LABORATOIRE DE PHYSIQUE STATISTIQUE
DE L'ÉCOLE NORMALE SUPÉRIEURE

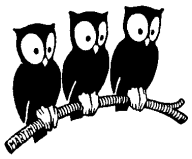

HABILITATION A DIRIGER LES RECHERCHES
DE l'UNIVERSITÉ PARIS VI

Spécialité : Biophysique

Présentée par

Frédéric PINCET

Du modèle à la réalité : liaison individuelle et adhésion biologique

Soutenance prévue le 12 Avril 2005 devant le jury composé de :

Mme Elisabeth CHARLAIX
Mme Sophie CRIBIER
M. Philippe DETERRE
M. Jean-François JOANNY
M. Éric PEREZ
M. François SCHWEISGUTH

Sommaire

1. Curriculum Vitae

Frédéric Pincet

Né le 21 Avril 1968 à Pabu (22), marié, 3 enfants

1988 Reçu au concours d'entrée de l'ENS, Paris (Mathématiques)

1989 Licence de physique, Paris 6 (mention AB)

1ère année Magistère Interuniversitaire de Physique (mention B)

1990 Maîtrise de physique, Paris 6 (mention B)

DEA de physique des liquides, Paris 6 (mention B)

2ème année Magistère Interuniversitaire de Physique (mention B)

dec 1990 – mars 1992 Séjour au Department of Chemical Engineering, Rensselaer Polytechnic Institute, Troy, New York, USA sous la direction du Professeur Georges Belfort, dans le cadre de mon service national.

1992 Reçu à l'Agrégation de mathématiques

3ème année Magistère Interuniversitaire de Physique (mention TB)

Magistère Interuniversitaire de Physique (mention B)

1994 Doctorat d'Université de l'Université P. et M. Curie (Paris 6), mention très honorable avec les félicitations du jury : « Mesures directes d'interactions spécifiques et non spécifiques entre membranes biologiques modèles », sous la direction d'Eric Perez.

1993 – 1996 Agrégé préparateur au département de physique de l'ENS.

Avril-mai et octobre-novembre 1996 Séjours aux departments of physics and pathology, The University of British Columbia, Vancouver, Canada, dans l'équipe d'Evan Evans.

1996 Recruté au CNRS au Laboratoire de Physique Statistique de l'ENS.

2000 Promotion au grade de Chargé de recherche de 1ère classe

2. Résumé

les chiffres en indice supérieur renvoient aux publications du § 5

Je fais partie de l'équipe "Surfaces Moléculaires Organisées" dont les recherches sont centrées sur les interactions entre molécules ou entre surfaces et sur l'adhésion cellulaire. Une grande partie des travaux que j'ai effectués est axée sur des problèmes issus de la biologie.

En 1996, j'ai été recruté au CNRS (section 05) avec pour mission d'élargir les capacités du groupe à travailler sur des systèmes proches du vivant. Pour cela, j'ai développé trois dispositifs distincts qui permettent de :

1. Mesurer l'énergie d'adhésion de vésicules lipidiques (ou de cellules dans certains cas) par détermination d'angles de contact.
2. Mesurer la force de séparation de deux cellules vivantes et adhérentes.
3. Mesurer la force de rupture d'un lien biologique unique.

Ce projet nécessitant une longue période de développement et d'apprentissage devait s'inscrire dans la durée (deux à quatre ans). Ces techniques utilisent toutes la manipulation d'objets microscopiques à l'aide de micropipettes. Leur mise en place m'a permis de réaliser des travaux fondamentaux et interdisciplinaires, où physique, chimie et biologie sont étroitement liées. Elle a également suscité un nombre croissant de collaborations avec chimistes et biologistes.

Ainsi, en collaboration avec P. Sinay (chimie, ENS), j'ai étudié le rôle d'un glycolipide dans l'embryogenèse et obtenu la première quantification d'une nouvelle classe d'interaction en biologie : la reconnaissance sucre-sucre[12,13,21,25]. P. Deterre (biologie, hôpital Pitié-Salpétrière), a observé qu'une mutation naturelle d'un récepteur de chimiokine protège de façon significative des maladies cardiovasculaires. Nous avons mis en évidence une modification de l'adhésion induite par ce récepteur et montré qu'elle peut expliquer cette observation épidémiologique[20]. Avec S. Dufour (biologie, Institut Curie), nous avons caractérisé l'adhésion produite par différents types de cadhérines et prouvé que le réseau d'actine est réorganisé pour renforcer les jonctions adhérentes provoquées par certaines cadhérines entre deux cellules vivantes[23]. Nous avons aussi étudié la modulation de l'adhésion induite par les cadhérines en présence de nectines[25].

Par ailleurs, j'ai mené plusieurs autres études : énergie de liaisons hydrogène[16] et de liaisons de chélation[27], mise en évidence d'un état intermédiaire de la fusion membranaire (l'hémifusion)[14,19] avec S. Cribier (physique, IBPC), manipulation de microgouttes d'huile (émulsion) et influence du pH sur leur adhésion[28] avec D. Langevin (physique, LPS, Orsay). D'autres travaux sont actuellement en cours sur les liens uniques protéine-membrane et protéine-ARN.

Dans le même temps, nous avons développé un modèle statistique d'adhésion par sites d'accrochage et l'avons validé par des mesures d'adhésion de vésicules fonctionnalisées[15]. Nous avons aussi étudié les propriétés mécaniques de cellules adhérentes et avons montré, en collaboration avec S. Dufour, que certaines cellules se comportent comme des sphères pleines élastiques obéissant à la théorie de l'adhésion développée par Johnson, Kendall et Roberts[26]. Je me suis enfin intéressé à des subtilités souvent ignorées mais importants dans l'interprétation des mesures de forces de rupture de liens unique (article en préparation). En reprenant le modèle de Kramers de diffusion entre états métastables, j'ai découvert l'origine d'apparentes contradictions entre différents travaux de référence sur le couple streptavidine-biotine.

La diversité de ces études m'a permis de publier dans des revues de haut niveau de physique, chimie et biologie.
Par ailleurs, l'expertise, acquise dans la manipulation par micropipettes, m'a permis de créer un pôle d'envergure nationale et internationale. J'ai ainsi conseillé et assisté une dizaine d'équipes. Souvent, il s'agissait d'aider à la mise au point d'un système de micromanipulation afin d'accomplir une tâche bien spécifique sur un problème donné. Certains groupes ont mené leur étude au laboratoire afin de bénéficier de nos dispositifs. Trois d'entre eux, venus dans un premier temps travailler sur nos systèmes expérimentaux vont dupliquer un de nos appareils de micromanipulation dans leur propre laboratoire (F. Bruckert, CEA, Grenoble ; D. van Effenterre – équipe de D. Roux - , CRPP, Bordeaux ; J. Rothman, New York).

Avant d'évoluer vers la matière vivante, mes thèmes de recherche portaient sur des systèmes modèles. Au cours de ma thèse, j'ai utilisé un appareil à force entre surface (SFA) afin de caractériser des interactions spécifiques et non spécifiques entre membranes modèles. Durant la première partie au department of chemical engineering du RPI, Troy, NY, j'ai étudié les interactions entre protéines et membranes polymériques [1,4]. J'ai effectué la deuxième partie au Laboratoire de Physique Statistique de l'Ecole Normale Supérieure de Paris. J'y ai d'abord étudié le rôle cryoprotecteur d'un sucre, le tréhalose. Puis j'ai entrepris la mesure des interactions entre des bases complémentaires de l'ADN [3]. Cette étude s'est poursuivie après ma thèse pendant deux années alors que j'occupais un poste d'agrégé préparateur [6,7]. Durant cette période, en collaboration avec P. Bassereau (Institut Curie, Paris), j'ai aussi élucidé l'origine des défauts (« trous ») observés dans les bicouches supportées [9]. Enfin, lors de deux séjours au laboratoire d'E. Evans (UBC, Vancouver, Canada), j'ai mis au point une nouvelle méthode de mesure d'énergies d'une liaison faible [8].

3. Activité de recherche

les chiffres en indice supérieur renvoient aux publications du § 5

Au cours de ma thèse (1990 – 1994) et pendant trois années en tant qu'agrégé préparateur (1993 – 1996) j'ai essentiellement étudié les interactions spécifiques et non spécifiques entre surfaces recouvertes d'une membrane (membrane polymérique ou bicouche lipidique) ou de protéines. Après mon recrutement au CNRS en 1996, j'ai développé plusieurs techniques de micromanipulations qui ont permis d'obtenir des résultats originaux dans de nombreux domaines. L'essentiel de ce manuscrit leur sera consacré et je ne parlerai que très peu (fin du rapport (§3.5)) des travaux antérieurs à mon recrutement et des travaux non directement associés aux micromanipulations. Je m'attacherai donc à détailler les parties concernant les trois systèmes que j'ai développés : mesure de l'énergie d'adhésion de vésicules lipidiques par détermination d'angles de contact (§3.1), mesure de la force de séparation de deux cellules adhérentes (§3.2), mesure de la force de rupture d'un lien unique (§3.3). Dans chaque chapitre, je décrirai le principe de l'expérience (§3.1.1., §3.2.1. et §3.3.1., resp.), puis je présenterai deux problématiques scientifiques traitées par chaque technique, l'une pourrait être qualifiée de « physique » (§3.1.2., §3.2.2. et §3.3.2., resp.), l'autre de plus « biologique » (§3.1.3., §3.2.3. et §3.3.3., resp.). Je terminerai chacune des parties en évoquant les autres sujets abordés avec chacune des techniques (§3.1.4., §3.2.4. et §3.3.4., resp.). Ensuite, j'expliquerai comment j'ai utilisé la micromanipulation pour des situations originales (§3.4.). Je conclurai en montrant que j'ai développé un pôle de micromanipulation français ouvert vers l'extérieur, et que je me suis attaché à diffuser le savoir acquis dans ce domaine le plus largement possible (§3.6.).
Pour chaque étude présentée, j'indiquerai, le cas échéant, les publications, collaborations et contrats de financement impliqués.

3.1 Adhésion de vésicules

3.1.1. Energie d'adhésion par mesure d'angle de contact

Cette technique a initialement été développée (Evans et Metcalfe, 1984) et décrite (Evans, 1980) par E. Evans. Son but est de mesurer l'énergie d'adhésion d'une vésicule géante (diamètre de quelques dizaines de microns) en contact avec un substrat rigide. Ce dernier peut être une bille, une lamelle de microscope ou encore une autre vésicule ayant une tension suffisamment élevée pour garder une forme sphérique. Le principe est décrit dans la figure 1. La vésicule (à droite sur la figure 1) est maintenue par une micropipette. Elle est mise en contact avec le substrat dont elle épouse la forme (s'il y a adhésion) jusqu'à atteindre une position d'équilibre décrite par l'équation d'Young-Dupré reliant l'angle de contact θ, la tension de la vésicule γ et l'énergie d'adhésion W_{adh} :

$$W_{adh}=\gamma(1-\cos\theta) \qquad (1)$$

γ est fixée par l'aspiration dans la pipette ΔP et la courbure de la vésicule, c :

$$\Delta P=2\gamma\left(\frac{1}{r_p}-c\right) \qquad (2)$$

Cette dernière relation peut être obtenue en appliquant deux fois la formule de Laplace sur la vésicule, une fois à l'extérieur de la pipette et une fois au niveau de l'hémisphère à l'extrémité de la « langue » située à l'intérieur de la pipette. En éliminant γ entre les relations (1) et (2), on obtient :

$$\Delta P = W_{adh}\left(2\frac{\left(\frac{1}{r_p}-c\right)}{1-\cos\theta}\right) = W_{adh} G \qquad (3)$$

où G ne dépend que de la géométrie du système (θ, r_p et c).
Expérimentalement, il est extrêmement délicat de mesurer précisément θ car, d'une part, il est difficile d'obtenir un angle entre des surfaces sur des distances de seulement quelques microns, et, d'autre part, physiquement, le module de courbure tend à adoucir la forme de la vésicule qui ne présente donc pas un angle net. La méthode la plus efficace pour obtenir θ est de calculer numériquement la forme qu'aurait une vésicule idéale sans module de courbure. Pour cela, deux propriétés fondamentales des vésicules géantes sont utilisées : elles gardent un volume et une surface constants à moins de 1% près, lors de l'expérience. Lorsque la vésicule épouse le substrat, elle réduit sa langue à l'intérieur de la pipette afin de gagner du volume et de la surface à l'extérieur. Ainsi, la mesure de l'avancée de la langue dans la pipette permet de connaître le volume et la surface extérieurs de la vésicule à tout instant, de prédire numériquement la forme de la vésicule idéale et donc de calculer θ et la courbure c.
Avec cette approche, une expérience s'effectue en mettant vésicule et substrat en contact tangentiel. L'aspiration à l'intérieur de la pipette, donc la tension de la vésicule, est ensuite variée par palier. L'angle de contact et la courbure de la vésicule à l'équilibre sont calculés pour chaque palier. La courbe ΔP en fonction de G peut alors être tracée. Il s'agit d'une droite dont la pente est W_{adh} (d'après l'équation (3)).

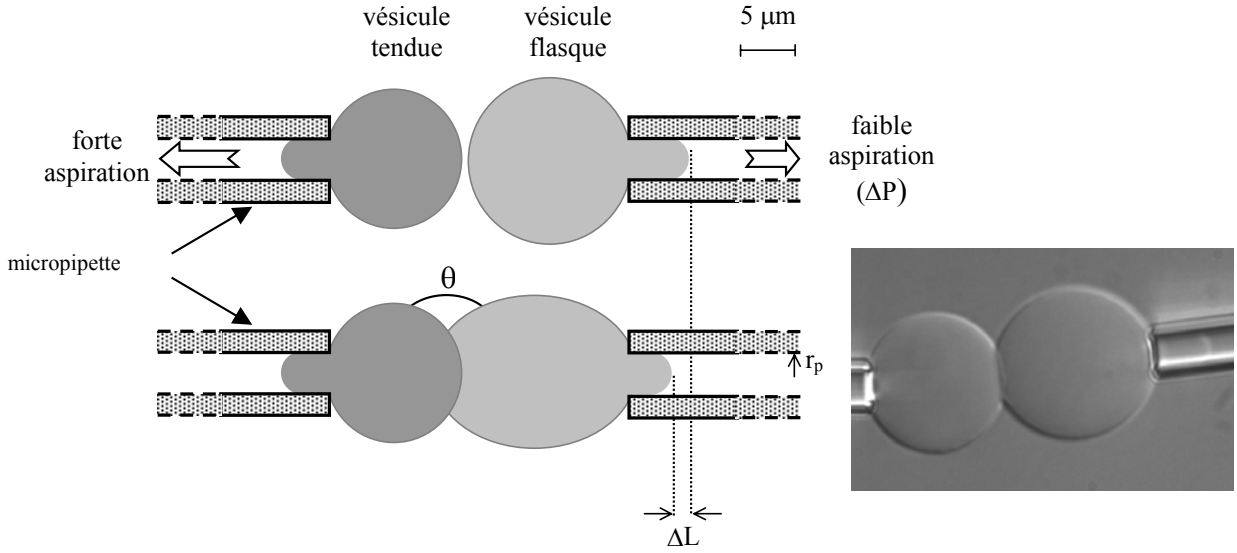

Figure 1 : Principe de l'expérience. Une vésicule faiblement aspirée (ΔP=10 – 200 Pa) est mise en contact tangentiel avec un substrat indéformable (ici, une autre vésicule, fortement aspirée). S'il y a adhésion, la vésicule épouse la forme du substrat. L'angle de contact θ est obtenu numériquement grâce à la mesure du déplacement de la langue ΔL. L'énergie d'adhésion peut alors être calculée grâce à l'équation (3).

3.1.2. Adhésion par sites mobiles : théorie et vérification expérimentale [15]

Collaboration : L. Lebeau (chimie, Illkirch)

L'adhésion de surfaces sur lesquelles diffusent des sites d'accrochage est un problème qui n'a été jusqu'à présent modélisé que par des approches utilisant les potentiels chimiques des composants. Ces modèles, déjà anciens (1985), ne permettaient pas de trouver une relation

entre les propriétés d'une liaison unique (énergie de liaison) et l'énergie d'adhésion macroscopique [Bell et al, 1984 ; Lipowski, 1996 ; Zuckerman et Bruinsma, 1995]. Deux raisons ont contribué à ce que les scientifiques de l'époque n'ont pas cherché à établir une telle relation. D'une part, l'approche avec les potentiels chimiques ne permettant pas de remonter au niveau moléculaire, il fallait envisager une autre théorie, d'autre part, les outils moléculaires nécessaires à la validation expérimentale d'une telle théorie n'existaient pas. Nous possédons maintenant, grâce à une collaboration étroite avec L. Lebeau (chimiste, Illkirch), de telles molécules. Par ailleurs, nous avons développé, avec l'aide de B. Derrida et de J. Vannimenus (LPS), une approche microcanonique simple qui permet de relier l'observable macroscopique (énergie d'adhésion globale) à l'énergie d'une liaison unique, e_l.

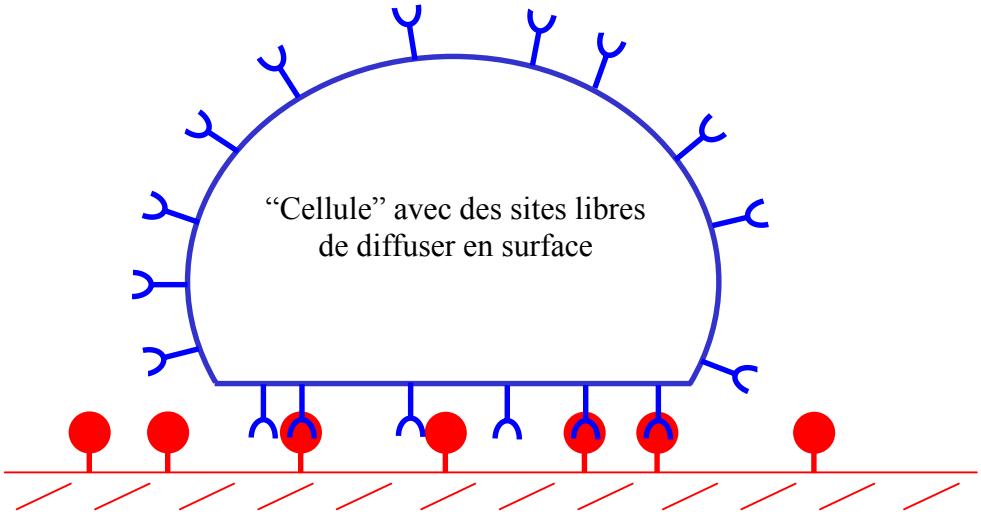

Figure 2: Schéma du modèle d'une cellule adhérant sur un substrat: la cellule est une capsule à la surface de laquelle des sites d'accrochages, ligands, circulent librement. Ces ligands peuvent se lier à des sites complémentaires, les récepteurs, immobiles à la surface du substrat.

Le principe du modèle, schématisé figure 2, est le suivant : une surface avec une densité de sites d'adhésion fixe d_R, fait face à une surface, la « cellule », d'aire A_t avec une densité d_L de sites libres de diffuser, les ligands. Au total, il y a donc $N=d_L A_t$ ligands. Les sites du substrat seront appelés récepteurs. Clairement, à l'équilibre, la densité de ligands sera plus élevée dans la zone de contact qu'à l'extérieur.

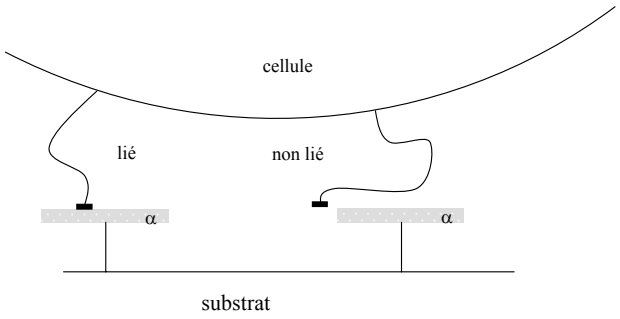

Figure 3: Modèle de l'interaction ligand-recepteur : si le ligand est dans l'aire d'attraction α du récepteur, il est lié (ligand de gauche). Sinon, il n'est pas lié (ligand de droite).

On fera l'hypothèse que chaque récepteur possède une aire d'attraction α, comme définie dans la figure 3 et que les zones d'attraction de deux récepteurs ne peuvent se chevaucher.

D'une manière générale, l'énergie d'adhésion peut se calculer à partir de l'énergie libre F :

$$W_{adh} = -\frac{\partial F}{\partial A_c}\Big)_{V,T} = k_B T \frac{\partial \ln Z}{\partial A_c}\Big)_{V,T} \qquad (4)$$

où Z est la fonction de partition du système.

Il reste donc à exprimer Z en fonction des différents paramètres. Le nombre total de récepteurs dans la zone de contact est : $d_R A_c$, ce qui implique que la surface totale de la zone où les ligands peuvent se lier au substrat est $A_l = \alpha d_R A_c$. Tout ligand présent dans A_l sera lié à un récepteur. L'énergie d'une configuration où n sites sont situés dans cette zone et N-n dans le reste de la « cellule » est ne_l. Par conséquent, la fonction de partition du système s'écrit :

$$Z = \sum_{n=0}^{N} \frac{N!}{n!(N-n)!} A_l^n \left(A_t - A_l\right)^{N-n} e^{\frac{ne_l}{k_B T}} = \left(A_t + A_l\left(e^{\frac{e_l}{k_B T}} - 1\right)\right)^N \qquad (5)$$

W_{adh} peut alors être directement obtenue à partir de l'équation (4) :

$$W_{adh} = A_t \alpha d_L d_R k_B T \frac{\left(e^{\frac{e_l}{k_B T}} - 1\right)}{\left(A_t + \alpha d_R A_c\left(e^{\frac{e_l}{k_B T}} - 1\right)\right)} \qquad (6)$$

Cette dernière équation donne de façon quantitative des résultats auxquels on pouvait s'attendre :

(i) W_{adh} diminue quand la zone de contact augmente puisque le réservoir formé par la partie extérieure de la « cellule » devient plus petit par rapport à A_c.

(ii) Quand le nombre de récepteurs dans la zone de contact est petit, W_{adh} est indépendante de A_c. C'est le régime linéaire où la fraction de ligands liés est petite.

(iii) Quand e_l est grande, tous les ligands sont liés et on a bien : $W_{adh} = Nk_B T/A_c$.

Pour affiner les prédictions de ce modèle analytique, il s'est avéré qu'une analyse numérique était la bienvenue. En effet, notre modèle utilise plusieurs hypothèses simplificatrices, dont certaines parfois inadaptées aux conditions expérimentales, notamment celle autorisant que plusieurs ligands se recouvrent. Avec M. Wouts (stagiaire MIP), nous avons pu montrer que l'énergie interne du système est pratiquement proportionnelle à l'aire de contact (il est en fait possible de démontrer de façon rigoureuse que cette approximation est très bonne). En faisant une telle hypothèse, nous avons pu retrouver une relation (toujours analytique) plus complexe entre W_{adh} et e_l. La première relation est en fait un développement limité au premier ordre de cette dernière.

Afin de valider le modèle, nous avons utilisé des billes de polystyrène commerciales recouvertes de superavidine, incubées dans une solution de molécules bi-fonctionnelles contenant une extrémité biotine (capable de se fixer sur les billes) et une extrémité formée d'une base de l'ADN (adénosine, A, ou thymidine, T) (cf figure 4). Nous avons aussi fabriqué des vésicules dont la membrane était composée à 90% de stearoyl-oleoyl-phosphatidylcholine (SOPC) et à 10% d'un lipide contenant A ou T dans sa tête polaire. Nous avions déjà mesuré les énergies de liaisons A/T, A/A et T/T auparavant avec un appareil à force entre surfaces (SFA, §3.5.1.).

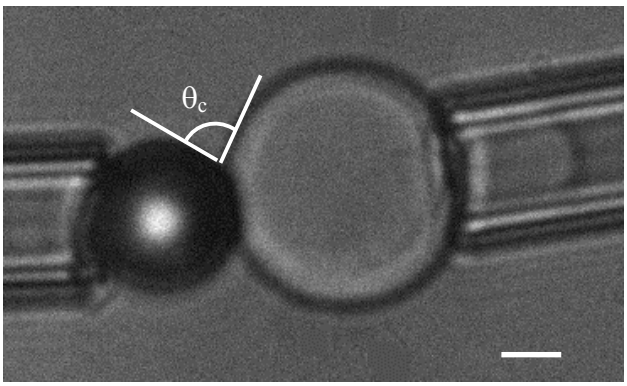

Figure 4: Une vésicule micromanipulée mise en contact avec une bille tenue par une micropipette. La barre d'échelle représente 5 µm. L'énergie d'adhésion est obtenue par mesure du déplacement de la « langue » de la vésicule dans la pipette de droite (voir 3.1.1.).

Nous avons donc pu, en mesurant l'énergie d'adhésion d'une de ces vésicules sur une de ces billes tester le modèle. Les résultats expérimentaux sont donnés figure 5.

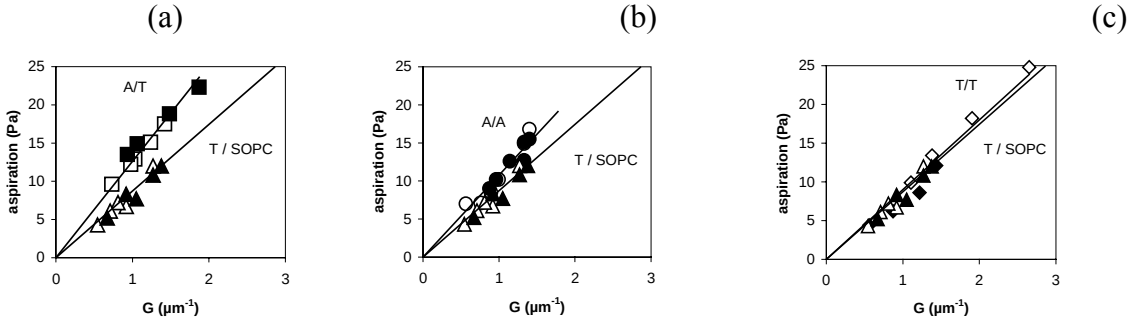

Figure 5: pression d'aspiration en fonction de G (cf. équation (3)) pour chaque interaction spécifique et comparaison avec la cas non spécifique où une vésicule de SOPC pure adhère sur une bille recouverte de T (T/SOPC). Les lignes sont des fits passant par l'origine et, d'après l'équation (3), leur pente est égale à W_{adh}. Les symboles noirs (vides) correspondent à une augmentation (diminution) de la pression d'aspiration. (a) bille A – vésicule T, (b) bille A – vésicule A, (c) bille T – vésicule T.

Afin de pouvoir appliquer l'équation (6), il est nécessaire d'estimer d_R et α. Dans notre cas, d_R est donné par le fournisseur des billes et α doit être de l'ordre de grandeur de l'aire moléculaire d'un lipide. d_L est connu grâce à la composition initiale du mélange lipidique utilisé pour fabriquer les vésicules. Les énergies de liaison déduites sont en excellent accord avec celles obtenues par SFA (cf. tableau 1). La précision des mesures est de l'ordre de 0,5 k_BT.

e_b (k_BT)	Valeur mesurée	Valeur SFA
A/T	3.2	3.6
T/A	3.4	3.6
A/A	2.3	1.9
T/T	1.7	1.5

Tableau 1 : valeurs des énergies de liaison déduites à partir des mesures de micromanipulation et de l'équation (6), comparées aux valeurs obtenues avec le SFA.

Ces résultats valident donc notre modèle qui pourra être appliqué à d'autres systèmes. La limitation principale du modèle est le besoin de connaître d_R et α. Ces paramètres ne sont pas toujours aussi faciles à estimer que pour les billes et, dans certains cas le recours à des simulations numériques s'avère nécessaire.

3.1.3. Une nouvelle classe d'interaction de molécules biologiques : l'interaction sucre – sucre [12,13,21,24]

Collaborations : P. Sinay (chimie, ENS)
Contrats l'Oréal 1997 et Physique et Chimie du Vivant 1998.

Les cellules biologiques sont entourées d'une couche appelée le glycocalix composée de molécules contenant des motifs chimiques de type sucres. Lorsque deux cellules se rencontrent, ce sont d'abord ces couches qui se « voient ». On pourrait donc s'attendre à ce que les interactions entre ces sucres jouent un rôle important en biologie. Or, jusqu'à ces dernières années, cela ne semblait pas être le cas. Des interactions entre sucres et protéines étaient bien connues. Par exemple, la formation de liens sucres – sélectines dans la réaction inflammatoire permet de forcer l'adhésion de globules blancs. En revanche, aucune interaction sucres – sucres pertinente en biologie n'avait été observée de façon certaine. Une étude menée par Hakomori [Hakomori, 1991], (biologiste, Seattle), semblait montrer qu'un sucre, le Lewis X (LeX), présent dans la tête polaire d'un glycolipide naturel est responsable de l'étape de compaction des embryons de rats. D'autres travaux allaient dans le même sens [Boubelik et al., 1998 ; Siuzdak et al., 1993 ; Henry et al., 1999 ; Geyer et al., 2000]. En effet, tout comme pour l'homme, il existe un stade où les cellules de rat, lors de l'embryogenèse, sont complètement recouvertes de ce glycolipide. A ce moment-là l'embryon s'écrase sur lui-même et devient lisse. C'est l'étape de compaction à partir de laquelle les cellules commencent à se différencier (les cellules à l'intérieur de l'embryon ne subissent pas les mêmes contraintes que celles présentes à la surface). Cette étape est vitale. Hakomori a observé qu'en présence de Lewis X soluble, ou lorsque le milieu était privé de calcium elle n'avait pas lieu. Il en a donc conclu qu'il existe une interaction spécifique Lewis X – Lewis X médiée par le calcium et que cette interaction est responsable de l'étape de compaction. Ses résultats restaient très controversés à cause des méthodes indirectes utilisées.
Afin d'obtenir des mesures quantitatives fiables, nous avons abordé ce problème par des expériences d'adhésion entre vésicules micromanipulées portant à leur surface le Lewis X. Pour cela, l'équipe de P. Sinay (chimie, ENS) a synthétisé un lipide fonctionnalisé portant le Lewis X dans sa tête polaire ainsi qu'un lipide témoin proche de celui-ci afin de mesurer les interactions non spécifiques. Nous avons mené les premières expériences de micromanipulation de vésicules avec ce glycolipide de synthèse où la forte mobilité orientationelle du Lewis X était assurée par la présence d'un long espaceur flexible. Grâce à la comparaison des énergies d'adhésion de vésicules portant le Lewis X ou le lipide témoin, mesurées en présence d'ions Ca^{2+} ou d'ions Na^{+}, la spécificité de l'interaction entre deux Lewis X a été démontrée, cette interaction est calcium dépendante (cf figure 6). L'énergie d'adhésion spécifique qui découle de ces mesures est faible.

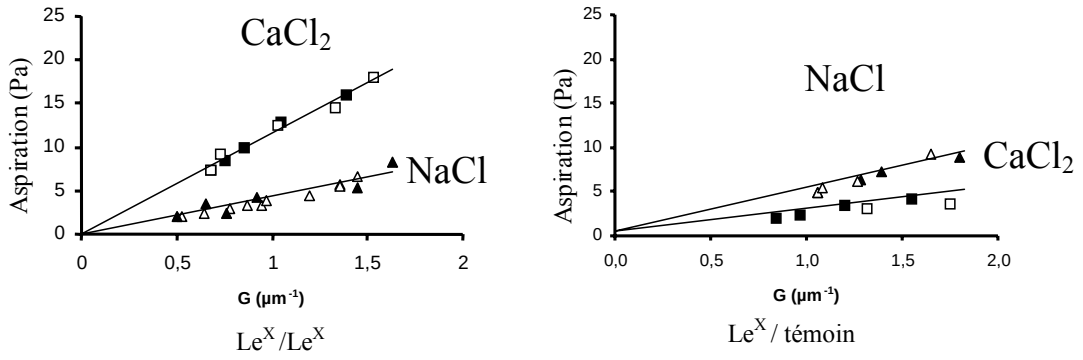

Figure 6 : à gauche, mesures d'adhésion entre deux vésicules composées de SOPC (90%) et de lipide LeX (10%) en présence de calcium (carrés) et sans calcium (triangle). Comme pour la figure 5, les pentes sont égales aux énergies d'adhésion. A droite, le même type de mesure entre une vésicule SOPC/LeX (90/10) et une vésicule composée de SOPC à 90% et de lipide témoin à 10%.

Dans un contexte cellulaire, la mobilité orientationnelle du Lewis X est très restreinte par rapport à celle des glycolipides de synthèse précédent. Le Lewis X naturel se compose de chaînes aliphatiques céramides qui imposent au Lewis X une orientation perpendiculaire à l'axe du céramide. En insérant ces Lewis X naturels dans les vésicules, et en mesurant leurs énergies d'adhésion, nous avons montré que non seulement la reconnaissance est possible avec la molécule naturelle, mais que l'adhésion est cinq fois plus forte qu'avec le glycolipide de synthèse doté d'un espaceur. Ceci illustre l'importance de l'orientation des Lewis X dans la reconnaissance et montre que la nature oriente naturellement bien le LewisX.
Enfin, nous avons testé le degré de spécificité de la reconnaissance en mesurant l'énergie d'adhésion entre une vésicule portant le Lewis X et une autre portant un isomère du Lewis X, le Lewis A structurellement très semblable au Lewis X. En présence d'ions Ca^{2+}, l'énergie d'adhésion n'augmente que lorsque les deux vésicules portent le Lewis X, montrant ainsi que la reconnaissance possible entre deux Lewis X devient impossible entre un Lewis X et un Lewis A.

Grâce à cette étude, nous avons pu obtenir la première quantification d'une interaction spécifique sucre – sucre jouant un rôle en biologie. Cette interaction hautement spécifique est très faible et est donc la plupart du temps occultée par d'autres interactions impliquant des protéines. Cependant, dans certaines conditions, comme ici dans l'embryogenèse où les cellules sont recouvertes de ce glycolipide, elle joue un rôle vital.

3.1.4. Autres études menées par mesures d'adhésion de vésicules

3.1.4.1. Liaisons de chélation [27]
Collaborations : C. Mioskowski (chimie, Illkirch)
Contrat Physique et Chimie du Vivant 2000
Dans le cadre de la thèse de David Tareste

La chélation entre un ion métallique et une molécule intervient dans de nombreux processus en chimie. Depuis plusieurs années, elle sert à ancrer des protéines sur des supports au moyen d'une étiquette polyhistidine, ou bien à élaborer des techniques de séparation en utilisant l'affinité d'un ion nickel pour le groupe NTA et pour la polyhistidine [Hochuli et al., 1988 ; Schmitt et al., 1994 ; Venien-Bryant et al., 1997 ; Wilson-Kubalek et al. 1998 ; Bischler et al.

1998 ; Lebeau et al., 2001]. Avec des monocouches de lipides portant ce complexe comme tête polaire, il est également possible d'utiliser la reconnaissance histidine-nickel pour produire des cristallisations bidimensionnelles de protéines à l'interface eau-air. L'ion nickel est alors partagé entre le groupement NTA et l'étiquette polyhistidine.
Nous avons entrepris de tester l'hypothèse selon laquelle deux groupes NTA peuvent se lier en partageant un Ni^{2+}, et de mesurer les énergies de liaison impliquées. Nous avons mesuré l'énergie d'adhésion entre monocouches de lipides dont la tête polaire porte un groupe NTA ayant fixé un Ni^{2+} (groupe NTA-Ni) ou non (groupe NTA) dans les conditions de chélation, c'est-à-dire à pH 8 fixé par le tampon tris. Les mesures ont été faites indépendamment au moyen de trois techniques différentes: la micromanipulation de vésicules fonctionalisées, le SFA et une technique souvent utilisée en chimie, la microcalorimétrie. Malgré des problèmes techniques tels que la relative instabilité des lipides, ou de l'ion nickel dans le NTA en présence de tris, nous avons pu obtenir des résultats fiables et concordants pour les trois techniques. Les énergies d'adhésion mesurées ont été analysées en reprenant pour chaque technique le modèle statistique approprié, et en tenant compte de la répulsion double-couche et de la quantité de Ni^{2+} ayant quitté les groupes NTA. Les résultats montrent qu'un groupe NTA-Ni se lie effectivement à un groupe NTA. L'énergie de liaison NTA-Ni et NTA-Ni-NTA a ainsi été mesurée, résultat qui permettra par exemple de prédire les rendements de techniques de séparation.

3.1.4.2. Comportement de chaînes courtes inhomogènes : effet polymère[22]
Collaboration : P. Sinay (chimie, ENS)

Les interactions qui gouvernent les systèmes colloïdaux dépendent souvent de molécules portées par leur surface [Ricoul et al., 1998 ; Helm et al. 1991 ; Luckham et al., 1993]. Ces molécules peuvent être des lipides fonctionnalisés, dont les groupes fonctionnels sont de tailles et flexibilités très diverses. Ce sont donc elles qui en premier lieu régiront les interactions avec l'environnement. Un bon modèle de ces systèmes est donné par des bicouches lipidiques portant de tels objets (figure7).

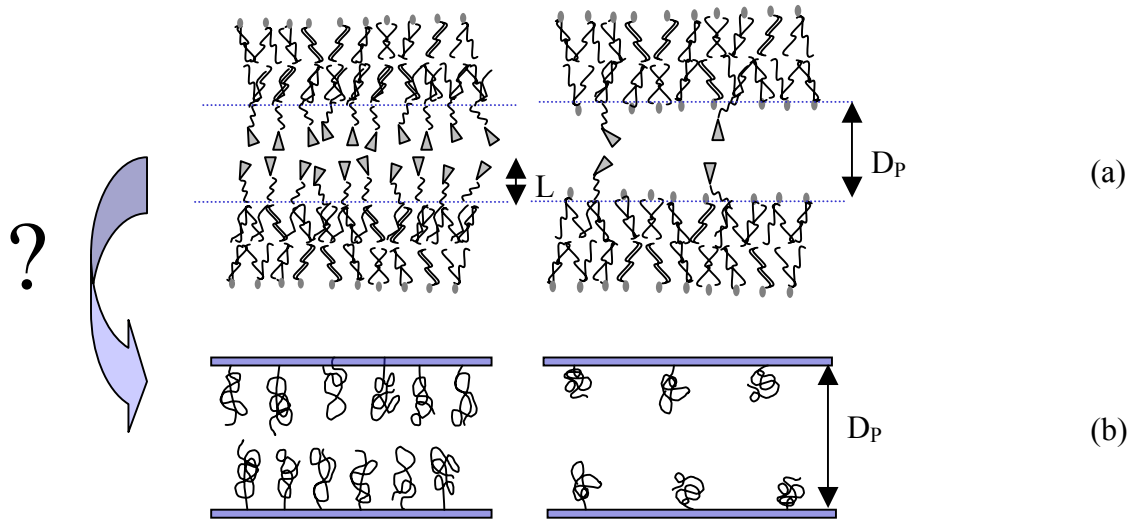

Figure 7 : (a) Schéma de bicouches lipidiques interagissant, portant une forte (gauche) ou faible (droite) densité de lipides fonctionnalisés. (b) On compare l'interaction produite par de telles bicouches à celle produites par des chaînes de polymères en régime brosse (gauche) ou champignon (droite).

On sait accéder expérimentalement aux interactions produites par ces systèmes, en revanche, il n'existe aucun modèle théorique permettant de les prédire. En dépit de tailles et flexibilités très réduites par rapport à celles des polymères, nous avons fait le pari qu'il était possible de décrire l'interaction stérique produite par ces fonctions en utilisant la théorie des polymères.
Pour des polymères ancrés à une surface, on parle de régime brosse lorsque les polymères sont suffisamment rapprochés pour interagir, de régime champignon, dans le cas contraire.
L'énergie d'interaction de deux brosses de polymère s'écrit [Alexander, 1977 ; de Gennes, 1981 ; de Gennes, 1987] :

$$E_{brush}(D_p) = \frac{\beta k_B T}{s^3}\left[\frac{D_p^{7/4}}{7(2L)^{3/4}} + \frac{(2L)^{9/4}}{5D_p^{5/4}} - \frac{24}{35}L\right] \qquad (7)$$

Elle dépend de leur distance de séparation (D_P), de l'épaisseur L de la brosse, de la distance de séparation moyenne s entre deux polymères, et d'un préfacteur β, ne dépendant ni de L, ni de s.
Pour des polymères en régime champignon, l'énergie d'interaction s'écrit [Kuhl et al, 1994 ; Dolan et Edwards, 1974] :

$$E_{mushroom}(D_p) = 36\Gamma k_B T e^{-\frac{D_p}{Rg}} \qquad (8)$$

Elle s'exprime comme une exponentielle décroissante de la distance de séparation (D_P) avec une longueur de décroissance égale au rayon de gyration du polymère. Γ est la densité surfacique de polymères ($\Gamma = 1/s^2$).
Les molécules avec lesquelles nous avons travaillé sont des glycolipides, composés d'une partie hydrophobe faite de trois chaînes aliphatiques ramifiées qui s'insèrent parfaitement dans des bicouches de phospholipides standards (SOPC). La fonction (le ou les sucres) se compose d'un, deux ou trois groupes rigides articulés entre eux. Ces sucres sont reliés aux chaînes hydrophobes par de petites chaînes de polymères (PEO) flexibles. Ces glycolipides ont été insérés dans des bicouches de phospholipides, elles-mêmes déposées sur substrat solide. D'une bicouche a une autre, la densité et la nature du glycolipide varie. Avec un SFA, nous avons mesuré les profils d'interactions de deux bicouches identiques en fonction de leur distance de séparation. Les molécules n'étant pas (ou très peu) chargées, les interactions en jeu sont l'attraction de van der Waals qui domine aux distances de séparation supérieures à la distance d'équilibre des deux bicouches, et les interactions stériques dues à la présence des fonctions qui dominent aux distances inférieures à la distance d'équilibre (les répulsions dues à l'hydratation et à la protrusion interviennent à des échelles beaucoup plus petites).
Les courbes obtenues pour deux glycolipides différents avec deux densités différentes (forte et faible) sont représentées figure 8.
Les profils ont été mesurés dans une gamme de distance où les interactions dominantes sont les répulsions stériques dues aux sucres. Les courbes en trait plein représentent les meilleurs ajustement obtenus en utilisant l'expression consacrée aux brosses de polymères (figure 8a), ou aux polymères en régime champignon (figure 8b). Notons que s et Γ sont obtenus indépendamment expérimentalement par mesure d'isothermes et ne sont donc pas ajustables. Quant à R_g, il s'agit ici d'un rayon de gyration effectif, ne pouvant en aucun cas être obtenu comme pour un polymère standard. Les ajustements obtenus sont bons avec des paramètres plausibles. Il semble donc que la théorie des polymères puisse nous fournir un bon modèle pour décrire les interactions produites par des chaînes courtes et inhomogènes.

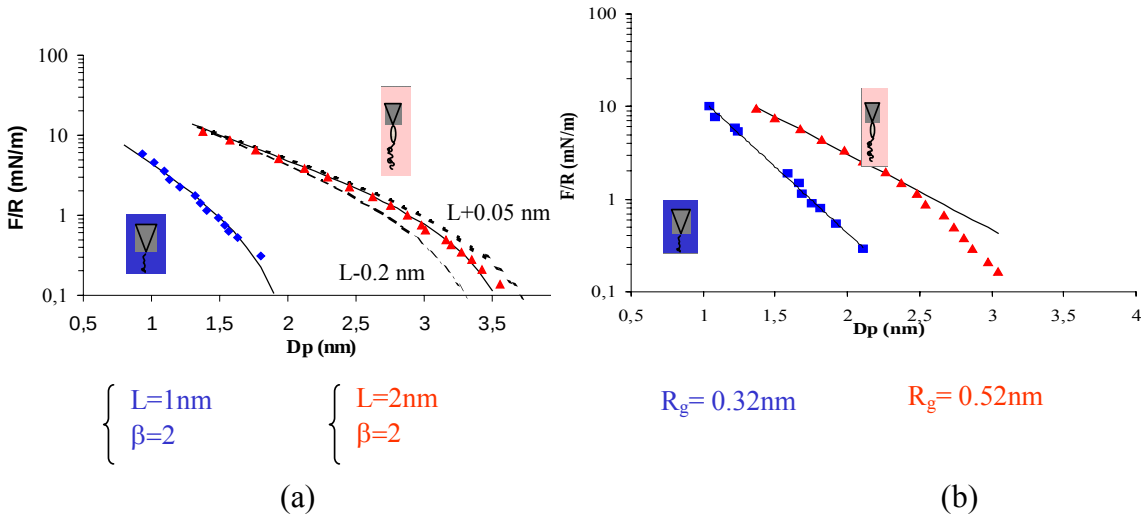

Figure 8 : profil force/ distance de deux bicouches composées de glycolipides (a) en forte densité (b) en faible densité, dans une gamme de distance ou les effets stériques dus aux sucres dominent. Les courbes bleues sont obtenues avec un glycolipide ne comportant qu'un groupement rigide, les courbes rouges sont obtenues avec un glycolipide comportant deux groupements rigides articulés.

Pour tester ce modèle, nous avons tenté de retrouver par le calcul les énergies d'adhésion de deux vésicules composées à 10% de glycolipides et à 90% de phospholipides standard (la SOPC). Nous avons mesuré l'énergie d'adhésion de quatre différentes paires de ces vésicules. Les énergies obtenues sont reportées tableau 2. On peut les comparer aux énergies calculées de façon théorique. Pour de telles vésicules, la densité de glycolipides est faible, c'est donc l'expression « champignon » (Eq. 2) que l'on a utilisée pour décrire l'interaction stérique produite par les sucres. Par ailleurs, contrairement aux bicouches déposées, les vésicules sont des objets fluctuants. Les répulsions de Helfrich, dues aux excitations thermiques de la membrane s'opposent donc également à l'attraction de van der Waals. L'énergie d'adhésion de deux vésicules est l'énergie qui à l'équilibre minimise la somme de ces trois interactions (van der Waals, Helfrich, stérique). Le calcul donne des valeurs comparables à celles obtenues expérimentalement, validant ainsi le modèle utilisé.

Vésicule 1 –vésicule 2	$E_{adh}(\mu J/m^2)$ mesurée	$E_{adh}(\mu J/m^2)$ calculée
	9.5 ± 0.5	9.8
	5.4 ± 1	5.9
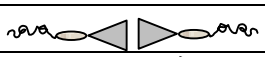	4.5 ± 2	4.0
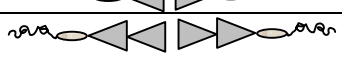	4.5 ± 2	3.0

Tableau 2 : Energies d'adhésion mesurées par micromanipulation de vésicules, et énergies d'adhésion calculées en considérant que les têtes des glycolipides se comportent comme des polymères en régime champignon.

Cette étude nous a permis de montrer que les interactions qui d'ordinaire régissent le comportement de surfaces de polymères s'appliquent également à des chaînes courtes et inhomogènes. Par conséquent, il devient possible de décrire le comportement de petites molécules linéaires et inhomogènes très utilisées en physique de la matière molle.

3.1.5 Bibliographie de la partie 3.1.

Alexander, S. *J. Phys. (Paris)*, **38**, 983-987, (1977).

Bell, G.I., M. Dembo, et P. Bongrand, *Biophys. J.* **45**, 1051–1064 (1984).

Bischler, N.; Balavoine, F.; Milkereit, P.; Tschochner, H.; Mioskowski, C.; Schultz, P., *Biophys. J.*, **74**, 1522-1532 (1998).

Boubelik, M., D. Floryk, J. Bohata, L. Draberova, J. Macak, F. Smid, et P. Draber, *Glycobiology*, **8**, 139 –146 (1998).

Dolan, A.; Edwards, F. *Proc. R. Soc. London A*, **337**, 509-516, (1974).

Evans, E., *Biophys. J.*, **31**, 425-431 (1980).

Evans E. et M., Metcalfe M., *Biophys. J.*, **45**, 715–720 (1984).

de Gennes, P.G., *Macromolecules*, **14**, 1637-1644 (1981).

de Gennes, P. G., *Adv. Colloid Interface Sci.***, 27**, 189-209, (1987).

Geyer, A., C. Gege, et R. R. Schmidt, *Angew. Chem. Int. Ed.*, **39**, 3246 –3249, (2000).

Hakomori, S., *Pure Appl .Chem,.* **63**, 473– 482 (1991).

Helm, C.; Knoll, W.; Israelachvili, J. N., *Proc. Natl. Acad. Sci. U.S.A*, **88**, 8169-8173, (1991).

Henry, B., H. Desvaux, M. Pristchepa, P. Berthault, Y. Zhang, J-M. Mallet, J. Esnault, et P. Sinay¨, *Carbohydr. Res*, **315**, 48–62 (1999) .

Hochuli, E.; Bannwarth, W.; Dobeli, H.; Gentz, R.; Stuber, D. *Bio-Technol.*, **6**, 1321-1325, (1988).

Kuhl, T. L., D.E. Leckband, D. Lasic, D., et J.N. Israelachvili, *Biophys. J.*, **66**, 1479-1488 (1994).

Lebeau, L.; Lach, F.; Venien-Bryan, C.; Renault, A.; Dietrich, J.; Jahn, T.; Palmgren, M. G.; Kuhlbrandt, W.; Mioskowski, C. *J. Mol. Biol.*, **308**, 639-647, (2001).

Luckham, P.; Wood, J.; Swart, R. *J. Colloid Interface Sci.*, **156**, 173-183, (1993).

Lipowski, R., *Phys. Rev. Lett.* **77**, 1652–1655, (1996).

Ricoul, F., Dubois, M., Belloni, L., Zemb, T., Andre-Barres, C., et Rico-Lattes, I., *Langmuir*, **14**, 2645-2655, (1998).

Schmitt, L., Dietrich, C., et Tampe, R., *J. Am. Chem. Soc.*, **116**, 8485-8491, (1994).

Siuzdak, G., Y. Ichikawa, T. J. Caulfield, B. Munoz, C.-H. Wong, et K. C. Nicolaou, *J. Am. Chem. Soc*, **115**, 2877–2881, (1993).

Venien-Bryan, C.; Balavoine, F.; Toussaint, B.; Mioskowski, C.; Hewat, E. A.; Helme, B.; Vignais, P. M. *J. Mol. Biol.*, **274**, 687-692, (1997).

Wilson-Kubalek, E. M.; Brown, R. E.; Celia, H.; Milligan, R.A., *Proc. Natl. Acad. Sci. USA*, **95**, 8040-8045, (1998).

Zuckerman, D., et R. Bruinsma, (1995), *Phys. Rev. Lett.*, **74**, 3900–3903, (1995).

3.2 Adhésion de cellules vivantes

3.2.1. Force de séparation de cellules adhérentes

Les cellules sont des objets très différents des vésicules. En effet, il n'est en général pas possible de parler de tension globale, mais plutôt de tension locale. De ce fait, l'approche présentée pour les vésicules (mesure d'angles de contact) s'avère caduque avec les cellules. J'ai donc mis au point une nouvelle technique permettant de quantifier l'adhésion de deux cellules. Le protocole expérimental est le suivant (figure 9). Deux cellules sont maintenues dans des micropipettes avec une aspiration contrôlée. Elles sont mises en contact afin que l'adhésion se développe. Après un temps de contact contrôlé, l'expérimentateur entreprend de séparer le doublet cellulaire formé. L'aspiration est fortement accrue au niveau d'une des deux pipettes (celle de droite sur la figure 9b), et reste plus faible dans l'autre. Un mouvement mécanique est exercé pour séparer les cellules. Deux cas se présentent alors. Si l'adhésion est plus forte que l'aspiration, le doublet reste formé et quitte la pipette. Si au contraire, l'aspiration domine, les cellules se séparent. Dans le premier cas, on rattrape le doublet et l'aspiration la plus faible est augmentée. On essaie alors de nouveau de séparer les cellules. Ce cycle est répété jusqu'à la rupture de l'adhésion au nième cycle.

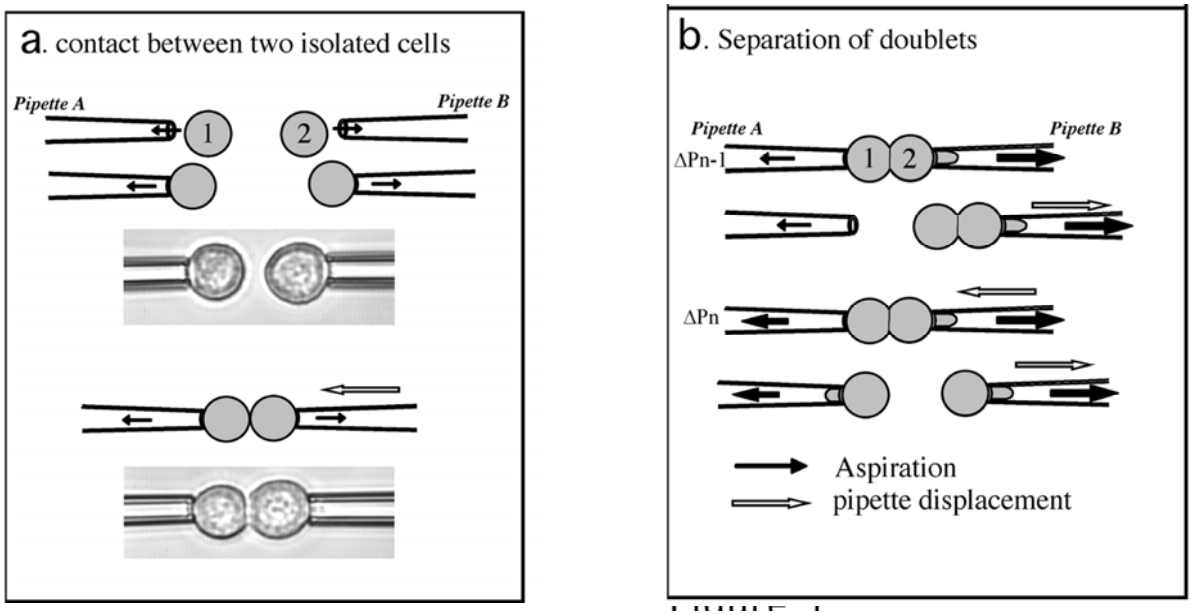

Figure 9 : Principe de l'expérience : Deux cellules sont attrapées par des micropipettes, mises en contact et séparées mécaniquement pour des valeurs croissantes d'aspiration jusqu'à la rupture de l'adhésion.

Nous avons montré à l'aide d'un microdynamomètre (une microaiguille) que la force de séparation, F_s, est bien approximée par : $F_s = (\Delta P_{n-1} + \Delta P_n)\, \pi\, r_p^2/2$

Où ΔP_{n-1} et ΔP_n sont respectivement les aspirations aux cycles n-1 et n au niveau de la pipette de rayon interne r_p (pipette de gauche dans la figure 9b).

Pour travailler dans des conditions où le comportement des cellules est proche de la réalité biologique, nous avons fabriqué une platine permettant de maintenir la température à 37°C durant l'expérience.

3.2.2. Un modèle de cellule : coque ou sphère pleine ? [26]

Collaboration : S. Dufour (biologie, institut Curie)

La cellule : un matériau actif

Une cellule vivante dont la taille typique est souvent de 10 µm peut être schématisée par un milieu visqueux enveloppé dans une membrane. Ce milieu possède la particularité de contenir le cytosquelette qui confère à la cellule ses propriétés mécaniques. Il est capable de se réorganiser en fonction des contraintes subies par la cellule. Le temps caractéristique de ces réorganisations est de quelques minutes. Le cytosquelette se présente sous trois formes dans la cellule : le cytosquelette cortical (formé de filament d'actine), les microtubules (tubuline) et les filament intermédiaires (souvent formés de kératine, de vimentine ou de desmine). Des photos de ces différents types de filaments sont données figure 10. Le cytosquelette cortical a une structure essentiellement bidimensionelle et est lié à la membrane de la cellule. Le globule rouge, par exemple ne possède qu'un cytosquelette cortical. Les microtubules et les filaments intermédiaires ont une structure tridimensionnelle. La plupart du temps, il n'y a pas de cytosquelette dans le noyau de la cellule.

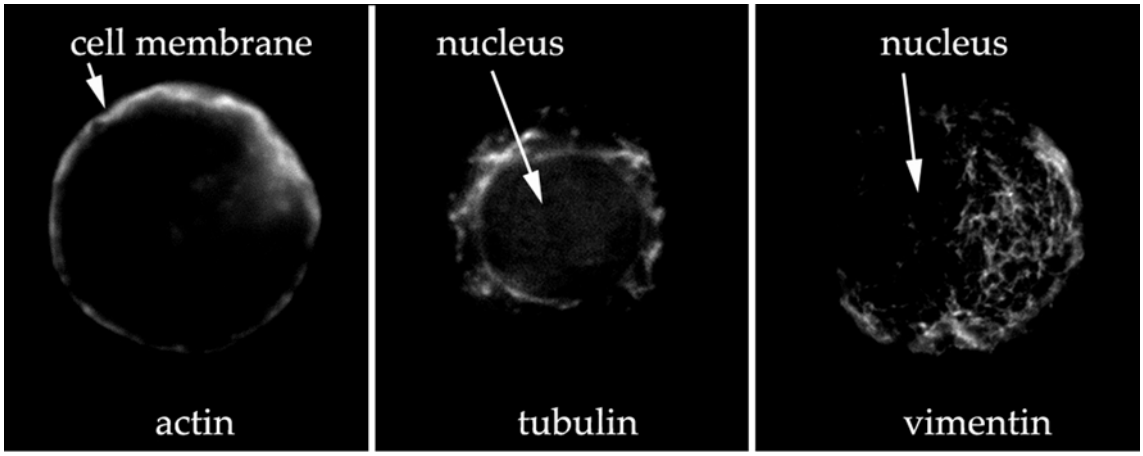

Figure 10: Trois des principaux types de cytosquelette, les filaments d'actine, les microtubules et les filaments intermédiaires (de gauche à droite). Ils sont visualisés à l'aide de certains anticorps fluorescents spécifiques à un composant du cytosquelette (ici, l'actine, la tubuline et la vimentine)

Dans le cas où des contraintes sont effectuées suffisamment rapidement par rapport au temps caractéristique de réorganisation du cytosquelette et où les déformations résultantes ne sont pas trop proches de la taille de la cellule, on peut donc imaginer que la cellule se comportera comme un matériau élastique classique. Suivant le type de cytosquelette (cortical ou tridimensionnel) qui dominera les propriétés mécaniques, une cellule pourra plutôt être modélisée par une capsule (coque élastique) ou par une sphère pleine. Voyons comment il est possible de déterminer le modèle le plus adapté à deux cellules adhérentes.

Capsules adhérentes

Pour simplifier la discussion, on va travailler sur le modèle présenté figure 11 d'une capsule adhérant sur un substrat plan et décrit dans [Brochard-Wyart, F. et de Gennes, P.G., 2003]. Le raisonnement pour l'adhésion de deux cellules (substrat en forme de capsule) est similaire et le résultat sera donné à la fin du paragraphe. On considère donc une capsule adhérente sur laquelle une force de traction est appliquée de façon normale à la zone de contact à l'aide d'un tube fin (la micropipette). Le problème est donc à symétrie cylindrique. Lorsque la force appliquée est nulle, la capsule s'apparente à une sphère tronquée. L'angle de contact θ_e entre la surface et la

capsule est lié à l'énergie d'adhésion de la capsule sur le substrat W_a par la relation d'Young-Dupré (cf. éq. (1) et (2)). Lorsqu'une force non nulle est appliquée, on peut écrire l'équilibre mécanique sur chaque section perpendiculaire à l'axe de symétrie.

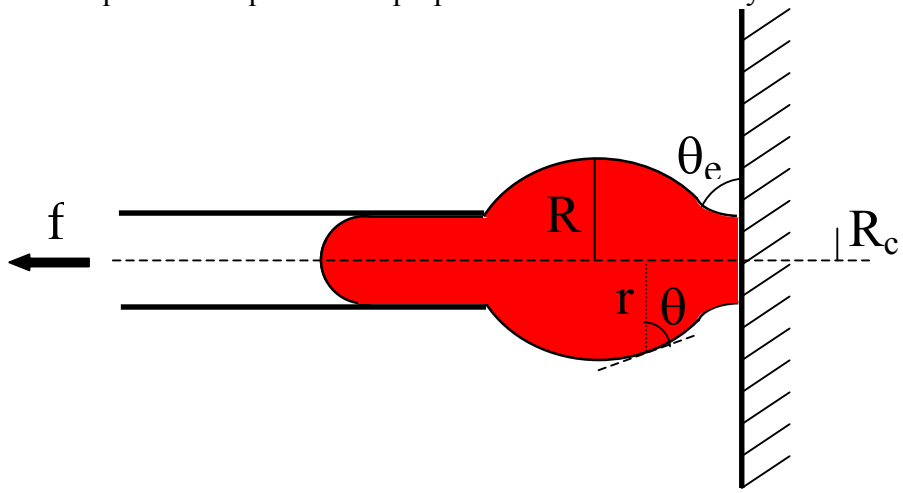

Figure 11 : schéma du système étudié. Une cellule est maintenue par une micropipette et adhère à un substrat. Une force est exercée pour rompre l'adhésion.

La cellule étant en surpression, on a alors : f+force de pression=force de tension. En appliquant cet équilibre à l'équateur et au contact, on obtient :

$$f\left(1-\frac{R_c}{R}\right)=2\pi R\tau\left(\frac{R_c}{R}\sin(\theta_e)-\left(\frac{R_c}{R}\right)^2\right) \qquad (9)$$

En général, on pourra prendre $R_c/R << 1$, soit:

$$f=2\pi R\tau\left(\frac{R_c}{R}\sin(\theta_e)-\left(\frac{R_c}{R}\right)^2\right) \qquad (10)$$

f est donc maximale pour :

$$f_{sep}=\pi R W_a \qquad (11)$$

C'est la force à la séparation. Dans le cas de deux capsules adhérentes, la relation (11) reste valable en prenant pour R la moyenne harmonique des rayons des deux capsules. Si elles sont identiques, on obtient donc :

$$f_{sep}=\frac{\pi R W_a}{2} \qquad (12)$$

Sphères élastiques adhérentes

Dans le cas de sphères pleines de module élastique K, l'équilibre mécanique peut s'écrire en minimisant les différents termes de l'énergie du système: énergie élastique, énergie mécanique due au déplacement et énergie de surface. Le calcul a été fait il y a plus de trente ans [Johnson et al., 1971 ; Maugis, 1980], c'est la théorie JKR (des noms Johnson, Kendall et Roberts). Le résultat obtenu est similaire à celui des capsules à un facteur 3/2 près :

$$f_{sep}=\frac{3\pi R W_a}{2} \qquad (13)$$

De la même façon que pour les capsules, dans le cas de deux sphères, la relation (13) reste valable en prenant pour R la moyenne harmonique des rayons des deux sphères. Si elles sont identiques, la relation s'écrit :

$$f_{sep}=\frac{3\pi R W_a}{4} \qquad (14)$$

On peut remarquer que pour obtenir la même force de séparation, l'énergie d'adhésion requise pour les capsules est plus grande que pour les sphères élastiques.

Le rayon de contact à force f fixée vérifie :

$$(R_c)^3 = \frac{R}{2K}\left[f + \frac{3\pi R W_a}{2} + \sqrt{3\pi R W_a f + \left(\frac{3\pi R W_a}{2}\right)^2} \right] \qquad (15)$$

De (15), on peut aisément déduire une relation simple entre le rayon de contact sous force nulle, R_{c0} et le rayon de contact à la séparation R_{csep} :

$$R_{csep} = \frac{1}{\sqrt[3]{4}} R_{c0} \qquad (16)$$

Caractérisation expérimentale des propriétés mécaniques de cellules

Afin de savoir si une cellule possède effectivement un comportement élastique, une approche possible consiste à appliquer une adhésion contrôlée et à comparer f_{sep} et W_a. Les relations (12) et (14) montrent qu'on attend alors un comportement du type :

$$\frac{f_{sep}}{R} \alpha \ W_a \qquad (17)$$

Si cette relation est vérifiée, le préfacteur permettra de déterminer si les cellules étudiées peuvent plutôt être assimilées à des capsules ou à des sphères dures. Nous avons effectué une telle étude sur des cellules de sarcome de souris (cellules S180). Ces cellules présentent l'avantage de ne pas être adhérentes entre elles naturellement [Friedlander et al., 1989]. Ici, l'adhésion a été induite par de longs polymères créant une force de déplétion. Le principe des forces de déplétion est bien connu et peut se comprendre qualitativement. Lorsque les cellules arrivent à proximité l'une de l'autre, le volume accessible au soluté (le polymère) est d'autant plus grand que les cellules sont proches. Ainsi, il s'exerce une force attractive d'origine entropique. Lorsque les cellules sont en contact, sa valeur est égale à la pression osmotique du soluté. De façon quantitative, l'expression de l'énergie d'adhésion est connue en fonction de la fraction volumique ϕ du polymère [de Gennes, 1985]:

$$W_a = \frac{k_B T}{\xi^2} = \frac{k_B T}{a^2} \phi^{1.5} \qquad (18)$$

Dans le cas du dextrane, cette même relation a été mesurée expérimentalement sur des vésicules lipidiques [Evans et Needham, 1988]. Il est donc possible de tester le comportement mécanique des cellules en les forçant à adhérer par force de déplétion pour différentes valeurs de ϕ.

La morphologie des S180 pendant la séparation est présentée figure 12. Les résultats obtenus pour deux tailles de dextrane (P.M. 4. 10^5 et 2.10^6) sont donnés figure 13. Ils montrent que les cellules semblent bien avoir un comportement élastique puisque la relation :

$$W_a \alpha \phi^{1.5} \qquad (19)$$

déduite de (12) et (14), est vérifiée.

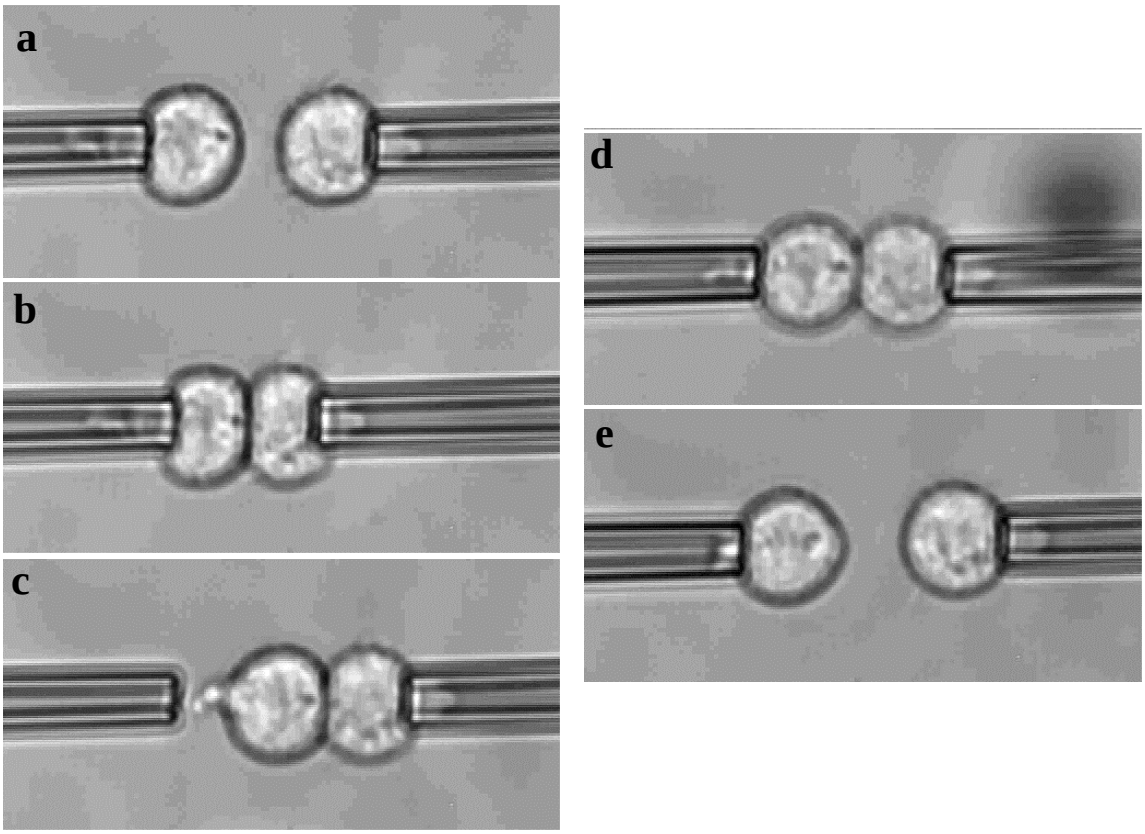

Figure 12 : Séparation de deux cellules S180 dont l'adhésion a été induite par les forces de déplétion.

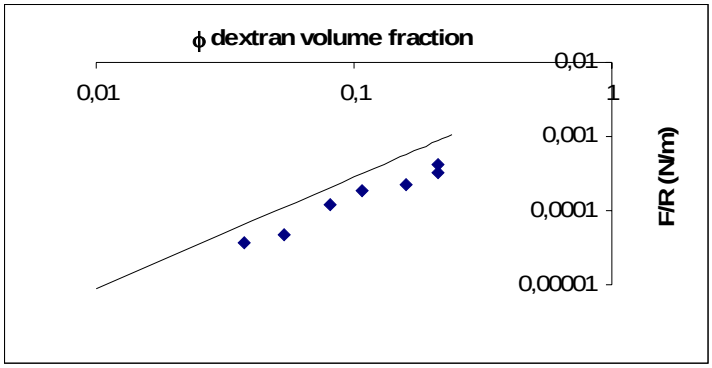

Figure 13 : force de séparation divisée par la moyenne harmonique des cellules en fonction de la fraction volumique en dextrane. La droite indique la pente attendue pour un comportement élastique.

Afin de déterminer si ces cellules ont plutôt un comportement de type sphère ou capsule, il est nécessaire de connaître le préfacteur. Les énergies d'adhésion qui seraient obtenues par les relations (12) et (14) sont présentées sur la figure 14 avec les valeurs théoriques et expérimentales déjà connues. Il y apparaît que les S180 ressemblent plus à des sphères qu'à des capsules. Pour confirmer cela, il est possible de mesurer le rayon de la zone d'adhérence en fonction de la force de traction appliquée, de voir si le comportement prévu par la relation (15) est vérifié et le cas échéant d'en déduire un module élastique K.

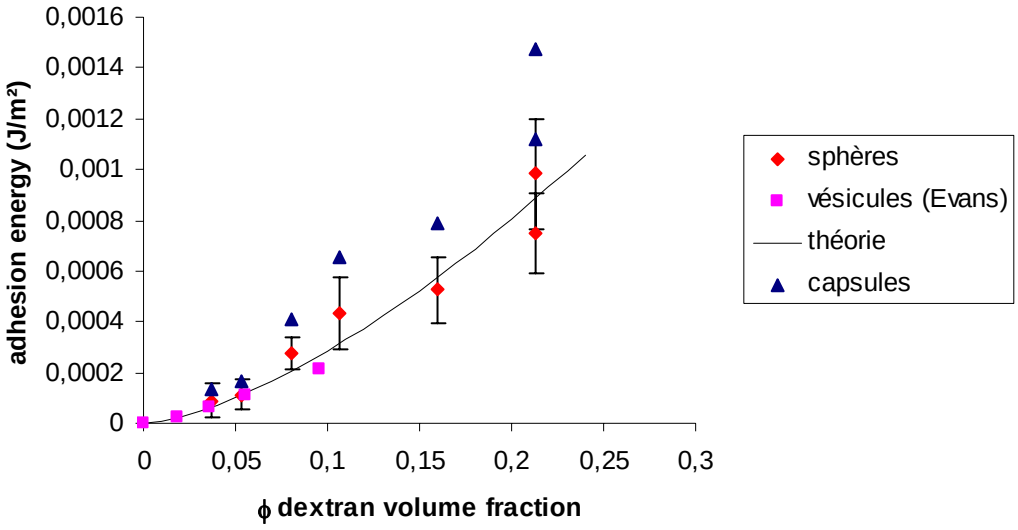

Figure 14 : énergie d'adhésion déduite de la force mesurée (figure 12) à partir des relations (12) (triangles) et (14) (losanges). Les valeurs prédites par la théorie (trait plein) et par les mesures expérimentales sur les vésicules (carrés) sont aussi indiquées.

La figure 15 montre qu'effectivement le comportement s'apparente à celui prévu par la théorie JKR et le fit permet d'obtenir un module élastique égal à : K = 3500 +/- 1500 Pa. Cette valeur est cohérente avec celle obtenue sur ces mêmes cellules avec un appareil à force entre surface : K = 4200 +/- 1000 Pa et avec les valeurs de la littérature sur d'autre cellules (K = 1000 – 5000 Pa) [Turner et Sens, 1999].

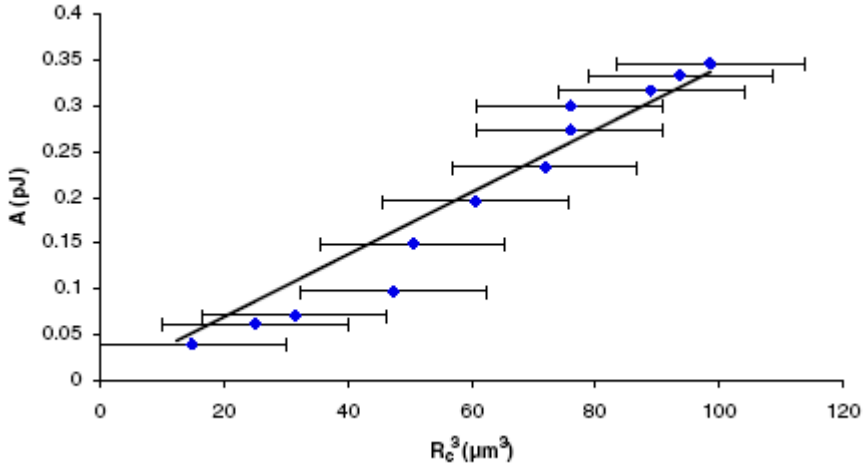

Figure 15 : Paramètre $A=\frac{R}{2}\left[f+\frac{3\pi RW_a}{2}+\sqrt{3\pi RW_a f+\left(\frac{3\pi RW_a}{2}\right)^2}\right]$ en fonction R_c^3. Dans le cas de la théorie JKR, cette courbe doit être une droite dont la pente est le module élastique K (cf relation 15). La barre d'erreur très large est due à la faible précision dans la mesure du rayon de contact R_c.

Enfin, une dernière vérification consiste à comparer le rayon de la zone de contact au moment de la séparation et à force nulle. On obtient alors : $R_{csep}=(0{,}645\pm0{,}12)R_{c0}$ qui est en accord avec la relation (16).

Toutes ces mesures indiquent que les cellules S180 ont un comportement élastique proche de celui décrit par la théorie JKR pour des sphères pleines en adhérence. Notons que ce résultat ne

sera pas vrai pour tous les types de cellules. Les globules rouges, par exemple, s'apparentent plus à des capsules bidimensionnelles.

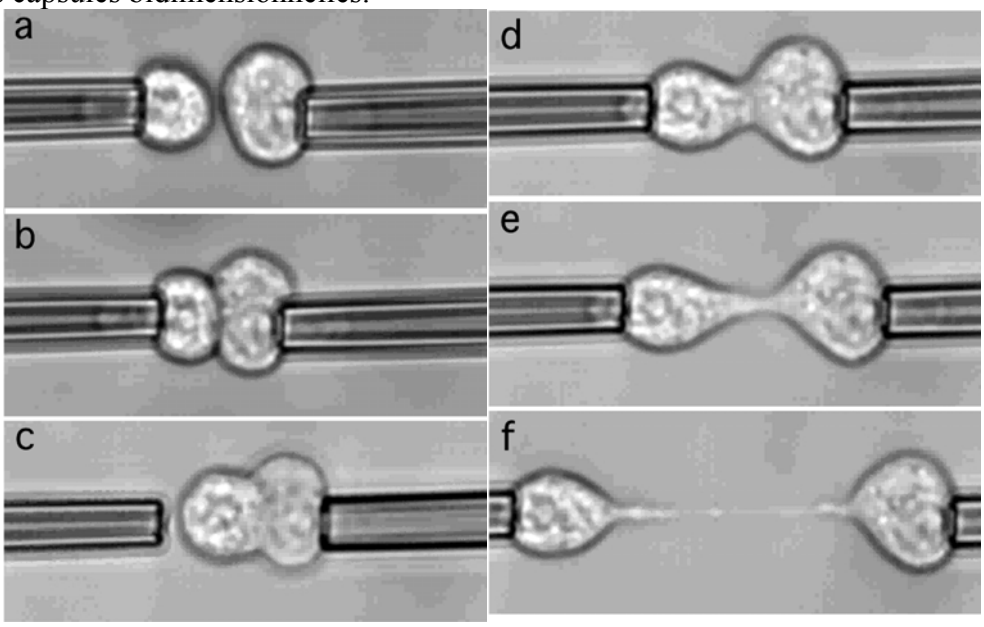

Figure 15 : (a),(b) Morphologie de cellules traitées avec la latrunculine pendant la séparation. Cette figure est à comparer à la figure 12.

On peut s'attendre à ce que le cytosquelette soit responsable des propriétés mécaniques des cellules S180. Pour le vérifier, il suffit de refaire le même type d'expériences en endommageant le cyosquelette à l'aide d'une drogue. Par exemple, la latrunculine empêche la polymérisation de l'actine quand elle est présente à concentration suffisamment élevée [Spector et al., 1989 ; Segal et al., 2001]. Les cellules ne présentent alors pas les mêmes déformations lors de la séparation que lorsque le cytosquelette reste intègre (cf figures 12 et 15).
Si, à partir de la force de séparation mesurée, on procède come précédemment en traçant l'énergie d'adhésion que donnerait la relation (14), on obtient un résultat incompatible avec l'énergie attendue (cf. figure 16). Le cytosquelette est donc bien à l'origine de ces propriétés mécaniques surprenantes des cellules. Il faut insister sur un point important : si le temps caractéristique des expériences avait été plus grand que le temps de réorganisation du cytosquelette, le résultat présenté ici ne serait évidemment plus valide.

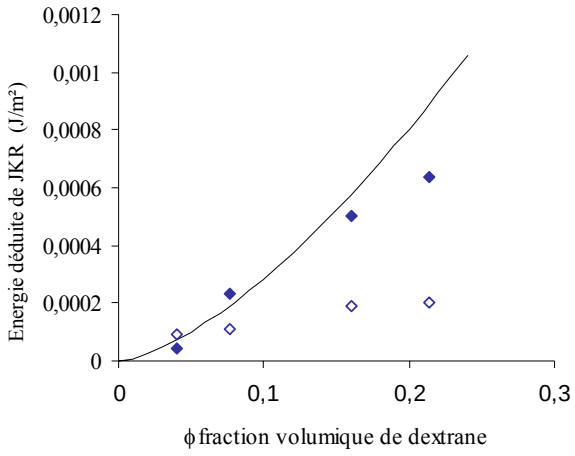

Figure 16 : énergie d'adhésion déduite de la force mesurée à partir de la relation (14) (losanges, pleins : 0,1 µM ; vides : 1,5 µM). Les valeurs prédites par la théorie (trait plein) sont aussi indiquées.

3.2.3. Adhésion cellulaire et épidémiologie des maladies cardiovasculaires, exemple du couple fraktalkine – CX3CR1 [20]

Collaboration : P. Deterre (biologie, Pitié-Salpétrière)
Contrat INSERM CardioVasculaire 2004
Dans le cadre de la thèse de M. Daoudi (biologie, Pitié – Salpétrière).

Les mesures d'adhésion de cellules telles qu'elles ont été présentées précédemment peuvent être utilisées pour essayer de comprendre certains problèmes biologiques et médicaux. La mesure quantitative de l'énergie d'adhésion ne donnera pas nécessairement d'information pertinente. En revanche, la variation de la force de séparation, qui représente bien la solidité du joint adhésif, avec un paramètre donné peut s'avérer intéressante. Par exemple, une telle approche nous a permis de mieux cerner l'origine d'une observation épidémiologique liée à une chimiokine, la fraktalkine et à son récepteur, le CX3CR1. Une mutation naturelle confère à celui-ci deux formes, sauvage et mutée. Cette dernière est associée à une diminution significative des risques cardiovasculaires chez l'homme [Moatti et al., 2001 ; McDermott et al., 2001 ; McDermott et al., 2003 ; Gugl et al., 2003]. Il a déjà été montré que le couple fraktalkine/CX3CR1 a deux fonctions dans l'organisme, une première liée au chimiotactisme, c'est-à-dire à la migration des cellules dans un gradient de soluté (ici, la fraktalkine), et une deuxième liée à l'adhésion cellulaire [Pan et al., 1997 ; Imai et al., 1997 ; Fong et al., 1998 ; Matloubian et al., 2000 ; Nakayama et al., 2003]. Les mesures de forces entre cellules exprimant le CX3CR1 et cellules exprimant la fraktalkine ont montré que la fonction adhésive différencie les deux formes de CX3CR1 (figure 17). En revanche, il n'y a pas de différence significative en ce qui concerne le chimiotactisme entre les deux formes de CX3CR1.

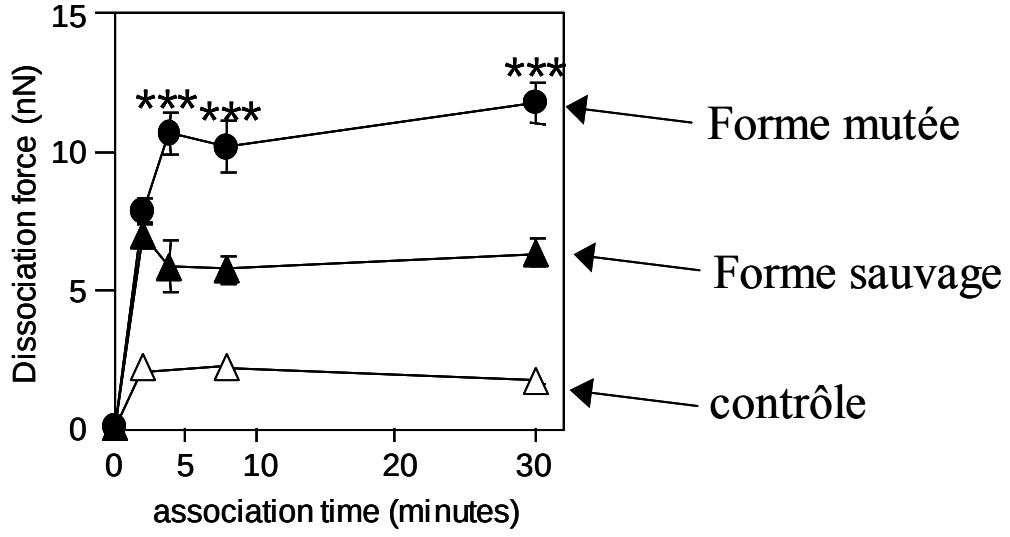

Figure 17 : force de séparation entre deux cellules de rein d'embryon humain en fonction du temps de contact. La première cellule exprime la fraktalkine et l'autre, soit, son récepteur, le CX3CR1, sous sa forme sauvage ou mutée, soit un autre récepteur non reconnu par la fraktalkine, le CCR5 (expérience contrôle). Les taux d'expression des différents récepteurs sont identiques.

L'augmentation d'adhésion avec le CX3CR1 mutée n'est effective qu'après 2-4 minutes de contact. Elle semble due à une signalisation intra-cellulaire différente pour les deux types de CX3CR1. Des expériences, dans lesquelles des drogues inhibant une protéine précise ont été

introduites, indiquent qu'un signal serait émis à partir du CX3CR1 muté et reviendrait vers lui. La protéine Gi et la protéine Rho sont impliquées dans cette signalisation car quand on les inhibe, on retrouve une adhésion similaire à celle obtenue avec le CX3CR1 sauvage. En revanche, la protéine Rac ne joue aucun rôle (figure 18).

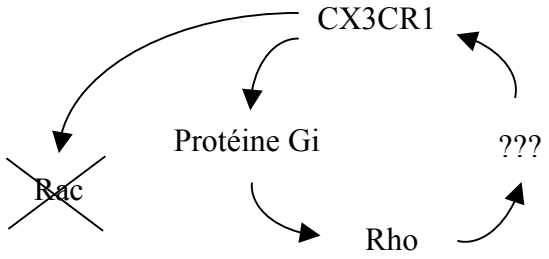

Figure 18: schéma de la signalisation induisant l'augmentation de l'adhésion par le CX3CR1 muté. Le signal émis par le CX3CR1 revient sur lui – même par une cascade complexe de signaux. Seules trois étapes sont représentées, il existe probablement beaucoup plus d'intermédiaires.

Grâce à ces mesures, nous pouvons mieux comprendre la différence physiologique entre les deux formes de CX3CR1. Il reste encore à compléter cette étude afin de décrypter complètement la signalisation qui en découle. Il sera alors plus aisé de comprendre le lien entre cette différence et les observations épidémiologiques, et de pouvoir, à terme, envisager des actions thérapeutiques.

3.2.4. Autre étude : adhésion induite par les cadhérines [23,25]

Collaboration : S. Dufour (biologie, Curie)
Contrats : Institut Curie 2001

Les cadhérines forment l'une des grandes classes de molécules d'adhésion [Gumbiner, 1996]. Elles interviennent par exemple dans le maintien de la cohésion des tissus. Nous avons caractérisé l'adhésion de cellules exprimant des cadhérines en mesurant la force nécessaire à la séparation de ces cellules. Cette étude a été conduite à trois niveaux : i. comparaison de plusieurs cadhérines, ii. processus de signalisation impliqués dans l'interaction de cellules S180 exprimant des cadhérines E., iii. adhésion induite simultanément par deux types de molécules d'adhésion, les cadhérines E et des nectines.
Ces expériences, effectuées par Y. Chu (étudiant en thèse), ont montré que la cinétique de l'adhésion des cellules est relativement lente (de l'ordre de la dizaine de minutes pour obtenir une adhésion maximale) et que les cadhérines E et N physiologiquement impliquées dans des joints adhésifs forts, par exemple dans la cohésion des tissus, induisent bien une adhésion plus forte que les cadhérines 7 impliquées dans des joints beaucoup plus labiles, par exemple lors de migrations cellulaires. Ce résultat démontre l'intérêt des micromanipulations par rapport aux techniques classiques d'agrégation qui ne parviennent pas à mettre en évidence cette différence.
Nous nous sommes intéressés en particulier à la cadhérine E et avons décrypté complètement la dynamique de l'adhésion qu'elle induit. Cette dynamique peut se décomposer en trois phases. Dans un premier temps, l'adhésion est rapidement initiée (en moins d'une minute) par les cadhérines présentes sur la membrane à proximité de la zone de contact. La seconde phase correspond à une augmentation régulière de l'adhésion essentiellement due à une réorganisation du cytosquelette cortical. Nos mesures montrent que cette réorganisation est déclenchée par des signaux passant par les protéines Rac et Cdc42. En revanche la voie Rho ne semble pas jouer de

rôle. Durant la troisième phase, l'adhésion croît beaucoup plus lentement, sans doute grâce à des réorganisation plus fines du cytosquelette.
Enfin, lors des expériences avec les nectines, nous avons montré que la présence simultanée des deux molécules d'adhésion, cadhérines et nectines, permet dans certaines conditions d'amplifier le rôle de chacune d'entre elles.

3.2.5. Bibliographie de la partie 3.2

Brochard-Wyart, F., et de Gennes, P.G., C.R. Physique, **4**, 281-287, (2003)

Evans, E., et Needham, D., *Macromolecules*, **21**, 1822-1831, (1988).

Fong, A. M., Robinson, L. A., Steeber, D. A., Tedder, T. F., Yoshie, O., Imai, T.,and Patel, D. D. , *J. Exp. Med.* **188,** 1413–1419 (1998).

Friedlander, D. R., Mege, R.-M., Cunningham, B. A.et Edelman, G. M.*, Proc. Natl. Acad. Sci. U.S.A.,* **86**, 7043-7047, (1989).

de Gennes, P-G., in *Scaling Concept in Polymer Physics* (Cornell University Press, Ithaca and London, 1985), 2nd ed.

Gugl, A., Renner, W., Seinost, G., Brodmann, M., Pabst, E., Wascher, T. C., Paulweber, B., Iglseder, B., and Pilger, E. *Atherosclerosis* **166,** 339–343 (2003).

Gumbiner, B. M., *Cell* **84,** 345-357, [1996].

Imai, T., Hieshima, K., Haskell, C., Baba, M., Nagira, M., Nishimura, M., Kakizaki, M., Takagi, S., Nomiyama, H., Schall, T. J., and Yoshie, O. *Cell* **91,** 521–530, (1997).

Johnson, K.L., Kendall, K., et Roberts. A.D., *Proc. R. Soc. Lon. Ser. A.*, **324**, 301-313, (1971).

Matloubian, M., David, A., Engel, S., Ryan, J. E., and Cyster, J. G. *Nat.Immunol.* **1,** 298–304 (2000).

Maugis, D., *J. Colloid Interf. Sci.,* **150**, 243-269, (1992).

McDermott, D. H., Halcox, J. P., Schenke, W. H., Waclawiw, M. A., Merrell, M. N., Epstein, N., Quyyumi, A. A., and Murphy, P. M. *Circ. Res.* **89,**401–407 (2001).

McDermott, D. H., Fong, A. M., Yang, Q., Sechler, J. M., Cupples, L. A., Merrell, M. N., Wilson, P. W., D'Agostino, R. B., O'Donnell, C. J., Patel, D. D., and Murphy, P. M. *J. Clin. Investig.* **111,** 1241–1250 (2003).

Moatti, D., Faure, S., Fumeron, F., Amara, M., Seknadji, P., McDermott, D. H., Debre, P., Aumont, M. C., Murphy, P. M., de Prost, D., et Combadiere, C, *Blood* **97,** 1925–1928 (2001).

Nakayama, T., Hieshima, K., Izawa, D., Tatsumi, Y., Kanamaru, A., and Yoshie, O. *J. Immunol.* **170,** 1136–1140 (2003).

Pan, Y., Lloyd, C., Zhou, H., Dolich, S., Deeds, J., Gonzalo, J. A., Vath, J., Gosselin, M., Ma, J., Dussault, B., Woolf, E., Alperin, G., Culpepper, J., Gutierrez-Ramos, J. C., and Gearing, D., *Nature* **387,** 611–617 (1997).

Segal, G., Lee, W., Arora, P. D., McKee, M., Downey, G. et McCulloch, C. A., *J. Cell Sci.*, **114**, 119-129, (2001).

Spector, I., Shochet, N.R., Blasberger, D. et Kashman, Y., *Cell Motil. Cytoskeleton,* **13**, 127-144, (1989).

Turner, M.S., et Sens, P., *Biophys. J.* **,76**, 564-572, (1999).

3.3 Rupture de lien unique

Qu'est-ce qu'un lien unique ?
Communément, dans tous les processus ayant trait à l'adhésion cellulaire, un lien ou une liaison unique représente un complexe moléculaire formé de deux molécules, un ligand et un récepteur. Souvent, on parle d'un lien spécifique en l'appelant « liaison clé-serrure » où le ligand est la clé et le récepteur la serrure. Une liaison très utilisée par la communauté scientifique est formée par le couple streptavidine-biotine qui permet de former l'une des liaisons non covalentes les plus « fortes ». D'une manière plus générale, on appellera ici liaison unique tout accrochage d'une seule molécule sur une autre entité. Cette entité pourra être le récepteur mentionné ci-dessus, mais aussi une surface sur laquelle la molécule serait accrochée ou une membrane dans laquelle elle serait ancrée.

Qu'est-ce que la force d'un lien ?
Une idée préconçue simple consiste à se dire qu'il est possible de mesurer la force d'un lien unique en exerçant une traction dessus et en détectant la force à laquelle le lien se rompt. Cette approche n'est pas correcte pour la simple raison que ces liaisons faibles, de corute durée de vie (de la microseconde à plusieurs jours), sont extrêmement sensibles aux fluctuations thermiques qui induiront leur rupture. Pour s'en convaincre de manière intuitive, il suffit d'imaginer su'une traction est appliquée très lentement sur le lien. Dans ce cas, au bout d'un temps fini, égal typiquement à la durée de vie du lien, le lien se rompt et la force mesurée est pratiquement nulle. L'agitation thermique a fourni tout le travail nécessaire à la rupture. En revanche, si la traction est appliquée très rapidement, une force finie sera mesurée. Evidemment, si l'expérience est effectuée deux fois dans des conditions similaires, les forces mesurées seront différentes, toujours à cause de l'agitation thermique. On ne peut donc pas parler de force d'un lien, mais seulement de distribution de la force de rupture du lien pour une condition de traction donnée.

3.3.1. Le Biomembrane Force Probe (BFP)

Une technique permettant de mesurer la force de rupture d'une liaison unique en variant la vitesse de traction sur le lien est le biomembrane force probe (BFP), initialement développé par E. Evans [Evans, 1998]. Son principe est le suivant. Un globule rouge est utilisé comme dynamomètre pour mesurer cette force. Le globule-ressort est maintenu dans une micropipette. Sa raideur est proportionnelle à sa tension qui dépend elle-même de l'aspiration via l'équation (2). Elle peut être variée sur trois ordres de grandeur. Une bille portant l'une des molécules à étudier est collée au globule (figure 19). La sonde ainsi formée est mise en contact avec un substrat contenant la molécule complémentaire. On tire ensuite sur la bille en rétractant la pipette à une vitesse donnée. Si un lien s'est formé, la force de traction est mesurée jusqu'à la rupture. La densité de molécules est choisie suffisamment faible pour que la probabilité de former un lien soit de l'ordre de 10 %. Ce contrôle permet de s'assurer qu'il s'agit dans plus de 90% des cas d'une liaison unique. L'étude de la force de rupture se fera en général en fonction du taux de charge (vitesse à laquelle la traction est appliquée sur le lien en pN/s). En pratique, la force s'exerçant entre les billes est obtenue par la mesure de la déformation du globule (logiciel de suivi de bille développé au laboratoire par V. Croquette, que nous avons adapté à cette technique). Les distributions de forces de rupture obtenues seront la signature du potentiel d'interaction entre les deux protagonistes.

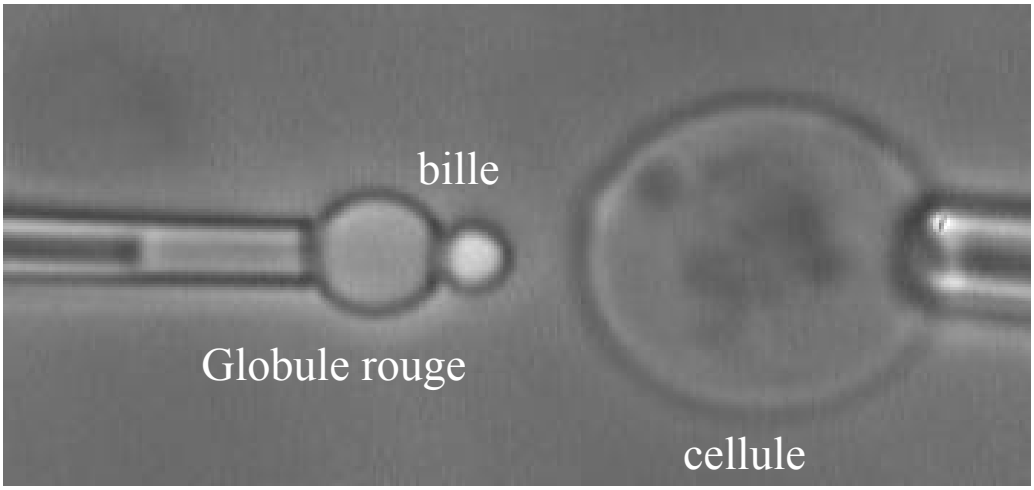

Figure 19 : Capteur de force à globule rouge : la bille, collée au globule rouge, porte l'une des molécules à étudier. Elle est mise en contact avec le substrat, ici une cellule, portant une molécule complémentaire. La déformation du globule lors de la séparation permet la mesure directe de la force de rupture.

3.3.2. Transition entre états métastable, explication du paradoxe streptavidine – biotine

Contrat BQR Paris 7 2000.
Dans le cadre de la thèse de J. Husson

Le couple streptavidine – biotine forme l'un des liens les plus étudiés. En effet, la molécule de biotine (la vitamine H) présente une formidable affinité pour la protéine streptavidine. Le complexe ainsi formé est très stable. C'est pourquoi il est fréquemment utilisé en biologie ou en chimie pour construire des assemblages solides de molécules (legos moléculaires). Avec un BFP, E. Evans a établi les distributions de forces de rupture sur plusieurs décades de taux de charges pour le couple streptavidine/biotine (figure 20). Nous avons refait ces mesures et retrouvé les mêmes histogrammes. Pourtant, ces résultats semblent en contradiction avec d'autres mesures effectuées par C. Bustamante, consistant à manipuler un brin d'ADN fonctionnalisé à chaque extrémité par une biotine à laquelle est greffée une bille recouverte de streptavidine (figure 21). Une force est alors appliquée sur l'une des billes par un flux hydraulique et la durée de vie du lien peut être mesurée. Les données expérimentales sont moins nombreuses que celles obtenues avec le BFP, mais il en ressort clairement que, pour une force inférieure à 80 pN, la durée de vie du lien est supérieure à une minute et, pour une force plus grande que 100 pN, la durée de vie est de quelques secondes. Les mesures avec le BFP indiquent que pour une force de 80 pN, la durée de vie devrait être au plus de 0,1 s, soit 3 ordres de grandeur plus faible. C'est le paradoxe straptavidine – biotine : la résistance du lien dans des conditions fixées semble dépendre de l'appareil de mesure.

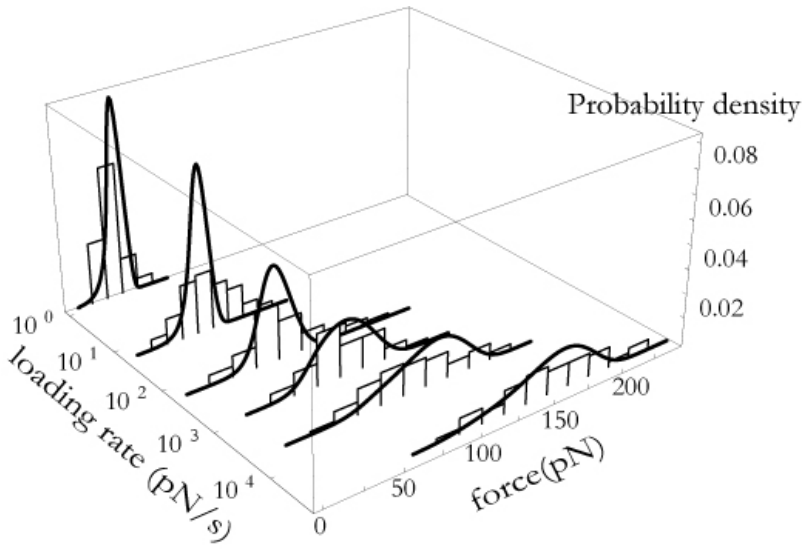

Figure 20 : histogrammes expérimentaux obtenus avec le couple streptavidine biotine à l'aide du BFP pour des taux de charge variant de 1 à 60000 pN/s. Les fits correspondent aux distributions attendus en appliquant le modèle de Kramers (équation 41) aux deux états métastables extrêmes du potentiel présenté figure 26.

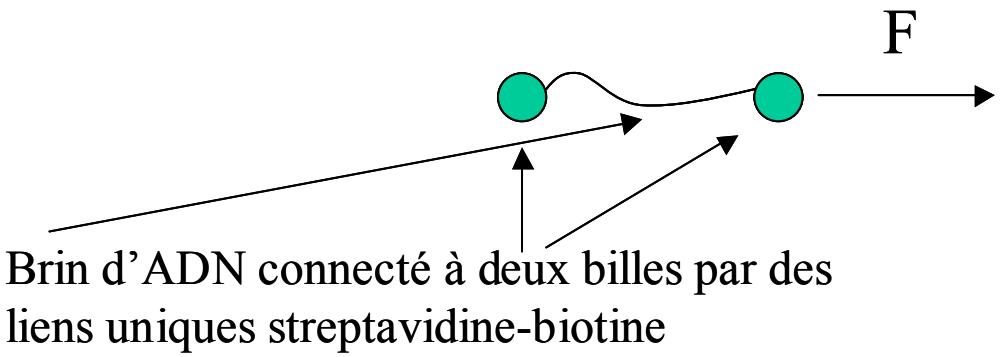

Figure 21 : Principe de l'epérience de C. Bustamante : un brin d'ADN est connecté à deux billes par des liens uniques straptavidine – biotine. L'une des billes est maintenues par une micropipette (ou des pincettes optiques) et l'autre est soumise à un flux imposant une force de traction sur les lien. La rupture d'un des deux liens est observée par le départ de la bille libre.

Nous avons expliqué l'origine de ce paradoxe et montré qu'en fait ces résultats expérimentaux apparemment contradictoires sont cohérents. Cette étude n'étant pas encore publiée, je vais, dans la suite de cette section, détailler plus précisément la théorie sous-jacente à la rupture d'un lien. La description présentée ici est largement inspirée de la revue sur les équations de Kramers donnée par Hänggi et al [1990].

Correspondance entre le panorama énergétique du lien et la distribution des forces de rupture?

Lors de la rupture du lien, le ligand suit en général un chemin privilégié. Le potentiel d'interaction des deux entités formant le lien, par la suite appelé le panorama énergétique du lien, peut donc de façon réaliste être considéré unidimensionnel. Il ressemblera par exemple à celui présenté dans la figure 22.

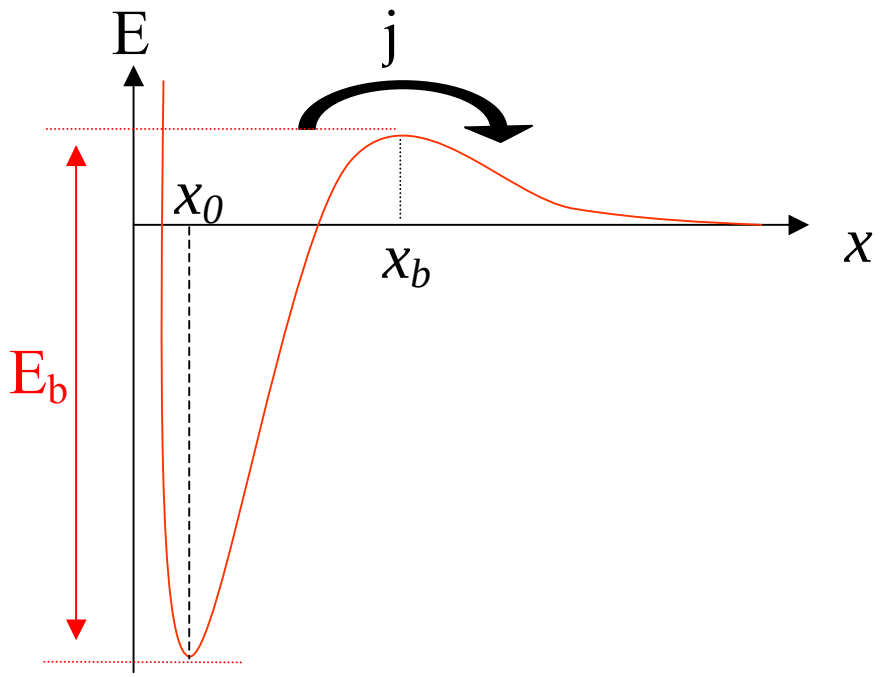

Figure 22 : Panorama énergétique d'un lien possédant une seule barrière. j est le flux sortant initial de l'état lié à l'état non lié (cf. texte).

Le problème de la rupture du lien s'apparente donc à l'échappement d'une particule piégée dans le potentiel E(x) ainsi défini et soumise à une force aléatoire (due à l'agitation thermique). C'est un problème ancien, popularisé par Kramers en 1940 [Kramers, 1940 ; Hänggi et al., 1990]. L'évolution de la position $\vec{r}$ et de la vitesse $\vec{v}$ de la particule sont données par l'équation de Langevin :

$$\begin{cases} \dfrac{d\vec{r}}{dt}=\vec{v} \\ M\dfrac{d\vec{v}}{dt}=-\text{grad}(E(\vec{r}))-\zeta\vec{v}+\vec{\xi}(t) \end{cases} \qquad (20)$$

Où ζ représente la viscosité et ξ vérifie :

$$\begin{cases} \langle\xi(t)\rangle=0 \\ \langle\xi(t)\xi(t')\rangle=2\zeta k_B T\delta(t-t') \end{cases} \qquad (21)$$

Pour simplifier, on prendra d'abord le cas où le panorama énergétique ne présente qu'une seule barrière. Il n'y aura donc qu'un état métastable. Les caractéristiques de ce panorama sont données dans la figure 22. La barrière présente en x_b est souvent réelle pour des liens biochimiques à cause des changements de conformation des molécules lors de l'association des deux entités formant le lien. Soit $\rho(x,v,t)$, la distribution de probabilité des états pour un lien déjà formé à l'instant t=0. Etudions l'évolution temporelle de $\rho(x,v,t)$. On supposera par ailleurs que la particule, une fois sortie, ne peut retourner dans l'état métastable; cela signifie qu'une fois le lien rompu, il ne se reformera pas (hypothèse du puits absorbant). A l'instant initial, la particule est piégée dans l'état métastable, et donc :

$$\int_0^{x_b}\int \rho(x,v,0)dvdx=1 \qquad (22)$$

Le système est similaire à tout instant, mais normalisé par la probabilité que la particule soit toujours piégée à l'instant t, $P(t)=\int_0^{x_b}\int \rho(x,v,t)dvdx$. Le flux d'échappement de l'état métastable

sera donc proportionnel à P(t). En supposant une constante « rethermalisation » de l'état lié, j, le coefficient de proportionnalité apparaît alors comme le flux initial d'échappement. P vérifie donc :

$$P(t)=1-\int_0^t jPdt \qquad (23)$$

Et, finalement :

$$P(t)=\exp(-jt). \qquad (24)$$

Il ne reste plus qu'à déterminer j pour pouvoir connaître P. Or j s'écrit aussi :

$$j=\int_0^{+\infty} v\rho(x_b,v,0)dv \qquad (25)$$

car on peut négliger les v<0 grâce à l'hypothèse du puits absorbant. La connaissance de ρ à l'instant initial permettra donc de déterminer j. A proximité du minimum de l'état métastable, le système est thermalisé. On a donc, dans cette région :

$$\rho(x,v)=Z^{-1}\exp\left\{-\left[\frac{1}{2}Mv^2+E(x)\right]/k_BT\right\} \qquad (26)$$

Or la grande majorité des états se situent dans cette région et donc :

$$\iint Z^{-1}\exp\left\{-\left[\frac{1}{2}Mv^2+U(x)\right]/k_BT\right\}dvdx=1 \qquad (27)$$

La relation (27) permet de calculer Z. En revanche, au niveau de la barrière ($x\sim x_b$), le système n'est plus thermalisé. Il est alors possible à partir de l'équation de Langevin de montrer que ρ vérifie l'équation de Fokker-Planck stationnaire :

$$\left[-\frac{\partial}{\partial x}v+\frac{\partial}{\partial v}[E'(x)+\zeta v]+\zeta k_BT\frac{\partial^2}{\partial v^2}\right]\rho(x,v)=0 \qquad (28)$$

En prenant $u=(x-x_b)+av$, on peut trouver une solution du type : $\rho(x,v)=\lambda(u)\exp\left\{-\left[\frac{1}{2}Mv^2+E(x)\right]/k_BT\right\}$. Avec des potentiels harmoniques au voisinage du minimum et de la barrière :

$$\begin{cases} E(x)=\frac{1}{2}\omega_0{}^2(x-x_0)^2 \\ E(x)=E_b-\frac{1}{2}\omega_b{}^2(x-x_b)^2 \end{cases} \qquad (29)$$

et en imposant que la solution en x_b ait comme comportement asymptotique la solution en x_0, on trouve, après calcul:

$$j=\frac{\left[\frac{\zeta^2}{4}+\omega_b^2\right]^{1/2}-\frac{\zeta}{2}}{\omega_b}\frac{\omega_0}{2\pi}\exp\left(-\frac{E_b}{k_BT}\right) \qquad (30)$$

Dans le cas très amorti où le temps caractéristique de l'observation est plus grand que le temps d'amortissement visqueux, cette expression se simplifie en :

$$j=\frac{\omega_b\,\omega_0}{2\pi\zeta}\exp\left(-\frac{E_b}{k_BT}\right) \qquad (31)$$

Ce même résultat peut aussi être dérivé à l'aide de l'équation de Smoluchowski. C'est l'expression classique de l'échappement d'un état métastable utilisé par exemple en cinétique chimique :

$$\frac{dP}{dt}=-\nu_0\exp\left(-\frac{E_b}{k_BT}\right)P \qquad (32)$$

avec $$\nu_0=\frac{\omega_b\,\omega_0}{2\pi\zeta}=\frac{1}{\tau_0} \qquad (33)$$

$\tau_0 \exp\left(\frac{E_b}{k_B T}\right)$ est la durée moyenne de présence dans l'état métastable (appelée durée de vie pour un lien biochimique). Il est important de remarquer que τ_0 dépend du potentiel et donc du lien considéré. La probabilité p(t)dt que le lien se rompe entre l'instant t et l'instant t+dt s'écrit donc :

$$p(t) = \nu_0 \exp\left(-\frac{E_b}{k_B T}\right) \exp\left(-\nu_0 \exp\left(-\frac{E_b}{k_B T}\right) t\right) \qquad (34)$$

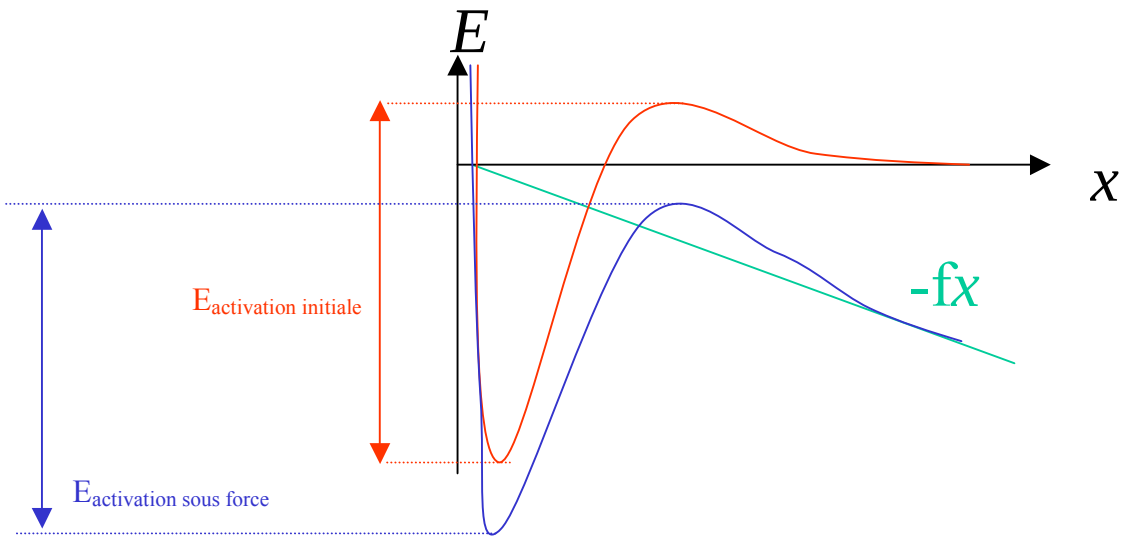

Figure 23: Le panorama énergétique sous force est incliné par rapport au panorama initial. L'énergie d'activation diminue quand la force augmente.

Lorsqu'une force f est appliquée sur le lien, le potentiel est incliné de la quantité –fx (cf. figure 23). En première approximation, il est possible de considérer que la position relative de x_0 et x_b ne change pas. On prendra pour simplifier $x_0=0$, ce qui conduit à la durée de vie du lien sous une force f :

$$\tau(f) = \tau_0 \exp(E_b/k_B T).\exp(-f x_b/k_B T) \qquad (35)$$

Dans le cas de l'approximation harmonique mentionnée ci-dessus (relations (29)), τ_0 ne change pas quand f varie. Comme on pouvait intuitivement le prévoir, la durée de vie du lien diminue quand la force augmente. La probabilité p(t) s'écrit alors :

$$p(t) = \nu_0 \exp\left(-\frac{E_b - f x_b}{k_B T}\right) \exp\left(-\nu_0 \exp\left(-\frac{E_b - f x_b}{k_B T}\right) t\right) \qquad (36)$$

Quantification de la rupture d'un lien à une barrière sous rampe de force.

Expérimentalement, il est souvent difficile d'exercer une force constante contrôlée sur un lien. La mesure consiste plutôt à appliquer sur ce lien une force croissant de façon linéaire dans le temps : f=rt ; r sera appelé le taux de charge. En faisant, comme précédemment, l'hypothèse que la position relative de x_0 et x_b ne varie pas avec la force, il est possible de trouver analytiquement la distribution de probabilité des forces de rupture en fonction du panorama énergétique. En effet, à tout instant, P vérifie une équation d'évolution similaire à (32):

$$\frac{dP(t)}{dt} = -\frac{P(t)}{\tau(f)} = -\frac{P(t)}{\tau_0 \exp\left(\frac{E_b}{k_B T}\right)} \exp\left(\frac{f x_b}{k_B T}\right) = -\upsilon P(t) \exp\left(\frac{f x_b}{k_B T}\right) \qquad (37)$$

Qui s'intègre immédiatement :

$$\tilde{P}(f)=\exp\left[-\frac{\upsilon k_B T}{r x_b}\left[\exp\left(\frac{f x_b}{k_B T}\right)\right]\right] \qquad (38)$$

La notation ~ correspond à la variable f. La densité de probabilité des forces de rupture vaut alors :

$$\tilde{p}(f)=-\frac{d\tilde{P}}{df}=\frac{\upsilon}{r}\exp\left(\frac{x_b f}{k_B T}\right)\tilde{P}(f) \qquad (39)$$

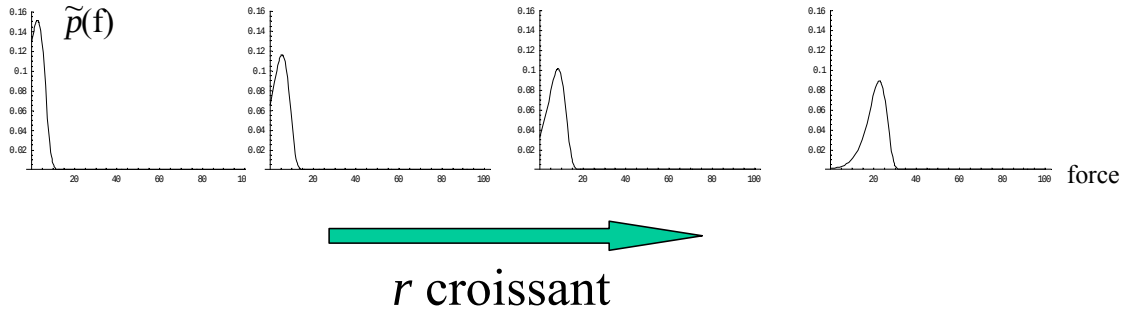

r croissant

Figure 24: exemple de variation de distribution de la force de rupture avec le taux de charge r pour un panorama énergétique choisi arbitrairement.

La connaissance de x_b, E_b, τ_0 et r permet de calculer $\tilde{p}(f)$. La distribution des forces variera donc avec r. Un exemple est donné dans la figure 24. La force la plus probable et la largeur du pic augmentent avec r. Le problème de l'analyse des expériences n'est pas tant de trouver la distribution de forces de rupture à partir du panorama énergétique que le contraire : être capable de retrouver le panorama énergétique à partir de la distribution de forces. Dans l'exemple présenté ici, la mesure de la force la plus probable f_m suffit. f_m s'obtient par : $\frac{dp}{df}(f_m)=0$, qui donne :

$$f_m=\frac{k_B T}{x_b}\left(\ln\left(\frac{x_b}{k_B T \upsilon}\right)+\ln(r)\right) \qquad (40)$$

A partir de cette relation, il est clair que, la courbe f_m en fonction de ln(r) doit donner une droite dont la pente permettra de déterminer x_b et l'ordonnée à l'origine donnera ν, c'est à dire E_b si τ_0 et connu. Cette description à déjà été utilisée avec succès dans plusieurs systèmes.

Quantification de la rupture d'un lien à plusieurs barrières, le paradoxe streptavidine-biotine

Le problème précédent peut se généraliser à plusieurs barrières, c'est-à-dire dans le cas où il y a plusieurs états métastables dans le panorama énergétique du lien. Il devient rapidement extrêmement complexe. En effet, dans ce cas, l'équation (37) devient en prenant l'exemple de 3 états métastables :

$$\begin{cases} \frac{dP_1}{dt}=-\upsilon_{12}(f)P_1(t)+\upsilon_{21}(f)P_2(t) \\ \frac{dP_2}{dt}=-(\upsilon_{21}(f)+\upsilon_{23}(f))P_2(t)+\upsilon_{12}(f)P_1(t)+\upsilon_{32}(f)P_3(t) \\ \frac{dP_3}{dt}=-(\upsilon_{32}(f)+\upsilon_{34}(f))P_3(t)+\upsilon_{23}(f)P_2(t) \end{cases} \qquad (41)$$

Les indices correspondent aux différents états (cf. figure 25), l'état 4 étant l'état non-lié. Pour déterminer l'évolution du système il est aussi nécessaire de connaître l'état initial, $P_1(0)$, $P_2(0)$ et $P_3(0)$.

Le taux de transition de l'état i vers l'état j=i+1 ou j=i-1 s'écrivent (cf. équations 32 et 33) :

$$\begin{cases} \nu_{i\,i+1}(f) = \left(\frac{(\kappa_{mi}\kappa_{bi})^{1/2}}{2\pi\zeta}\right) \exp\left(-\frac{E_{bi}(f) - E_{mi}(f)}{k_B T}\right) \\ \nu_{i\,i-1}(f) = \left(\frac{(\kappa_{mi+1}\kappa_{bi})^{1/2}}{2\pi\zeta}\right) \exp\left(-\frac{E_{bi}(f) - E_{mi+1}(f)}{k_B T}\right) \end{cases} \quad (42)$$

où E_{bi} représente l'énergie de la barrière i et E_{mi}, celle de l'état i. κ_m et κ_b sont les courbures au voisinage du minimum et de la barrière, respectivement.

Les paramètres du panorama énergétique impliqués sont nombreux :

- positions relatives des puits et des barrières
- hauteurs relatives des puits et des barrières
- courbures du potentiel à proximité des puits et des barrières.

Chaque nouvel état métastable apporte donc 3 nouveaux paramètres. Il est donc nécessaire de connaître certains de ces paramètres indépendamment des mesures de force de rupture. Une façon de procéder consiste à considérer que la barrière la plus élevée domine à tout instant (cette barrière ne sera pas toujours la même suivant la force appliquée) [Evans et Williams, 2002]. Dans ce cas, les calculs présentés pour une barrière restent valables et on s'attend à voir différents régimes suivant le taux de charge appliqué, chaque régime correspondant à une des barrières qui domine les autres. Cette approche pourra fonctionner dans certains cas, mais est en général trop réductrice. Ici, nous prendrons une autre méthode qui consiste à utiliser les résultats de simulations de dynamique moléculaire pour déterminer une partie des paramètres, vérifierons la cohérence des résultats sur le couple streptavidine – biotine et montrerons donc que l'apparent paradoxe streptavidine-biotine n'existe pas.

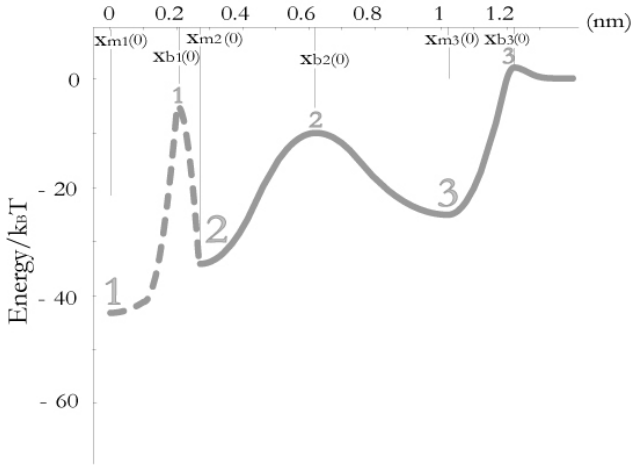

Figure 25 : Exemple de panorama énergétique à trois barrières.

Des simulations de dynamique moléculaire ont été effectuées sur le lien streptavidine -biotine. Les données obtenues par certaines de ces simulations sont présentées figure 26 où la trajectoire de la particule dans le potentiel énergétique est donnée. Les zones noires correspondent aux endroits où elle a été piégée, et donc aux états métastables.

Ces simulations permettent donc de déterminer avec une précision relativement bonne, les positions des minima et des barrières ainsi que les énergies des états métastables. Les paramètres restants sont donc :

- hauteurs relatives des barrières
- courbures du potentiel à proximité des puits et des barrières.

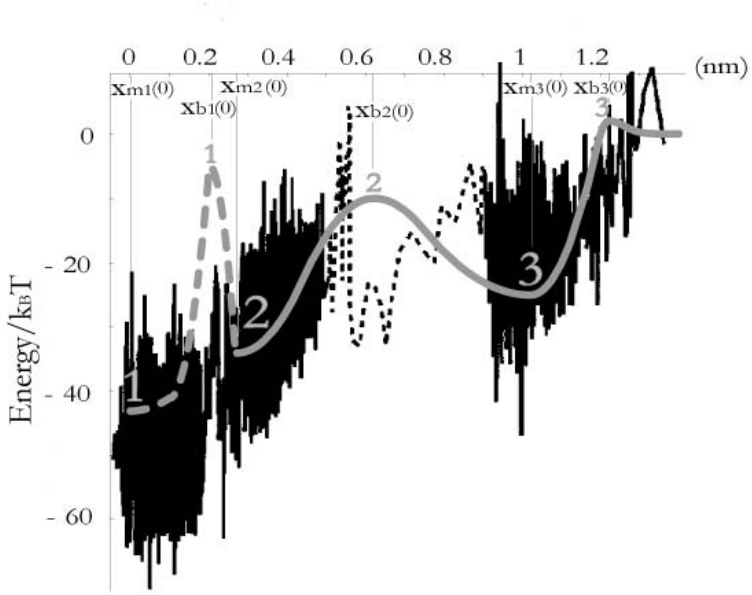

Figure 26 : Simulations de dynamique moléculaire sur le lien streptavidine - biotine. La biotine est retirée de la poche streptavidine dans laquelle elle est piégée en une nanoseconde. La trajectoire de la particule est présentée dans le potentiel déduit de ces simulations. Les zones sombres correspondent donc aux puits et trois barrières principales peuvent être déterminées. La ligne grise continue correspond au potentiel utilisé pour fitter les histogrammes expérimentaux (cf. figure 20).

En variant les paramètres qui restent dans les équations (41), il est possible de déterminer un panorama énergétique qui permet de fitter les histogrammes obtenus par le BFP avec une précision meilleure que l'erreur expérimentale (cf. figure 20) et qui est cohérent avec les simulations de dynamique moléculaire (cf. figure 26). Cependant, nous avons réalisé que la seule manière d'obtenir un tel fit est de prendre pour conditions initiales $P_1(0)=0$, $P_2(0)=1$ et $P_3(0)=0$. Cela signifie qu'avec le BFP, le lien n'a pas encore atteint son état le plus profond. Le contact entre la bille et le substrat durant moins de 1 seconde, ce résultat n'est pas surprenant. En effet, avec le potentiel de la figure 26, le temps de remplissage du puits le plus profond est de l'ordre de 10 s (cf. figure 27).

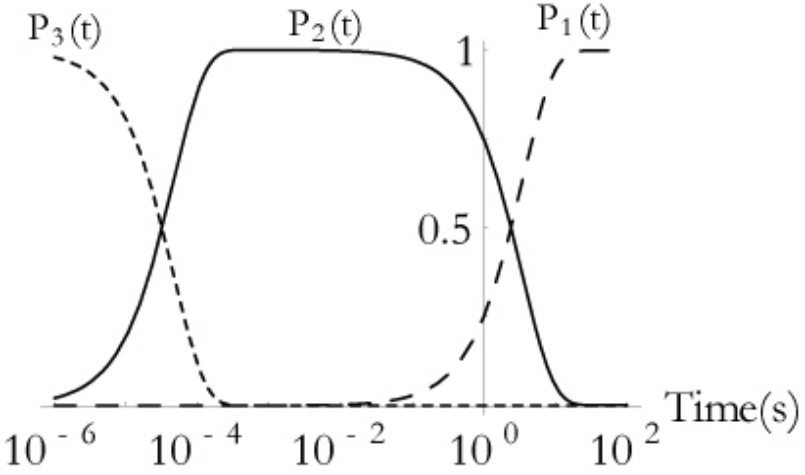

Figure 27 : Remplissage des différents puits du potentiel présenté figure 26 en fonction du temps t en partant des conditions initiales $P_1(0)=0$, $P_2(0)=0$ et $P_3(0)=1$ et en appliquant les relations (41) sans force de traction. Pour chaque puits, il y a une transition nette entre l'état où il est occupé et l'état où il est vide.

En revanche, dans les expériences de C. Bustamante (figure 21), le lien peut atteindre son état d'énergie le plus favorable puisque le temps d'attente avant que la force de traction soit appliquée est de l'ordre de plusieurs minutes.

Sur l'exemple du couple streptavidine, nous avons donc pu voir qu'il est possible de décrypter en détail le panorama énergétique d'une liaison complexe en utilisant en parallèle des simulations de dynamique moléculaire et des mesures de forces. Nous avons aussi vu que sur une échelle de temps « humaine », c'est-à-dire de l'ordre de la seconde, un lien n'était pas nécessairement dans son état le plus stable. Cela soulève le problème de constante d'association et de dissociation en chimie (k_{on} et k_{off}) qui devraient être définie pour chaque état métastable. Néanmoins, le couple présenté ici est un cas extrême et on peut donc s'attendre à ce que la plupart du temps, seul l'état le plus stable est important.

3.3.3. Solidité d'une ancre membranaire et vaccin antitumoral

Collaboration : D. Gillet (biologie, CEA, Saclay)
Contrat Nano Objet Individuel, 2000.
Dans le cadre de la thèse de J. Husson

Plusieurs protéines solubles ont un fort pouvoir anti-tumoral (Maini *et al.*, 1997), c'est par exemple le cas de certaines cytokines. Une stratégie consiste à utiliser ce potentiel dans l'élaboration de vaccins anti-cancéreux. Pour permettre aux cytokines d'agir à bon escient, il est nécessaire de les concentrer au niveau de la tumeur car leur administration par voie systémique chez l'homme provoque de graves effets secondaires (Maas *et al.*, 1993). Il est possible d'injecter *in vivo* des cellules tumorales transfectées avec des gènes de cytokine (GM-CSF, IL-2, IL-12, IL-18,...) de manière à ce que les cellules tumorales sécrètent elles-mêmes ces protéines (Chong *et al.*, 1998; Osaki *et al.*, 1999; Schmidt *et al.*, 1997). Cependant, cette approche présente encore de nombreux problèmes. Certaines cellules tumorales sont difficiles voire impossibles à transfecter. Les vecteurs viraux posent aussi des problèmes de sécurité (Alemany *et al.*, 2000; Marshall, 1999; Simon *et al.*, 1993). Ces procédures sont longues et coûteuses dans un contexte clinique. Enfin, le taux de production des cytokines est difficilement contrôlable avec des cellules transfectées (Schmidt *et al.*, 1995).
Une alternative à la transfection est la fixation de cytokines via une ancre membranaire soit lipidique soit protéique. Trois équipes ont commencé à développer des ancres membranaires lipidiques pour l'immunothérapie (McHugh *et al.*, 1999; van Broekhoven *et al.*, 2000) ou d'autres applications biotechnologiques (de Kruif *et al.*, 2000). A l'inverse, le choix de D. Gillet s'est porté sur une ancre protéique, le domaine T de la toxine diphtérique, qui, présente au moins trois avantages par rapport aux ancres lipidiques [Nizard *et al*., 2003] : longévité de la fixation (pas d'internalisation [McHugh *et al.*, 1999; van Broekhoven *et al.*, 2000], pas de formation de micelles [Roy *et al.*, 1997]), choix de la fixation sur l'une des deux extrémités, N- ou C-terminale de la cytokine, déclenchement contrôlé de l'ancrage par le pH sans altération de la cellule. Il a ancré les cytokines directement à la surface des cellules tumorales irradiées ou tuées, à l'aide du domaine T de la toxine diphtérique nécessitant seulement une courte incubation *in vitro*, voire directement *in vivo* par injection intra-tumorale.
Le domaine T de la toxine diphtérique (20 kDa) possède la propriété de se lier aux membranes lipidiques à pH acide. D. Gillet a montré que le domaine T pouvait être utilisé comme une ancre permettant de lier aux membranes des protéines solubles fusionnées à son extrémité N- ou C-terminale [Liger *et al.*, 1998; Nizard *et al.*, 1998 ; Chenal et al., 2002]. Ceci a été réalisé avec

l'IL-2 humaine, l'IL-3 de souris et la protéine ZZ, capable de lier les IgG. L'ancrage se fait par incubation de la protéine de fusion avec les cellules à pH 5 pendant 15 à 60 minutes. Les protéines restent associées à la surface de la plupart des cellules plus de 48 h. A titre de modèle, ce procédé a été appliqué à l'ancrage membranaire de l'IL-2 [Liger *et al.*, 1998; Nizard *et al.*, 2003]. Elle possède un puissant pouvoir anticancéreux par stimulation de la prolifération des cellules T cytotoxiques et auxiliaires et des cellules NK [Maas *et al.*, 1993].

L'équipe de D. Gillet a montré que des cellules murines de lymphome T (RMA), ou de mélanôme (B16) tapissées d'IL-2 par l'intermédiaire du domaine T, étaient capables d'induire une immunité anti-tumorale protectrice chez la souris syngénique C57Bl/6 [Nizard *et al*., 2003]. Le développement d'ancres membranaires adaptées à l'élaboration de vaccins anti-cancéreux très efficaces implique de connaître dans le détail leur mode d'interaction avec les membranes cellulaires. L'objectif de cette étude est de mesurer à l'échelle de la molécule unique les forces d'extraction des ancres protéiques que nous développons. A terme, ce travail permettra de comparer les efficacités des ancres membranaires protéiques et lipidiques. Il permettra également de mieux comprendre la nature de ces interactions.

D'autre part, le domaine T présente une transition structurale à pH acide qui lui permet de s'insérer dans la membrane. Nous avons comparé les forces mises en jeu dans l'ancrage de la protéine à pH neutre et à pH acide. Cette transition conduisant à une conformation de type molten globule, les informations obtenues permettront de mieux comprendre cet état particulier des protéines souvent impliqué dans leur trajectoire de repliement, et parfois impliqué dans la physiologie même de certaines protéines (toxines bactériennes, protéines anti-apoptotiques de la famille Bcl-2…).

Deux protéines dérivées du domaine T et biotinylées respectivement du coté N- et C-terminal ont été produites chez la bactérie *E. coli*. Les extrémités biotinylées des protéines ont été utilisées comme des poignées pour manipuler les protéines dans le dispositif de mesure de force (figure 28).

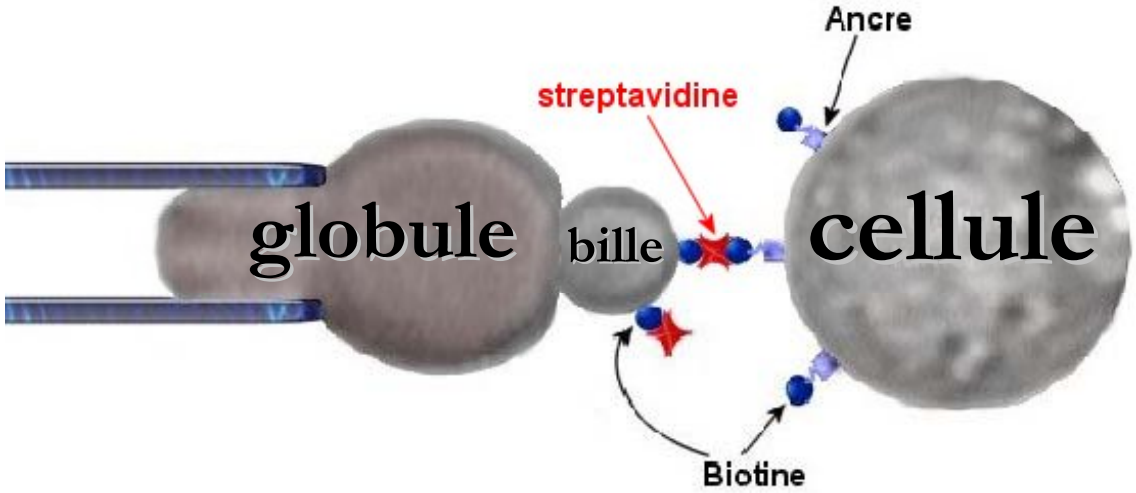

Figure 28 : Principe de l'extraction de l'ancre membranaire à l'aide du BFP. Une protéine (streptavidine), utilisée comme poignée, est fixée sur la bille et permet, une fois au contact de la membrane, de tirer sur une ancre fonctionnalisée avec une biotine afin de sonder sa fixation. On déduit la force qu'elle subit de la déformation du globule rouge. Les échelles ne sont pas respectées (les molécules sont évidemment beaucoup plus petites).

Nos expériences consistent donc à extraire, à l'aide du BFP, une ancre unique de la membrane de cellules. L'ancre utilisée est le domaine T de la toxine diphtérique sur une cellule de souris (mélanome, B16).

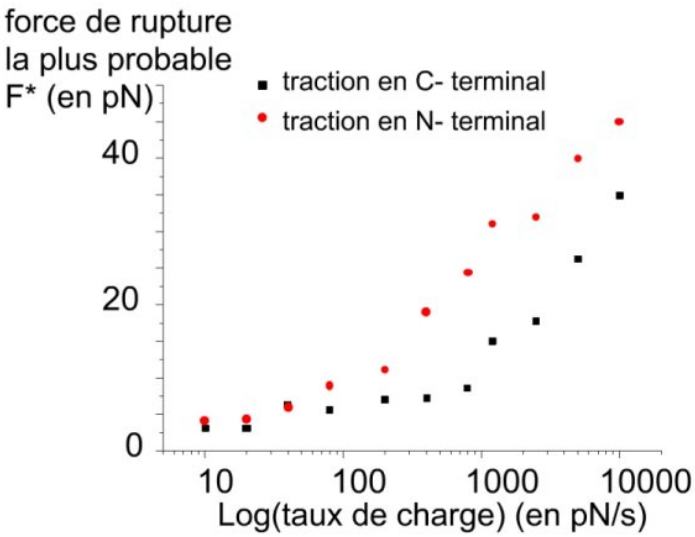

Figure 29 : force d'extraction la plus probable du domaine T en tirant par le coté N-terminal (ronds) ou le coté C-terminal (carrés)

Nous avons étudié le domaine T fonctionnalisé avec une biotine soit en son extrémité N-terminale, soit en son extrémité C- terminale. Les forces d'extraction mesurées montrent qu'il y a une différence nette selon l'extrémité où s'effectue la traction (figure 29). Il en résulte qu'une cytokine est plus robustement ancrée si elle est fusionnée à l'extrémité N-terminale du domaine T. Par ailleurs, les expériences pour lesquelles la protéine a été ancrée à pH physiologique montre que les force d'extraction sont plus faibles que pour les protéines ancrées à pH acide. Ce résultat conforte l'hypothèse selon laquelle il faut effectuer le greffage de l'ancre à pH acide.

3.3.4. Autres études effectuées avec le BFP

3.3.4.1. un peptide cellule perméant : la pénétratine
Collaborations : A. Prochiantz et A. Joliot (biologie, ENS)
Contrat Nano Science 2003

Certains peptides dits cellule-perméants possèdent la faculté de traverser les membranes des cellules en l'absence de récepteur chiral [Joliot et Prochiantz, 2004 ; Wadia et al., 2004]]. Leur utilisation comme vecteurs de médicaments est envisagée par de nombreuses compagnies pharmaceutiques. Ce passage à travers les membranes est aussi observé pour des protéines entières (dont ces peptides sont dérivés) et cela pourrait correspondre à un nouveau mode de transduction du signal (concept de protéines messagères). Si le passage a déjà été clairement démontré en utilisant des marqueurs fluorescents, son mécanisme reste inconnu. Les tentatives de sa caractérisation au niveau physico-chimique ont été infructueuses car le plus souvent fondées sur l'utilisation de vésicules lipidiques. Ces dernières ne permettent pas de prendre en compte la complexité des membranes biologiques (distribution asymétrique des lipides, présence de sucres, hétérogénéités de la membrane telles que les rafts, zones enrichies en cholestérol et glycosphingolipides) [Derossi et al., 1998 ; Thorén et al., 2000 ; Magzoub et al., 2001 ; Chritiaens et al., 2002]. Nous sommes allés au-delà de ces expériences classiques. La pénétration implique que la molécule se lie avec la membrane avant de s'en dissocier. Nous travaillons sur un de ces liens en sondant directement et en détails l'association d'un peptide unique avec la membrane cellulaire. La comparaison d'un peptide cellule-perméant avec

différents peptides mutés non cellule-perméants permet de déterminer le rôle de chaque partie du peptide dans le mécanisme d'association. Pour cette étude, nous utilisons le BFP pour sonder le lien entre le peptide et une membrane de cellule vivante.

Le projet est encore en cours. Nous tentons de répondre aux questions suivantes :

- Quel est le rôle des différents constituants membranaires ?
- Le mécanisme de passage est-il le même pour tous ces peptides ?
- Y a-t-il des effets coopératifs impliquant la multimérisation de peptides ?
- Où le passage se fait-il préférentiellement dans la membrane?

Le principe de l'expérience est similaire à celui de l'ancre membranaire (partie 3.3.3, voir figure 28). Cette fois-ci, le peptide, biotinylé, est directement fixé à la bille et doit s'accrocher à la membrane de la cellule pendant l'expérience.

Nous nous sommes intéressés en particulier à la pénétratine, peptide cellule-perméant découvert par A. Prochiantz. Ce peptide constitue la troisième hélice alpha de l'homéodomaine d'une homéoprotéine, antennapedia. Nous disposons d'un peptide muté dans lequel un acide aminé a été modifié pour changer les interactions hydrophobes avec la membrane.

Deux types de cellules ont été étudiés, des cellules de rein, les K562 et des neurones d'embryons de souris. Afin de tester le rôle des sucres membranaires, deux séries d'expériences avec les K562 ont été effectuées. Lors de la première série, l'accrochage du peptide sur la cellule était observé en présence d'acide colominique qui joue alors le rôle de compétiteur des sucres membranaires. Pour la deuxième série, des K562 traitées à la tunicamycine ont été utilisées. Les sucres membranaires étaient alors dégradés.

Les conclusions des expériences effectuées à ce jour sont les suivantes :

- Le peptide muté se lie moins fortement aux K562 car les forces de rupture observées pour des taux de charges supérieurs à 1000 pN/s sont plus faibles qu'avec la pénétratine sauvage. Cela met en évidence l'importance du tryptophane. Ce résultat confirme l'observation selon laquelle ce peptide muté n'est pas cellule-perméant.
- L'homéodomaine se lie plus fortement aux K562 que la pénétratine sauvage. L'action du peptide semble donc renforcée en utilisant l'homéodomaine complet.
- Les sucres membranaires sont indispensables à la formation du lien. En effet, en présence d'acide colominique, la fréquence de formation des liens peptide-membrane est réduite d'un facteur proche de 3 et, d'un facteur 10 avec des K562 traitées à la tunicamycine. Pour l'homéodomaine, l'effet est encore plus dramatique puisque 100 fois moins de liens sont formés avec ces mêmes cellules traitées.
- La force du lien dépend de la nature de la cellule car le peptide est plus fortement lié aux neurones qu'aux K562. Ce résultat demande à être confirmé avec l'homéodomaine (expériences en cours).

3.3.4.3. extraction d'hélice alpha de membranes de vésicules.

Collaboration : R. Hodges (chimie, Calgary, Canada)

Dans le cadre de la thèse de Y. Gambin

Certaines inclusions monomoléculaires présentant un caractère hydrophile-hydrophobe-hydrophile sont capables de modifier, y compris en faible concentration, la structure de phases lamellaires inverses. Ces lamelles, formées par deux monocouches d'un tensioactif non-ionique entourant une faible épaisseur d'eau, sont séparées par du dodécane. Les inclusions sont des protéines ou peptides dont la partie centrale hydrophobe est formée par une hélice [Ben Shaul et

al., 1996 ; Harroun et al., 1999]. Elles rapprochent localement les deux lamelles voisines en y incorporant leurs parties hydrophiles et agissent donc comme des « boutons-pressions ».
Les modifications structurales de l'ensemble du système ont été bien analysées, en particulier l'influence de la concentration des inclusions sur l'espacement entre lamelles ainsi que leur effet sur les fluctuations de ces dernières [Taulier et al., 2000]. En revanche, on ne dispose pas d'information quantitative quant à la résistance de ces inclusions. Le but de ce projet est donc d'étudier l'extraction (et donc la rupture) de ces " boutons-pressions ".
Pour cela, nous avons synthétisé trois peptides (hélices alpha) biotinylés de longueurs transmembranaires différentes. Ces peptides ont été insérés dans des vésicules lipidiques géantes d'où ils sont arrachés avec le BFP à la manière de l'ancre membranaire mentionnée précédemment (partie 3.3.3, figure 28). Le peptide le plus court est plus petit que l'épaisseur de la membrane des vésicules, le plus long est plus grand alors que la longueur du peptide intermédiaire correspond exactement à l'épaisseur de la membrane (voir figure 31).

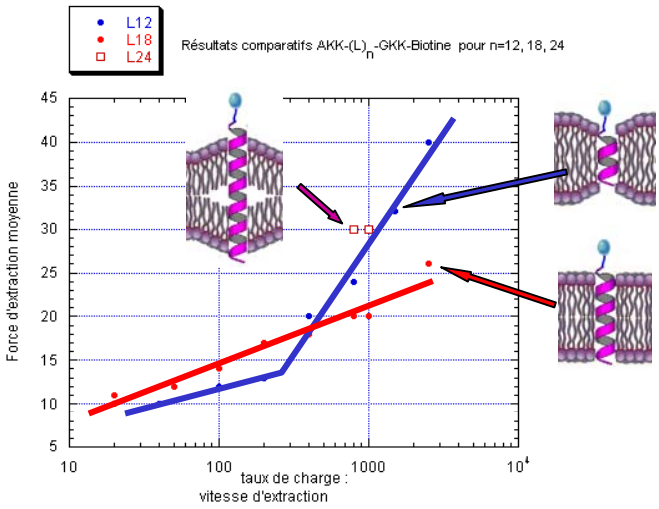

Figure 31 :Forces les plus probables mesurées pour les trois hélices alpha à différents taux de charge.

La comparaison des forces d'extraction pour ces hélices montre que l'inadéquation entre les tailles des parties hydrophobes joue un grand rôle dans l'ancrage des peptides dans la membrane. Les expériences montrent que si l'on tire doucement sur les peptides, l'ancrage le plus solide est celui de l'ancre la plus longue, comme attendu. En revanche, si on tire plus brusquement sur l'hélice, c'est alors l'hélice la plus courte, la moins hydrophobe, qui oppose le plus de résistance à l'arrachement.

3.3.5 Bibliographie de la partie 3.3

Alemany, R., Balague, C., and Curiel, D. T., *Nat Biotechnol* **18**, 723-727, (2000).

Ben Shaul, A., Ben-Tal, N. et Honig, B., *Biophys. J.*, **71**, 130-137, (1996).

Chenal, A., Nizard, P., et Gillet., D., *J. Toxico.-toxin Rev.*, **21**, 321-358, (2002).

Chong, H., Todryk, S., Hutchinson, G., Hart, I. R., and Vile, R. G., *Gene Ther* **5**, 223-232, (1998).

Christiaens, B., Symoens, S., Vanderheyden, S., Engerborghs, Y., Joliot, A., Prochiantz, A., Vanderkerckhove, J., Rosseneu, M., et Vanloo, B., *Eur. J. Biochem.*, **269**, 2918-2926, (2002).

Derossi, D., Chassaing, G., et Prochiantz, A., *Trends in Cell Biol.*, **8**, 84-87, (1998).

el-Shami, K. M., Tzehoval, E., Vadai, E., Feldman, M., and Eisenbach, L., *J Interferon Cytokine Res* **19**, 1391-1401, (1999).

Evans, E., *Faraday Discuss*., **111**, 1-16, (1998).

Evans, E., P. Williams, P., Dynamic force spectroscopy. *In* Physics of Bio-Molecules and Cells. F. Julicher, P. Ormos, F. David, and H. Flyvbjerg, editors. Springer Verlag, Berlin, Germany. 145 – 204, (2002).

Graf, M. R., Jadus, M. R., Hiserodt, J. C., Wepsic, H. T., and Granger, G. A., *J Immunol* **163**, 5544-555, (1999).

Grakoui, A., Bromley, S. K., Sumen, C., Davis, M. M., Shaw, A. S., Allen, P. M., and Dustin, M. L., *Science* **285**, 221-227, (1999).

Hänggi, P. , P. Talkner, and M. Borkovec. Reaction-rate theory: fifty years after Kramers. *Rev. Mod. Phys.*, 62:251-342, (1990).

Harroun, T.A., Heller, W.T., Weiss, T.M., Yang, L., et Huang, H.W. , *Biophys. J.*, **76**, 937-945, (1999).

Kramers, H.A., *Physica* (Utrecht) **7**, 284-304 (1940)

de Kruif, J., Tijmensen, M., Goldsein, J., and Logtenberg, T., *Nat Med* **6**, 223-227, (2000).

Joliot, A., et Prochiantz, A., *Nature Cell Biol.*, **6**, 189-196, (2004).

Liger, D., Nizard, P., Gaillard, C., vanderSpek, J. C., Murphy, J. R., Pitard, B., and Gillet, D., *Protein Eng*, **11**, 1111-1120, (1998).

Maas, R. A., Dullens, H. F., and Den Otter, W., *Cancer Immunol Immunother* **36**, 141-148, (1993).

Magzoub, M., Kilk, K., Eriksson, L.E.G., Langel, U., et Gräslund, A., *BBA*, **1512**, 77-89, (2001).

Maini, A., Morse, P. D., Wang, C. Y., Jones, R. F., and Haas, G. P.,*Anticancer Res* **17**, 3803-3808, (1997).

Marshall, E., *Science* **286**, 2244-2245**,** (1999).

McHugh, R. S., Nagarajan, S., Wang, Y. C., Sell, K. W., and Selvaraj, P., *Cancer Res* **59**, 2433-2437, (1999).

Nizard, P., Gross, DA., Gaillard, C., and Gillet, D., *FEBS Lett* **433**, 83-88, (1998)

Nizard, P., Gross, D.A., Babon, A., et Gillet, D., *J. Immunother.*, **26**, 63-71, (2003).

Osaki, T., Hashimoto, W., Gambotto, A., Okamura, H., Robbins, P. D., Kurimoto, M., Lotze, M. T., and Tahara, H., *Gene Ther* **6**, 808-815, (1999).

Roy, M. O., Uppenberg, J., Robert, S., Boyer, M., Chopineau, J., and Jullien, M., *Eur Biophys J* **26**, 155-162, (1997).

Schatz, P. J., *Biotechnology (N Y)* **11**, 1138-1143, (1993).

Schmidt, W., Maass, G., Buschle, M., Schweighoffer, T., Berger, M., Herbst, E., Schilcher, F., and Birnstiel, M. L., *Gene* **190**, 211-216, (1997).

Schmidt, W., Schweighoffer, T., Herbst, E., Maass, G., Berger, M., Schilcher, F., Schaffner, G., and Birnstiel, M. L., *Proc Natl Acad Sci U S A* **92**, 4711-4714, (1995).

Simon, R. H., Engelhardt, J. F., Yang, Y., Zepeda, M., Weber-Pendleton, S., Grossman, M., and Wilson, J. M., *Hum Gene Ther* **4**, 771-780, (1993).

Smith, P. A., Tripp, B. C., DiBlasio-Smith, E. A., Lu, Z., LaVallie, E. R., and McCoy, J. M., *Nucleic Acids Res* **26**, 1414-1420, (1998).

Soo Hoo, W., Lundeen, K. A., Kohrumel, J. R., Pham, N. L., Brostoff, S. W., Bartholomew, R. M., and Carlo, D. J., *J Immunol* **162**, 7343-7349, (1999).

Taulier, N., Nicot, C., Waks, M., Ober, R., Gulik-Krzywicki, T., Hodges, R.S., et Urbach, W., *Biophys. J.*, **78**,: 857-865,(2000).

Thorén, P.E.G., Persson, D., Karlsson, M., et Nordén, B., *FEBS Lett.*, **482**, 265-268, (2000).

van Broekhoven, C. L., Parish, C. R., Vassiliou, G., and Altin, J. G., *J Immunol* **164**, 2433-2443, (2000).

Wadia, J.S., Stan, R.V., et Dowdy, S.F., *Nature Medicine*, **10**, 1-6, (2004).

3.4. Autres utilisations des expériences de micromanipulation

Les manipulations par micropipettes ainsi que l'expérience acquise sur de nombreux objets à caractère biologique (vésicules, cellules, …) ont permis d'utiliser les dispositifs expérimentaux dans des contextes très différents de ceux présentés précédemment. Ces études sont décrites dans les paragraphes suivants.

3.4.1. Une nouvelle méthode de mesure d'énergie de liaison : la nanotitration de liens faibles [8]

Collaboration : E. Evans (physique, Vancouver, Canada) et L. Lebeau (chimie, Illkirch)

Avec E. Evans, nous avons mis au point une nouvelle technique de mesure d'énergie de liaison. Elle consiste à contrebalancer l'attraction spécifique par un potentiel répulsif ajustable: une force électrostatique double-couche. Pour valider cette approche, nous nous sommes attachés à retrouver l'énergie de liaison spécifique de deux bases complémentaires de l'ADN, A et T, déjà mesurée par ailleurs (§3.1.2.).

Dans le cas présent, nous avons utilisé deux vésicules chargées et fonctionnalisées par des lipides contenant soit A soit T dans leur tête polaire. Par ailleurs, la charge totale de ces deux vésicules est contrôlée, pour l'une d'entre elle par certains lipides A qui sont modifiés pour porter une charge négative, pour l'autre par des lipides négatifs non fonctionnalisés, en l'occurrence la dioleoyl-phosphatidylsérine (DOPS) (cf. figure 32). Lorsque les charges sont écrantées par du sel, les vésicules peuvent s'approcher et adhérer, leur distance de séparation – déterminée par l'équilibre entre force électrostatique double couche et attraction de van der Waals - autorise le contact moléculaire entre les surfaces. Des liens entre nucléosides des deux surfaces peuvent se former. Ensuite, quand l'écrantage est progressivement réduit, les vésicules se séparent spontanément à une concentration donnée de sel, C*. Cette concentration correspond à l'écrantage pour lequel l'énergie électrostatique double couche et l'énergie de liaison de chaque lipide A chargé sont équilibrées.

L'énergie électrostatique double-couche pour un nucléoside dépend de la densité de charges ρ_e sur la vésicule opposée (en nombre de charges par nm^2) et de la concentration en sel monovalent c_i (mol/l):

$$\mathrm{Sinh}\,(E_{dl}/2k_BT) \sim 1.36\,\rho_e/\sqrt{c_i} \qquad (43)$$

En pratique, des forces de déplétion[21] doivent être appliquées pour forcer le contact initial des vésicules. Celles-ci sont ensuite transférées dans un chambre où la force ionique est plus faible. Si elles restent en contact, elles sont transférées dans une autre chambre avec une force ionique encore plus faible. Ce processus est répété jusqu'à la séparation des surfaces.

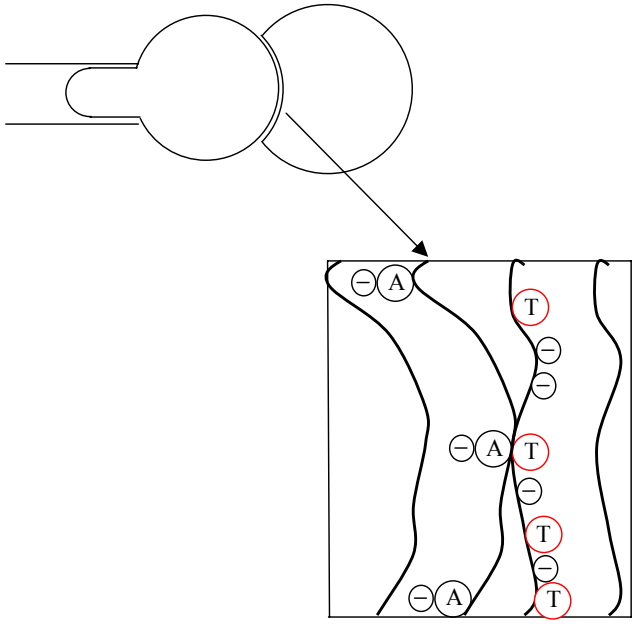

Figure 32: Une vésicule portant le lipide A chargé négativement (gauche) en contact avec une vésicule portant le lipide T , neutre, et un lipide chargé (droite).

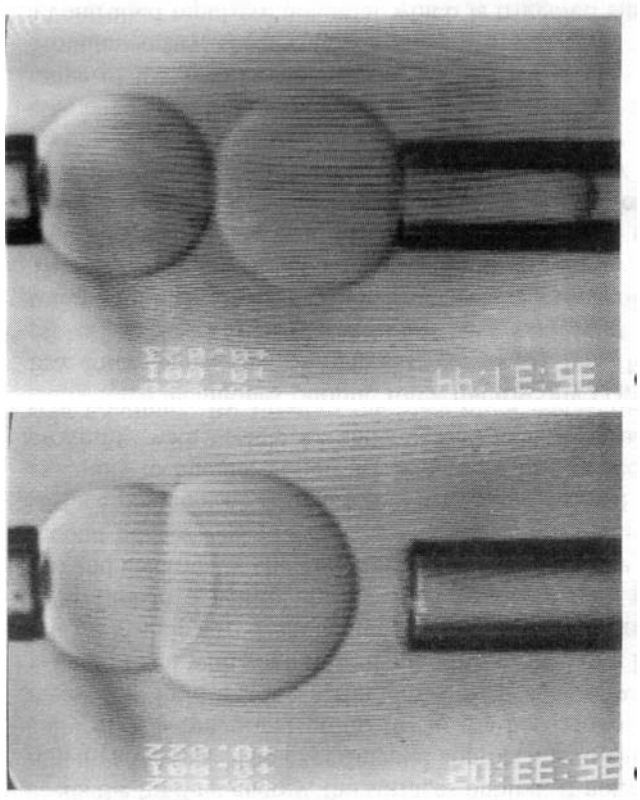

Figure 33: Deux vésicules mises en contact (haut) et adhérant dans une solution sans polymère indiquant que les liens entre nucléosides persistent (bas).

Des bornes inférieure et supérieure à l'énergie de liaison sont alors obtenues directement à partir de la concentration en sel avant et après la séparation respectivement. La composition lipidique des vésicules peut aussi être variée. Les résultats sont reportés dans le tableau 3.

Vesicule #1	Vesicule #2	C* (mM)	Énergie de liaison (k_BT)
DOSPA/SOPC (5:95)	DOST/SOPS/SOPC (5:5:90)	$1 < C^* < 10$	$1.83 < E_b < 3.83$
DOSPA/SOPC (5:95)	DOST/SOPS/SOPC (5:10:85)	$1 < C^* < 10$	$2.97 < E_b < 5.18$
DOSPA/SOPC (5 :95)	DOSA/SOPS/SOPC (5 :5 :90)	$5 < C^* < 50$	$0.90 < E_b < 2.37$

Tableau 3: Compositions des vésicules utilisées et bornes inférieure et supérieure de l'énergie du lien correspondant.

Ces valeurs sont en bon accord avec celles obtenues en utilisant le SFA (partie 3.5.1):

Énergie de liaison (k_BT)	Valeur expérimentale	Valeur SFA
A/T	$2.97 < E_b < 3.83$	3.6
A/A	$0.90 < E_b < 2.37$	1.7

Tableau 4 : Comparaison des valeurs d'énergies de liaison obtenue par nanotitration et par le SFA

Cette nouvelle méthode de titration de liens faibles fournit une approche relativement simple pour évaluer des énergies de liaison entre 2 et 25 k_BT.

3.4.2. une étape intermédiaire de la fusion membranaire : l'hémifusion [14,19]

Collaboration : S. Cribier (physique, IBPC, Paris)
Contrats Physico Chimie du Vivant 1999 et Dynamique et Réactivité des Assemblages Biologiques 2001.
Dans le cadre de la thèse de J. Heuvingh.

La fusion membranaire est un phénomène biologique qui, malgré son omniprésence, reste fort mal compris [Cohen et al., 1984 ; Almers et Tse, 1990 ; Melikyan et al., 1995 ; Durrer et al., 1996 ; Jahn et Südhof, 1999 ; McNew et al., 2000 ; Kuzmin et al., 2001 ; Kozlovsky, 2002]. Avec S. Cribier, nous avons cherché à saisir certaines de ses caractéristiques en utilisant des systèmes modèles contenant un minimum de composants.
Nous avons mis en évidence par fluorescence l'hémifusion de vésicules contenant des lipides fonctionnalisés avec des bases de l'ADN. Cette hémifusion se caractérise par le partage des couches externes des vésicules, mais chacune des couches internes reste indépendante. Ce phénomène peut s'expliquer en termes de transition de phases car la présence des bases de l'ADN induit une distance d'équilibre entre les membranes tellement faible que la phase bicouche n'est plus stable. Nous avons estimé numériquement la distance d'équilibre entre deux bicouches, elle décroît de 2,6 nm sans force spécifique à 1,4 nm en présence de forces spécifiques. Ce rapprochement est similaire à ce qui se produit dans la fusion membranaire au sein des cellules biologiques. En particulier, certaines protéines, appelées SNARE, sont impliquées dans la fusion membranaire (voir §4.) car elles permettent justement de rapprocher considérablement les membranes.
Nous avons vérifié qu'il n'existe pas de pore entre les vésicules et donc que les contenus internes restent bien distincts (figure 34).
Nous avons aussi quantifié nos mesures pour essayer de mieux comprendre la structure de l'interface dans l'état hémifusionné. Un modèle de diffusion en « cacahouète » où les lipides

des couches externes peuvent librement diffuser d'une vésicule à l'autre a été utilisé. A partir des tailles des vésicules et de l'aire de contact, nous avons ainsi pu déterminer les intensités de fluorescence de chacune des vésicules et les comparer aux intensités mesurées pour chaque expérience. L'accord avec les expériences est étonnamment bon. Compte tenu des contraintes géométriques et énergétiques, la structure à l'interface ne peut alors être composée que de pédoncules reliant les vésicules.

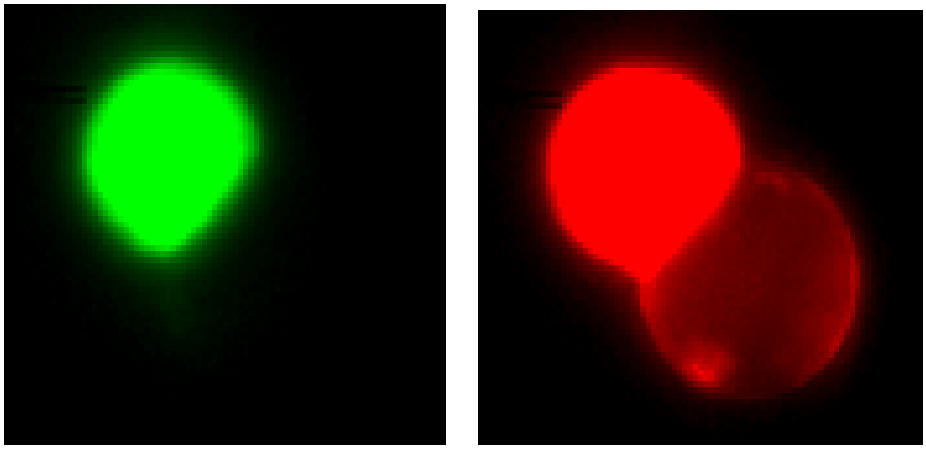

Figure 34 : fluorescence de deux vésicules à l'équilibre : la vésicule supérieure contenait initialement dans sa membrane des lipides marqués par la rhodamine et en volume de petites molécules de dextrane marquées à la fluorescéine. Elle contient aussi un lipide portant de l'adénine. La vésicule inférieure contient un lipide portant de la thymine, mais aucun marqueur fluorescent. A l'équilibre, la rhodamine (à gauche) est effectivement passée d'une vésicule à l'autre (hémifusion), mais la fluorescéine est restée dans la vésicule supérieure (à droite).

Grâce à cette étude, nous avons mis en évidence et caractérisé une structure intermédiaire possible lors de la fusion membranaire.

3.4.3. Ouverture spontanée de pores en milieu aqueux.

Collaboration : S. Cribier (physique, IBPC, Paris)
Dans le cadre de la thèse de N. Rodriguez.

En ajoutant un sel, de la dithionite, à des vésicules composées de deux lipides dont les courbures spontanées sont très différentes, nous avons pu nucléer des pores de façon reproductible et contrôlée, en milieu aqueux. De tels pores avaient déjà été observés en présence de glycérol [Sandre et al., 1999 ; Karatekin et al., 2003]. L'un des deux lipides utilisés ici, plus soluble, contient un marqueur fluorescent, la NBD qui est oxydé par la dithionite. Nous interprétons cette ouverture de pores de la façon suivante. La membrane de la vésicule serait lentement solubilisée par le lipide le plus soluble en présence de dithionite. Sa tension augmenterait jusqu'à atteindre la tension de rupture à laquelle un pore se forme pour relâcher la tension. Le milieu intérieur peut alors s'échapper et le pore se referme. La cinétique d'ouverture et de fermeture de ces pores a déjà été décrite [Brochard-Wyart et al., 2000]. A priori, les ordres de grandeurs des viscosités en présence impliquent des tailles de pores trop petites et des durées de vie trop courtes pour être observées. Cependant la réduction de la tension de ligne au bord du pore due à la présence des lipides marqués ainsi que la réduction constante de la surface de la vésicule permettent de ralentir la cinétique du phénomène et peuvent dans certaines conditions suffire à observer des pores [Fumimasa et al., 2001]. La vitesse de fermeture du pore est alors suffisamment lente pour laisser le temps à des particules initialement présentes à

l'intérieur de la vésicule de s'échapper (figure 35). Ce résultat prouve que de tels pores peuvent être formés de façon contrôlée en milieu aqueux et ouvre de nombreuses perpectives notamment dans le domaine de la vectorisation d'objets.

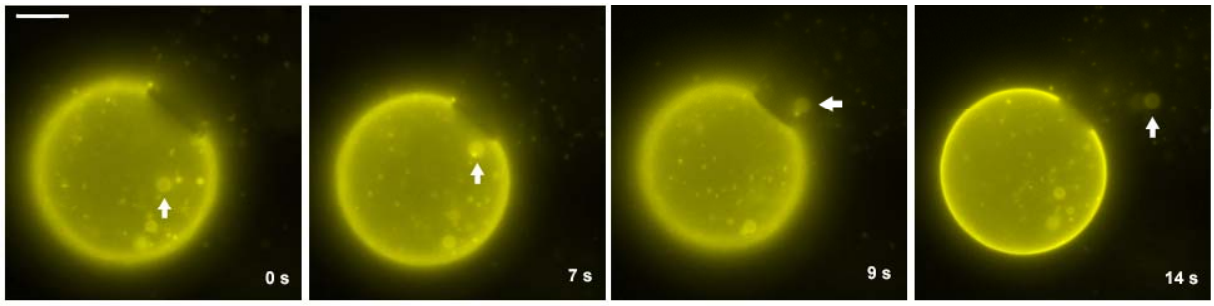

Figure 35 : un pore est ouvert à la surface d'une vésicule. Une petite vésicule initialement présente à l'intérieur de la grande s'en échappe (indiqué par la flèche). La barre représente 5 µm.

3.4.4. micromanipulation de gouttes d'émulsions [29]

Collaboration : D. Langevin (physique, LPS, Orsay), J-F. Argillier (chimie, IFP, Rueil-Malmaison)

L'utilisation d'émulsions aqueuses pour faciliter le transport d'huiles lourdes est actuellement envisagée. Le comportement de ces émulsions est essentiellement contrôlé par l'interface entre l'eau et les gouttes d'huile [Mclean et Kilpatrick., 1997 a et b ; Yarranton et al., 2000 ; Kumar et al., 2001 ; Salager et al., 2001 ; Sjoblom et al., 2003]. Les surfactants présents dans le pétrole, comme les asphaltènes ou les acides naphténiques, et les surfactants synthétiques éventuellement ajoutés à l'émulsion, sont en compétition à ces interfaces. Afin de caractériser ces émulsions, dont les propriétés intéressent au plus haut point l'Institut Français du Pétrole (IFP), nous avons effectué des mesures de coalescence de gouttes microscopiques micromanipulées à différents pH en présence de plusieurs surfactants. Les expériences ont été effectuées par S. Poteau (étudiante en thèse à l'IFP). Les résultats montrent que la coalescence n'a pas lieu à des pH extrêmes (élevés ou faibles). Une interaction entre asphaltènes et maltènes a été détectée. Elle facilite le réarrangement moléculaire au niveau de l'interface. Tous ces résultats corroborent et expliquent ce qui a été observé à l'IFP au niveau macroscopique par des mesures de tension de surface.

3.4.5. mise en évidence d'un seuil de densité de récepteurs pour la capture spécifique d'objets microscopiques par une cellule biologique [18]

Collaboration : N. Henry (physique, institut Curie, Paris)

L'équipe de N. Henry a greffé des ligands (ici la biotine) à la surface de cellules avec une densité connue. Des mesures d'agrégation ont permis de montrer que des particules recouvertes d'une densité élevée du récepteur correspondant, la streptavidine, n'adhèrent sur les cellules qu'une fois une densité critique de ligand atteinte. Cette densité critique dépend de plusieurs paramètres dont la longueur de l'espaceur entre la cellule et le ligand, et l'intensité des collisions cellule-particule. Nous avons pu, en mesurant des angles de contact par micromanipulation (figure 36), estimer le nombre de liens impliqués dans l'adhésion. Les résultats montrent que le processus de capture de la particule par la cellule est extrêmement dynamique. Au début, très peu de liens participent à l'adhésion (de l'ordre de la dizaine) alors

qu'après quelques minutes, plusieurs dizaines de milliers sont impliqués. Cela explique pourquoi très peu de particules (la plupart du temps une ou deux) semblent pouvoir être capturées par la cellule : les premières particules adhérentes mobilisent tous les ligands disponibles.

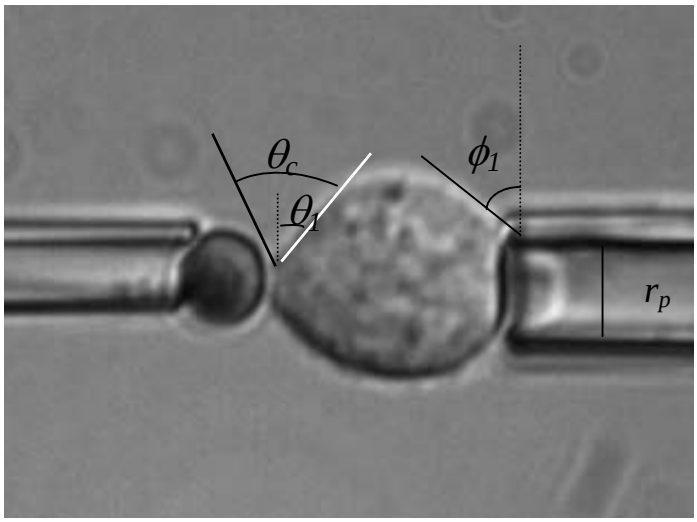

Figure 36 : une particule (bille de latex) recouverte de récepteurs (streptavidine) est micromanipulée et mise en adhésion avec sur une cellule portant le ligand. La mesure de l'angle de contact particule/cellule (θ_c) et cellule/pipette (ϕ_1) permet de déduire le nombre de liens impliqués. Le diamètre des billes est de l'ordre de 3 microns.

3.4.6. Bibliographie de la partie 3.4.

Almers, W., et Tse, F.W., *Neuron*, **4**, 813-818 (1990).

Brochard-Wyart, F., de Gennes, P.G., et Sandre, O, *Physica A*, **278**,32–51, 2000.

Cohen, F.S., Akabas, MH Zimmerberg J and Finkelstein A., *J. Cell Biol.*, **98**, 1054-1062 (1984).

Durrer, P., Galli, C., Hoenke, S., Corti, C., Glück, R., Vorherr, T., et Brunner, J., *J. Biol. Chem.*, **271**, 13417-13421 (1996).

Fumimasa Nomura, F., Nagata, M., Inaba, T., Hiramatsu, H., Hotani, H., et Takiguchi, K., *PNAS*, **98**, 2340-2345, (2001).

Jahn, R., et Südhof, T.C., Annu. Rev. Biochem. **68**, 863-911, (1999).

Karatekin, E., Sandre, O, Guitouni, H., Borghi, N., Puech, P.-H., et Brochard-Wyart, F., *Biophys. J.*, **84**, 1734–1749 (2003).

Kozlovsky, Y. & Kozlov, M. M. *Biophys J* **82,** 882-95, (2002).

Kumar, K., Nikolov, A. D., et Wasan, D. T. *Ind. & Engin. Chem. Res.***, 40**, 3009-3014, (2001).

Kuzmin, P. I., Zimmerberg, J., Chizmadzhev, Y. A. & Cohen, F. S, *Proc Natl Acad Sci U S A* **98,** 7235-40, (2001).

Mclean, J. D., et Kilpatrick, P. K. *J. Coll. and Intfc. Sc*, **196**, 23-34, (1997a).

Mclean, J. D., et Kilpatrick, P. K. *J. Coll. and Intfc. Sc.***, 189**, 242-253, (1997b).

McNew, J.A**.,** Weber, T., Parlati, F., Johnston, R.J., Melia, T.J., Söllner, T.H., et Rothman**.,** J.E., *J. Cell Biol.*, **150**, 105-118 (2000).

Melikyan, G.B., White, J.M., et Cohen, F.S., *J. Cell Biol.*, **131**, 679-691 (1995).

Salager, J. L., Briceno, M. I.; Brancho, C. L. Heavy Hydrocarbon Emulsions. In *Encyclopedic Handbook of Emulsion Technology;* Marcel Dekker: New York,; pp 455-495, 2001.

Sandre, O., Moreaux, L., et Brochard-Wyart, F., *PNAS.*, **96**, 10591–10596 (1999).

Sjoblom, J., Aske, N., Auflem, I. H., Brandal, O., Havre, T. E., Saether, O., Westvik, A., Johnsen, E. E., Kallevik, H., *Adv. in Col. Intfc. Sc.*, **100**, 399-473, (2003).

Yarranton, H. W., Hussein, H.; et Masliyah, J. H., *J. Coll. and Intfc. Sc.*, **228**, 52-63 (2000).

3.5. autres travaux: propriétés physiques de couches d'amphiphiles, fonctionnalisées ou non

3.5.1. Mesures directes d'interactions moléculaires spécifiques entre bases complémentaires de l'ADN [3,6,7,16]

Collaboration : L. Lebeau et C. Mioskowski (chimie, Illkirch)

Les forces liées à la reconnaissance moléculaire jouent un rôle essentiel à tous les niveaux d'organisation de la matière vivante. Leur portée n'est en général pas connue et presque aucune mesure directe de ces forces n'a été faite. Nous avons abordé leur étude dans un cas simple: deux bases complémentaires de l'ADN, l'adénosine et la thymidine, A et T.

Nous avons étudié cette interaction avec un SFA en déposant des bicouches de lipides fonctionnalisés avec A ou T (voir §3.1.2. et §3.4.1.). Trois types d'expériences ont été menées : mesures de forces entre deux surfaces recouvertes d'adénosine (A/A), entre deux surfaces de thymidine (T/T) et, entre une surface d'adénosine et une surface de thymidine (A/T). Les valeurs obtenues pour l'énergie d'adhésion reflètent l'interaction préférentielle de A et T, et permettent de trouver les énergies de liaison de ces molécules.

A toutes les distances et dans tous les cas, les forces sont attractives mais ne s'avèrent pas toujours préférentielles pour A et T: entre 20 et 60 nm, l'attraction A/A entre deux surfaces recouvertes de lipides A est plus forte que l'attraction A/T elle-même supérieure à T/T. Cependant, à 38 nm, l'interaction A/T présente une cassure de pente allant dans le sens d'une plus forte attraction et les courbes A/T et A/A se croisent à 19 nm. Afin de préciser ces comportements très spécifiques, nous avons modifié T (molécule MeT) en éliminant la liaison hydrogène clef qui permet l'appariement avec A: la force A/MeT suit, aux distances supérieures à 38 nm, le même profil que A/T. Mais à 38nm, A/MeT ne présente pas la cassure de pente observée pour A/T. Ainsi, le régime de forces conduisant à la préférence de A pour T commence à 38 nm (figure 37).

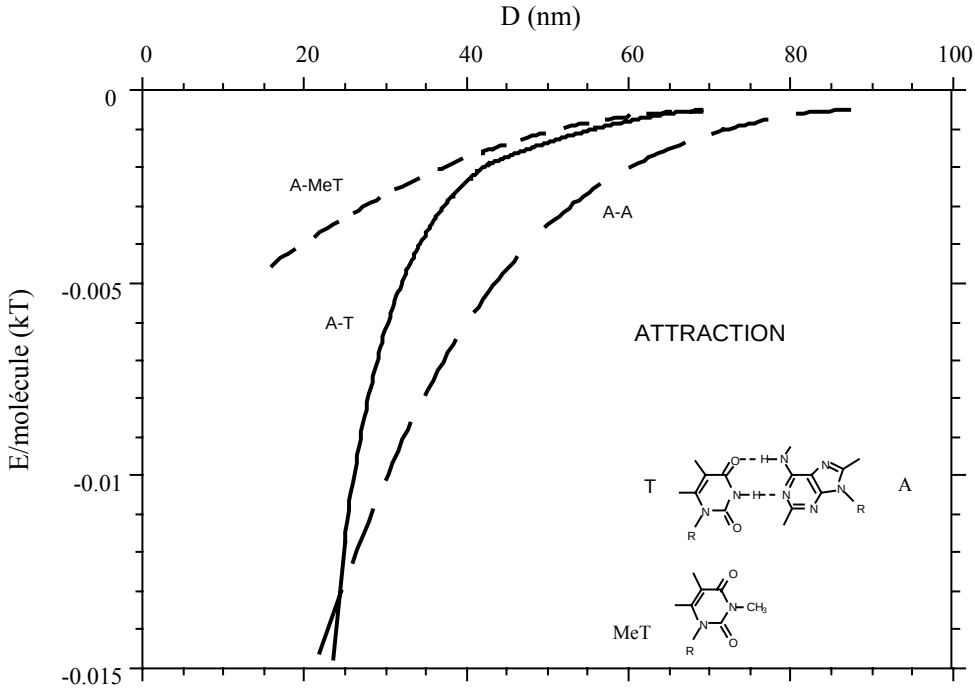

Figure 37 : Attractions entre nucléosides ramenées à une molécule en fonction de la distance de séparation. Le MeT ne peut pas s'apparier avec A

Les forces attractives observées dans tous les cas de figure sont nouvelles. Les données actuelles suggèrent que cette attraction pourrait être due à la formation de petits domaines (taille env. 60 nm), dans les monocouches, dans lesquels les bases seraient ordonnées ce que nous avons observé par ailleurs (§3.5.2).
Lors de la thèse de D. Tareste, en utilisant d'autre lipides formant des liaisons hydrogène par l'intermédiaire de groupement carboxyles, nous avons trouvé des interactions similaires. En particulier, l'énergie d'une liaison hydrogène est pratiquement la même dans l'eau pour un lien N-H -- O et pour un lien C-O -- H : 1 k_BT.

3.5.2. Une monocouche de type "liquide-expansé" peut s'accompagner d'un ordre translationnel [10]

Collaborations : M. Goldmann (physique, Paris V) et L. Lebeau (chimie, Illkirch).

Une monocouche lipidique à l'interface eau-air dont l'isotherme de compression indique une forte compressibilité est automatiquement assimilée à une couche désordonnée (état liquide-expansé) [Gaines, 1966 ; Langmuir, 1933]. Les lipides A et T contredisent cette règle. En effet, les bases de l'ADN ayant une tendance à mettre leurs plans parallèles (π-stacking) [Saenger, 1984], une organisation des têtes polaires est probable et la formation de domaines est envisageable bien que l'isotherme de compression des lipides indique un état liquide-expansé. Afin de vérifier cette hypothèse, nous avons effectué des expériences de diffraction de rayons X en incidence rasante au LURE (synchrotron). Les résultats indiquent qu'un ordre bidimensionnel est induit par les bases de l'ADN (cf.figure 38).
La largeur du pic de diffraction permet d'estimer la taille caractéristique de ces domaines. A l'aide d'un modèle rudimentaire que nous avons développé, il est possible, à partir de cette largeur de remonter à l'énergie d'empilement des lipides, e_s, dans le cas des bases de l'ADN. Schématiquement, ce modèle suppose que les domaines sont unidimensionnels (les bases

s'alignent avec leurs plans parallèle). Supposons qu'un base ait une probabilité p d'être empilée à la précédente. La probabilité d'obtenir une chaîne de n bases est alors : $P(n)=p^{n-1}(1-p)$. La longueur moyenne des chaînes est : $<n>=(1-p)^{-1}$. Une approche simple consiste à exprimer la probabilité p en fonction de e_s exprimée en k_BT: $p=\exp(e_s)/(1+\exp(e_s))$. Dans le cas présent, la taille typique des domaines est de 12 nm pour les lipides T, ce qui correspond à 35 molécules. On en déduit donc une énergie de « stacking » de 3,5 k_BT, ce qui est très proche de la valeur de la littérature (4,3 k_BT).

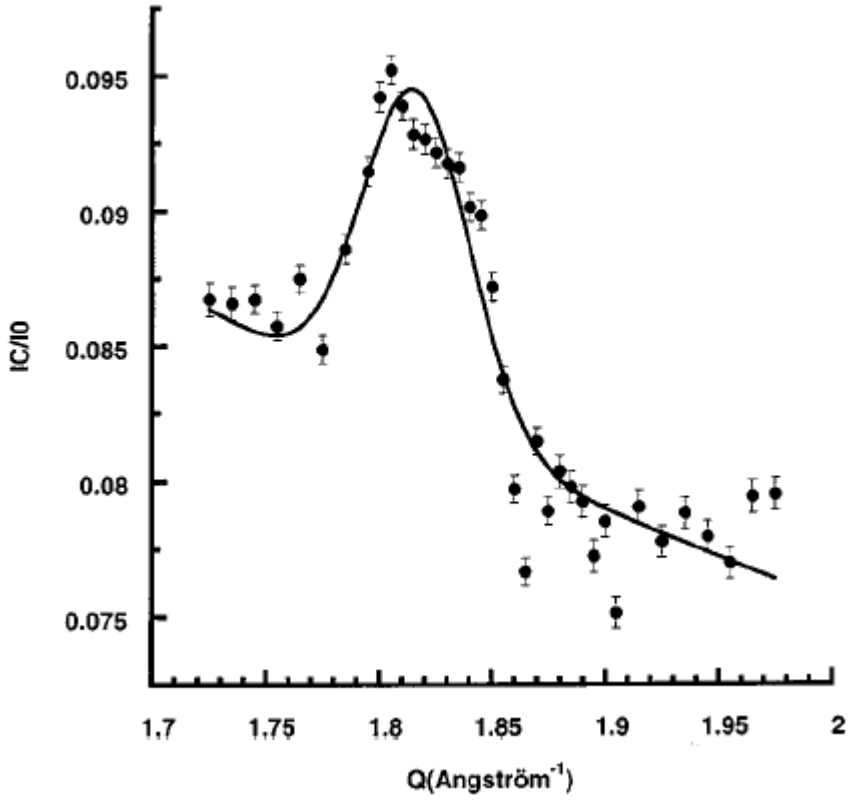

Figure 38 : spectre de diffraction de rayons X pour une monocouche de lipide T à l'interface eau/air. Le trait plein est un fit du pic (gaussienne) et de la ligne de base (lorentzienne). IC/I0 est l'intensité relative et Q est le vecteur d'onde en A^{-1}.

Une monocouche ayant un isotherme du type liquide-expansé n'est donc pas obligatoirement désordonnée. Du point de vue des mesures d'interaction entre surfaces, cet ordre « macroscopique » pourrait être à l'origine des attractions à grandes distances observées (§3.5.1.). Par ailleurs, il est possible, à partir des spectres de diffraction de rayons X aux petits angles d'estimer une énergie d'empilement des molécules impliqués dans les domaines.

3.5.3. transition réversible entre structures amphiphiles et huiles

Les bicouches de lipides fréquemment étudiés comme membranes biologiques modèles possèdent une cohésion mécanique leur permettant de résister à de nombreuses sollicitations telles que l'application d'une pression locale ou d'une tension [Israelachvili et al., 1977 ; Wolfe et al., 1991 ; Helm et al., 1992 ; Olbrich et al, 2000]. Par exemple, lorsque dans un SFA, on comprime deux bicouches de lécithine l'une contre l'autre, les surfaces demeurent à une certaine distance à cause des répulsions à courte portée. Nous avons montré que, lorsque les bicouches sont fluides et que les têtes polaires des lipides forment des liaisons hydrogène entre

les deux bicouches, il n'en est pas de même. Nous avons fait ces mesures avec des lipides fonctionnalisés par A et T. Dans ce cas, en comprimant les couches, on voit la distance diminuer entre les surfaces au lieu de rester constante: les bicouches perdent leur cohésion à cause de la formation de complexes hydrophobes entre les lipides fonctionnels des deux surfaces (figure 39). En appliquant la loi de Darcy, nous avons vérifié que ces complexes s'écoulent comme un liquide visqueux.

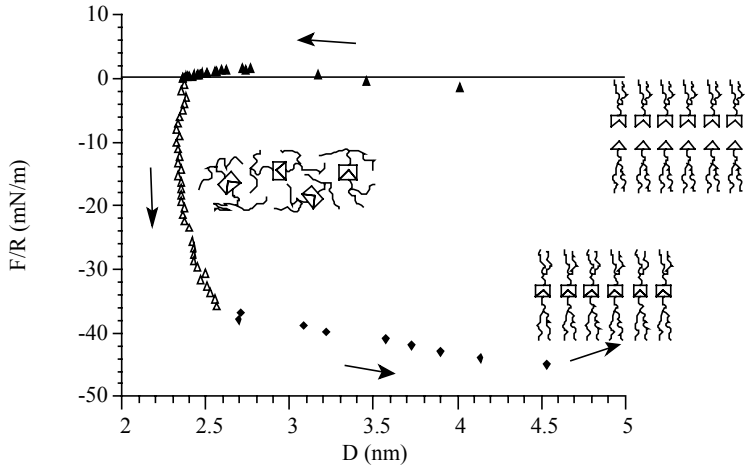

Figure 39 : courbe de force obtenue dans un SFA entre deux bicouches lipidiques fonctionnalisées. Les flèches indiquent l'évolution dans le temps. Le contact entre les couches est obtenu pour D = 4 - 5 nm. Puis, les couches se déstabilisent pour permettre la réduction de la distance.

D. Tareste, au cours de sa thèse a trouvé un résultat similaire avec des lipides dont les têtes polaires sont des nitrilotriacétates (NTA).
Dans les deux cas (A/T et NTA), lorsqu'on bloque les liaisons hydrogène, la cohésion mécanique est conservée comme pour des lipides non fonctionnels.
Une telle transition n'est pas nécessairement anodine car il est possible que, lors de la fusion membranaire, des complexes similaires se forment afin de combler les zones « vides » dans les modèles actuels de réorganisation des membranes.

3.5.4. Trous dans des bicouches lipidiques [9]

Collaboration : P. Bassereau (physique, Institut Curie, Paris).

Lors des mesures de forces avec le SFA, les molécules fonctionnalisées sont souvent des lipides déposés sur le mica sous forme de bicouches par la méthode de Langmuir-Blodgett (§3.1.4.2., §3.5.1., §3.5.2., §3.5.3., §3.5.4. et §3.5.6.). Cependant, plusieurs études menées par AFM ont montré que, contrairement à ce qui était imaginé auparavant, ces bicouches ne sont pas parfaitement lisses et uniformes, mais qu'elles sont parsemées de trous exposant le substrat (du mica en général) [Bourdieu et al., 1991 ; Hui et al., 1995]. L'origine de ces trous n'était pas comprise. Pourtant leur rôle peut être important, notamment dans le cas de mesures de forces. En collaboration avec P. Bassereau, et en effectuant des mesures sur un AFM, nous avons conclu que ces trous, d'une profondeur égale à l'épaisseur de la bicouche, sont dus à l'équilibre, au niveau de la ligne triple mica/eau/air, entre les lipides à l'interface eau/air et les lipides sur le mica. Il est alors possible d'estimer l'énergie d'adsorption des lipides sur le substrat. En effet, la proportion de trous sera déterminée par la balance énergétique entre l'état où la bicouche est déposée sur le substrat et l'état où le substrat est nu et les lipides à l'interface eau/air : $\rho=\exp(-\Delta E/k_BT)$, où ΔE est la différence d'énergie libre entre les deux états pour une molécule. Il est

possible de montrer que ΔE peut simplement s'écrire : $\Delta E=E_a-\alpha\gamma$, où Ea est l'énergie d'adsorption, α un coefficient et γ est la tension à laquelle la deuxième couche est déposée. La courbe $\ln(\rho)=f(\gamma)$ doit alors être une droite dont l'ordonnée à l'origine donne E_a. La figure 40 donne l'exemple d'une bicouche sur du mica. Cette bicouche est formée de DMPE en première couche et de DOPC en deuxième couche. La régression linéaire donne une énergie d'adsorption de 5,2 $\pm$0,5 k_BT pour le DMPE sur le mica.

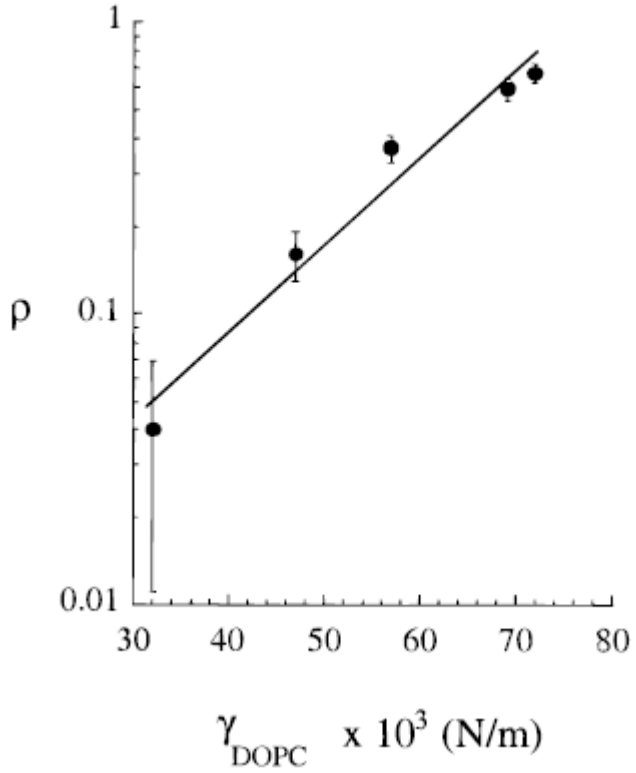

Figure 40 : Rapport entre la surface couverte par les trous et la surface couverte par la bicouche en fonction de la tension de la deuxième couche lors du dépôt (ici, la DOPC).

Cette étude a par ailleurs permis de montrer qu'une simple mesure de rapport de prélèvement, c'est à dire le rapport entre l'aire déposée et l'aire du substrat, lors d'un dépôt de Langmuir-Blodgett permet d'obtenir l'énergie d'adsorption du lipide sur le substrat. En effet, le rapport de prélèvement donne directement la fraction de la surface couverte de trous. Il est alors possible d'appliquer la méthode présentée auparavant.

3.5.5. Charges de lipides supposés neutres [11]

Collaboration : S. Cribier (physique, IBPC, Paris).

Les phospholipides tels que la dioleoylphosphatidylcholine (DOPC) sont censés avoir une charge totale nulle à pH 5,5 (pH de l'eau ultrapure laissé quelques minutes en contact avec l'air). Cependant, lorsqu'on met deux vésicules de ces lipides en contact, elles n'adhèrent pas sauf si le milieu aqueux contient du sel (quelques millimolaires). Nous avons mis en évidence par mesure de forces entre bicouches (SFA), qu'une répulsion à longue portée (plusieurs centaines de nanomètres) peut être observée. Cette répulsion est parfaitement décrite par les forces électrostatiques double-couche avec une longueur de Debye correspondant à la concentration en sel attendue, i.e. de l'ordre de $10^{-5,5}$ M. Il existe donc une charge résiduelle correspondant à une charge pour environ 1000 lipides. Cette charge n'a pas pas été observée

pour la Dimyristoylphosphatidylethanolamine (DMPE). Cette charge électrostatique faible est sans doute due à des impuretés qui existent même dans les lots de lipides les plus purs. En parallèle, nous avons effectué des expériences d'électrophorèse qui ont permis de confirmer ce résultat et d'obtenir le signe de ces charges : elles sont négatives. Ces impuretés, indécelables par les méthodes chimiques classiques, peuvent totalement changer les résultats de mesures entre couches de lipides puisqu'elles sont aptes à empêcher l'adhérence de vésicules dans certaines conditions.

3.5.6. Mécanisme de la cryoprotection: interaction de molécules cryoprotectrices avec les membranes [2]

Collaboration : J. Wolfe (U.N.S.W., Kensington,Australie)

Les dommages induits par le gel à la matière vivante sont importants. Pendant le refroidissement, le milieu extracellulaire commence à geler. Comme les solutés qui s'y trouvent ne sont pas solubles dans la glace, leur concentration augmente pendant la congélation et comprime osmotiquement la cellule en la déshydratant. Il en résulte des fortes contraintes anisotropes qui sont responsables des dommages causés par le gel.
La plupart des molécules cryoprotectrices sont des sucres, notamment le tréhalose. Leur action est d'abord de limiter osmotiquement la déshydratation, mais de nombreux cryobiologistes font l'hypothèse d'une liaison lipides/sucres dont l'effet serait de modifier les forces à courte portée entre membranes et d'agir sur leur élasticité.
J'ai voulu vérifier cette hypothèse en mesurant l'effet de concentrations élevées en sucre sur la force entre deux bicouches lipidiques, et en déterminant (mesures effectuées par J. Wolfe) le partage du sucre entre une phase lamellaire de lipides et une phase aqueuse. Les résultats sont d'une part que le sucre ne s'adsorbe pas sur les bicouches et, d'autre part, qu'aucune modification des forces n'est observée avec des concentrations élevées en sucre.

3.5.7. Colmatage de membranes polymériques par des protéines [4]

Collaboration : G. Belfort (chimie, Troy, NY, USA)

J'ai effectué ce travail lors de mon séjour au laboratoire de bioséparation et biocatalyse dirigé par le professeur G. Belfort au Rensselaer Polytechnic Institute (RPI) à Troy, NY. G. Belfort tentait en particulier de résoudre le problème non compris du colmatage qui limite la séparation de molécules biologiques par des filtres [Belfort et al., 1993 ; Fane et Fell.,1983 ; Mattiasson, 1983 ; Nystrom et al., 1990 ; McDonogh et al., 1990 ; Robertson et Zydney, 1990]. Nous avons testé les différentes hypothèses sur l'origine de ce colmatage, en mesurant l'interaction entre diverses protéines et l'acétate de cellulose, une membrane fréquemment utilisée. Nous avons montré que le colmatage de cette membrane est dû davantage à la dénaturation des protéines qu'à l'adsorption de la protéine sur le filtre.

3.5.8. Les protéines dénaturées se comportent-elles comme un polymère flexible ? [1]

Collaboration : G. Belfort (chimie, Troy, NY, USA)

Les protéines dénaturées étaient souvent assimilées à des polymères flexibles bien qu'aucune preuve directe n'ait été apportée. Nous avons testé, au RPI, cette hypothèse avec deux protéines, en comparant les forces entre deux couches dans le cas natif puis dans le cas dénaturé. Il est

apparu que l'albumine dénaturée se comporte effectivement comme un polymère flexible, ce qui n'est pas le cas de la ribonucléase.

3.5.9. Étude de l'influence de la colle dans le SFA [5]

Collaboration : J. Wolfe (U.N.S.W., Kensington, Australie)

L'influence de la colle qui est utilisée pour fixer les feuilles de mica dans les expériences avec le SFA était controversée. Les attractions à longue distance observées entre surfaces hydrophobes lui étaient parfois attribuées. En collaboration avec J. Wolfe, nous avons effectué une étude prouvant que la colle ne contamine pas l'appareil.

3.5.10. Bibliographie de la partie 3.5.

Belfort, G.; Pimbley, J. M.; Greiner A., Chung, K-Y., *J. Membr. Sci.*, **77,** 1-22, (1993)**.**

Bourdieu, L.; Silberzan, P.; Chatenay, D. *Phys. Rev. Lett.*, *67*, 2029-2032, (1991).

Fane, A.G., Fell, C. J.; Suzuki, A., *J. Membr. Sci.*, **16**, 195-210, (1983).

G. Gaines, Insoluble monolayers at liquid-gas interfaces (Interscience publishers, New York, 1966).

Helm, C. A., Israelachvili, J. N. & McGuiggan, P. M. (1992) *Biochemistry* **31,** 1794-1805.

Hui, S. W.; Viswanathan, R.; Zasadsinski, J. A.; Israelachvili, J. N. *Biophys. J.*, *68*, 171-178, (1995).

Israelachvili, J. N., Mitchell, D. J. & Ninham, B. W. (1977) *Biochimica et Biophysica Acta* **470,** 185-201.

Langmuir, I., J. Chem. Phys., **1**, 756-776 (1933).

McDonogh, R. M.; Bauser, H., Stroh, N., Chmiel, H., *Desalination*, **79**, 217-231, (1990).

Mattiasson, E., *J. Membr. Sci.*, **16**, 23-36 (1983).

Nystrom, M., Laatikainen, M., Turku, M.; Jarvinen, P., *Prog. Colloid Polym. Sci.*, **52**, 321-329, (1990).

Olbrich, K., Rawicz, W., Needham, D. & Evans, E. (2000) *Biophys J* **79,** 321-327.

Parsegian, V. A., et Gershfeld, N. L., *Biophys. J.*, **64,** 222A, (1993).

Robertson, B. C., et Zydney, A. L., *J. Colloid Interface Sci.*, **134**, 563-575, (1990).

Saenger, W. Principles of Nucleic Acid Structure (Springer-Verlag, New York, 1984)

Wolfe, J., Perez, E., Bonanno, M. & Chapel, J. P. (1991) *Eur Biophys J* **19,** 275-281.

3.6. Conclusion : un pôle micromanipulation français ouvert vers l'extérieur

Au milieu des années 90, les techniques de micromanipulation étaient pratiquement inexistantes en France. J'ai construit trois techniques de micromanipulation qui m'ont permis de mener des études de pointe et variées en physique, chimie et biologie et de participer de façon active au développement de ces approches, au niveau national et international. Depuis lors, d'autres équipes que la notre ont été intéressées par la micromanipulation et ont souhaité monter leur propre système afin de résoudre un problème précis. Outre les nombreuses collaborations

initiées, l'expérience que j'avais acquise m'a permis d'aider ces équipes et de les conseiller quand un problème se présentait à eux. J'ai ainsi interagi avec de nombreuses équipes en France et à l'étranger. Trois de ces équipes, F. Bruckert (Grenoble), D. Roux (Bordeaux) et J. Rothman, New York), sont venues faire des expériences préliminaires sur notre équipement afin de vérifier la faisabilité de leur projet, et ont décidé de s'inspirer de l'un de nos systèmes expérimentaux pour réaliser le leur.

4. Programme de recherches : Machinerie cellulaire ; signalisation, fusion et transmigration

Les techniques de micromanipulation que j'ai développées sont maintenant parfaitement opérationnelles. Les premières études et les publications relatives sont achevées. Je souhaite maintenant élargir l'éventail de mes recherches en m'intéressat à la physique de quelques aspects de la machinerie cellulaire, en particulier, la signalisation (§4.1.), la fusion membranaire (§4.2.) et la transmigration (§4.3.). Je désire également travailler sur quelques projets de physique « pure » (§4.4.). Certains de ces projets sont déjà entamés.

4.1. Signalisation intra cellulaire

Contrat Dynamique et Réactivité des Assemblages Biologiques 2004

Lors des travaux sur la fraktalkine (§3.2.3.) et sur les cadhérines (§3.2.4.), j'ai déjà été sensibilisé au problème omniprésent de la signalisation cellulaire. L'adhésion y est omniprésente. En effet, elle est assurée par des familles de récepteurs portés à la surface des cellules, en particulier les cadhérines, impliquées dans l'adhérence entre cellules, et les intégrines permettant l'adhérence à la matrice extracellulaire. L'interaction de ces récepteurs avec leurs ligands spécifiques forme des complexes adhésifs qui activent des voies de signalisation cytoplasmique, induisent une réorganisation du cytosquelette et régulent l'expression génique. Plusieurs faits expérimentaux suggèrent l'existence d'un « dialogue » entre cadhérines, intégrines et le cytosquelette aboutissant à une modulation de l'adhérence. J'aimerais donc caractériser ce dialogue en collaboration avec une équipe de biologistes (S. Dufour) spécialiste des cadhérines et de l'adhérence et une équipe de chimistes-biologistes (J. Parello, San Diego) spécialiste des intégrines. Nous utiliserons des approches utilisant la micromanipulation, l'imagerie, la mutagenèse dirigée et la synthèse de nouveaux effecteurs agonistes ou antagonistes de l'adhérence.

4.2. fusion membranaire

La fusion membranaire n'est pas un domaine qui m'est complètement étranger, puisque je l'ai déjà abordée sur des systèmes modèles (§3.4.2. et §3.4.3.). Cependant, j'aimerais maintenant passer à des objets plus biologiques, car la fusion est un problème central de la machinerie cellulaire. En effet, les cellules biologiques contiennent des vésicules qui permettent le transport de composés variés entre les différents compartiments cytoplasmiques. Ce trafic membranaire, indispensable à la vie de la cellule et à sa division nécessite la fusion entre la membrane de la vésicule de transport et celle du compartiment cible. La fusion membranaire est contrôlée par deux protéines: la v-SNARE et la t-SNARE qui sont implantées respectivement dans la membrane de la vésicule et dans celle du compartiment cible. Quand les protéines SNARE s'assemblent, elles accrochent ensemble les deux membranes et exercent une force sur celles-ci, conduisant ainsi à la fusion. Cependant, le mécanisme de fusion n'est pas connu. Une meilleure connaissance de celui-ci (structure des complexes, nombre de complexes, énergies impliquées dans la fusion des membranes etc…) pourrait permettre de mieux maîtriser certaines pathologies et servir au développement de nouvelles thérapies. J'aimerais, en collaboration avec J. Rothman, obtenir des informations sur les changements conformationnels et les énergies impliquées dans l'assemblage des membranes. Pour cela, il est possible d'incorporer des protéines SNARE dans des membranes de cellules ou des bicouches lipidiques et de mesurer

leurs énergies d'adhésion à l'aide d'une machine à force entre surfaces (SFA) et par micromanipulation de cellules et de vésicules. La haute résolution en distance du SFA donnera aussi des renseignements sur la conformation des protéines, comme l'ont confirmé des expériences préliminaires. Cette collaboration se met actuellement en place.

4.3. Transmigration

Dans les années à venir, j'aimerais aussi aborder un autre thème fondamental en biologie pour lequel je suis convaincu qu'une étude physique peut apporter des informations pertinentes : la diapédèse, c'est-à-dire la migration de cellules à travers des couches cellulaires. Ce phénomène joue un rôle notamment lors du passage de globules blancs à travers les parois de vaisseaux sanguins. Etre capable de visualiser (lumière directe et fluorescence) la diapédèse constituerait déjà une première étape car jusqu'à présent aucune visualisation nette n'a jamais été obtenue. Ensuite, des mesures de forces ainsi que des contraintes mécaniques exercées sur les cellules traversant un tissu devraient permettre de quantifier ces phénomènes. Je suis actuellement en train de définir avec l'équipe de P. Deterre de l'hôpital Pitié-Salpétrière différentes approches pour entamer cette étude. Nous avons déjà envisagé la construction d'une chambre permettant la visualisation de la diapédèse dans des conditions proches de celles qui existent dans un vaisseau sanguin.

4.4. projets de physique « pure » fondés sur l'expérience acquise

Simultanément, je souhaiterais mettre à profit l'expérience que j'ai acquise pour entamer des travaux n'ayant que peu de lien avec la biologie. Le premier thème, déjà entamé dans le cadre de la thèse d'O. Marnette, concerne les transitions de phase dans les systèmes bidimensionnels de sphères dures polydisperses. Ces systèmes bidimensionnels de sphères dures ont un lien étroit avec les transitions vitreuses, mais modélisent aussi les interactions dans d'autres systèmes comme les réseaux de vortex dans des supraconducteurs. C'est la polydispersité qui joue le rôle de désordre. Le projet est de faire des phases bidimensionnelles de sphères dures avec des microbilles traitées de façon appropriée et piégées à l'interface de deux liquides. Le diagramme de phases pourra être exploré par observation directe au microscope en faisant varier la densité surfacique et la polydispersité des particules. Pour chaque condition, les positions des sphères dures et les fonctions de corrélation de paires caractéristiques de l'état du système seront mesurées. Selon les calculs théoriques, ce diagramme de phases est très riche et devrait montrer des transitions liquide/solide, ou des transitions vitreuses selon la densité et la polydispersité. La mesure de la diffusivité, par suivi individuel de particules, permettra de mettre en évidence cette transition vitreuse qui, par des observations statiques, reste indétectable. La faisabilité de l'étude a été démontrée au cours du séjour récent de G. Bryant au LPS qui a réussi à former des phases de sphères dures à l'interface entre deux liquides. La modélisation théorique des expériences sera faite avec W. Krauth par simulations Monte-Carlo qui permettent d'obtenir toutes les propriétés d'équilibre (diagramme de phases, facteur de structure) mais aussi les caractéristiques dynamiques du système. Ce projet est très étroitement relié au travail d'une autre équipe de théoriciens de l'ENS (P. Le Doussal), très actifs dans le domaine des systèmes désordonnés bidimensionnels.
Le deuxième travail que je souhaiterais mener à bien concerne l'étude de la forme d'une poutre flexible adhérant sur un substrat avec une adhésion contrôlée. Nous envisageons pour le moment de commencer avec un système macroscopique (poutre de diamètre ~ 1mm). Puis, si

les résultats s'avèrent satisfaisants, nous continuerons sur des systèmes à l'échelle microscopique. Cette étude se fera en collaboration avec Y. Pomeau du laboratoire et T. Frisch de l'IRPHE à Marseille.

La dernière étude concerne l'osmophorèse, phénomène décrit au début des années 80, mais pour le moment non encore observé de manière certaine. Il prédit qu'une capsule semi-perméable doit se déplacer en présence d'un gradient de soluté. Il s'agit d'une sorte de moteur osmotique. J'ai déjà conçu et fait construire par J. Quintas (mécanicien du laboratoire) un système expérimental qui j'espère permettra de mettre en évidence ce phénomène. Cette étude est menée en collaboration avec M. Jaeger (Marseille) qui a longuement travaillé sur sa quantification et grâce à qui il sera possible de trouver les paramètres optimaux pour espérer voir un effet de façon certaine (i.e. sans artefact dû à d'autres sources de mouvement comme des convections naturelles, des mouvements par effet Marangoni,…).

5. Publications dans des revues scientifiques

5.1. Revues avec comité de lecture

1. F.Pincet, E.Perez, G.Belfort, "Do denatured proteins behave like polymers?",. *Macromolecules*, **27**, 3424-3425 (1994).

2. F.Pincet, E.Perez, J.Wolfe, "Do trehalose and dimethyl sulfoxide affect inter-membrane forces?", *Cryobiology*, **31**, 531-539 (1994).

3. F.Pincet, E.Perez, G.Bryant, L.Lebeau, C. Mioskowski, "Long-range attraction between nucleosides with short-range specificity", *Physical Review Letters*, **73**, 2780-2783 (1994).

4. F.Pincet, E.Perez, G.Belfort, "Molecular interactions between proteins and synthetic membrane polymer films", *Langmuir*., **11**, 1229-1235 (1995)

5. F. Pincet, E. Perez et J. Wolfe, "Does the glue contaminate the Surface Forces Apparatus?"; *Langmuir*., **11**, 373-374 (1995)

6. F. Pincet, E. Perez, L. Lebeau et C. Mioskowski,""H-Bond specific interactions between nucleosides have long-range", *Faraday Transactions*, **91**, 4329-4330 (1995)

7. F. Pincet, E. Perez, G.Bryant, L. Lebeau , C. Mioskowski, "Specific Forces Between DNA bases", *Mod. Phys. Lett. B.*, **10**, 81-99 (1996)

8. F. Pincet, W. Rawicz, E. Perez, L. Lebeau , C. Mioskowski and E. Evans, "Electrostatic nanotitration of weak biochemical bonds", *Physical Review Letters*, **79** (10), 1949-1952 (1997).

9. P. Bassereau, F. Pincet, "Quantitative Analysis of Holes in Supported Bilayers Providing the Adsorption Energy of Surfactants on Solid Substrate", *Langmuir*, **13**, 7003-7007 (1997).

10. E. Perez, F. Pincet, M. Goldman, C. Mioskowski, L. Lebeau, "Translational order in liquid-expanded lipid-expandedlipid monolayers functionalized with nucleosides", *Eur. Phys. J. B*, **6**, 1-4 (1998).

11. F. Pincet, S. Cribier, E. Perez, "Bilayers of neutral lipids bear a small but significant charge", *Eur. Phys. J. B,* **11**, 127-130 (1999)

12. F. Pincet, T. Le Bouar, Y. Zhang, J. Esnault, J.M. Mallet, E. Perez, P. Sinay, "Ultraweak sugar-sugar interactions for transcient cell adhesion", *Biophys. J.* **80**,1354-1358 (2001)

13. J. Esnault, JM. Mallet, Y. Zhang, P. Sinay, T. Le Bouar, F. Pincet, E. Perez, "New highly hydrophobic lewis x glycolipids: synthesis and monolayer behaviour", *European Journal of Organic Chemistry,* **2001**, 253-260 (2001)

14. F. Pincet, L. Lebeau, S. Cribier, "Short-range specific forces are able to induce hemifusion" *Eur. Biophys. J.* **30** (2001) 91-97.

15. F. Pincet, E. Perez, J.-C. Loudet, L. Lebeau "From macroscopic adhesion energy to molecular bonds: a test of the theory", *Physical Review Letters*, **87**, 178101 1-4, (2001)

16. D. Tareste, F. Pincet, E. Perez, S. Rickling, C. Mioskowski, and L. Lebeau "Energy of Hydrogen Bonds Probed by the Adhesion of Functionalized Lipid Layers ", *Biophys. J.* **83**, 3675-3681, (2002)

17. G. Bryant, S. R. Williams, L. Qian, I. K. Snook, E. Perez, and F. Pincet, "How hard is a colloidal "hard-sphere interaction? ", Phys. Rev. E **66**, 060501(R) (2002)

18. S. Sarda, D. Pointu, F. Pincet, and N. Henry, "Specific Recognition of Macroscopic Objects by the Cell Surface: Evidence for a Receptor Density Threshold Revealed by Micrometric Particle Binding Characteristics", Biophys. J. **86**: 3291-3303 (2004)

19. J. Heuvingh**,** F. Pincet, S. Cribier "Hemifusion and fusion of giant vesicles induced byreduction of inter-membrane distance", Eur. Phys. J. E **14**, 269–276 (2004)

20. M. Daoudi, E. Lavergne, A. Garin, N. Tarantino, P. Debré, F. Pincet, C. Combadière, and P. Deterre, "Enhanced adhesive capacities of the naturally occurring I249-M280 variant of the chemokine receptor CX3CR1", J. Biol. Chem., **279**, 19649-19657 (2004).

21. C. Gourier, F. Pincet, E. Perez, Y. Zhang, J.-M. Mallet, P. Sinay, "Specific and non specific interactions involving LeX determinantquantified by lipid vesicle micromanipulation", Glycoconjugate J., **21**, 165-174 (2004).

22. C. Gourier, F.Pincet, T. Le Bouar, Y. Zhang, J. Esnault, J.-M. Mallet, P. Sinay, and E. Perez, "Can Small Complex Chains Be Treated as Polymers?", *Macromolecules,* **37**, 8778-8784, (2004).

23. Y. Chu, W. Thomas, O. Eder, F. Pincet, E. Perez, J.-P. Thiery, and S. Dufour, "Force measurements in E-cadherin-mediated cell doublets reveal rapid adhesion strengthened by actin cytoskeleton remodelling through Rac and Cdc42", *J. Cell. Biol.*, **167**, 1183-1194 (2004).

24. C. Gourier, F. Pincet, E. Perez, Y. Zhang, Z. Zhu, J.-M. Mallet, and P. Sinay, "The natural Lewix X bearing lipids promote membrane adhesion. Influence of ceramide on carbohydrate-carbohydrate recognition", *Angewandte Chemie* (2005), accepté, sous presse.

25. C. Martinez-Rico, F. Pincet, E. Perez, J.-P. Thiery, K. Shimizu, Y. Takai, and S. Dufour, "Separation force measurements reveal different types of modulation of E-cadherin-based adhesion by nectin-1 and –3", *J. Biol. Chem.*, (2005), accepté, sous presse.

26. Y. Chu, S. Dufour, J.-P. Thiery, E. Perez, and F. Pincet, "Johnson-Kendall-Roberts theory applied to living cells", *Physical Review Letters*, **94,** 028102 1-4 (2005)

27. D. Tareste, F. Pincet, M. Brellier, C. Mioskowski, and E. Perez, "The binding of two chelating molecules by a metal ion", *Journal of the American Chemical Society*, (2005), accepté sous presse..

28. N. Rodriguez, F. Pincet, S. Cribier, "Giant vesicles formed by gentle hydration and electroformation : a comparison by fluorescence microscopy", *Coll. Surf. Sc. B.,*(2005) , accepté sous presse.

29. S. Poteau, J.-F. Argillier, D. Langevin, F. Pincet, and E. Perez, "Influence of pH on stability and dynamic properties of asphaltenes and other amphiphilic molecules at the oil water interface", *Energy & Fuels*, (2005), accepté sous presse.

5.2. autres publications

1. F. Pincet, "Mesures directes d'interactions spécifiques et non spécifiques entre membranes biologiques modèles".Thèse de doctorat de l'université Paris VI (1994).

2. F. Pincet, E. Perez, L. Lebeau et C. Mioskowski,"En direct des forces qui animent l'ADN", *La Recherche*, **26**, 684 (Juin 1995)

3. F. Pincet, "Phénomène d'adhésion : lipides, de la bicouche à la molecule unique", *Les écoles Physique et Chimie du Vivant, CNRS : Cahier n°2 : Energies et Forces de l'interaction entre macromolécules biologiques : l'aspect quantitatif*, 39-45 (2000).

4. F..Pincet, E. Perez, J.C. Loudet, L. Lebeau, "Interactions between bio-functionnalised surfaces", 5th *European adhesion conference*, 21 (2000).

5. F..Pincet, E. Perez, J.C. Loudet, L. Lebeau, "Des molécules reconnaissantes si attachantes…", *CNRS info* **399**, 6 (2002).

6. F. Pincet "Mechanical measurements of intermolecular and adhesive forces", *Atelier de Formation n°48, INSERM: Role of mechanical constraints in cell biology: nanomanipulations by optical and magnetic tweezers*, 21 (2003).

7. F. Pincet, C. Gourier, D. Tareste, E. Perez, "Energies of weak biochemical bonds from physical and colloidal methods", *Recent Res. Devel. Surface & Colloids*, **1**, 343-366 (2004).

8. F. Pincet, "Adhesion of a Cell on a Substrate", *Dekker Encyclopedia of Nanoscience and Nanotechnology*, 11 - 21 (2004).

6. Conférences

6.1. Conférences invitées

1. F. Pincet, E.Perez, G.Bryant, L.Lebeau, C. Mioskowski, "Mesures directes de forces spécifiques entre monocouches d'amphiphiles fonctionnalisés", Réunion des instituts de la Montagne Sainte Geneviève, 6-7 mai 1994, intitulée "Des films moléculaires aux biomembranes".

2. F. Pincet, "Interactions between membranes decorated with specific nucleosides", CIAR SSSI spring meeting, Ladysmith, Vancouver island, B.C., Canada, 27-30 avril 1996.

3. F. Pincet, "Phénomènes d'adhésion : lipides, de la bicouche à la molécule unique", Ecole Physique et Chimie du Vivant, intitulée "Energies et forces de l'interaction entre macromolécules biologiques : l'aspect quantitatif", 25-27 octobre 1999, Garchy.

4. F. Pincet, S. Cribier, "Vésicules fonctionnalisées : approche de la fusion membranaire", Groupe d'Etude des Interactions Molécules Membranes 8, Anglet, 6-9 octobre 1998.

5. F. Pincet, "Phénomène d'adhésion : lipides, de la bicouche à la molecule unique", *Les écoles Physique et Chimie du Vivant, CNRS : Energies et Forces de l'interaction entre macromolécules biologiques : l'aspect quantitatif*, septembre 1999.

6. F. Pincet, E. Perez, M. Goldman, C. Mioskowski, L. Lebeau, "Les nucléosides en tant qu'adhésifs", Séminaire Adhésion – Agrégation des Micro-organismes, Nancy, 21-23 février 2000.

7. F. Pincet, "Adhérence de membranes : de la surface macroscopique à la liaison unique", Regards de physiciens sur les systèmes d'intérêt biologique, MOLBIO2000, 5-6 juin 2000, Lyon .

8. F. Pincet, "Mesure d'adhésion entre vésicules : de la surface macroscopique à la liaison unique", Journée "Techniques de mesure de forces colloïdales ou moléculaires", CRPP, février 2001, Bordeaux, France.

9. F. Pincet, "hemifusion de bicouches lipidiques par transition de phase", réunion du réseau PCV "aspects physicochimiques de la fusionmembranaire" :, Toulouse, 16 mai 2001, F. Pincet.

10. F. Pincet., "Rôle de la proximité des membranes dans la fusion", Réunion du club exocytose, avril 2002, Paris.

11. F. Pincet, "Machine de force d'Israelachvili (forces entre surfaces solides)", Journées INRA : Biopolymères aux interfaces dans les mousses, émulsions, matériaux et systèmes biologiques, Nantes, 25-26 novembre 2002.

12. F. Pincet, "Mechanical measurements of intermolecular and adhesive forces", atelier de formation INSERM n°148: Role of mechanical constraints in cell biology: nanomanipulations by optical and magnetic tweezers, novembre 2003.

13. F. Pincet, 9èmes journées de la matière condensée, Nancy, 30 août – 1er septembre 2004 : "Adhésion de cellules vivantes : du modèle physique à l'application biologique".

6.2. Conférences internationales avec comité de lecture

(auxquelles viennent s'ajouter plusieurs dizaines de conférences présentées par des co-auteurs)

1. F. Pincet, E. Perez, L. Lebeau and C. Mioskowski, "Specific interactions between nucleosides", EUCHEM conference de "the Swedish Chemical Society": "Surface Forces in Science and Technology", Skytteholm, Sweden, 14-18 June 1995.

2. F. Pincet, E. Perez, L. Lebeau, C. Mioskowski, "Forces involved in recognition of DNA bases", 70th Colloid and Surface Science Symposium, Clarkson university, Postdam, N.Y., USA., 16-19 juin 1996.

3. F. Pincet, E. Perez, L. Lebeau and C. Mioskowski, E. Evans, "Specific Interactions between complementary bases of DNA", Congrès de l'EBSA, Orléans, 13-17 juillet 1997.

4. F. Pincet, E. Evans, E. Perez, "Nucleoside lipids as adhesives", Amphiphiles at Interfaces : From Structure Control to Properties, Pékin, 24-29 mai 1999.

5. F. Pincet, L. Lebeau, E. Perez, "Adhesion of functionalized surfaces", 74th Colloid and Surface Science Symposium, Bethlehem, Pennsylvanie, USA, 18-23 juin 2000.

6. F. Pincet, E.Perez, "Specific Adhesion: From Macroscopic Surfaces to Single Bonds", 3rd European Biophyics Congress, Munich, Allemagne, 9-13 Sep. 2000.

7. F. Pincet, E.Perez, "Specific Adhesion between Biological Membranes", International Conference on Colloid and Surface Science, Tokyo, Japon, 5-8 Nov. 2000.

8. F. Pincet, C. Gourier, E. Perez, "Cell adhesion : theory and experiment", 76th ACS Colloid and Surface Science Symposium, Ann Arbor, USA, 23-26 juin 2002.

9. F. Pincet, C. Gourier, E. Perez, "Adhesion of a cell on a substrate: theory and experiment"., Congrès de l'ECIS, Paris, 21-27 septembre 2002.

10. Y. Chu, S. Dufour, J. P. Thiery, E. Perez and F. Pincet "Probing of depletion induced cell adhesion by micromanipulation and influence of the cytoskeleton", 77th Colloid and Surface Science Symposium, Atlanta, Georgia, USA, 15-18 juin 2003.

11. F. Pincet, J. Husson, C. Gourier, E. Perez, "How to interpret single bond measurements", 78th Colloid and Surface Science Symposium, Yale, New Haven, Connecticut, USA, 20-23 juin 2004.

12. F. Pincet and J. Husson "A Solution to the Streptavidin-Biotin Paradox?", MRS 2005 Spring Meeting, San Francisco, 28 mars – 1 avril 2005.

13. F. Pincet, S. Cribier and N. Rodriguez, "Controlled Object Delivery in Aqueous Medium through Large Pores", MRS 2005 Spring Meeting, San Francisco, 28 mars – 1 avril 2005.

6.3. Autres conférences

1. F. Pincet, E. Perez, G. Bryant, L. Lebeau, C. Mioskowski, "Interactions physico-chimiques et adhésion membranaire"IIème Forum de la biologie, les 21 et 22 novembre 1994.

2. F. Pincet, S.Cribier, E. Perez, E.Evans, "reconnaissance moléculaire et adhésion cellulaire", Rencontre de la Montagne Sainte Geneviève, Institut Curie, 22-23 avril 1997.

3. F. Pincet, "Direct measurement of binding energies", GDR Modélisation des Assemblages Moléculaires Complexes, IBPC, Paris, 18-19 septembre 1997.

4. F. Pincet, E. Perez, "mesures directes d'énergie de liaison", GDR Films Moléculaires Bidimensionnels, Aix les Bains, 20-22 octobre 1997.

5. F. Pincet, E. Evans, E.Perez., "Vésicules fonctionnalisées comme outil d'étude de la fusion membranaire", GDR Films Moléculaires Bidimensionnels, Roscoff, 30 septembre-3 octobre 1998.

7. Séminaires sur invitation

1. "Interactions spécifiques et non spécifiques entre membranes biologiques modèles". Laboratoire de Physique Théorique, ENS, Paris, Novembre 1994.

2. "Le SFA: une nouvelle technique pour mesurer les interactions spécifiques?" Laboratoire d'Etude des fluides granulaires et supramoléculaires, Rouen, Janvier 1995.

3. "Mesures directes d'interactions spécifiques et non spécifiques entre molécules d'intérêt biologique", Institut Curie, Paris. Juin 1995.

4. "Interactions spécifiques et non spécifiques entre molécules d'intérêt biologique", Laboratoire de Physique des Matériaux Industriels, Pau. Janvier 1996.

5. "Interactions spécifiques et non spécifiques entre molécules d'intérêt biologique", Institut de Chimie de Surfaces et Interfaces, Mulhouse. Janvier 1996.

6. "Mesures directes d'interactions spécifiques et non spécifiques", Laboratoire de Dynamique des Phases Condensées, Montpellier. Février 1996.

7. "Direct measurements of specific interactions between DNA base", Department of Chemical Engineering, Rensselaer Polytechnic Institute, Troy, NY, USA, Juin 1996.

8. "Reconnaissance moléculaire et adhéson cellulaire", Spectrometrie Physique, Grenoble, Mars 97.

9. "La reconnaissance moléculaire entre nucléosides: effets collectifs et individuels", Institut de Physique, Université Louis Pasteur, Strasbourg. Mars 97.

10. "Reconnaissance moléculaire et adhésion cellulaire", Laboratoire de Physique de la Matière Condensée, ENS, Paris. Avril 97.

11. "Energy and force measurements : from macroscopic surfaces to single bonds", Laboratoire d'Immunologie, INSERM U 387, Hopital de Sainte-Marguerite, Marseille, 25 avril 2000.

12. "Adhérence de membranes : de la surface macroscopique à la liaison unique", Magistère interuniversitaire de Physique de l'ENS, 28 avril 2000

13. "adhérence de membranes: de la surface macroscopique à la liaison unique", Laboratoire de Physique des Lasers, Institut Galilée, Villetaneuse, 20 octobre 2000.

14. "Adhérences par sites : liaison unique et comportements collectifs", Séminaire Matière Molle et Biologie, Jussieu, 19 janvier 2001.

15. "Liaison unique et comportements collectifs", Institut Curie, 6 juin 2001.

16. "Adhérences par sites : liaison unique et comportements collectifs", Service de Physique Théorique, séminaire général, 16 octobre 2001.

17. "Un modèle simple d'adhérences par sites, vérification expérimentale et applications", ENS, Séminaire biophysique, 23 novembre 2001

18. "Adhérences par sites, fusion membranaire et liaison unique", IUSTI, Marseille, 21 juin 2002. 14 mars 2003.

19. "Dynamique de l'adhésion cellulaire: de la cellule à la molécule", Laboratoire de Physique du Solide, Orsay.

20. "Adhésion cellulaire: de la cellule à la molécule", Institut Charles Sadron, Strasbourg, 3 juin 2003

21. "Modèles d'adhésion cellulaire. Exemples d'applications", Physico-chimie, pharmacotechnie, biopharmacie, Chatenay-Malabry, 3 février 2004

22. "Une physique appliquée à la biologie ? Exemple de l'adhésion cellulaire", CRPP, Pessac, 7 octobre 2004.

8. Longs séjours à l'étranger

1. "Mesures directes d'interactions polymères-protéines", au **Department of Chemical Enginnering, Rensselaer Polytechnic Institute, Troy, New York, USA**, décembre 1990-mars 1992

2. "énergie de liaison entre bases de l'ADN", **Department of Physics and Pathology, University of British Columbia, Vancouver, British Columbia, Canada,** avril-mai 1996 puis octobre-novembre 1996.

9. Direction de thèses et encadrement de chercheurs

1. J. Heuvingh : **Thèse** de doctorat de l'université Paris 11 (spécialité Champs, Particules, Matière) co-encadrée avec S. Cribier et intitulée: "Hémifusion de vésicules géantes : caractérisation d'un état intermédiaire vers la fusion, en présence de forces spécifiques" soutenue la 19 novembre 2002. J. Heuvingh est maintenant A.T.E.R. à Paris 5.

2. N. Rodriguez : étudiant en troisième année de **thèse** (université Paris 6) sur le sujet : "formation et dynamique depores dans des vésicules géantes"**,** co-encadrée par S. Cribier.

3. J. Husson: étudiant en troisième année de **thèse** (université Paris 6), intitulée: "comment interpréter les forces de rupture de liens uniques. Exemple d'une ancre membranaire", co-encadrée par Eric Perez.

4. C. Berger: **postdoc** hollandais, mai 2002 – avril 2003, sur le thème: "lien unique entre un ARN et une protéine".

J'ai aussi participé à l'encadrement des thésitifs suivants :

5. T. Le Bouar: **Thèse** de doctorat de l'université Paris 6, intitulée: "étude de la reconnaissance entre oligosaccharides impliqués dans l'adhésion cellulaire", dirigée par E. Perez et soutenue le 16 septembre 1997.

6. D. Tareste : **Thèse** de doctorat de l'université Paris 6, intitulée: "liaisons par chélation et liansons hydrogène : une mesure directe", dirigée par E. Perez et soutenue le 20 septembre 2002.

7. O. Marnette: étudiant en deuxième année de **thèse** (université Paris 6), intitulée: "Transitions de phases dans les systèmes de sphères dures à deux dimensions", dirigée par Eric Perez.

8. Y. Chu: étudiant en quatrième année de **thèse** (université Paris 6), intitulée: "Adhésion de cellules exprimant des cadhérines", dirigée par Sylvie Dufour (Institut Curie).

9. M. Daoudi: étudiant en quatrième année de **thèse** (université Paris 6), intitulée: "Une mutation naturelle d'un récepteur de chimiokine : de l'adhésion à la pathologie", dirigée par Philippe Deterre (Pitié-Salpétrière).

Participation à des jurys de thèses:
S. Pierrat: "Etude de l'adhésion cellulaire à différentes échelles: de la molécule unique à la cellule" Thèse soutenue le 28 avril 2004 à l'Institut Curie , Paris (rapporteur)

10. Encadrement de stagiaires

1. Elsa Joo (Magistère Interuniversitaire de Physique, septembre-octobre 1996)
2. Thierry Guillet (Magistère Interuniversitaire de Physique, juillet 1997)
3. Karim Benabed (DEA de physique théorique, février 98)
4. Cécile Leduc (Magistère de physique, Lyon, juin-juillet 1998)
5. Karol Borejsza (Magistère Interuniversitaire de Physique, septembre 1998)
6. Jean Christophe Loudet (DEA de physique des liquides, janvier-juin 1999)
7. Raphaël Voituriez (DEA de physique théorique, février 1999)
8. Mehdi Daoudi (Maîtrise de biologie, janvier-septembre 1999)
9. Thomas Blon (IUT mesures physiques, Orsay, avril-juin 1999)
10. Julien Heuvingh (DEA Champs Particules Matière, juin 1999)
11. Olivier Legrand (Magistère Interuniversitaire de Physique, septembre 1999)
12. Florence Rosset (IUT mesures physiques, Orsay, novembre 99 - février 2000)
13. Samir Bouchouicha (IUT mesures physiques, Orsay, avril 2000 - juin 2000)
14. Marc Wouts (Cursus mixte Math-physique, ENS, février-mai 2001)
15. Bénédicte Faure (DEA de physique des solides, février-mars 2002)
16. Nicolas Rodriguez (DEA de physique des solides, février-mars 2002)
17. Samir Belkacem (IUT mesures physiques, Orsay, avril 2002 - juin 2002)
18. Sylvain Condamin (DEA de physique théorique, février 2002)
19. Cristian Vergu (Magistère Interuniversitaire de Physique, juillet 2003)
20. Marie Camille Delsuc (DEA Biophysique, janvier-juin 2004)
21. Juliette Simonet (Magistère Interuniversitaire de Physique, juillet 2004)
22. Mariem Chalbi (M2 « Ingénierie physique de la santé », février-juillet 2005)

11. Collaborations en France et a l'étranger

1. **G. Belfort (chimiste) du Department of Chemical Engineering, Rensselaer Polytechnic Institute, Troy, New-York, U.S.A**., dans le cadre de mon service national, thème : interaction protéine/polymère (1990-92).

2. **J. Wolfe (physicien) du Biophysics Department**, **U.N.S.W., Kensington, Australie**, thème : mécanisme d'action des molécules cryoprotectrices (Avril-Juillet 1993).

3. **L. Lebeau et C. Mioskowski (chimistes) du laboratoire de synthèse bio-organique, CNRS, Illkirch** thèmes: mesure des forces et énergie entre bases complémentaires de l'ADN (1992-2001), puis entre molécules formant des liaisons par chélation (1999-2004).

4. **P. Bassereau** (physicienne), Institut Curie, Paris, thème : formation de trous dans des bicouches supportées (1994-1997).

5. **E. Evans (physiciens) des departments of physics and pathology, UBC, Vanvouver, Canada**, thème: nanotitrage de liens faibles (1996).

6. **M. Goldman (physicien) de l'université Paris 5**, thème : ordre translationnel dans des monocouhes de type « liquide expansé » (1996-1998).

7. **J.-P. Thiery et S. Dufour (biologistes), de l'Institut Curie, Paris**, thème : adhésion de cellules exprimant des cadhérines (depuis 1997).

8. **S. Cribier (physicienne) de l'IBPC, Paris**, thèmes : hémifusion et fusion membranaire (1996-2002), puis formation de pores dans les membranes (depuis 2001)

9. **P. Sinay (chimiste) du département de chimie, ENS, Paris**, thème : interaction entre oligosaccharides (depuis 1997).

10. **C. Branlant (biologiste), CNRS, Nancy**, thème : lien unique ARN-protéine (1999-2003).

11. **P. Deterre (biologiste), Hôpital de la Pitié Salpétrière, Paris**, thème : étude d'une mutation naturelle d'un récepteur de chimiokine : de l'adhésion à la pathologie (depuis 2001).

12. **D. Gillet (biologiste) , CEA, Saclay**, thème : ancre protéique membranaire utilisée dans des vaccins antitumoraux.

13. **N. Henry (physicienne) de l'institut Curie, Paris**, thème : capture de particules par des cellules biologiques (2002-2004).

14. **A. Prochiantz et A. Joliot du département de biologie, ENS**, **Paris**, thème : mécanisme de traversée d'une membrane par un peptide cellule perméant (depuis 2002).

15. **R. Hodges (chimiste), Université d'Alberta, Calgary, Canada**, thème : lien unique peptide-membrane (deuis 2002).

16. **J. Rothman, Cellular Biochemistry and Biophysics ,Sloan-Kettering Institute, New York**, thème : fusion membranaire et protéines SNARE (depuis 2003).

17. **J-P. Wolffe (médecin), Université Paris 13,** thème : identification des protéines impliquées dans la reconnaissance spermatozoïde-ovocyte.

12. Contrats

Pour chaque contrat, j'ai indiqué la partie correspondante dans le rapport d'activité.
Contrat l'Oréal 1997 : §3.1.3.
Contrat Physico-Chimie du Vivant 1998 : §3.1.3.
Contrat Nano Objet individuel 1999 : §3.3.4.2.
Contrat Physico-Chimie du Vivant 1999 : §3.4.2.
Contrat Physico-Chimie du Vivant 2000 : §3.1.4.
Contrat Nano Objet Individuel 2000 : §3.3.3.
Contrat BQR Paris 7 2000 : §3.3.2.
Contrat Institut Curie 2001 : §3.2.4.
Contrat Dynamique et Réactivité des Assemblages Biologiques 2001 : §3.4.2.
Contrat Nano Science 2003 : §3.3.4.1.
Contrat INSERM Cardiovasculaire 2004 : §3.2.3.
Contrat Dynamique et Réactivité des Assemblages Biologiques 2004 : §4.1.

13. Enseignement

13.1 Formation initiale

Magistère Interuniversitaire de Physique (MIP) de l'ENS :

1. travaux dirigés de mathématiques (cours de J.P. GAZEAU, 1ère année du MIP), années 93/94, 94/95 et 95/96 (30 heures par an).
2. travaux dirigés de physique non linéaire (cours de P. MANNEVILLE, 1ère année du MIP), années 93/94, 94/95 et 95/96 (20 heures par an).
3. travaux dirigés du cours sur les surfaces et les interfaces (cours de J. DAILLANT, 2ème année du MIP), années 94/95 et 95/96 (20 heures par an).
4. Responsable des projets informatiques (1ère année du MIP), années 93/94, 94/95 et 95/96 et d'un projet expérimental (1ère année du MIP), années 94/95 et 95/96.
5. travaux pratiques d'optique (1ère année du MIP) années 93/94, 94/95 et 95/96.
6. travaux dirigés du cours « Physique statistique et biologie » (cours de B. Derrida, 2ème année du MIP), années 2000/01 et 01/02 , (18 heures par an)

Université Paris 6 :

1. cours magistral: « nanomanipulations de molécules biologiques », maîtrise de physique, années 95/96, 96/97 et 97/98 (12 heures par an).

Université d'Evry val d'Essonne :

1. cours magistral: « optique », licence de physique, années 2001/02, 02/03 et 03/04 (19,5 heures par an).

Université Paris 5 :

1. cours magistral « Micromanipulations », DESS Ingénierie Physique pour la Santé, années 2002/03, 03/04 (8 heures par an) et 04/05 (10 heures).

autres activités liées à l'enseignement :

1. Participations au jury de concours d'entrée aux grandes écoles.
    a. correcteur de l'épreuve de physique du concours d'entrée (mathématiques) à l'école normale supérieure de Paris, de 1994 à 1997.
    b. examinateur de l'épreuve de travaux pratiques de physique du concours d'entrée (physique) à l'école normale supérieure de Paris 1994, 96, 97 et 98.
    c. correcteur de l'épreuve de physique I du concours d'entrée (physique) à l'école Polytechnique, de 1997 à 2005.
2. Interrogations orales (« colles ») en classes préparatoires
    a. mathématiques mathématiques en classe de mathématiques supérieures à l'Institut Supérieure d'Electronique de Paris, de 1993 à 2005 (87 heures par an).
    b. Mathématiques en classe de mathématiques spéciales au lycée Michelet (Vanves) 1995/96 (48 heures).

13.2. Formation permanente

1. cours intitulé « Micromanipulaciones con micropipetas » (en Espagnol, école doctorale, université d'Hermosillo, Sonora, Mexique)(6h) (2003).
2. cours « Adhésion biologique: de la cellule à la molécule, du modèle au réel », Rencontres Non Linéaires de Peyresc, Peyresc (2,5 heures) (2004).

14. Responsabilités administratives et autres

1. Secrétariat du concours d'entrée à l'ENS (physique) (1995).
2. correspondant en physique des séminaires intermagistères (1997/98).
3. Responsable des séminaires du département de physique de l'ENS (1999/2000).
4. Organisation du minicolloque "Physiciens et biologistes: quels échanges?" aux Journées de la matière condensée, Nancy, 30 aout-4septembre 2004
5. Organisation des journées X-ENS-UPS destinées aux professeurs de classes préparatoires (mai 2003, mai 2004 et mai 2005)

15. Publications en annexe

1. Y. Chu, S. Dufour, J.-P. Thiery, E. Perez, and F. Pincet, “Johnson-Kendall-Roberts theory applied to living cells”, *Physical Review Letters*, **94,** 028102 1-4 (2005)

2. Y. Chu, W. Thomas, O. Eder, F. Pincet, E. Perez, J.-P. Thiery, and S. Dufour, “Force measurements in E-cadherin-mediated cell doublets reveal rapid adhesion strengthened by actin cytoskeleton remodelling through Rac and Cdc42”, *J. Cell. Biol.*, **167**, 1183-1194 (2004).

3. C. Gourier, F.Pincet, T. Le Bouar, Y. Zhang, J. Esnault, J.-M. Mallet, P. Sinay, and E. Perez, “Can Small Complex Chains Be Treated as Polymers?”, *Macromolecules,* **37**, 8778-8784, (2004).

4. M. Daoudi, E. Lavergne, A. Garin, N. Tarantino, P. Debré, F. Pincet, C. Combadière, and P. Deterre, “Enhanced adhesive capacities of the naturally occurring I249-M280 variant of the chemokine receptor CX3CR1”, J. Biol. Chem., **279**, 19649-19657 (2004).

5. S. Sarda, D. Pointu, F. Pincet, and N. Henry, “Specific Recognition of Macroscopic Objects by the Cell Surface: Evidence for a Receptor Density Threshold Revealed by Micrometric Particle Binding Characteristics”, Biophys. J. **86**: 3291-3303 (2004)

6. J. Heuvingh**,** F. Pincet, S. Cribier "Hemifusion and fusion of giant vesicles induced byreduction of inter-membrane distance", Eur. Phys. J. E **14**, 269–276 (2004)

7. F. Pincet, T. Le Bouar, Y. Zhang, J. Esnault, J.M. Mallet, E. Perez, P. Sinay, "Ultraweak sugar-sugar interactions for transcient cell adhesion", *Biophys. J.* **80**,1354-1358 (2001).

8. F. Pincet, E. Perez, J.-C. Loudet, L. Lebeau "From macroscopic adhesion energy to molecular bonds: a test of the theory", *Physical Review Letters*, **87**, 178101 1-4, (2001)

9. F. Pincet, W. Rawicz, E. Perez, L. Lebeau , C. Mioskowski and E. Evans, "Electrostatic nanotitration of weak biochemical bonds", *Physical Review Letters*, **79** (10), 1949-1952 (1997).

10. P. Bassereau, F. Pincet, "Quantitative Analysis of Holes in Supported Bilayers Providing the Adsorption Energy of Surfactants on Solid Substrate", *Langmuir*, **13**, 7003-7007 (1997).

Johnson-Kendall-Roberts Theory Applied to Living Cells

Yeh-Shiu Chu,[1] Sylvie Dufour,[1] Jean Paul Thiery,[1] Eric Perez,[2] and Frederic Pincet[2,*]

[1]*UMR 144, Centre National de la Recherche Scientifique et Institut Curie, 26 rue d'Ulm, 75248 Paris Cedex 05, France*

[2]*Laboratoire de Physique Statistique de l'Ecole Normale Supérieure, UMR8550, Centre National de la Recherche Scientifique et Universités Paris 6 et 7, 24 rue Lhomond, 75251 Paris Cedex 05, France*

(Received 19 December 2003; published 18 January 2005)

Johnson-Kendall-Roberts (JKR) theory is an accurate model for strong adhesion energies of soft slightly deformable material. Little is known about the validity of this theory on complex systems such as living cells. We have addressed this problem using a depletion controlled cell adhesion and measured the force necessary to separate the cells with a micropipette technique. We show that the cytoskeleton can provide the cells with a 3D structure that is sufficiently elastic and has a sufficiently low deformability for JKR theory to be valid. When the cytoskeleton is disrupted, JKR theory is no longer applicable.

DOI: 10.1103/PhysRevLett.94.028102 PACS numbers: 87.17.–d, 68.35.Np, 82.35.Lr, 87.80.Fe

A quantitative understanding of the adhesion of living cells is not often possible, and the study reported here is one of the rare exceptions. In contrast, the adhesion of solid elastic bodies has been extensively studied in the past, and a complete mathematical description has been derived [1]. In general, when the contacting surfaces adhere only weakly and deform little, the Derjaguin-Muller-Toporov approach [2] allows prediction of the behavior of the system. At higher adhesion and deformability, when adhering surfaces are subject to a separating force, there is a finite, nonzero contact area at separation. In this case, Johnson-Kendall-Roberts (JKR) theory [3] gives the relation between the pull off force F_s and the adhesion energy W_{adh} via the radii of curvature of the materials. For solid, homogeneous spheres,

$$W_{\mathrm{adh}} = 2F_s/(3\pi R_m), \tag{1}$$

where R_m is the harmonic mean of the radii of the two spheres.

Many experimental studies on simple elastic materials have verified this description [4]. Similarly, the relation between F_s and W_{adh} has been recently derived for spherical shells [5]:

$$W_{\mathrm{adh}} = F_s/(\pi R_m). \tag{2}$$

However, the adhesion of soft bodies such as cells is much more difficult to characterize. Several attempts to probe the adhesion strength of two biological cells have been made using techniques including shear flow or centrifugation [6]. Adhesion experiments using micromanipulation were conducted more than a decade ago [7,8] using red blood cells, which have well-defined membrane elasticity and a relatively simple, liquid interior. In contrast, it is much more difficult to extract quantitative results from adhesion measurements involving nucleated cells, which are often characterized by an irregular surface with folds and wrinkles and whose interior exhibits a complex rheology. Chien's group has developed a model inspired by Evans's results [9] involving the mechanical equilibrium of the cell membrane. Using this model, they measured the adhesion between cytolytic T cells and target cells [10,11]. Treating the separation of the cells as a peeling process, they analyzed their experiments in terms of adhesion energies and junction avidity.

The present study involves living cells that do not spontaneously adhere. We cause them to adhere through a depletion effect in the suspending medium. We show that, when the cytoskeleton of the cells has a complete 3D structure that maintains a slightly deformable spherical shape, JKR theory is applicable to relate the separation force to the adhesion energy. It gives an elastic modulus coherent with the one independently measured with a surface force apparatus (SFA) and with those found in the literature [12]. In this case, where the 3D cytoskeleton is responsible for their spherical shape, the cells do not behave like shells but like elastic spheres.

The general principle of our approach consists of micromanipulating two murine sarcoma S180 cells [13] with micropipettes, making them adhere in a highly concentrated dextran solution and balancing the depletion-induced adhesion by the aspiration pressure in a micropipette.

It is well documented that nonadsorbing, water-soluble polymers can induce an attraction of phospholipid bilayers [14,15]. The adhesion energy W_{adh} induced by the depletion of dextran has been measured experimentally on lipid vesicles [16] and analyzed theoretically [17]. de Gennes has derived the expression of W_{adh} as a function of the volume fraction of polymers ϕ:

$$W_{\mathrm{adh}} = (k_B T/a^2)\phi^{1.5}, \tag{3}$$

where $k_B T$ is the thermal energy and a the size of a monomer.

For this study, we used a protocol similar to that used by Chien's group [11]. It is described in Fig. 1. Before analyzing the adhesion behavior, we establish that the adhesion observed in the polymer solution is due only to this depletion effect. It was already known that S180 cells are devoid of intrinsic intercellular adhesion properties [18]

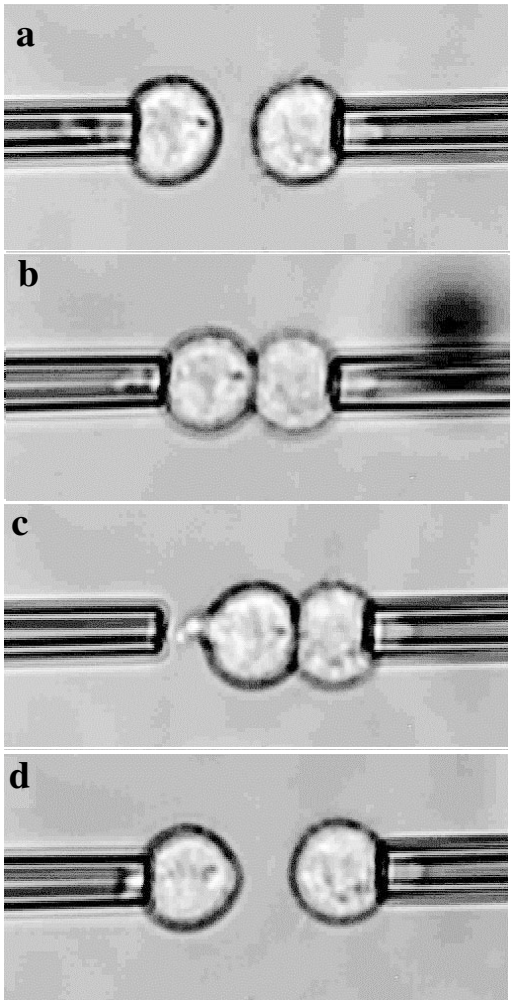

FIG. 1. (a),(b) Two cells, held under weak aspiration by micropipettes, are placed in contact and 1 s later became adherent. Separation process (c),(d): One cell is held by the right micropipette under strong aspiration. The aspiration applied to the other cell is increased and the right micropipette displaced away. Either the cell leaves the left micropipette (c) or both cells separate (d). In the first case, the cell is reseized by the left micropipette (b), the aspiration incremented, and the right micropipette displaced again. This cycle is repeated until the cells separate and the separation force is deduced from the last aspiration pressures. During the measurements, the pipettes were moved at a velocity of about 20 μm/s. The whole process of separation lasted 1 min at most. The aspiration level on pressure employed in each cycle was monitored continuously.

because they do not express cell-cell adhesion receptors at their surface. This is consistent with our observation that S180 cells brought to close contact do not adhere without dextran. In contrast, in the presence of dextran, S180 cells do adhere when they are mechanically pushed together with the micropipettes. Equilibrium under zero compression is reached after this mechanical constraint is removed (after less than a second). Further, the observation that adhering cells separated immediately after transfer in a dextran-free chamber shows that no receptor was activated during the adhesion phase. This indicates that the adhesion of S180 cells observed here was purely a depletion effect.

During separation, the cells appear elastic and slightly deformable (see Fig. 1) and the contact area at separation remains finite. Therefore, it is interesting to analyze the separation process with JKR theory and with the spherical shell model.

As shown by Yeung and Evans [19], the cells may display viscoelastic behaviors that could induce force gradients. To avoid any artifact due to this problem, we have checked that the aspiration force in the pipette equals the force transmitted to the contact zone: we used a direct method of probing this transmitted force by aspirating a cell in a 4–5 μm micropipette with a gentle suction and placing the opposite side of the cell on a spring (a microneedle with a known stiffness), the results of these force experiments indicate that, in the range of force, time, and velocity used, the measured force equals exactly the aspiration one.

Thus, it is possible to test the validity of JKR and spherical shell theories on these cells. The separation force F_s is close to the average of the aspiration forces of the penultimate cycle $n-1$ and the last cycle n:

$$F_s = \pi(\Delta P_{n-1} + \Delta P_n)R_p^2/2, \tag{4}$$

where R_p is the pipette inner radius, ΔP_i being the aspiration during cycle i.

The adhesion energy predicted by JKR and spherical shells theories can be calculated from the measurements of F_s and the radii of the cells. These values can be compared (Fig. 2) to the theoretical [17] expression for the energy due to the depletion effects [Eq. (3)] and the experimental measurements [16] of that energy. Figure 3 shows a very

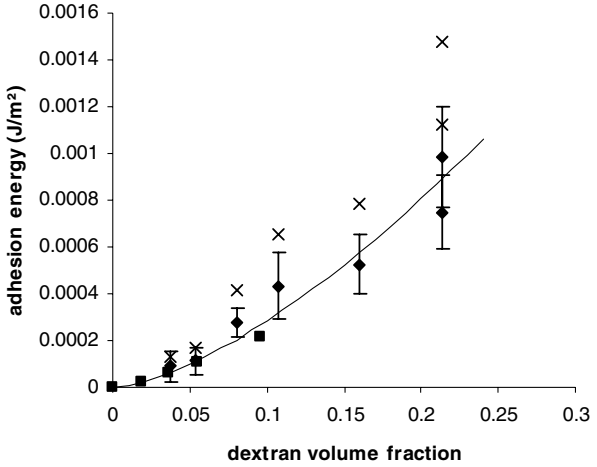

FIG. 2. Adhesion energy, as deduced from JKR theory [diamonds, Eq. (1)] and spherical shells [crosses, Eq. (2)] as a function of the volume fraction of dextran. Two sizes of dextran molecules (4.6×10^5 and 2×10^6 MW) were used. The results can be compared to the theoretical ones given by de Gennes [17] (line) and to experimental ones obtained by Evans by contact angle measurements on lipid vesicles [16] (squares).

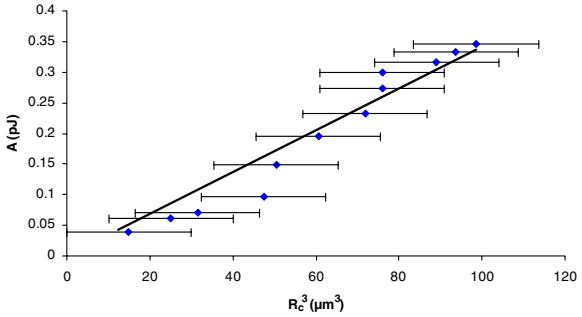

FIG. 3 (color online). Parameter $A = \frac{R_m}{2}[-F + 3\pi R_m W_{\text{adh}} + \sqrt{-6\pi R_m W_{\text{adh}} F + (3\pi R_m W_{\text{adh}})^2}]$ plotted as a function of R_c^3. As indicated in Eq. (5), in the case of JKR theory, the slope gives the elastic modulus. The large error bars are due to the low accuracy in the measurement of the contact radius in optical microscopy. The points are taken from three different experiments at various dextran volume fractions.

good agreement with JKR theory while spherical shells theory does not seem to be suitable.

To check that JKR theory is indeed valid, we have measured the variation of the contact area R_c during the separation process and deduced the elastic modulus K from the relation [3]:

$$(R_c)^3 = \frac{R_m}{2K}[-F + 3\pi R_m W_{\text{adh}} + \sqrt{-6\pi R_m W_{\text{adh}} F + (3\pi R_m W_{\text{adh}})^2}], \quad (5)$$

where F is the (positive) pulling force. The results are plotted in Fig. 3 and give $K = 3500 \pm 1500$ Pa. To check this value, we have conducted SFA [20] experiments between two layers of cells in which the reduction of the two layers of thickness with the load is measured (Fig. 4). These measurements give $K = 4200 \pm 1000$ Pa, which is in excellent agreement with values obtained by micromanipulation and with values from the literature [12] (1–5 kPa). As a final proof of the validity of the JKR theory, the ratio between the contact radius at separation and the one under zero load was measured. The obtained value is 0.65 ± 0.12, again in excellent agreement with the expected one, 0.63. Therefore, the main features of JKR theory are verified here. This result may seem surprising as living cells in general display very complex mechanical behaviors and JKR should obviously not be valid for all types of cells. In the present case, the cytoskeleton is responsible for the shape of the cells and its 3D elastic properties. We have verified by imaging actin, tubulin, and vimentin filaments that the S180 cells have an extended 3D cytoskeleton (data not shown). However, elasticity is expected of only the behavior of the cytoskeleton for shape changes that are sufficiently rapid that there is no time for the cytoskeleton to exhibit plastic flow during the detachment. This is the case here. These experiments lasted a few tens of seconds, whereas the time taken by a cell to regain its spherical shape after it has been expelled from a pipette was a few minutes.

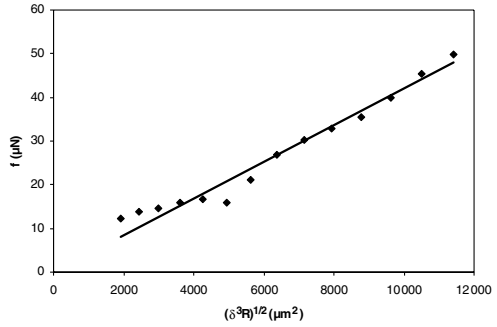

FIG. 4. Force between two layers of S180 cells deposited on mica surfaces in a SFA function of the parameter $(\delta^3 R)^{1/2}$ where δ is the reduction of the two cell layers thickness under compression and R the radius of the substrate. For δ smaller than the cell size, the slope gives the elastic modulus [3].

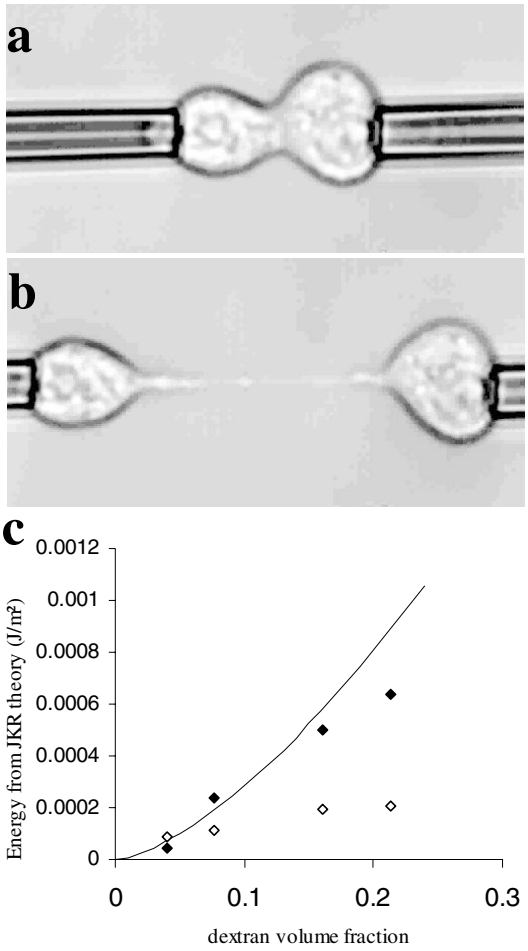

FIG. 5. (a),(b) Morphology of the cells treated with Lat B during the separation process. Note the difference from Fig. 1. (c) Adhesion energy as it would be obtained through JKR theory [Eq. (1)] as a function of the dextran volume fraction in the presence of 0.1 μM (filled diamonds) or 1.5 μM (empty diamonds) latrunculine B. The solid line is the expected value deduced from the applied depletion force [17].

To confirm the assumption that the cytoskeleton is responsible for the elastic behavior of the cell, the same micromanipulation experiments were done in the presence of 0.1 or 1.5 μM of Latrunculin B (Lat) which inhibits actin polymerization and sequesters actin monomers [21,22]. When the cell is made more deformable by alteration (0.1 μM Lat) or disruption (1.5 μM Lat) of the actin cytoskeleton network, there is a drastic change in the adhesion measurements as shown in Fig. 5. In the first concentration, JKR theory seems to work correctly at low dextran concentrations (weak forces) while it is not applicable at higher ones. In 1.5 μM Lat, the measured apparent adhesion is weak and independent of the dextran concentration. In these cases, the cells present a much larger deformation and take a long time (up to several minutes) to recover their initial shape, and it is meaningless to try to deduce adhesion energies with the approach presented here. The actin cytoskeleton is mostly cortical in round cells in suspension and allows the mechanical connection of the membrane to the tridimensional elastic structure of the rest of the cell. It is therefore not surprising that in this case JKR and spherical shell theories are not valid anymore.

These measurements show that JKR theory can reasonably be applied to predict the adhesion energy of these cells. Micropipette experiments are ideal to measure such an adhesion as the aspiration pressure gives a good measurement of the separation force. Whether such measurements are valid for cells of other kinds remains open. The applicability of JKR theory to the adhesion of other living cells could be checked directly using depletion forces, as here. However, these results suggest that the deformation of the cell during the detachment process is a good indicator of whether JKR or spherical shells theories are applicable: if the cells present a small deformation with a finite contact area at separation, this suggests a nearly elastic behavior of the cytoplasm and therefore the likelihood that these theories will be applicable.

*Corresponding author.
Electronic address: Frederic.Pincet@lps.ens.fr

[1] D. Maugis, J. Colloid Interface Sci. **150**, 243 (1992); B. D. Hughes and L. R. White, J. Chem. Soc., Faraday Trans. 1 **76**, 963 (1980).
[2] B. V. Derjaguin, V. M. Muller, and Y. P. Toporov, J. Colloid Interface Sci. **53**, 314 (1975).
[3] K. L. Johnson, K. Kendall, and A. D. Roberts, Proc. R. Soc. London A **324**, 301 (1971).
[4] J. N. Israelachvili, E. Perez, and R. K. Tandon, J. Colloid Interface Sci. **78**, 260 (1980); E. D. Shchukin, in *Microscopic Aspects of Adhesion and Lubrification*, edited by J. M. Georges (Elsevier, Amsterdam, 1982), pp. 389–402; E. D. Shchukin, E. A. Amelina, and V. V. Yaminsky, Colloids Surf. **2**, 221 (1981).
[5] F. Brochard-Wyart and P. G. de Gennes, C.R. Phys. **4**, 281 (2003).
[6] A. S. G. Curtis and J. M. Lackie, *Measuring Cell Adhesion* (John Wiley & Sons, New York, 1990).
[7] N. Mohandas and E. Evans, J. Clin. Invest. **76**, 1605 (1985).
[8] E. Evans, D. Berk, A. Leung, and N. Mohandas, Biophys. J. **59**, 849 (1991).
[9] E. Evans and A. Leung, J. Cell Biol. **98**, 1201 (1984).
[10] K.-l. P. Sung, L. A. Sung, M. Crimmins, S. J. Burakoff, and S. Chien, Science **234**, 1405 (1986).
[11] A. Tozeren, K.-l. P. Sung, and S. Chien, Biophys. J. **55**, 479 (1989).
[12] M. S. Turner and P. Sens, Biophys. J. **76**, 564 (1999).
[13] For the experiments, the same type of cells was used: murine sarcoma S180 cell. S180 cell cultures were trypsinized with 0.05% trypsin, 0.02% EDTA (*in vitrogen*), and seeded at sufficiently high density to yield a nearly confluent culture 18 to 24 h later. At that point, cells were treated with 0.01% trypsin in HMF (magnesium-free HEPES-based buffer containing 10 mM calcium, *p*H 7.4). After centrifugation, the cell suspension was pipetted gently in HCMF (calcium- and magnesium-free, HEPES-based) to yield isolated cells. Micromanipulation measurements were performed on a Leica inverted microscope at 37 °C. All surfaces in contact with the cells were precoated with bovine serum albumin (10 mg/ml; fraction V, Sigma). Before the assay, the chamber was charged with CO2-independent medium (*in vitrogen*) supplemented with 1% FCS, penicillin (100 IU/ml), and streptomycin (100 μg/ml). Pipettes were filled with sterile isotonic sucrose solution (300–330 mOs) and preincubated in bovine serum albumin. The pressure sensor to control the aspiration pressure was a Validyne, model DP103-38, ranging from 0 to 50 000 Pa.
[14] E. Evans, D. J. Klinggenberg, W. Rawicz, and F. Szoka, Langmuir **12**, 3031–3037 (1996).
[15] E. Evans and B. Kukan, Biophys. J. **44**, 255 (1983).
[16] E. Evans and D. Needham, Macromolecules **21**, 1822 (1988).
[17] P-G. de Gennes, in *Scaling Concept in Polymer Physics* (Cornell University Press, Ithaca and London, 1985), 2nd ed.
[18] D. R. Friedlander, R.-M. Mege, B. A. Cunningham, and G. M. Edelman, Proc. Natl. Acad. Sci. U.S.A. **86**, 7043 (1989).
[19] A. Yeung and E. Evans, Biophys. J. **56**, 139 (1989).
[20] J. Israelachvili and G. E. Adams, J. Chem. Soc., Faraday Trans. 1 **74**, 975 (1978).
[21] I. Spector, N. R. Shocket, D. Blasberger, and Y. Kashman, Cell Motil. Cytoskeleton **13**, 127 (1989).
[22] G. Segal, W. Lee, P. D. Arora, M. McKee, G. Downey, and C. A. McCulloch, J. Cell Sci. **114**, 119 (2001).

Force measurements in E-cadherin–mediated cell doublets reveal rapid adhesion strengthened by actin cytoskeleton remodeling through Rac and Cdc42

Yeh-Shiu Chu,[1] William A. Thomas,[3] Olivier Eder,[1] Frederic Pincet,[2] Eric Perez,[2] Jean Paul Thiery,[1] and Sylvie Dufour[1]

[1]UMR144 Centre National de la Recherche Scientifique (CNRS)-Institut Curie and [2]UMR8550 CNRS-ENS, 75248 Paris Cedex 05, France
[3]Department of Natural Sciences, Colby-Sawyer College, New London, NH 03257

We have used a modified, dual pipette assay to quantify the strength of cadherin-dependent cell–cell adhesion. The force required to separate E-cadherin–expressing paired cells in suspension was measured as an index of intercellular adhesion. Separation force depended on the homophilic interaction of functional cadherins at the cell surface, increasing with the duration of contact and with cadherin levels. Severing the link between cadherin and the actin cytoskeleton or disrupting actin polymerization did not affect initiation of cadherin-mediated adhesion, but prevented it from developing and becoming stronger over time. Rac and Cdc42, the Rho-like small GTPases, were activated when E-cadherin–expressing cells formed aggregates in suspension. Overproduction of the dominant negative form of Rac or Cdc42 permitted initial E-cadherin–based adhesion but affected its later development; the dominant active forms prevented cell adhesion outright. Our findings highlight the crucial roles played by Rac, Cdc42, and actin cytoskeleton dynamics in the development and regulation of strong cell adhesion, defined in terms of mechanical forces.

Introduction

Prominent among the transmembrane adhesion molecules, cadherins play a key role in establishing and maintaining intercellular adhesion. Cadherin-mediated adhesion is thought to develop by several discrete, sequential steps (Braga, 2002; Jamora and Fuchs, 2002). E-cadherin initiates intercellular contacts by homophilic ligation in the presence of calcium. This triggers association of the cytoplasmic domain of cadherin with the actin cytoskeletal network via α-catenin (α-cat) and β-catenin (β-cat; Vestweber and Kemler, 1985; Kemler, 1993). In epithelial cells, the recruitment of E-cadherin and actin to regions of intercellular contact is essential for the formation and stabilization of adherens junctions (Yonemura et al., 1995; Adams et al., 1996; Yap et al., 1997).

In addition to promote cell adhesion, cadherins often function as ligand-activated cell surface receptors, triggering signals that regulate cell shape, migration, proliferation, differentiation, and survival. These two functions show considerable interdependence, with the regulatory processes exercising feedback control over cell adhesion, often through inside-out signaling (for review see Gumbiner, 2000). GTPases of the Rho family—Rho, Cdc42 and Rac—are known to mediate cadherin-actin signaling and actin reorganization (Braga et al., 1997, Braga, 2002; Yap and Kovacs, 2003). Rho family GTPase activity is also involved in the formation and development of cadherin-dependent cell–cell contacts (Kim et al., 2000; Vasioukhin et al., 2000; Noren et al., 2001; Ehrlich et al., 2002). However, details on the initiation, progressive organization and regulation of E-cadherin–based adhesion remain unclear.

In recent years, several high resolution techniques (e.g., flow chamber assay, atomic force microscopy, and surface force analysis) have been used to investigate aspects of cadherin–cadherin interactions at the level of individual molecules (Baumgartner et al., 2000; Sivasankar et al., 2001; Perret et al., 2002); nevertheless, analysis of the mechanical aspects of cadherin-mediated adhesion at the cellular level has proven more difficult. Various assays used in multiple studies of cadherin-dependent intercellular adhesion (Nose et al., 1988; Friendlander et al., 1989; Steinberg and Takeichi, 1994; Angres et al., 1996; Niessen and Gumbiner, 2002; Duguay et al., 2003) have yielded a basic understanding of the underlying processes. However, these assays typically analyze the behavior of large

J.P. Thiery and S. Dufour were co-principal investigators.

The online version of this article contains supplemental material.

Correspondence to Sylvie Dufour: Sylvie.Dufour@curie.fr

Abbreviations used in this paper: α-cat, α-catenin; β-cat, β-catenin; BFA, brefeldin A; Ecad-Δcyto, E-cadherin lacking the cytoplasmic domain; Jasp, Jasplakinolide; LatB, Latrunculin B; SF, separation force; TC, trypsin-calcium.

The Journal of Cell Biology, Vol. 167, No. 6, December 20, 2004 1183–1194
http://www.jcb.org/cgi/doi/10.1083/jcb.200403043

Supplemental Material can be found at:
http://www.jcb.org/cgi/content/full/jcb.200403043/DC1

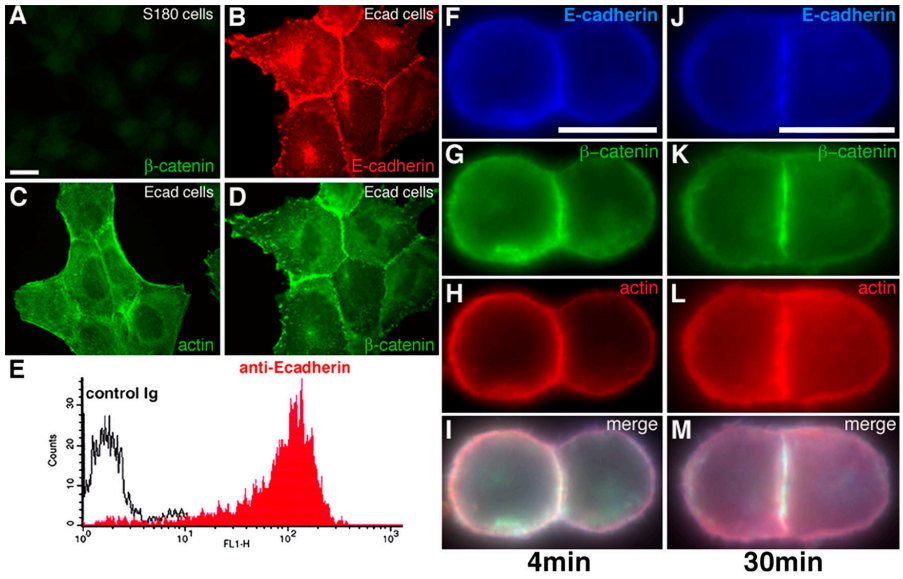

Figure 1. **Adhesive properties of Ecad cells.** Immunodetection of β-cat (A and D), E-cadherin (B), and actin (C) in S180 cells (A) and Ecad cells (B–D). E, FACS analysis on isolated Ecad cells in suspension, after TC treatment, with an antibody directed against the extracellular domain of E-cadherin. Immunodetection of E-cadherin (F and J), β-cat (G and K), and actin (H and L) in doublets formed in suspension for 4- (F–I) or 30-min (J–M). Merged images are shown in I and M. Bars: (A) 20 μm; (F and J) 10 μm.

populations of cells, providing little insight into adhesion at the level of individual cells.

We used a dual pipette assay for measuring the forces required to separate two adherent cells (Daoudi et al., 2004) maintained in suspension to avoid the complicating impact of cell–matrix adhesion and signaling (Monier-Gavelle and Duband, 1997; Gimond et al., 1999). The assay can be used for simultaneous measurement of separation force (SF), a quantitative estimate of cell adhesiveness, and detection of fluorescent proteins involved in adhesion. In this study, we used this assay to quantify intercellular adhesion in terms of mechanical forces at the cellular level and to investigate the mechanisms of adhesion specifically regulated by E-cadherin and the actin cytoskeleton.

Results

Characterization of E-cadherin–expressing cells and measurement of SF between cells by a dual pipette assay

S180 cells contain no detectable β-cat (Fig. 1 A) or cadherins (not depicted) and display minimal cell–cell adhesion in tissue culture (Friendlander et al., 1989; Dufour et al., 1999). By contrast, S180 cells stably transfected to express E-cadherin (Ecad clone) displayed characteristic intercellular adhesion in culture, with E-cadherin, β-cat and actin all detected concentrated at sites of cell–cell adhesion (Fig. 1, B–D). Ecad cells that had been dissociated by trypsin-calcium (TC) treatment (see Materials and methods) expressed E-cadherin on the cell surface (Fig. 1 E) and readily formed doublets or aggregates in suspension. Cell adhesion sites matured over time, becoming enriched in E-cadherin, β-cat and actin, and increasing in area (Fig. 1, F–I vs. J–M). In doublets of S180 cells transiently transfected with pEcad-GFP, E-cadherin–GFP molecules were concentrated at cell–cell interface (Video 3, frames 1–5, available at http://www.jcb.org/cgi/content/full/jcb.200403043/DC1) but were redistributed uniformly in the membrane after separation of the adherent cells (see next paragraph; Video 3, frames 9–12).

The micromanipulation assay was used to quantify the force required to separate pairs of adherent cells. Cadherin expressing cells held by gentle aspiration at the tips of two micropipettes (Fig. 2 A) were first brought gently into contact and held for a predetermined time (Fig. 2, B and Video 1, available at http://www.jcb.org/cgi/content/full/jcb.200403043/DC1). Fig. 2 D illustrates an example of a doublet of Ecad cells obtained after 4 min of contact (a 4-min doublet), the right pipette withdrawn to visualize the resulting adhesion (Fig. 2 C). Such a doublet was cyclically brought back into contact with the left pipette and then withdrawn to the right, each time after a step-wise increase in the strength of aspiration by the left pipette, until the cells were separated (see Materials and methods; Fig. 2, D–I; Video 2, available at http://www.jcb.org/cgi/content/full/jcb.200403043/DC1). The SF was defined as the aspiration force required to separate the doublet, such that one cell remained in each pipette when the right pipette was withdrawn (Fig. 2 I). SF was considered to be zero for pairs of cells that did not form adherent doublets in this assay.

Dependence of SF on cadherin's homophilic interaction and its activity

We measured SF for pairs of Ecad cells after different times of contact (Fig. 3 A). Adhesion was initiated rapidly, with cells adhering to each other after only a few seconds of contact (not depicted), but measurements for contact periods of <30 s were not reproducible. At 30 s of contact, a mean force of 20 nN was required to separate adherent cells. From 30 s to 30 min of contact (30-s doublets and 30-min doublets, respectively), the force required to separate the cells increased rapidly. It stabilized at ~200 nN after 1 h of contact (60-min doublets). Anti–E-cadherin significantly reduced the SF of 4-min doublets (Fig. 3 D), and S180 cells lacking cadherins displayed no detectable adhesion after 4 min (Fig. 3 D) or 30 min of contact (not depicted), both results clearly indicating that the doublet formation was E-cadherin dependent.

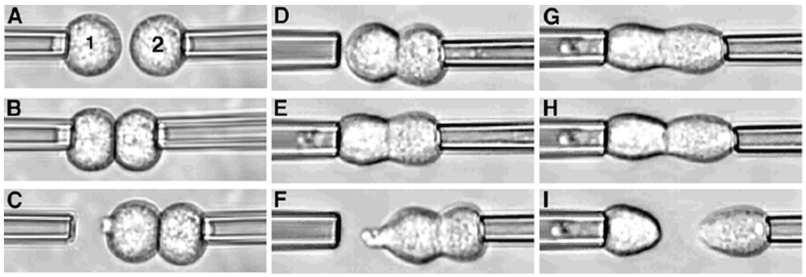

Figure 2. **Dual micropipette assay.** (A) Two cells in suspension (1 and 2) are held under weak aspiration by micropipettes, and placed in contact (B; Video 1). The formation of contact is checked (C) after displacement of the right pipette. (D) Second cell is held by the micropipette under strong aspiration. (E–I) First cell is held by the micropipette and the aspiration applied is increased as the right micropipette displaced, step by step, until the adherent cells are separated (I; Video 2).

We determined the "maximal" SF using doublets not separated during the dissociation procedure (see Materials and methods). The mean SF for such Ecad "preexisting doublets" (Fig. 3 B) was much higher than that for 60-min doublets (350 nN vs. 200 nN). By contrast, an SF of only 50 nN was obtained for preexisting doublets of S180 cells.

Homophilic interaction is thought to be key to cadherin functions. In our assay, cells expressing similar levels of either E- or N-cadherin (unpublished data) readily formed homotypic doublets and rapidly developed strong adhesion, but the SF displayed by Ecad cells was considerably higher than that of Ncad cells (Table 1). Heterotypic interaction was not detected. Ecad-Ncad pairs held together for times up to 30 min were separated immediately upon withdrawal of the right pipette therefore no SF could be measured.

Calcium dependence is a characteristic feature of E-cadherin–mediated adhesion so we assessed the calcium requirement of Ecad cell adhesion in our assay (Fig. 3 C). For 4-min doublets, no SF could be measured below 100 μM calcium ($CaCl_2$) and by 400 μM calcium, the SF reached a maximum equivalent to that obtained in the control buffer (containing 2 mM $CaCl_2$; Fig. 3 A).

Ecad cells dissociated by TE treatment to degrade surface cadherins progressively recovered cadherins at the cell surface, as shown by FACS analysis performed 4 and 12 h after TE treatment (Fig. 3 E, white peaks). Treatment of cells with 10 μM brefeldin A (BFA; a vesicular transport blocking agent; Misumi et al., 1986) abolished the recovery of E-cadherin at the surface, demonstrating that the drug effectively blocked cadherin export from the cytoplasmic and other newly synthesized pools (Fig. 3 E, black peaks). However, preincubation of TC-treated Ecad cells (retaining their cadherins at the surface) with 10 μM BFA for 1 h had no effect upon the measured SF at 30 min (Fig. 3 F). This indicates that adhesion between the cells of a doublet is mediated mainly by E-cadherins already present at the cell surface, and that export of cadherins from the cytoplasmic pool plays only a minor role at times shorter than 30 min.

Thus, in our experimental system, the SF of paired cells is a function of the type of cadherin expressed, the functional state of cadherin at the cell surface and the duration of contact between cells.

Modulation of SF by E-cadherin expression level

To test the effect of cadherin concentration on cell adhesion, we generated various stably transfected S180 clones differing

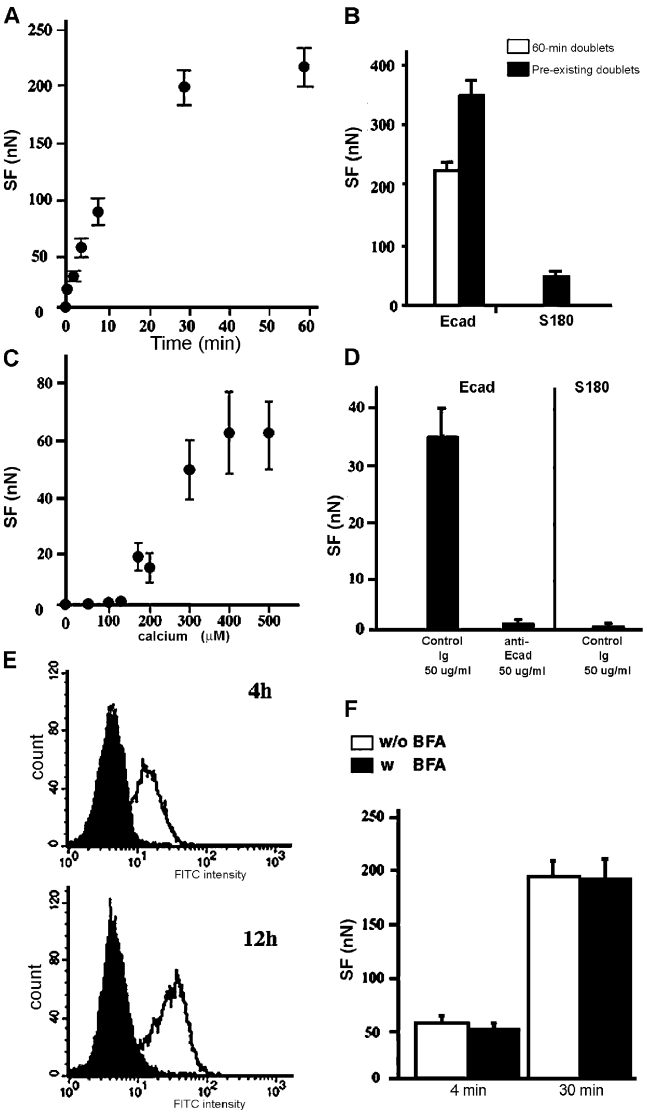

Figure 3. **Characterization of Ecad cell adhesion.** (A) SF measurements for Ecad cells held in contact for 0.5–60 min. (B) SF required to separate 60-min doublets (white bar) and preexisting doublets (black bars), selected as described in Materials and methods. (C) Dose-response curve of force measurements for 4-min doublets in various concentrations of calcium. (D) The effect of a control or anti–E-cadherin antibody on SF in Ecad or S180 cells. (E) FACS analysis of E-cadherin expression on the surface of Ecad cells treated with 10 μM BFA (black peaks) for 4 and 12 h or untreated (white peaks). (F) The mean SFs measured for 4- or 30-min Ecad doublets treated with 10 μM BFA (black bars) for 1 h or untreated doublets (white bars).

Table I. **Homophilic and heterophilic interactions between Ecad and Ncad cells**

Cell pair	Ecad-Ecad (homophilic)	Ncad-Ncad (homophilic)	Ecad-Ncad (heterophilic)
Formation of doublets	Yes	Yes	No
SF at 4 min (nN)	52.6 ± 7.0	7.7 ± 1.4	0
SF at 30 min (nN)	194 ± 14.9	46.9 ± 7.8	0

in the amount of E-cadherin expressed at the cell surface. Clones were selected by FACS, on the basis of homogeneous cadherin expression in all cells of the population. Western blot analyses with anti–E-cadherin and anti–β-cat were used to quantify the levels of these two proteins in each clone. The highest value obtained, that of the Ecad clone, was set at 100% and was treated as the reference clone in the analysis (E100). Clones were renamed based on their E-cadherin levels on Western blots. Clones E2, E14, E38, E41, and E58 were selected for further analysis; their total cadherin levels relative to the Ecad (100%) were 2%, 14%, 38%, 41%, and 58%, respectively (Fig. 4 A). The relative levels of β-cat were similar to those of cadherins, indicating that β-cat content could be used to estimate cadherin content in cells. By contrast, α-cat and p120 levels, and the pattern of tyrosine phosphorylation, were similar in all the clones studied (unpublished data). The results obtained by flow cytometry analysis (Fig. 4 B) were similar to those obtained by Western blotting.

We compared the adhesiveness of these clones (Fig. 4 C, black curve) by measuring the SF for 30-min doublets prepared from each of them. E2 cells, which had the lowest levels of cadherin expression, displayed no significant adhesion at 30 min. Mean SF for the other clones were 8.5 nN for E14, 21 nN for E38, 19.8 nN for E41, 38.1 nN for E58, and 89.5 nN for E100 (Fig. 4 C). Furthermore, the rate of increase of SF, calculated by its augmentation in the first 30 min of contact for the E14–E100 clones, varied linearly with the square of cadherin expression level (Fig. 4 C, red curve). Thus, the SF for 30-min doublets is primarily determined by the amount of E-cadherin expressed at the cell surface.

Role of the cytoplasmic partners of cadherins in the modulation of SF

We determined the role of the E-cadherin cytoplasmic domain and its partners in the establishment of cell adhesion by comparing SF in cells expressing wild-type and cytoplasmically modified E-cadherins. Parental S180 cells were transiently cotransfected with pEGFPC1 and a plasmid encoding E-cadherin, E-cadherin lacking the cytoplasmic domain (Ecad-Δcyto) or E-cadherin–α-cat chimera (EαMC; Ozawa, 2002; Fig. 5 A). FACS analysis revealed that GFP-producing cells expressed higher levels of E-cadherin or Ecad-Δcyto (Fig. 5 B, bottom) than EαMC (Fig. 5 C, bottom), whereas the GFP-positive EαMC transfectants expressed an amount of mutant E-cadherin similar to that of the E-cadherin in the expressor clone E58 (Fig. 5 C, bottom). Only cells expressing E-cadherin were shown to coexpress β-cat (Fig. 5, B and C, top), indicating that the lack of a β-cat binding site prevented the mutated cadherins from recruiting this cytoplasmic partner.

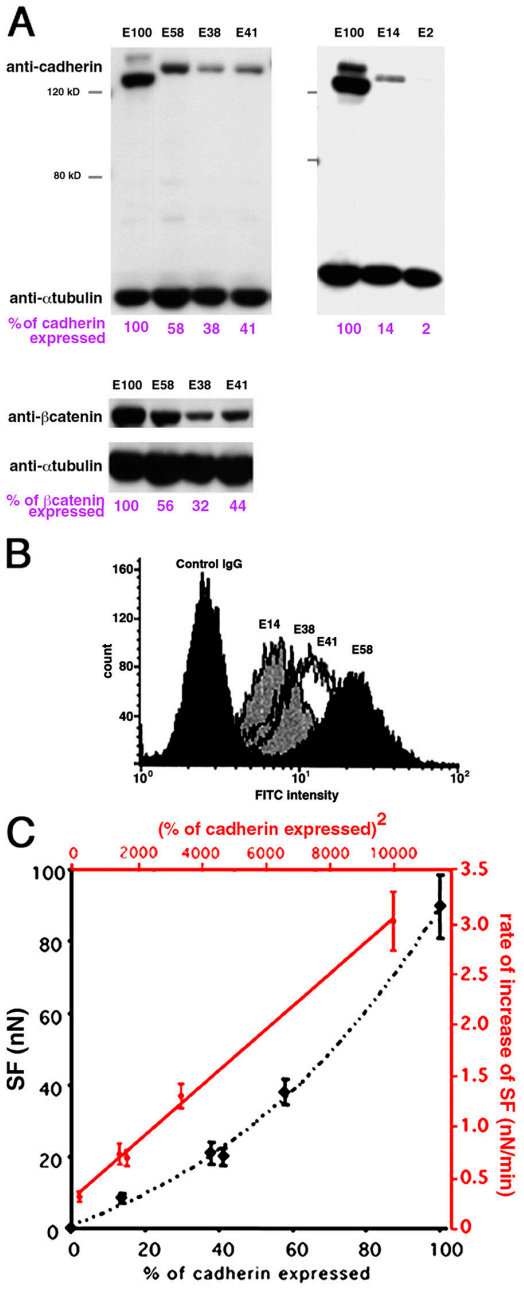

Figure 4. **SF depends on cadherin expression at the surface.** (A and B) Characterization of clones differing in E-cadherin expression level. (A) Western blot analysis of cell extracts with anti–E-cadherin or β-cat, paired with an anti–α-tubulin. Quantification of cadherin and β-cat in cell extracts is indicated in violet. (B) FACS analysis of E-cadherin expression on the cell surface of four different clones. (C) SF (y axis, nN) measured for 30-min doublets of various clones (x axis, relative cadherin content in %). In red, the rate of increase of SF (y axis, nN/min) varies linearly with the square of the % cadherin expression (x axis). The equation for the best fitting red line is $Y = 3 \times 10^{-4} X + 0.2661$.

GFP-positive cells were held in contact for 30 s, 4 min, and 30 min. Cells expressing the Ecad-Δcyto did not exhibit a time-dependent increase in SF in contrast to the cells expressing E-cadherin or EαMC (Fig. 5, D and E). The Ecad-Δcyto (Fig. 5 F) and EαMC (Fig. 5 G) proteins accumulated at the contact zone (Fig. 5, F and G, arrows) in doublets. Moreover, E58 cells and EαMC transfectants expressing the same range

of E-cadherin and EαMC chimera (Fig. 5 C, bottom), respectively, also displayed a similar time-dependent increase in SF. Together, these results indicate that the E-cadherin cytoplasmic domain and its connection to the actin cytoskeleton play a crucial role in the strengthening of cell–cell adhesion.

Role of the cytoskeleton in E-cadherin–mediated intercellular adhesion

The recruitment of actin microfilaments to cell–cell contacts has been shown to promote strong cadherin-mediated adhesion (Imamura et al., 1999). We assessed the impact of the actin cytoskeleton on the establishment of cell adhesion by measuring SF for paired Ecad cells in the presence of either Latrunculin B (LatB) or cytochalasin D, both of which inhibit actin polymerization (Flanagan and Lin, 1980; Spector et al., 1983), or Jasplakinolide (Jasp), a drug inhibiting actin disassembly or promoting actin filament aggregation in a dose-dependent manner (Bubb et al., 1994; Cramer, 1999).

We determined the effects of Jasp and LatB on actin by labeling Ecad doublets with an anti-actin mAb (not depicted) or phalloidin-TRITC (Fig. 6, B and C, respectively). Under control conditions, paired cells displayed a uniform distribution of surface E-cadherin and cortical actin over most of the cell with higher density colocalization of both molecules at the cell–cell interface (Fig. 6 A). Treatment with Jasp at 0.1 μM caused cortical actin and E-cadherin to redistribute in a nonuniform manner everywhere. However, at the contact zone both molecules were still noticeably colocalized. Jasp at 1 μM dramatically reduced the thickness of cortical actin, produced actin aggregates throughout the cytoplasm and eliminated the characteristic E-cadherin/actin colocalization at the cell–cell interface. Immunostaining of actin with mAb or phalloidin gave similar results and showed that, for doublets in suspension, Jasp at both 0.1 and 1 μM mainly induces a disorganization of the actin network reflecting the aggregation/polymerization activity of this drug described by Cramer (1999). LatB at 0.1 μM had no marked effect on the localization of E-cadherin and actin in paired cells in suspension (Fig. 6 C) but 1 μM LatB treatment induced the formation of large actin aggregates in the cytoplasm, E-cadherin clusters at the cell surface and higher levels of E-cadherin staining in

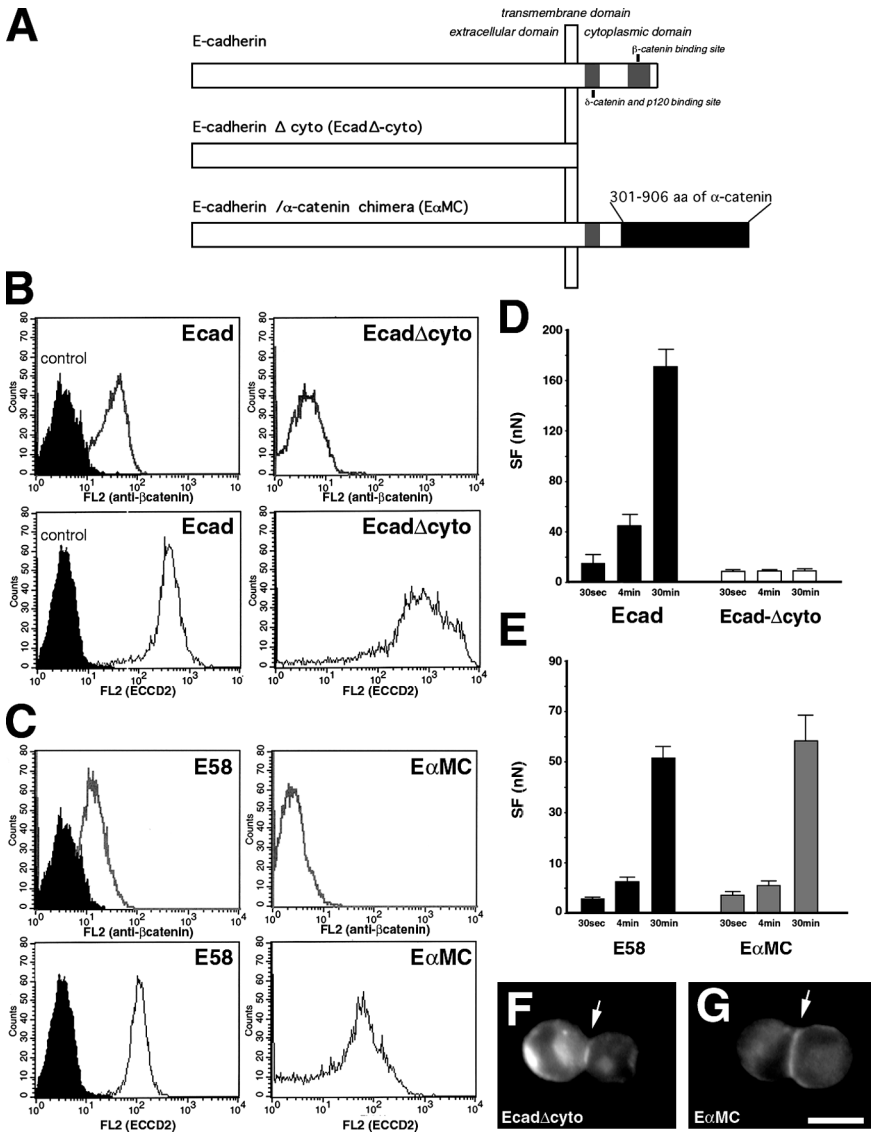

Figure 5. **The time-dependent increase in SF depends on the connection of cadherin to the actin cytoskeleton.** (A) Schematic representation of the structure of wild-type cadherin, E-cadherin lacking the cytoplasmic domain (Ecad-Δcyto), and E-cadherin–α-cat chimera (EαMC) expressed by transiently transfected S180 cells. FACS analysis of transiently cotransfected cells expressing Ecad (B), Ecad-Δcyto (B), EαMC (C), or E58 cells (C) with anti–β-cat (B and C, top, white peaks), anti–E-cadherin ECCD2 antibody (B and C, bottom, white peaks), or control antibodies (black peaks). (D and E) Mean SF for 30-s, 4- and 30-min doublets of GFP-positive cells expressing E-cadherin (D, black bars), Ecad-Δcyto (D, white bars), EαMC chimera (E, gray bars), and doublets of E58 cells (E, black bars). Immunodetection of Ecad-Δcyto (F) and EαMC (G) proteins in representative doublets formed after 30-min aggregation in suspension. Bar, 10 μm.

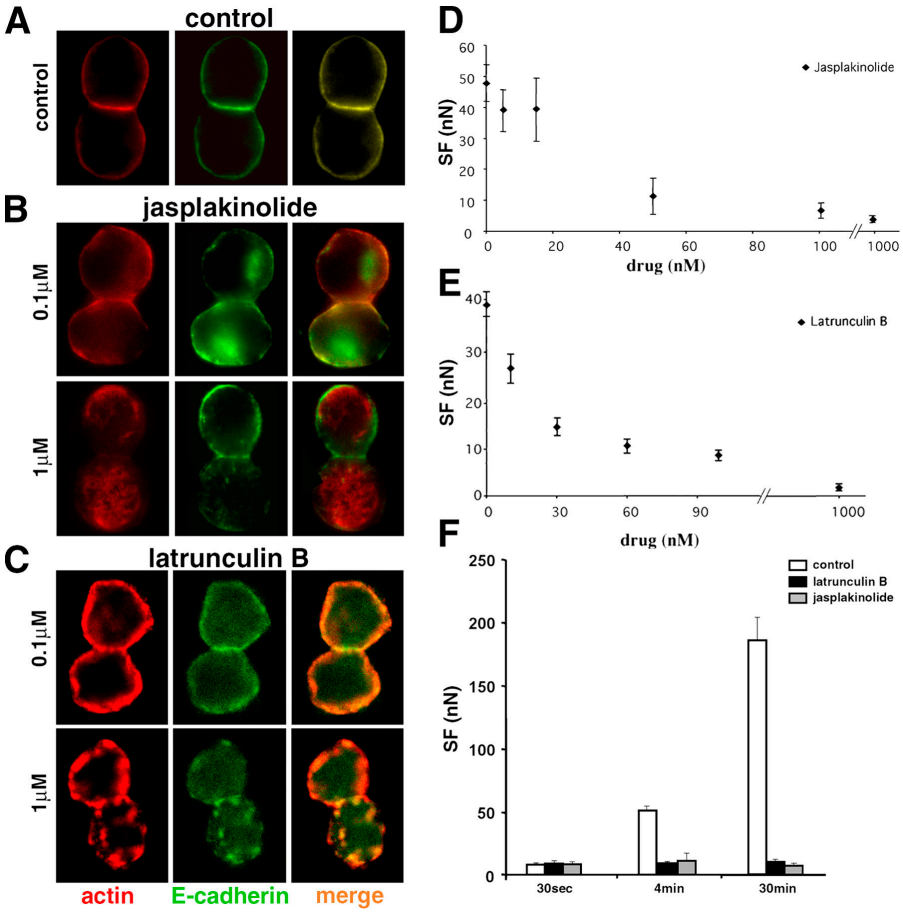

Figure 6. **Drugs affecting actin polymerization perturb actin cytoskeleton organization and decrease SF.** Confocal analysis of Ecad doublets formed in suspension under control conditions (A), in the presence of Jasp (B) or LatB (C), and labeled for actin and E-cadherin. Merged images are shown in right panels. The images correspond to a medial transverse plane of the doublet. Dose-response curve of SF for 4-min Ecad doublets in medium containing Jasp (D) or LatB (E). (F) Mean SF for 30-s, 4- and 30-min doublets in the presence of 0.1 μM LatB (black bars), 0.1 μM Jasp (gray bars), or in control medium (white bars).

the cytoplasm. FACS analysis demonstrated that LatB or Jasp, at concentrations up to 0.3 μM, does not affect E-cadherin expression at the cell surface (unpublished data).

Jasp (Fig. 6 D), LatB (Fig. 6 E), and cytochalasin D (not depicted) all reduced the SF for Ecad 4-min doublets in a dose-dependent manner. The IC_{50} for LatB was 21.2 nM, although at this concentration the drug had no visible effect on the distribution of E-cadherin and actin in cells in suspension (Fig. 6 C). Ecad cells treated with 0.1 μM LatB or Jasp formed doublets that displayed initial SF (30 s of contact) identical to that of untreated cells but the treatment abolished the time-dependent increase in SF characteristic of control doublets (Fig. 6 F). Maximal inhibition of adhesion for LatB was achieved at 0.5 μM and was fully reversible upon removal of the drug.

To test whether LatB's effect on SF might be due to changes in cell viscoelasticity and deformability, we used a depletion force-induced adhesion test (Evans and Needham, 1988) on S180 cells with and without LatB. SFs measured in the presence of LatB at up to 0.1 μM were similar to those of the control condition. This result demonstrates that treatment of cells with LatB at concentrations as high as 0.1 μM does not interfere with force measurements in the dual pipette assay (unpublished data).

Thus, the time-dependent increase in the SF for Ecad cells depends principally on actin polymerization and actin cytoskeleton dynamics.

Activation of Rac and Cdc42, but not of Rho, during formation of aggregates of Ecad cells in suspension

We used GTPase pull down assays to test the effect of E-cadherin–mediated intercellular adhesion on endogenous activity of Rho-like GTPases in Ecad cells in suspension. The levels of endogenous active and total Rho-like GTPases were monitored in S180 cells and Ecad cells at different times during a 60-min aggregation assay (Fig. 7A). In S180 cells no change was observed in the activation levels of Rac, Cdc42, and Rho during the assay. In clear contrast with this result, activation of Rac was observed in Ecad cells as soon as 5 min after the start of aggregation and reached a maximum by the end of the assay (Fig. 7 B). The kinetics of activation for Cdc42 were comparable to those described for Rac, but activation of Rho followed a very different pattern (gray, white, and black bars, respectively; Fig. 7 B). The levels of activated Rho in Ecad cells did not significantly change throughout the aggregation assay (Fig. 7 B). Results from total lysates indicated that the differences observed in band densities after precipitation were not due to variations in the total amount of protein. Each GST pull-down assay was repeated three times.

Requirement of Rac and Cdc42, but not of Rho, for E-cadherin mediated adhesion, as evaluated by SF measurements

We transiently transfected Ecad cells with pEGFPC1 alone (transfection control), or with vectors encoding the GFP-tagged consti-

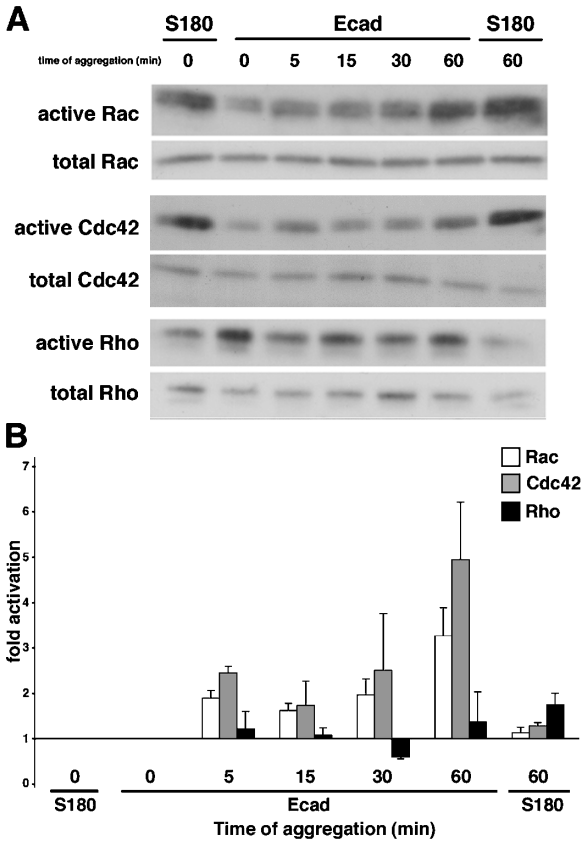

Figure 7. **Activation of small GTPases during Ecad cell aggregation.** Representative Western blot analysis of GTP-bound (active) and total Rac, Cdc42, and Rho on S180 and Ecad cells taken at different times of the aggregation assay in suspension (A). (B) Fold activation of the Rac (white bars), Cdc42 (gray bars) and Rho (black bars) GTPases; the activation level at time 0 serves as the reference level. Activation fold represents the mean ± SEM from three independent experiments.

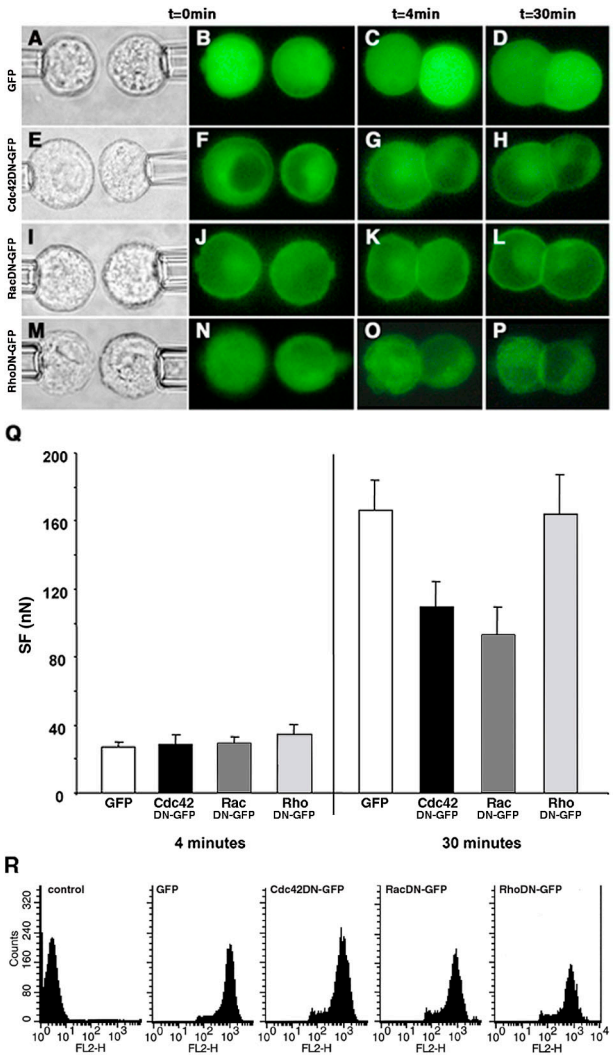

Figure 8. **The effect of dominant negative GTPase protein expression on SF.** Distribution of GFP-tagged proteins in transfected Ecad cells producing GFP (B–D), and the Cdc42DN (F–H), RacDN (J–L), and RhoDN (N–P) before contact (B, F, J, and N), in 4-min doublets (C, G, K, and O) and in 30-min doublets (D, H, L, and P). Each row represents a series of real-time images of a doublet monitored by light transmission or epifluorescence microscopy before and at 4 and 30 min of contact. Q, SF measured for 4- and 30-min Ecad doublets producing either GFP (white bars), Cdc42DN (black bars), RacDN (dark gray bars), or RhoDN (light gray bars). (R) FACS analysis of transiently transfected Ecad cells, positive for GFP, Cdc42DN, RacDN, or RhoDN, and immunostained with an antibody directed against the extracellular domain of E-cadherin (FL2 channel).

tutively inactive constructs, Cdc42DN, RacDN, and RhoDN or the GFP-tagged constitutively active constructs, Cdc42DA, RacDA, and RhoDA. In suspended isolated cells, GFP (Fig. 8 B) was distributed uniformly throughout the cytoplasm. For Cdc42DN (Fig. 8 F), RacDN (Fig. 8 J), RhoDN (Fig. 8 N), and RacDA (Fig. 9, G and H), we observed homogeneous fluorescence in the cytoplasm and more intense fluorescence close to the cell membrane. This distribution was also observed for Cdc42DA and RhoDA, but to a lesser extent (unpublished data).

GFP-positive cells were held in contact for 4 or 30 min. In the transfection control cells, GFP remained uniformly distributed in the cytoplasm as cell adhesion developed (Fig. 8, C and D) whereas DN-forms of Rho GTPases were recruited at the cell–cell contact zone within 4 min (Fig. 8, G, K, and O) and were markedly accumulated at 30 min (Fig. 8, H, L, and P). By contrast, the Cdc42DA and RhoDA were not recruited (Fig. 9, C and D, and E and F, respectively).

Force measurements showed that all 4-min doublets (GFP controls and all DN-GTPases) developed similar SFs (Fig. 8 Q). Even at 30 min, variations in Rho levels had no impact; neither RhoDN nor RhoDA affected the adhesive phenotype of paired cells or the SF measured between them (Fig. 8, O–Q; Fig. 9, B, E, and F).

In striking contrast to these results are those for the other two GTPases. Production of Cdc42DN or RacDN significantly reduced adhesion (by 35% and 44%, respectively) relative to that of the control group in 30-min doublets (Fig. 8 Q). Dominant active forms had an even stronger effect. Although cells producing the Cdc42DA did adhere when pushed into contact, the contact interface less developed (Fig. 9, C and D) than for control cells or for cells producing any of the inactive constructs (Fig. 8, C and P), and a much lower SF was required to separate 4- and 30-min Cdc42DA doublets than for even the dominant negative forms of Cdc42 or Rac (Fig. 9 B vs. Fig. 8 Q). This indicates that no time-dependent strengthening of adhesion occurred in the presence of Cdc42DA. RacDA had the most dramatic effect of

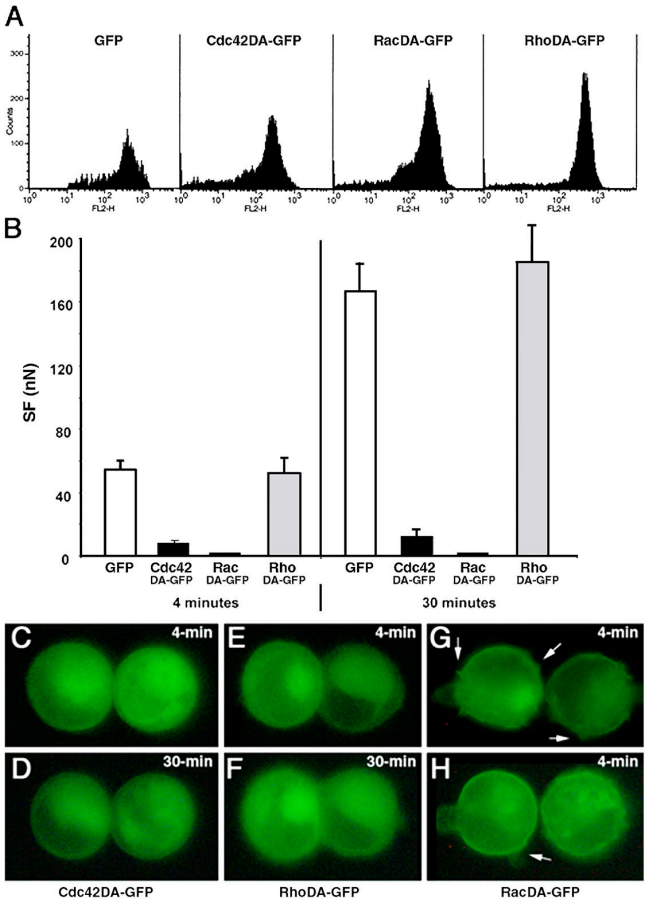

Figure 9. **The effect of dominant active GTPase protein expression on SF.** (A) FACS analysis of transiently transfected Ecad cells, positive for GFP, Cdc42DA, RacDA or RhoDA, and immunostained with an antibody directed against the extracellular domain of E-cadherin (FL2 channel). (B) SF measured for 4- and 30-min Ecad doublets producing GFP (white bars), Cdc42DA (black bars), RacDA (dark gray bars) and RhoDA (light gray bars). Real-time images showing the distribution of GFP-tagged proteins in 4-min (C, E, G, and H) and 30-min (D and F) doublets of Ecad cells producing Cdc42DA (C and D), RhoDA (E and F), or RacDA (G and H). Arrows in G and H indicate the membrane protrusions specifically observed in RacDA transfectants.

all. Cells transfected with RacDA were irregular in shape, with membrane protrusions easily visible on fluorescence microscopy and they did not form adhesive doublets at all (Fig. 9, G and H). These results suggest major changes in the membrane dynamics of RacDA transfectants.

FACS analysis showed that the transfected cells producing GFP, DN-forms (Fig. 8 R) or DA-forms (Fig. 9 A) of Rho GTPases expressed E-cadherin at their surface. Thus, the observed decrease in the SF of cells producing mutant forms of GTPases could not be accounted for by a loss of E-cadherin from the cell surface.

Discussion

In the dual pipette assay described here, we initiated adhesion between two cells by pushing them together and then measured the SF required to separate them. We manipulated cells in suspension using micropipettes, an approach that eliminates matrix-mediated signaling, minimizes the contribution of generalized membrane events, and bypasses the initiation of intercellular adhesion through lamellipodial and filopodial activities, as typically occurs during cell–cell adhesion on a substratum. The assay was not designed to quantify the strength of molecular interactions between individual adhesive receptors present at the cell surface. Instead, for the first time, it provides an overall quantification in terms of mechanical force of the adhesive properties conferred on the cell by adhesion receptors during the development of adhesion. In this cellular context, the assay provides insight into the functioning of specific cell surface receptors, their cytoplasmic partners and their connections to the cytoskeleton.

We used S180 cells stably transfected with the E-cadherin cDNA to investigate E-cadherin–dependent adhesive mechanisms and to minimize interference by other adhesion receptors; no classical intercellular adhesion molecules were detectable in the S180 cells, and they do not form doublets (however, they do form very weak cadherin-independent adhesions after very extended contact times; Fig. 3 B).

By contrast, S180 cells expressing E-cadherin display significant adhesion after a few seconds of contact, and a SF of a few to several hundred nanoNewtons can be measured, depending on the duration of contact and cadherin levels expressed at the cell surface. SF increased linearly over time for the first 30 min and then reached a plateau. Forces then continued to develop slowly between 30 and 60 min. Overall, our results clearly demonstrate that cadherins are required to initiate and to sustain the rapid intercellular adhesion that develops during the first hour of contact.

Here, we report a requirement for homophilic interactions between functional cadherin molecules (E or N) for the rapid development of strong adhesion (Table 1), although heterotypic cadherin interactions have been reported in other studies. N-cadherin expressing lens cells and E-cadherin expressing liver cells were found to form heterotypic junctions in primary cultures (Volk et al., 1987), and cadherins have been observed to interact in a heterophilic fashion in flow chamber and cell sorting assays (Niessen and Gumbiner, 2002; Duguay et al., 2003). In our assay, however, heterotypic contacts between E- and N-cadherin expressing cells were unable to induce the formation of doublets. This cannot be interpreted to completely exclude the possibility of the heterophilic interaction among different types of cadherins because heterotypic interactions may be constrained by the geometry of our assay or may simply produce adhesion too weak to be detected by our technique.

In this assay, the SF measured between two adherent cells considered to be identical in terms of E-cadherin expression because they are derived from the same clone. The comparison of SF in clones expressing different levels of E-cadherin shows that SF is a function of cadherin density at the cell surface, with greater SF resulting from higher levels of expression (Fig. 4 C). The curve best describing the relationship between force and cadherin expression level for 30-min doublets is a second-order polynomial function. In addition, the rate of increase of SF, an index representing how fast a pair of cells can interact each other to form a doublet within 30 min, associates linearly with

the square of the percentage of cadherin expression (for clones with 14–100% expression). These two relationships clearly indicate a direct link between two parameters, E-cadherin density on two "identical" interacting cells and SF, in our dual pipette assay. Thus, we demonstrate that E-cadherin expression is the main parameter regulating initiation and development of E-cadherin–mediated adhesion.

We identified three phases in the kinetics of adhesion in paired cells: (1) initial contact (up to 30 s); (2) rapid increase of SF with duration of contact (30 s–30 min of contact); and (3) a phase in which the increase of SF after 30 min continues much more slowly over time. Table II chronologically summarizes the mechanisms required during the development of E-cadherin adhesion in paired cells.

The deletion of the cytoplasmic domain of E-cadherin does not affect the initiation of adhesion (Fig. 5 D). Similarly, treatment of cells with LatB or Jasp has no effect on the SF measured for 30-s doublets (Fig. 6 F). These results indicate that the actin cytoskeleton is not required during the first phase of adhesion and we deduce, therefore, that SFs recorded during this phase reflect the trans-interactions of E-cadherin extracellular domains at the contact zone. In contrast, deleting the E-cadherin cytoplasmic domain or perturbing actin polymerization by drugs does affect the second and third phases of adhesion, abolishing the time-dependent increase in the measured SF. Thus, a controlled actin polymerization activity is essential for the development and stabilization of cadherin-mediated adhesion over time. Furthermore, the accumulation of the Ecad-Δcyto at the contact zone suggests that the rapid increase in SF with time is most likely due to an "inside-out" signaling rather than solely the increase in the number of binding sites. Together, our results indicate that the connection of the cadherin–catenin complex with actin cytoskeleton and its reinforcement is the prominent process controlling the second phase of adhesion whereas the third stage probably corresponds to contact stabilization through higher order cytoskeletal rearrangements, as previously described (Yonemura et al., 1995; Adams et al., 1996; Yap et al., 1997; Yap and Kovacs, 2003).

We also found that the inhibition of intracellular protein transport by BFA did not affect SF measured for Ecad cells during the initial and second phases of adhesion. This argues strongly that the early stages of adhesion in paired cells depend on interactions between cadherins already present at the contact zone or recruited from membrane regions proximal to it.

GTPases of the Rho family (Rho, Cdc42, and Rac) are known to participate in the signaling cascades activated by cadherin-mediated intercellular adhesion (Braga et al., 1997, Fukata and Kaibuchi, 2001; Nakagawa et al., 2001; Braga, 2002; Charasse et al., 2002; Kovacs et al., 2002; Yap and Kovacs, 2003), and their dominant negative forms have been shown to affect the organization of actin filaments and the recruitment and stabilization of cadherin and β-cat at cell–cell contact sites in cells attached to a substratum (Braga et al., 1997; Takaishi et al., 1997; Jou and Nelson, 1998). Our results support and extend these findings. We observed that the formation of Ecad cell aggregates in suspension was accompanied with the activation of Rac and Cdc42, but not Rho (Fig. 7). Because neither Rac nor Cdc42 was activated during aggregation of S180 cells (lacking cadherins), we conclude that this activation in Ecad cells was specifically mediated by E-cadherin interactions.

In paired cells in suspension, overproduction of Cdc42DN and RacDN attenuated the normal time-dependent increase in SF between 4 and 30 min of contact (Fig. 8). This attenuation was not caused by a decrease of the E-cadherin expression levels in the transfectants. Therefore, although Rac and Cdc42 GTPases are not involved in the first phase of adhesion, they clearly are involved late in the second phase of adhesion. Other reports (Braga et al., 1997; Kovacs et al., 2002; Lambert et al., 2002) have shown these GTPases are involved in nascent contacts between epithelial cells. The pushing together of isolated cells in our assay circumvents the need for filopodial or lamellipodial activity and may abolish the potential primary effect of these GTPases during the early stages of cell–cell contact. Our results are consistent with the observations that cadherin ligation can activate Rac and Cdc42 (Kim et al., 2000; Kovacs et al., 2002) and that inhibitory forms of Cdc42 and Rac disturb E-cadherin–mediated adhesion in gyratory cell aggregation assays (Fukata et al., 1999). They also confirm that Rac/Cdc42 are involved in the development of adhesion after 4 min and in strengthening the mechanical link between cadherin and actin filaments, reinforcing adhesion, as previously suggested (Ehrlich et al., 2002).

Dominant active forms of Cdc42 and Rac had more pronounced effect. Overproduction of Cdc42DA protein in paired Ecad cells in suspension resulted in much weaker than normal adhesion, with a dramatically lower SF (Fig. 9). RacDA protein drastically altered E-cadherin–based adhesion, preventing both its initiation and subsequent development. Transfectants producing RacDA had normal levels of E-cadherin at the cell surface, but the molecules were completely unable to mediate adhesion. Because even cells treated with LatB or Jasp generated some SF (Fig. 6 F), we suspect that Rac may affect cadherin activity directly, independently of actin remodeling, by an unknown mechanism. We do not exclude the possibility that activated Rac also modified the state of the actin cytoskeleton and otherwise affected general membrane dynamics. Such a possibility is consistent with our observation that RacDA-producing cells, unlike the other transfectants, displayed notable membrane protrusions (Fig. 9, G and H).

The results with the dominant active constructs evoke an interesting speculation. The Cdc42DA and RacDA proteins overproduced in isolated cells probably compete with endogenous Cdc42 and Rac activation, primed at sites of cadherin–cadherin interaction, when cells are pushed into contact. In a sense, they would "swamp out" the adhesion-based signal with an overbearing background noise. Thus, if Rac/Cdc42 activation occurs independently of and before cadherin ligation, it prevents E-cadherin–mediated adhesion. This interpretation would be consistent with the frequent overproduction of Rho family GTPases (Sahai and Marshall, 2002) and the associated loss of intercellular adhesiveness observed in tumor cells during metastasis. Moreover, sustained activation of Rac also disrupts cadherin junctions in keratinocytes (Braga et al., 2000).

Table II. **Chronological order of mechanisms required during the development of adhesion in paired Ecad cells**

	Time (min)	0–0.5	0.5–4	4–30	30+
Molecular manipulation or drug treatment	**Effects**	**First phase of adhesion**	**Second phase of adhesion**		**Third phase of adhesion**
Deletion of E-cadherin cytoplasmic domain	No interaction with cytoplasmic partners	−	+	+	+
Without calcium anti-cadherin antibody	Nonfunctional cadherins	+	+	+	+
E-cadherin–α-catenin chimera	Direct interaction with the actin cytoskeleton	−	−	−	−
Latrunculin	Inhibition of actin polymerization	−	+	+	+
Jasplakinolide	Aggregation/ polymerization of actin				
Brefeldin A	Inhibition of vesicular transport	−	−	−	nd
Actin network organization and membrane dynamics					
Cdc42DN/RacDN	Inhibition of filopodia/ lamellipodia and membrane ruffles	−	−	+	nd
Cdc42DA/RacDA	Stimulation of filopodia/ lamellipodia and membrane ruffles	+	+	+	+
RhoDN/RhoDA	Inhibition/induction of stress fibers; cell contractility	−	−	−	−
Dependency		E-cadherin	E-cadherin	E-cadherin	E-cadherin
			Actin polymerization	Actin polymerization	Actin dynamics
				Actin remodelling through Rac/Cdc42 activation	
		Membrane dynamics	Membrane dynamics	Membrane dynamics	

+, sensitive.
−, insensitive.
nd, not done.

Finally, Rho is not activated during Ecad cell aggregation in suspension, nor does overproduction of either RhoDA or RhoDN in any way affect the intercellular adhesion or the measured SF in our paired cell assay. Several reports (Braga et al., 1997; Takaishi et al., 1997; Noren et al., 2001) suggest a role for Rho in the establishment of adherent junctions regulated by E-cadherin in epithelial cell lines or keratinocytes adhering to ECM and indeed, under physiological conditions, most cells are in contact with ECM (circulating cells excepted). The paired, suspended cells used here differ from cells attached to ECM in two major aspects: (1) they are round and nonpolarized, so their capacity to establish intercellular junctions in three dimensions is not subject to shape constraints associated with 2D-substrata; and (2) they are exempt from matrix-dependent signaling and matrix-dependent actin cytoskeleton remodelling.

The assay described here provides a new tool for investigating the cytomechanics of intercellular adhesions. It will allow us to compare the adhesiveness of cells expressing different types of cadherin, visualize the contributing molecules, and elucidate the mechanisms involved.

Materials and methods

Reagents

LatB, cytochalasin D, and Jasp were purchased from Calbiochem. BFA, phalloidin-TRITC, anti-actin and DECMA-1 mAb were obtained from Sigma-Aldrich. The pAbs to P, E, N-cadherins, and the ECCD-2 mAb were obtained from Takara Biomedicals. The rabbit inhibitory antibody directed against the extracellular domain of chicken E-cadherin has been described elsewhere (Thiery et al., 1984). The mAbs directed against β-cat, α-cat, p120, and phosphotyrosine were obtained from Becton Dickinson Biosciences. The mAbs anti–α-tubulin and secondary antibodies conjugated to HRP were purchased from Amersham Biosciences. The secondary antibodies were obtained from Jackson ImmunoResearch Laboratories. The anti-Rac and anti-RhoA mAbs were purchased from Upstate Biotechnology and Santa Cruz Biotechnology, Inc., respectively. Rabbit anti-Cdc42 antibody was provided by P. Chavrier (UMR144 CNRS-Institut Curie). Expression vectors encoding mutant forms of Rho, Rac, and Cdc42 GTPases fused to GFP (Roux et al., 1997; Gauthier-Rouviere et al., 1998; Ory et al., 2000) were obtained from M. Lambert (U440 INSERM/UPMC-Institut du Fer à Moulin). The GST-CRIB PAK1 and GST-RBD Rhotekin were described elsewhere (Ren and Schwartz, 2000; Patel et al., 2002) and were provided by F. Niedergang (UMR144 CNRS-Institut Curie) and I. Ader (U528 INSERM-Institut Curie), respectively. pEαMC encoding an E-cadherin–α-cat chimera and pEcad-GFP were a gift of M. Ozawa (Kagoshima University, Kagoshima, Japan; Ozawa, 2002 and 1998, respectively). pEGFPC1 was obtained from CLONTECH Laboratories, Inc.

Cell lines, constructs and transfections

We produced the pCE-EcadΔcyto expression vector encoding an E-cadherin with a deletion of its cytoplasmic domain, as follows: a DNA fragment was amplified from pCE-Ecad using 5′-AAAGACCAGGTGACCACG and 5′-ATCTGTACGTACCTACGGACCGACCACCGTTCTCCTCCG primers to introduce sites for RsrII and SnaBI (underlined sequences) and a stop codon at the end of the transmembrane domain of E-cadherin. The 195-bp PCR fragment was digested by BstE2 and SnaB1 and ligated into theBstE2 and SnaB1 sites of pCE-Ecad.

The Ecad and Ncad clones are S180 cells stably transfected to express chicken E- and N-cadherin and are described elsewhere (Friedlander et al., 1989 and Dufour et al., 1999, respectively). Clones with different levels of mouse E-cadherin expression were obtained by stable transfection of S180 cells with the pCE-Ecad eukaryotic expression vector and pAG60 as described previously (Boyer et al., 1992). Alternatively, cells at 80% confluence were transiently transfected with 5 μg DNA: 12 μg lipofectamine 2000 (Invitrogen) or a mixture of 0.8 μg of pEGFPC1 and 8 μg DNA (pEcad, pEcadΔcyto, or pEαMC): 15 μg lipofectamine 2000 for 5 h and incubated in culture medium. After 15–48 h of transfection, we selected the GFP-positive cells for force measurements.

Tissue culture, cell dissociation, and drug treatments

Cells were maintained in DME with 10% FCS, and confluent cultures were routinely treated with TE buffer (0.05% trypsin + 0.02% EDTA). For force measurements and cell aggregation assay, cell dissociation was performed in TC buffer (0.01% trypsin + 10 mM calcium) as described previously (Nakagawa and Takeichi, 1995). Before SF measurement, cells were resuspended in working medium—a CO_2-independent medium (Invitrogen) supplemented with 1% FCS—and used immediately. When necessary, drugs or similar amounts of solvents (as a control) were added to isolated cells in working medium 30 min to 2 h (Invitrogen) before force measurements. Cell aggregation assays are performed as described elsewhere (Dufour et al., 1999).

Western blotting

Extraction of cell monolayers and Western blot analysis were performed as described previously (Dufour et al., 1999) with a mixture of antibodies directed against α-tubulin and β-cat or E-cadherin and revealed by ECL detection (Amersham Biosciences). Quantitative analysis was done using the ImageQuant program on a representative Western blot of three independent experiments. The α-tubulin content was used to normalize for protein level. The levels of β-cat and E-cadherin of E100 cells were set at 100% in comparisons of transfected clones.

Pull down assay and the determination of the activity of Rho-like GTPases

Cell aggregation assays were performed as described above. 10^6 cells were used for each point of the kinetics. Cells were lysed on ice in lysis buffer and the Rac, Cdc42, and RhoA activity pull down assays were performed as described previously (Patel et al., 2002; Arthur and Burridge, 2001). Precipitation was performed in the presence of 0.5% BSA with GST-CRIB (30 μg) and GST-RBD (30 μg) and revealed by Western blotting.

Microscopy

Immunodetection of cadherins on cultured cells was performed as described previously (Dufour et al., 1999). Preparations were viewed by epifluorescence microscopy, using a DMRBE microscope (Leica) equipped with an objective of 63× (PL APO, NA/1.32-0.6 oil) and of 100× (NA/1.4) and with a cooled CCD camera (Hamamatsu C5985). Acquisitions were controlled by a Power Macintosh workstation operating IP-Lab software. Alternatively, preparations were analyzed by TCS4D confocal microscopy based on a DM microscope interfaced with an argon/krypton laser. Cadherin expression on the cell surface of TC- or TE-treated cells was analyzed by flow cytometry as described previously (Beauvais et al., 1995) with specific antibody directed against the extracellular domain of cadherins. Samples from three independent experiments were analyzed.

Measurement of SF between cells

We used a micromanipulation technique described previously in Daoudi et al. (2004). In brief, forces were measured on the stage of an inverted epifluorescence microscope (Leica) equipped with objectives of 63× (PL FLUOTAR; NA/0.7; C PLAN NA/0.75) and with a cooled CCD C5985 (Hamamatsu) or Coolpix 5000 camera (Nikon). Image acquisition was described in the previous paragraph. Cells were manipulated at 37°C with two micropipettes, each held by one micromanipulator connected to a combined hydraulic/pneumatic system and a pressure sensor making it possible to control and measure the aspiration applied to the cells. Micropipettes were pulled (model P-2000; Sutter Instrument), cut, and fire polished with a homemade microforge, such that their i.d. was 4.0–5.5 μm. The aspiration applied to the left pipette was measured by a pressure sensor (model DP103-38; Validyne). Aspiration was monitored continuously during the separation process (Fig. 3), and the values recorded for each of the last two cycles in the series (P_{n-1} and P_n) were used to calculate the SF for each doublet using the equation: $SF = \pi (d/2)^2 (P_{n-1}+P_n)/2$ where d is the i.d. of left pipette. Results for 30–50 measurements were used to obtain the mean force of separation for a specific contact time in at least three independent experiments.

Online supplemental material

Real-time (Videos 1 and 2) and time-lapse (Video 3) films are included as online videos. Video 1 shows two Ecad cells held by micropipettes and put in contact. Video 2 shows the separation process for a 4-min Ecad doublet and a SF of 47.5 nN was calculated. Videos 1 and 2 were taken under a 63× objective. Video 3 shows the separation process of a S180 cell doublet transiently expressing E-cadherin tagged with GFP. Images were taken under a 100× objective. For the details, refer to video legends. Online supplemental material is available at http://www.jcb.org/cgi/content/full/jcb.200403043/DC1.

We thank F. Niedergang, I. Ader, and M. Ozawa for reagents; and C. Burger, J.-B. Sibarita, V. Fraisier, D. Meur, and D. Morineau for help with imaging and computerized video microscopy. We thank K.M. Yamada, R.J. Thomas-Mudge, M.J. Morgan, P. Nassoy, S.Y. Lee, and B. Janssens for helpful discussions.

This work was supported by the CNRS, the Institut Curie (Physicochimie des structures biologiques complexes), the Association pour la Recherche sur le Cancer (grant 5653), and EEC contract QLGI-CT-2001-00869. Y.-S. Chu benefited from a France-Taiwan Ministry of Foreign Affairs Ph.D. fellowship.

Submitted: 4 March 2004
Accepted: 27 October 2004

References

Adams, C.L., W.J. Nelson, and S.J. Smith. 1996. Quantitative analysis of cadherin-catenin-actin reorganization during development of cell–cell adhesion. *J. Cell Biol.* 135:1899–1911.

Angres, B., A. Barth, and W.J. Nelson. 1996. Mechanism for transition from initial to stable cell–cell adhesion: kinetic analysis of E-cadherin–mediated adhesion using a quantitative adhesion assay. *J. Cell Biol.* 134:549–557.

Arthur, W.T., and K. Burridge. 2001. RhoA inactivation by p190RhoGAP regulates cell spreading and migration by promoting membrane protrusion and polarity. *Mol. Biol. Cell.* 12:2711–2720.

Baumgartner, W., P. Hinterdorfer, W. Ness, A. Raab, D. Vestweber, H. Schindler, and D. Drenckhahn. 2000. Cadherin interaction probed by atomic force microscopy. *Proc. Natl. Acad. Sci. USA.* 97:4005–4010.

Beauvais, A., C.A. Erickson, T. Goins, S.E. Craig, M.J. Humphries, J.P. Thiery, and S. Dufour. 1995. Changes in the fibronectin-specific integrin expression pattern modify the migratory behaviour in the embryonic environment. *J. Cell Biol.* 128:699–713.

Boyer, B., S. Dufour, and J.-P. Thiery. 1992. E-cadherin expression during the acidic FGF-induced dispersion of a rat bladder carcinoma cell line. *Exp. Cell Res.* 201:347–357.

Braga, V.M. 2002. Cell-cell adhesion and signalling. *Curr. Opin. Cell Biol.* 14: 546–556.

Braga, V.M., L.M. Machesky, A. Hall, and N.A. Hotchin. 1997. The small GTPases Rho and Rac are required for the establishment of cadherin-dependent cell–cell contacts. *J. Cell Biol.* 137:1421–1431.

Braga, V.M., M. Betson, X. Li, and N. Lamarche-Vane. 2000. Activation of the small GTPase Rac is sufficient to disrupt cadherin-dependent cell-cell adhesion in normal human keratinocytes. *Mol. Biol. Cell.* 11:3703–3721.

Bubb, M.R., A.M. Senderowicz, E.A. Sausville, K.L. Duncan, and E.D. Korn. 1994. Jasplakinolide a cytotoxic natural product induces actin polymerization and competitively inhibits the binding of phalloidin to F-actin. *J. Biol. Chem.* 269:14869–14871.

Charasse, S., M. Meriane, F. Comunale, A. Blangy, and C. Gauthier-Rouvière. 2002. N-cadherin–dependent cell–cell contact regulates Rho GTPases and β-catenin localization in mouse C2C12 myoblasts. *J. Cell Biol.* 158: 953–965.

Cramer, L.P. 1999. Role of actin-filament disassembly in lamellipodium protrusion in motile cells revealed using the drug jasplakinolide. *Curr. Biol.* 9:1095–1105.

Daoudi, M., E. Lavergne, A. Garin, N. Tarantino, P. Debre, F. Pincet, C. Combadiere, and P. Deterre. 2004. Enhanced adhesive capacities of the naturally occurring Ile249-Met280 variant of the chemokine receptor CX3CR1. *J. Biol. Chem.* 279:19649–19657.

Dufour, S., A. Beauvais-Jouneau, A. Delouvée, and J.P. Thiery. 1999. Differential function of N-cadherin and cadherin-7 in the control of embryonic cell motility. *J. Cell Biol.* 146:501–516.

Duguay, D., R.A. Foty, and M. Steinberg. 2003. Cadherin-mediated cell adhesion and tissue segregation: qualitative and quantitative determinants. *Dev. Biol.* 253:309–323.

Ehrlich, J.S., M.D. Hansen, and W.J. Nelson. 2002. Spatio-temporal regulation of Rac1 localization and lamellipodia dynamics during epithelial cell-cell adhesion. *Dev. Cell.* 3:259–270.

Evans, E., and D. Needham. 1988. Attraction between lipid bilayer membranes in concentrated solutions of nonabsorbing polymers: comparison of mean-field theory with measurements of adhesion energy. *Macromolecules.* 21:1822–1831.

Flanagan, M.D., and S. Lin. 1980. Cytochalasins block actin filament elongation by binding to high affinity sites associated with F-actin. *J. Biol. Chem.* 255:835–838.

Friendlander, D.R., R.-M. Mege, B.A. Cunningham, and G.M. Edelman. 1989. Cell sorting-out is modulated by both the specificity and amount of different cell-cell adhesion molecules (CAMs) expressed on cell surfaces. *Proc. Natl. Acad. Sci. USA.* 86:7043–7047.

Fukata, M., and K. Kaibuchi. 2001. Rho-family GTPases in cadherin-mediated cell-cell adhesion. *Nat. Rev. Mol. Cell Biol.* 2:887–897.

Fukata, M., S. Kuroda, M. Nakagawa, A. Kawajiri, N. Itoh, I. Shoji, Y. Matsuura, S. Yonehara, H. Fujisawa, A. Kikuchi, and K. Kaibuchi. 1999. Cdc42 and Rac1 regulate the interaction of IQGAP1 with beta-catenin. *J. Biol. Chem.* 274:26044–26050.

Gauthier-Rouviere, C., E. Vignal, M. Meriane, P. Roux, P. Montcourier, and P. Fort. 1998. RhoG GTPase controls a pathway that independently activates Rac1 and Cdc42Hs. *Mol. Biol. Cell.* 9:1379–1394.

Gimond, C., A. van Der Flier, S. van Delft, C. Brakebusch, I. Kuikman, J.G. Collard, R. Fassler, and A. Sonnenberg. 1999. Induction of cell scattering by expression of beta1 integrins in beta1-deficient epithelial cells requires activation of members of the rho family of GTPases and downregulation of cadherin and catenin function. *J. Cell Biol.* 147:1325–1340.

Gumbiner, B.M. 2000. Regulation of cadherin adhesive activity. *J. Cell Biol.* 148:399–403.

Imamura, Y., M. Itoh, Y. Maeno, S. Tsukita, and A. Nagafuchi. 1999. Functional domains of α-catenin required for the strong state of cadherin-based adhesion. *J. Cell Biol.* 144:1311–1322.

Jamora, C., and E. Fuchs. 2002. Intercellular adhesion, signalling and the cytoskeleton. *Nat. Cell Biol.* 4:E101–E108.

Jou, T.S., and W.J. Nelson. 1998. Effects of regulated expression of mutant RhoA and Rac1 small GTPases on the development of epithelial (MDCK) cell polarity. *J. Cell Biol.* 142:85–100.

Kemler, R. 1993. From cadherins to catenins: cytoplasmic protein interactions and regulation of cell adhesion. *Trends Genet.* 9:317–321.

Kim, S.H., S. Li, and D.B. Sacks. 2000. E-cadherin-mediated cell-cell attachment activated Cdc42. *J. Biol. Chem.* 275:36999–37005.

Kovacs, E.M., R.G. Ali, A.J. McCormack, and A.S. Yap. 2002. E-cadherin homophilic ligation directly signals through Rac and phosphatidylinositol 3-kinase to regulate adhesive contacts. *J. Biol. Chem.* 277:6708–6718.

Lambert, M., D. Choquet, and R.-M. Mege. 2002. Dynamics of ligand-induced Rac1-dependent anchoring of cadherins to the actin cytoskeleton. *J. Cell Biol.* 157:469–479.

Monier-Gavelle, F., and J. Duband. 1997. Cross talk between adhesion molecules: control of N-cadherin activity by intracellular signals elicited by β1 and β3 integrins in migrating neural crest cells. *J. Cell Biol.* 137: 1663–1681.

Misumi, Y., K. Miki, A. Takatsuki, G. Tamura, and Y. Ikehara. 1986. Novel blockade by brefeldin A of intracellular transport of secretory proteins in cultured rat hepatocytes. *J. Biol. Chem.* 261:11398–11403.

Nakagawa, M., M. Fukata, M. Yamaga, N. Itoh, and K. Kaibuchi. 2001. Recruitment and activation of Rac1 by the formation of E-cadherin-mediated cell-cell adhesion sites. *J. Cell Sci.* 114:1829–1838.

Nakagawa, S., and M. Takeichi. 1995. Neural crest cell-cell adhesion controlled by sequential and subpopulation-specific expression of novel cadherins. *Development.* 121:1321–1332.

Niessen, C.M., and B.M. Gumbiner. 2002. Cadherin-mediated cell sorting not determined by binding or adhesion specificity. *J. Cell Biol.* 156:389–399.

Noren, N.K., C.M. Niessen, B.M. Gumbiner, and K. Burridge. 2001. Cadherin engagement regulates Rho family GTPases. *J. Biol. Chem.* 276:33305–33308.

Nose, A., A. Nagafuchi, and M. Takeichi. 1988. Expressed recombinant cadherins mediate cell sorting in model systems. *Cell.* 54:993–1001.

Ory, S., Y. Munari-Silem, P. Fort, and P. Jurdic. 2000. Rho and Rac exert antagonistic functions on spreading of macrophage-derived multinucleated cells and are not required for actin fiber formation. *J. Cell Sci.* 113:1177–1188.

Ozawa, M. 1998. Identification of the region of alpha-catenin that plays an essential role in cadherin-mediated cell adhesion. *J. Biol. Chem.* 273: 29524–29529.

Ozawa, M. 2002. Lateral dimerization of the E-cadherin extracellular domain is necessary but not sufficient for adhesive activity. *J. Biol. Chem.* 277: 19600–19608.

Patel, J.C., A. Hall, and E. Caron. 2002. Vav regulates activation of Rac but not Cdc42 during FcgammaR-mediated phagocytosis. *Mol. Biol. Cell.* 13: 1215–1226.

Perret, E., A.M. Benoliel, P. Nassoy, A. Pierres, V. Delmas, J.-P. Thiery, P. Bongrand, and H. Feracci. 2002. Fast dissociation kinetics between individual E-cadherin fragments revealed by flow chamber analysis. *EMBO J.* 21:2537–2546.

Ren, X.D., and M.A. Schwartz. 2000. Determination of GTP loading on Rho. *Methods Enzymol.* 325:264–272.

Roux, P., C. Gauthier-Rouviere, S. Doucet-Brutin, and P. Fort. 1997. The small GTPases Cdc42Hs Rac1 and RhoG delineate Raf-independent pathways that cooperate to transform NIH3T3 cells. *Curr. Biol.* 7:629–637.

Sahai, E., and C.J. Marshall. 2002. RHO-GTPases and cancer. *Nat. Rev. Cancer.* 2:133–142.

Sivasankar, S., B. Gumbiner, and D. Leckband. 2001. Direct measurements of multiple adhesive alignments and unbinding trajectories between cadherin extracellular domains. *Biophys. J.* 80:1758–1768.

Spector, I., N.R. Shochet, Y. Kashman, and A. Groweiss. 1983. Latrunculins: novel marine toxins that disrupt microfilaments organization in cultured cells. *Science.* 219:493–495.

Steinberg, M.S., and M. Takeichi. 1994. Experimental specification of cell sorting tissue spreading and specific spatial patterning by quantitative differences in cadherin expression. *Proc. Natl. Acad. Sci. USA.* 91:206–209.

Takaishi, K., T. Sasaki, H. Kotani, H. Nishioka, and Y. Takai. 1997. Regulation of cell–cell adhesion by Rac and Rho small G proteins in MDCK cells. *J. Cell Biol.* 139:1047–1059.

Thiery, J.-P., A. Delouvée, W.J. Gallin, B.A. Cunningham, and G.M. Edelman. 1984. Ontogenic expression of cell adhesion molecules: L-CAM is found in epithelia derived from the three primary germ layers. *Dev. Biol.* 102: 61–78.

Vasioukhin, V., C. Bauer, M. Yin, and E. Fuchs. 2000. Directed actin polymerization is the driving force for epithelial cell-cell adhesion. *Cell.* 100: 209–219.

Vestweber, D., and R. Kemler. 1985. Identification of a putative cell adhesion domain of uvomorulin. *EMBO J.* 4:3393–3398.

Volk, T., O. Cohen, and B. Geiger. 1987. Formation of heterotypic adherens-type junctions between L-CAM-containing liver cells and A-CAM-containing lens cells. *Cell.* 50:987–994.

Yap, A.S., and E.M. Kovacs. 2003. Direct cadherin-activated cell signaling: a view from the plasma membrane. *J. Cell Biol.* 160:11–16.

Yap, A.S., W.M. Brieher, M. Pruschy, and B.M. Gumbiner. 1997. Lateral clustering of the adhesive ectodomain: a fundamental determinant of cadherin function. *Curr. Biol.* 7:308–315.

Yonemura, S., M. Itoh, A. Nagafuchi, and S. Tsukita. 1995. Cell-to-cell adherens junction formation and actin filament organization: similarities and differences between non-polarized fibroblasts and polarized epithelial cells. *J. Cell Sci.* 108:127–142.

Can Small Complex Chains Be Treated as Polymers?

C. Gourier,*,† F. Pincet,† T. Le Bouar,† Y. Zhang,‡ J. Esnault,‡ J.-M. Mallet,‡ P. Sinay,‡ and E. Perez†

Laboratoire de Physique Statistique de l'Ecole Normale Supérieure, UMR 8550 associée au C.N.R.S. et aux Universités Paris 6 et Paris 7, 24 rue Lhomond, 75231 Paris Cedex 05, France, and Département de Chimie de l'Ecole Normale Supérieure, UMR 8642, 24 rue Lhomond, 75231 Paris Cedex 05, France

Received December 15, 2003; Revised Manuscript Received June 23, 2004

ABSTRACT: The interactions of supramolecular systems often depend on small and complex molecules. It is tempting though dangerous to apply polymer theory to these molecules that are normally considered to be too small to be polymers and too large to be rigid. Here, forces and adhesions between surfaces bearing several types of such molecules with both flexible and rigid parts are measured. The force/distance profiles follow closely the description given by polymer theory. It is shown for a wide variety of systems containing these molecules that if one obtains an effective radius of gyration R_g of the molecules, polymer theory can be used to predict their adhesion energy. Conversely, if the adhesion energy for bilayers containing such small and complex molecules is measured, polymer theory allows to deduce the effective R_g of the molecule.

I. Introduction

Many colloidal systems or surfaces bear a wide variety of molecules that determine the interactions of those surfaces with their environment.[1−4] These molecules may have various sizes and flexibilities, and it is tempting to predict their behavior with polymer theory. The lower size threshold for a molecule made of the same monomers to be considered as a polymer is not clear and depends on bond flexibility. The situation is difficult enough for homopolymers, but for a complex (or heterogeneous) molecule made of different parts, predictions are even more complex. This paper addresses this question and aims to test the relevance of polymer theory for surfaces bearing linear heterogeneous molecules of intermediate size. Here, force/distance profiles and adhesion measurements are compared with expected behaviors obtained by applying polymer theory to heterogeneous molecules.

A good example of such systems is provided by bilayers of lipids with flexible segments in their headgroups. These segments (oligosaccharides, polysaccharides, peptides, etc.) govern the bilayer equilibrium distance and determine their adhesion energy. For neutral lipids these two parameters result from a competition between the van der Waals forces and the steep short-range repulsions which depend strongly on the headgroup size of the lipids.[4,5] By contrast, polymer chains produce a repulsion of the brush or mushroom type.[6−9] Many flexible segments present on membranes are larger than usual lipid headgroups but presumably too small to be considered as polymers. Functionalized lipids often provide such intermediate size headgroups,[4] but few studies address the question of the short-range part of the force/distance profile. Kuhl et al.[10] reported such interactions and showed the validity of polymer theory for surfaces bearing linear and homogeneous molecules of small size (2000 M_w PEO chains). Here, we focus on molecules of similar sizes but with heterogeneous headgroups in which flexible parts are combined with more rigid ones.

II. Material and Methods

Four glycolipids were synthesized with different headgroup flexibilities and sizes (500−1500 M_w) (Figure 1). These headgroups are composed of some of the following patterns: a short linear and flexible PEO chain (P), a lactose (L), and a more rigid and complex sugar (Lex).[11] The names of the glycolipids reflect their compositions: PLex, PL, PLLex, PLLexLex (Figure 1).

Two techniques, the surface force apparatus (SFA)[12] and vesicle micromanipulation,[13] were used to measure interactions between layers made of those glycolipids. SFA experiments allowed the measurement of force/distance profiles between two mica surfaces in a crossed cylindrical geometry (with a radius of curvature R of about 2 cm), each bearing a glycolipid layer immersed in pure water.[12] In practice, the mica surfaces were coated with lipid bilayers by the Langmuir−Blodgett (LB) method. The monolayers in contact with mica were composed of a phospholipid (DOPC = 1,2-dioleoyl-*sn*-glycero-3-phosphocholine or DMPE = 1,2-dimyristoyl-d_{54}-*sn*-glycero-3-phosphoethanolamine) while the outer ones were composed either of pure glycolipids or of a mixture consisting of the phospholipid used for the inner layer and between 10% and 25% (mol/mol) of one of the glycolipids (Figure 2).

The second technique involved measurement of the adhesion energy between two osmotically controlled giant vesicles prepared from a mixture of one of the glycolipids and SOPC (1-stearoyl-2-oleoyl-*sn*-glycero-3-phosphocholine) in a 1:9 molecular ratio. The vesicles were manipulated in aqueous NaCl solution (200 mM) using the micropipet aspiration technique developed by Evans[13] and illustrated in Figure 3. The negative pressure (ΔP) in the pipet controls the positive hydrostatic pressure in the vesicle and thus the mechanical tension τ_m in the vesicle membrane. One of the vesicles is held with low pressure and remains deformable while the other one is held under a high aspiration pressure to be almost rigid. The free energy of adhesion was measured using the contact angle θ_c and the tension τ_m of the flaccid vesicle membrane: $E_{adh} = \tau_m(1 - \cos\theta_c)$. The measurement of θ_c was numerically deduced from geometrical parameters as indicated by Evans.[13]

III. Polymer and Bilayer Interactions

When a surface is coated with polymers at elevated concentrations such that the molecules are close enough

† UMR 8550.
‡ UMR 8642.
* Corresponding author: e-mail gourier@lps.ens.fr.

10.1021/ma035905m CCC: $27.50
Published on Web 10/16/2004

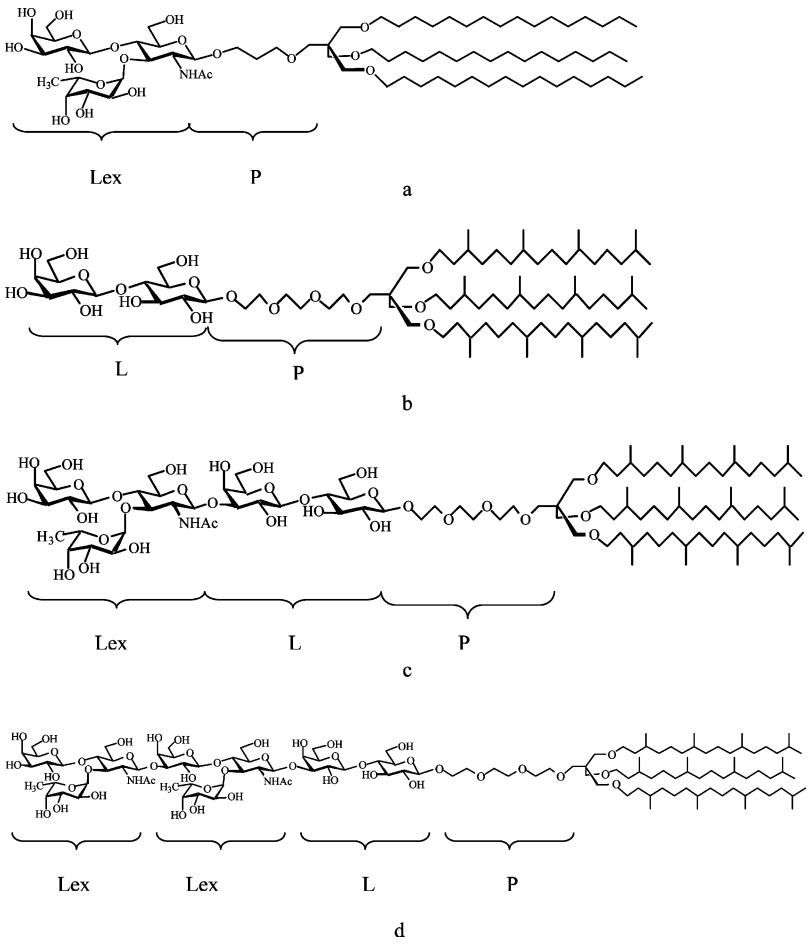

Figure 1. Glycolipids: (a) PLex is a Lex group connected to an aliphatic tail by a very short PEO chain, (b) PL is a lactose group connected to an aliphatic tail by a short PEO chain. (c) PLLex molecule is made of a PL molecule and one Lex group connected to the L group. (d) PLLexLex molecule is made of a PL molecule and two Lex group in series connected to L.

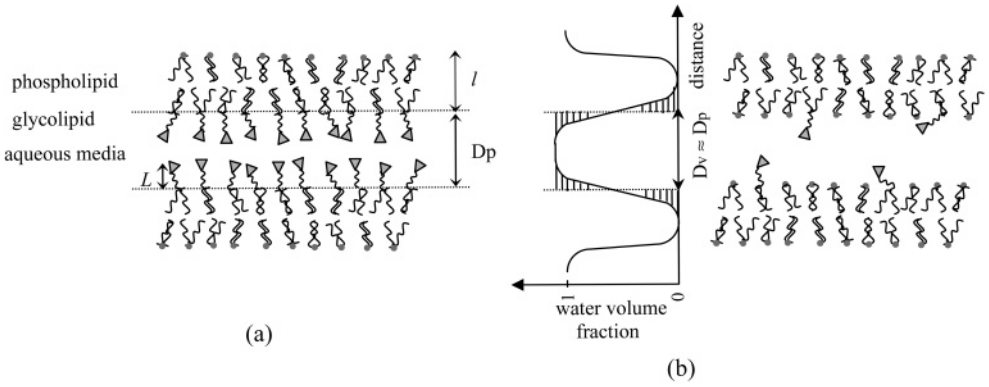

Figure 2. Representation of lipid bilayers in SFA experiments (a) for full coverage of glycolipids in the SFA experiments and (b) for partial coverage of glycolipids in SFA experiments or in vesicle experiments (in reality, in vesicles, the outer layer also contains some glycolipids). Lipid chains connected to circles symbolize phospholipids, whereas lipid chains connected to triangles (sugar headgroups) through small wiggles (PEO chains) symbolize glycolipids. The curve represents the water volume fraction (0 around the aliphatic chains and 1 in the gap between the layers). The distance D_v is taken between the water density-weighted interface; the four striped zones have the same areas. D_p is the distance between the surfaces as defined by the limit between the aliphatic tails and the headgroup of the glycolipids. When the density of glycolipids is small, which is always the case in vesicle experiments, the definitions of D_p and D_v give rise to similar distances D.

to overlap, the resulting layer is called a brush. In this case, the distance s between the polymer chains is smaller than twice the brush thickness L. Alexander and de Gennes[14–16] have derived the expression for the repulsion of two such brushes as a function of the separation distance D_p of the coated surfaces (Figure 2). For $D_p < 2L$, it is given by

$$E_{\text{brush}}(D_p) = \frac{4\beta k_B T}{s^3}\left[\frac{{D_p}^{7/4}}{7(2L)^{3/4}} + \frac{(2L)^{9/4}}{5{D_p}^{5/4}} - \frac{24}{35}L\right] \quad (1)$$

where β is an unknown numerical factor,[17] independent of s and L.

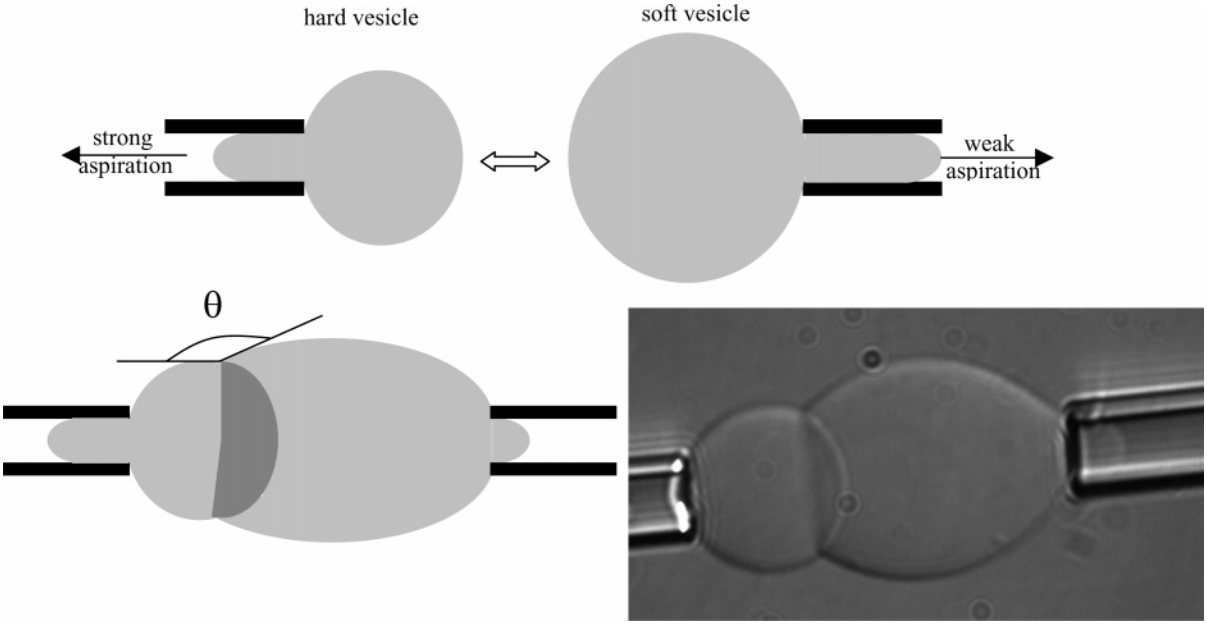

Figure 3. Principle underlying the measurement of adhesion energy by the micromanipulation of vesicles. The two osmotically controlled vesicles held in micropipets by aspiration are observed in interference contrast microscopy. The suction pressure applied to the micropipets allows the control of the tension of the vesicle bilayers. One of them (left) is pressurized into a tight-rigid sphere with large bilayer tension, whereas the adherent vesicle (right) is held with low pressure and remains deformable. The adhesion energy W_{adh} is obtained by determining the contact angle θ_c of the two vesicles and the tension τ_m of their membrane: $W_{adh} = \tau_m(1 - \cos \theta_c)$.

As the separation distance D_p approaches zero, eq 1 can be approximated[10] by

$$E_{brush}(D_p) \propto e^{-\pi D_p/L} \quad (2)$$

In contrast, low polymer surface concentrations with no chain overlap ($s > 2L$) correspond to the mushroom regime which produces an exponential repulsion profile as the surfaces get close to the contact:[10,18]

$$E_{mushroom}(D_p) = 36\Gamma k_B T e^{-D_p/R_g} \quad (3)$$

where Γ is the density of anchored polymers ($\Gamma = 1/s^2$) and R_g is the radius of gyration of the polymer.

One may note that at the limit between brush and mushroom regimes ($s \approx 2L$) steric repulsion due to the polymer effect can be described by either eq 2 or eq 3, which supposes that for intermediate polymer surface concentration L/π has to tend to R_g.

Lipid bilayers involving glycolipids such as those mentioned above differ from pure phospholipid bilayers by the presence of protruding large headgroups. A schematic of such lipid bilayers (either in SFA or in vesicles experiments) is given in Figure 2: a layer of thickness l comprising the phospholipids and/or the aliphatic tails of the glycolipids, from which protrude large linear and heterogeneous groups (the glycolipid headgroups: PEO plus polysaccharides). These prominent chains give rise to steric interactions that we may consider similar to those produced by polymers.

The equilibrium distance between two of these lipid bilayers is obtained by minimizing (relative to their separation distance) the free energy of interaction between them. This energy is comprised of many contribution elements: van der Waals attraction, steric repulsion due the protruding headgroups, undulation (or Helfrich) repulsion[19] which comes from spontaneous membrane undulations under thermal fluctuations and interactions due to hydration,[20] and protrusion effects.[21] One may note that these latter two interactions are not relevant here since the repulsions they generate have shorter range than the distances involved in the present SFA or vesicles experiments. At distances longer than the equilibrium distance, van der Waals attraction dominates the interaction profile, while at shorter distances, steric repulsion due to glycolipid headgroup and Helfrich undulations is predominant.

In SFA experiments, the bilayers are fixed on mica surfaces, and the distance between the surfaces can be modified through the mechanical force which is applied to the surfaces. Therefore, at separation distances smaller than the equilibrium distance, the interaction between the bilayers is repulsive due exclusively to the steric repulsions of the glycolipid headgroups. Indeed, the bilayers are not free to fluctuate and do not generate Helfrich repulsion. The particular characteristics of this technique permit the testing of the polymer aspect of the steric interaction.

By contrast, in the vesicle adhesion energy experiments, lipid bilayers are free to fluctuate, and the distance separating two vesicles is thus the equilibrium distance that results from the minimization of the free energy.

In the case of two interacting bilayers as shown in Figure 2b, the van der Waals attraction contributes to the interaction energy with a power law distance dependence given by[22]

$$E_{vdW}(D_v) = \frac{H}{12\pi}\left[\frac{1}{D_v^2} - \frac{2}{(D_v + l)^2} + \frac{1}{(D_v + 2l)^2}\right] \quad (4)$$

where H is the Hamaker constant and l the bilayer thickness.

The Helfrich entropic repulsion also follows a power law distance dependence.[19] The expression derived in ref 23 is suitable for lipid bilayers and will be used here:

$$E_{\text{Helfrich}}(D_v) = \frac{(k_B T)^2}{1.6\pi^2 k_c} \frac{1}{D_v^2} \quad (5)$$

where k_c is the bilayer rigidity modulus of curvature.

These two contributions depend on the separation distance D_v between the vesicles defined as the distance between the density-weighted interfaces (Figure 2b) because of the soft nature of bilayers.

IV. Results and Discussion

Polymer-like Interactions from SFA Force/Distance Profiles. The four force/distance profiles probed with the SFA technique were respectively those of monolayers of purePLex (Figure 4a), pure PLLex (Figure 4b), a 1:3 PLex/DMPE mixture (Figure 5a), and a 1:9 mixture of PLLex/DOPC (Figure 5b). Figures 4 and 5 display the short-range portion of the profiles due, as explained above, to the glycolipid headgroups. This steric interaction can be compared directly with the one given by the polymer theory. Because of the high glycolipid density, the brush character of surfaces fully covered with glycolipids (PLex or PLLex) (eq 1) can first be tested by fitting their force/distance profiles (Figure 4) using eq 1. For our systems, s, L, and D_p in eq 1 can respectively be seen as the distance between two glycolipids, the thickness of the layer made of the glycolipid headgroups, and the distance between the surfaces defined by the limit between the aliphatic tails and the headgroup of the glycolipids (see Figure 2a). s is not an adjustable parameter since it has been obtained independently by compression isotherm measurements before Langmuir−Blodgett deposition. In this study s is equal to 0.95 ± 0.05 nm for both PL and PLLex. The fit parameters β and L are given in Table 1. Figure 4 shows that fits are very good and accurate. Indeed, their ranges of adjustment are extremely narrow. The short and long dashed line in Figure 4b show how the best fit is changed when L is shifted by +0.05 nm and −0.2 nm from its optimal value. Similarly, a small variation of β would lead to a significant vertical translation of the curves.

The small thickness $L = s$ obtained for PLex layer indicates that despite the high coating density of PLex molecules, conditions approach the limit ($L = s/2$) between the brush and the mushroom regime. According to eqs 2 and 3, in that limit, L/π should tend to R_g. By reducing the PLex density by a factor of 4 (1:3 PLex/DMPE mixture), the mushroom regime should therefore be fully reached. Indeed, the force/distance profile (Figure 5a) has successfully been fitted with the exponential law given by eq 3. Like s, $\Gamma = 1/s^2$ is not an adjustable parameter since it has been obtained independently by compression isotherm measurements. For the 1:3 PLex/DMPE mixture $\Gamma = 0.35$ nm^{-2}. From the fit (Figure 5a), an effective R_g value of 0.32 nm (see Table 1) could be obtained. As expected, this value is close to that obtained for L/π (0.33 nm).

For a layer of pure PLLex, the thickness value ($L = 2$ nm $= 2s$, see Table 1) shows that the system is far from the mushroom regime. Nevertheless, if the PLLex molecule is diluted by a factor 10 in DOPC (1:9 of PLLex/DOPC mixture), the mushroom regime should be reached ($\Gamma = 0.1$ nm^{-2}). Indeed, the corresponding force/distance profile (Figure 5) fits well with the exponential law of eq 3. The strong difference between the R_g value (0.52 nm, Table 1) and the L/π value (0.64 nm) obtained with a brush regime (eq 2) shows that in this case the layer is far from the limit between brush and mushroom regimes.

In the Appendix, we demonstrate that fitting force/distance profiles of high glycolipid surface densities (pure PLex and pure PLLex layers) with the mushroom regime is not appropriate. Conversely, eq 1 relative to

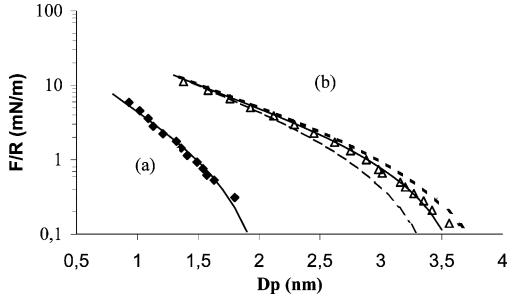

Figure 4. Force/distance profile for surfaces covered by a (a) PLex and (b) PLLex. The solid lines are best fits for β, L with the brush regime obtained from eq 1. The short and long dashed lines have been plotted to show the accuracy of the fit: they are the best fits for β with the brush regime obtained from eq 1 when shifting L by +0.05 nm and −0.2 nm from the value given in Table 1. A variation of β leads to a vertical translation of the curves. D_p is defined in Figure 2a.

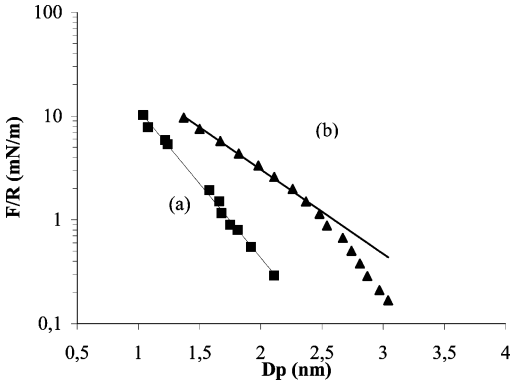

Figure 5. Force/distance profiles between surfaces covered by a monolayer of (a) a 1:3 mixture of PLex/DMPE and (b) a 1:9 mixture of PLLex/DOPC. The solid lines are fits of the mushroom regime at short distances obtained from eq 3. When the repulsion decreases at longer distances, the data points cannot be fitted anymore because the exponential approximation stops being valid. D_p is defined in Figure 2a.

Table 1. Values (in nm) of the Radius of Gyration R_g and of the Parameters β and L As Defined in the Text[a]

	β	L	R_g
PLex 100%			
Figure 6a —	**0.1**	**1.0**	
Figure 6a - - -	1.2	0.8	
Figure 6a ⎯			0.21
PLLex 100%			
Figure 6a —	**0.1**	**2.0**	
Figure 6a - - -	2.96	1.2	
Figure 6a ⎯			0.37
PLex/DMPE 1:3			
Figure 7a —			**0.32**
Figure 7a - - -	0.1	1.9	
Figure 7a ⎯	1.2	1.2	
PLLex/DOPC 1:9			
Figure 7a —			**0.52**
Figure 7a - - -	0.1	4.7	
Figure 7a ⎯	2.96	1.7	

[a] β, L: obtained by fitting force/distance profiles with eq 1 (brush regime). R_g: obtained by fitting force/distance profiles with eq 3 (mushroom regime).

Table 2. Vesicles' Free Adhesion Energy, Measured and Calculated, and Interaction Parameters for the Calculation of the Adhesion Energy; Equilibrium Distance D_{eq} and Calculated Adhesion Energy Are Obtained by Minimizing the Sum of the Different Energetic Contributions (E_{vdW}, $E_{mushroom}$, $E_{Helfrich}$)

	E_{adh} (μJ/m^2) measured	E_{adh} (μJ/m^2) calculated	R_g (nm)	D_{eq} (nm)	E_{vdW} (μJ/m^2)	$E_{mushroom}$ (μJ/m^2)	$E_{Helfrich}$ (μJ/m^2)
PL−PL	9.5 ± 0.5	9.8	0.41[a]	3.3	15.7	4.8	1.1
PLLex−PL	5.4 ± 1	5.9	0.47[b]	4.1	9.1	2.4	0.7
PLLex−PLLex	4.5 ± 2	4.0	0.52[c]	4.7	6.4	1.8	0.6
PLLexLex−PLLex Lex	4.5 ± 2	3.0	0.52 ± 0.07[d]	5.2	4.9	1.4	0.5

[a] Estimated from the molecular structure (see text). [b] Averaged from the R_g values of PLLex and PL. [c] Deduced from the fits of the force/distance profiles measured by SFA. [d] Calculated from the adhesion energy data (see text).

the brush regime is not suitable for coherently fitting the repulsion produced by the 1:3 of PLex/DMPE mixture and the 1:9 of PLLex/DOPC mixture.

The SFA experiments have shown that the steric repulsion due to large linear and heterogeneous groups (the glycolipid headgroups) are close to those produced by polymers in a brush or mushroom regime. By fitting force/distance profiles, an effective value of the gyration radius of PLex and PLLex headgroups is obtained. It is therefore tempting to use these effective radii of gyration to test whether we can predict the adhesion energy of two vesicles bearing such molecules.

Vesicles Adhesion Energy. Giant vesicles composed of a mixture (approximately 1:9) of PL, PLLex, or PLLexLex and SOPC have been used to measure the adhesion energy of the four following pairs: PLLex−PLLex, PL−PL, PLLex−PL, and PLLexLex−PLLexLex. The experimental results (Table 2) show that, as expected, the adhesion energies vary monotonically with the size of the headgroups. The larger the headgroups, the larger the steric repulsion and therefore the smaller the adhesion energies.

As mentioned above, the adhesion energy of two bilayers results from the balance between the van der Waals attraction and the repulsion that includes entropic (Helfrich undulations) and steric contributions (polymer effect). Note that when the density of glycolipids is small, which is always the case in vesicle experiments, D_p and D_v resolve to a common distance D. Assuming the additivity of these three contributions (the approximation of additivity introduces an error smaller than the experimental one),[24] the adhesion energy is calculated by minimizing the sum of these contributions (eqs 1−5). This requires the knowledge of several parameters: H and l (eq 4), k_c (eq 5), and R_g and Γ (eq 3) since the polymer effect of the glycolipid heads is of the mushroom type as suggested by SFA results for a small concentration of glycolipids. In the case of vesicles made with PLLex and SOPC, all these parameters are known. R_g, obtained by SFA experiments, is equal to 0.52 nm, and Γ, given by monolayer compression isotherms, is about 0.1 nm^{-2}. For SOPC, the Hamaker constant H is equal to 7×10^{-21} J,[25] but for pure glycolipid vesicles like those formed of digalactosyldiglyceride (DGDG), H is higher ($H = 25 \times 10^{-21}$ J).[25] H was therefore chosen equal to 9.5×10^{-21} J for the vesicles with 87% of SOPC and 13% of glycolipid in surface. The thickness used in the fits is that of SOPC: $l = 4.06$ nm (as measured in ref 5). k_c is equal to 9×10^{-20} J, as in ref 24. The adhesion energy for PLLex vesicles, calculated with these parameters, is equal to 4.0 μJ/m^2, and the details of energetic contributions as well as the related equilibrium distances can be found in Table 2. This result is in excellent agreement with the value experimentally measured (4.5 ± 2 μJ/m^2).

For both the PL−PL pair and the antisymmetric PLLex−PL pair, all the parameters required to calculate the adhesion energy are the same as for the PLLex−PLLex system, except the R_g value which is unknown for the PL molecule. Nevertheless, the PL headgroup is a linear and flexible chain with 16 beads, of which 14 have C−C or C−O bonds (≈0.15 nm) and two are sugar cycles (≈0.4 nm). These can be seen as ideally flexible chains for which R_g is given by $R_g = aN^{3/5}/6^{1/2}$ (a being the weighted average bead size and N the number of beads).[10,26] a is roughly equal to 0.18 nm; therefore, $R_g \approx 0.41$ nm. For the asymmetric PLLex−PL system, R_g can be taken equal to 0.47 nm, which is the averaged of the R_g of the PL−PL system (0.41 nm) and of the PLLex−PLLex one (0.52 nm obtained from the force/distance fits). As can be seen in Table 2, the calculated adhesion energies are consistent with the ones obtained experimentally. Moreover, the adhesion energy is very sensitive to a small variation of R_g as illustrated below in the discussion of the PLLexLex case.

The good agreement between the calculated adhesion energies and the experimental values confirms the above-mentioned SFA results, stressing that the interaction of lipids with large headgroups can be described in the same way as for polymers.

We have just seen that the use of independently obtained effective R_g values allows for the accurate prediction of the adhesion energy. It is interesting to test whether the reverse is true. Is it possible in the last system (the PLLexLex−PLLexLex pair) to deduce a consistent R_g value of the complex PLLexLex chain from the measured adhesion energy and its calculation? Given the error bar, the adhesion energy of the PLLexLex−PLLexLex system lies (see Table 2) between 2.5 and 6.5 μJ/m^2. Therefore, R_g should be equal to 0.52 ± 0.07 nm. This is compatible with the fact that it should be slightly larger than the one of PLLex. Therefore, even for a very complex molecule that produces small adhesion energy, the accuracy of the R_g value is still high.

V. Conclusion

In this work, we have used two very different techniques: the surface force apparatus which gives force/distance profiles and a micromanipulation system for measuring the adhesion energy of vesicles. With each technique, we have studied four different configurations involving either different molecules or different densities. Moreover, the molecules differed by the length of the flexible chain and its composition and also by the introduction of one or two rigid groups.

The SFA experiments allowed to directly observe the influence of the steric repulsion produced by the glycolipid headgroups on the force/distance profiles, show-

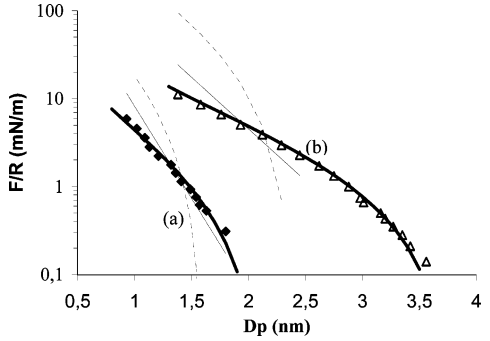

Figure 6. Force/distance profile for surfaces covered by a (a) PLex and (b) PLLex. The solid bold lines are best fits for β, L with the brush regime obtained from eq 1 (the same as in Figure 4). The solid thin lines are the best fits obtained with the mushroom regime (eq 3). The short dashed lines are the best fits obtained by fixing $\beta = 1.2$ for PLex and $\beta = 2.96$ for PLLex (see Figure 7).

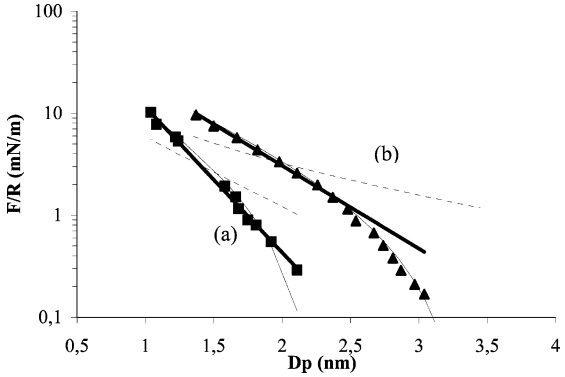

Figure 7. Force/distance profiles between surfaces covered by a monolayer of (a) a 1:3 mixture of PLex/DMPE and (b) a 1:9 mixture of PLLex/DOPC. The solid bold lines are the best fits with the mushroom regime at short distances obtained from eq 3 (the same as in Figure 5). The short dashed lines are the best fits obtained with the brush regime (eq 1) with $\beta = 0.1$ (value which provides the best "brush" fits for the pure PLex and pure PLLex force/distance profiles (see Figure 4 or Figure 6). The solid thin lines are the best fits obtained with the brush regime by allowing β to be different from 0.1.

ing their polymer-like nature. For the PLex and PLLex chains, a value of their effective R_g could be deduced from experiments. For the PL chain (linear and without rigid moiety), a value of R_g could be obtained from a crude structural argument. With these effective R_g values the calculation for three systems of the adhesion energy of two bilayers bearing these molecules has been done. The excellent agreement with the micropipet experimental value could show that the use of independently obtained R_g values allows accurate prediction of the vesicles' adhesion energies. For the more complex PLLexLex chain, a reliable R_g could be deduced from the measured adhesion energy and the calculation using polymer scaling theory.

Finally, this extended study shows that the behavior of small linear heterogeneous molecules is consistent with polymer scaling theory. This conclusion supported by the present study is likely to have some limitations, such as, if the rigid part were much larger than the flexible part of the molecules. However, this point will remain unclear until measurements are done with such molecules. Nevertheless, the main conclusion applies to a majority of the functionalized lipids used in soft matter physicochemistry.

Appendix

Figure 4 shows that the relationship describing the interaction between two polymer brushes (eq 1) provides a good description of the interaction between surfaces with high glycolipid densities.

Figure 5 illustrates that a mushroom interaction (eq 3) can nicely account for the interaction between surfaces with low density of glycolipids close to the contact.

In eq 3, only R_g is a fit parameter since Γ is independently obtained by compression isotherm measurements. The force at $D = 0$ is therefore fixed. In pure Plex and PLLex layers Γ is equal to 1.1 and 0.35 nm^{-2} (0.1 nm^{-2}) in the 3:1 PLex/DMPE mixture (9:1 PLLex/DOPC mixture). Figure 6 clearly shows that attempts to fit the force/distance profiles of the dense layers (pure PLex (curve a) and pure PLLex (curve b)) with the mushroom relation (eq 3) do not give satisfactory results.

In eq 1, not only L but also β are parameters. However, β depends neither on L nor on s. To determine whether the brush interaction (eq 1) could also describe the force/distance profile obtained with low density of glycolipids, β should be fixed to the value obtained for high coverage of glycolipids ($\beta \approx 0.1$ for both PLex and PLLex layers). Figure 7 shows that the best fits obtained are still very far from experimental curves. Better fits (see Figure 7) could be obtained by also fitting β (see Table 1). However, with such β values the fits for the denser surfaces are irrelevant (see Figure 6 and Table 1).

The main conclusion of this Appendix is that the steric repulsion due to the glycolipid headgroups can be well described by the polymer theory. As in the case of real polymers, the expressions depend on the surface densities of the glycolipids.

References and Notes

(1) Ricoul, F.; Dubois, M.; Belloni, L.; Zemb, T.; Andre-Barres, C.; Rico-Lattes, I. *Langmuir* **1998**, *14*, 2645.
(2) Pincet, F.; Perez, E.; Lebeau, L.; Mioscowski, C. *Phys. Rev. Lett.* **1994**, *73*, 2780.
(3) Helm, C.; Knoll, W.; Israelachvili, J. N. *Proc. Natl. Acad. Sci. U.S.A.* **1991**, *88*, 8169.
(4) Luckham, P.; Wood, J.; Swart, R. *J. Colloid Interface Sci.* **1993**, *156*, 173.
(5) Rand, R. P.; Parsegian, V. A. *Biochim. Biophys. Acta* **1989**, *988*, 351.
(6) Taunton, H. J.; Toprakcioglu, C.; Fetters, L. J.; Klein, J. *Nature (London)* **1988**, *332*, 712.
(7) Israelachvili, J. N. In *Intermolecular and Surface Forces*; Academic Press Limited: London, 1991; p 450.
(8) Taunton, H. J.; Toprakcioglu, C.; Fetters, L. J.; Klein, J. *Macromolecules* **1990**, *23*, 571.
(9) De L. Costello, B. A.; Luckam, P. F.; Tadros, Th. F. *J. Colloid Interface Sci.* **1993**, *156*, 72.
(10) Kuhl, T. L.; Leckband, D. E.; Lasic, D. D.; Israelachvili, J. N. *Biophys. J.* **1994**, *66*, 1479.
(11) Henry, B.; Desvaux, H.; Pristchep, A. M.; Berthault, P.; Zhang, Y. M.; Mallet, J. M.; Esnault, J.; Sinay, P. *Carbohydr. Res.* **1999**, *315*, 48.
(12) Israelachvili, J. N.; Adams, G. E. *J. Chem. Soc., Faraday Trans. 1* **1978**, *74*, 975.
(13) Evans, E. *Colloids Surf.* **1990**, *43*, 327.
(14) Alexander, S. *J. Phys. (Paris)* **1977**, *38*, 983.
(15) de Gennes, P. *Macromolecules* **1981**, *14*, 1637.
(16) de Gennes, P. *Adv. Colloid Interface Sci.* **1987**, *27*, 189.
(17) Milner, S. T. *Europhys. Lett.* **1988**, *7*, 695.
(18) Dolan, A.; Edwards, F. *Proc. R. Soc. London A* **1974**, *337*, 509.
(19) Helfrich, W. *Z. Naturforsch.* **1978**, *33A*, 305.
(20) Parsegian, V. A.; Rand, R. P. *Biochim. Biophys. Acta* **1989**, *988*, 351.

(21) Israelachvili, J. N.; Wennerström, H. *J. Phys. Chem.* **1992**, *96*, 520.
(22) Lis, L. J.; Mcalister, M.; Fuller, N.; Rand, R. P.; Parsegian, V. A. *Biophys. J.* **1982**, *37*, 657.
(23) Evans, E. *Langmuir* **1991**, *7*, 1900.
(24) Evans, E.; Parsegian, V. A. *Proc. Natl. Acad. Sci. U.S.A.* **1986**, *83*, 7132.
(25) Evans, E.; Needham, D. *J. Phys. Chem.* **1987**, *91*, 4219.
(26) Doi, M.; Edwards, S. F. *The Theory of Polymer Dynamics*; Oxford Science Publications: New York, 1986; Chapter 2, p 8.

MA035905M

THE JOURNAL OF BIOLOGICAL CHEMISTRY
Vol. 279, No. 19, Issue of May 7, pp. 19649–19657, 2004

Printed in U.S.A.

Enhanced Adhesive Capacities of the Naturally Occurring Ile^{249}–Met^{280} Variant of the Chemokine Receptor CX3CR1*

Received for publication, December 9, 2003, and in revised form, February 25, 2004
Published, JBC Papers in Press, February 27, 2004, DOI 10.1074/jbc.M313457200

Mehdi Daoudi, Elise Lavergne, Alexandre Garin, Nadine Tarantino, Patrice Debré, Frédéric Pincet‡, Christophe Combadière, and Philippe Deterre§

From the Laboratoire d'Immunologie Cellulaire, INSERM U543, Faculté de Médecine Pitié-Salpêtrière, 91 Boulevard de l'Hôpital, 75013 Paris, France and the ‡Laboratoire de Physique Statistique de l'Ecole Normale Supérieure, CNRS UMR 8550, 24 rue Lhomond, 75005 Paris, France

It was recently shown that individuals carrying the naturally occurring mutant CX3CR1-Ile^{249}–Met^{280} (hereafter called CX3CR1-IM) have a lower risk of cardiovascular disease than individuals homozygous for the wild-type CX3CR1-Val^{249}–Thr^{280} (CX3CR1-VT). We report here that peripheral blood mononuclear cells (PBMC) from individuals with the CX3CR1-IM haplotype adhered more potently to membrane-bound CX3CL1 than did PBMC from homozygous CX3CR1-VT donors. Similar excess adhesion was observed with CX3CR1-IM-transfected human embryonic kidney (HEK) cell lines tested with two different methods: the parallel plate laminar flow chamber and the dual pipette aspiration technique. Suppression of the extra adhesion in the presence of pertussis toxin indicates that G-protein mediated the underlying transduction pathway, in contrast to the G-protein-independent adhesion previously described for CX3CR1-VT. Surprisingly, HEK and PBMC that expressed CX3CR1-IM and -VT were indistinguishable when tested with the soluble form of CX3CL1 for chemotaxis, calcium release, and binding capacity. In conclusion, only the membrane-anchored form of CX3CL1 functionally discriminated between these two allelic isoforms of CX3CR1. These results suggest that each form of this ligand may lead to a different signaling pathway. The extra adhesion of CX3CR1-IM may be related to immune defenses and to atherogenesis, both of which depend substantially on adhesive intercellular events.

Adhesion, a critical stage in cell trafficking and migration (1, 2), requires the presence of numerous adhesion molecules, such as integrins, that need divalent ions to function. Recent studies show that two chemokines, namely, CX3CL1 and CXCL16, are not only chemoattractant as soluble molecules, but also function as adhesion molecules since they are membrane-anchored, regardless of the presence of divalent ions (3–7). The best known of these is CX3CL1, also called fractalkine. It is expressed on the surface of many types of cells, in particular interleukin-1- and tumor necrosis factor-activated endothelial (4) and dendritic cells (8), as a membrane molecule containing the classic chemokine domain, a mucin-like stalk, and a transmembrane domain tethering it to the cell membrane. CX3CL1 may be cleaved by TACE and released from cells (9, 10). In this soluble form, it behaves like a chemoattractant molecule, just as other chemokines do. The transmembrane feature of the native CX3CL1 protein, combining it with its receptor, CX3CR1, produces a strongly adhesive pair (4, 5, 11) that mediates the rapid capture and firm adhesion of leukocytes. Because this activity persists in the absence of divalent cations, it is thought to be independent of integrins (5, 11, 12). This adhesive feature is also independent of the G_i pathway, since it is still present after pertussis toxin (PTX)[1] treatment (4, 5, 11).

The CX3CR1 molecule is expressed on leukocytes, especially monocytes (4) and cytotoxic cells (13, 14), on dendritic cells (15), and on neurons and microglial cells (16, 17). Recently, we identified two common polymorphisms in strong linkage disequilibrium in the *CX3CR1* gene: V249I and T280M (18). We also found that these mutations are associated with more rapid progression to AIDS (18, 19), although two studies have failed to confirm this association (20, 21). A recent work indicates that these mutations are linked to earlier immunological failure in response to antiretroviral therapy (22). It seems unlikely that CX3CR1, which functions as an HIV co-receptor *in vitro* (23–25), has the same role under pathophysiologic conditions. The effect of the mutation is probably related to the role of cytotoxic T cells, as pointed out recently (13, 14).

These two mutations are also associated with reduced prevalence of acute coronary events and atherosclerosis (26–28), but not with peripheral arterial diseases (29). The causal mechanism of these effects remains unclear. Previous studies, including ours, have hypothesized that the mutation might decrease the affinity of CX3CL1 to its receptor (18, 28). Moreover the CX3CR1-Ile^{249} variant has repeatedly been found to be expressed less often by PBMC than is CX3CR1-Val^{249} (18, 26). We show here that the situation is more complex. We investigated possible differences in the molecular properties of these variants and found that, although they responded similarly to soluble CX3CL1, they behaved very differently as adhesion molecules. Surprisingly, the mutated Ile^{249} CX3CR1 genotype was associated with enhanced adhesiveness.

* This work was supported in part by Grant 7516 from the Association pour la Recherche sur le Cancer (to P. D.), by the French Ministry of Research (ACI Jeunes Chercheurs, to C. C.), and by the French Association for AIDS Research (ANRS). The costs of publication of this article were defrayed in part by the payment of page charges. This article must therefore be hereby marked "*advertisement*" in accordance with 18 U.S.C. Section 1734 solely to indicate this fact.

§ To whom correspondence should be addressed: Laboratoire d'Immunologie Cellulaire INSERM U 543, Faculté de Médecine Pitié-Salpêtrière, 91, boulevard de l'Hôpital 75013 Paris, France. Tel.: 33-1-40-77-98-93; Fax: 33-1-40-77-97-34; E-mail: deterre@ccr.jussieu.fr.

[1] The abbreviations used are: PTX, pertussis toxin; AIDS, acquired immunodeficiency syndrome; BSA, bovine serum albumin; DMEM, Dulbecco's modified Eagle's medium; HBSS, Hank's balanced saline solution; HEK, human embryonic kidney cell line clone 293; HIV, human immunodeficiency virus; MAP, mitogen-activated protein; PBMC, peripheral blood mononuclear cells; PBS, phosphate-buffered saline; FITC, fluorescein isothiocyanate.

EXPERIMENTAL PROCEDURES

CX3CR1 Variant Constructs—Open reading frames corresponding to CX3CR1-Val^{249}–Thr^{280} (CX3CR1-VT) and CX3CR1-Ile^{249}–Met^{280} (CX3CR1-IM) were amplified from genomic DNA prepared from PBMC from two healthy donors with the corresponding genotypes. To do that, we used HindIII-tailed forward primer (LT5-CX3CR1, GCGCATATAAGCTTGCCACCATGGATCAGTTCCCTGAATCAG) and XhoI-tailed reverse primer (LT3-CX3CR1, GCGGATATGTCGACCTCGAGTCACGAGTCAGAGAAGGAGCAA). The PCR-cycling conditions were 95 °C for 5 min followed by 30 cycles at 95 °C for 1 min, 52 °C for 1 min, and 72 °C for 1 min. The PCR product was then digested with HindIII and XhoI (Promega, Charbonnières, France), subcloned into the mammalian expression vector pCDNA3.1(+) (Invitrogen, Cergy-Pontoise, France), and then sequenced on both strands with the BigDye Terminator kit (Applied Biosystems, Warrington, UK).

Cell Culture and Transfection—HEK cells were cultured in Dulbecco's modified Eagle medium (DMEM) supplemented with 10% fetal calf serum, 1 mM sodium pyruvate, 2 mM glutamine, 100 units/ml penicillin, and 100 μg/ml streptomycin (Invitrogen). To generate stably transfected clones, we used Transfast (Promega) in accordance with the manufacturer's instructions. We transfected 10^6 HEK cells in 3-cm dishes with 2 μg of each pcDNA3.1 construct (Invitrogen) with CX3CR1 inserts encoding the *CX3CR1* variant gene. Clones were derived by selection in 1 mg/ml G418 (Invitrogen). The clones thus obtained were assayed for CX3CL1 binding, and those expressing high levels of CX3CR1 were selected for further study. The clones were maintained in DMEM medium containing G418 and were checked with CX3CL1 binding for CX3CR1 expression before each experiment. To obtain transiently transfected HEK cells, we used JetPei™ (cationic polymer transfection reagent, Qbiogene, Illkirch, France) in accordance with the manufacturer's instructions. We used 3 μg of each pcDNA3.1 construct to transfect 4×10^5 HEK cells in a 6-well plate. After 2 days, transfected cells were resuspended by incubation with PBS for 30 min at 37 °C and were checked with CX3CL1 binding for CX3CR1 expression before use. For CX3CL1 transfection in HEK, we used pBlast plasmid (InvivoGen, Toulouse, France) with a CX3CL1 insert or with no insert. For stable expression, clones were derived by selection in 5 μg/ml blasticidin (Euromedex, Mundolsheim, France) for at least 1 month. The clones thus obtained were assayed for CX3CL1 staining by flow cytometry, and those expressing high levels of CX3CL1 were selected for further study. The clones were maintained in DMEM medium containing blasticidin and were checked before each experiment for CX3CL1 expression by flow cytometry. PBMC were isolated from heparinized venous blood from healthy volunteers by one-step centrifugation on a Ficoll-separating solution (Biochrom KG, Berlin, Germany).

Flow Cytometry—The cells (10^5 PBMC or 2.5×10^5 HEK) were tested for CX3CR1 expression by flow cytometry after staining by fluorescein isothiocyanate (FITC)-conjugated anti-CX3CR1 monoclonal antibody (MBL, Nagoya, Japan). As a control, the cells were incubated without any antibody. We verified that this produced the same signal as an isotype antibody control. The different PBMC subsets were quantified sequentially, in 2 ways: first, by discriminating lymphocytes and monocytes according to their width and granulometry (SSC *versus* FSC diagram), and second, by staining with various antibodies as follows. The lymphocytes (CD3+CD4+, CD3+CD8+) and the NK cells (CD4-, CD8low, CD16+, CD56+) were analyzed with FITC-anti-CD3, phycoerythrin (PE)-conjugated anti-CD16 plus anti-CD56, and AlloPhycoCyanin (APC)-conjugated anti-CD4 or anti-CD8. The monocytes (CD3-, CD4 low, CD8-, CD14+) were analyzed with FITC-anti-CD4, PE anti-CD14, APC anti-CD8, and peridinin chlorophyll A protein (PerCP) anti-CD3. All antibodies were from BD Biosciences (Le Pont de Claix, France). FACScalibur™ performed fluorescent analysis with CellQuestPro™ software (BD Biosciences).

^{125}I-CX3CL1 Binding Assay—PBMC (10^6 cells per sample) or HEK cells (2×10^5 or 2×10^6 cells per sample, for stable clones or transiently transfected cells, respectively) were washed in PBS and suspended in 200 μl of PBS containing 2.5 mg/ml bovine serum albumin (BSA, fraction V, Sigma) and 0.005% azide with 50 pM ^{125}I-CX3CL1 (Amersham Biosciences) in the presence or absence of 50 nM unlabeled human CX3CL1 (TEBU, Le Perray en Yvelines, France). After 2 h at 37 °C, unbound chemokines were separated from cells by centrifugation in 1 ml of PBS supplemented with 10% sucrose. Gamma emissions were then counted in the cell pellet. For association studies, cells were incubated with 50 pM ^{25}I-CX3CL1 under the same conditions as above (PBS+BSA+azide, 37 °C) for increasing periods of time and washed.

Calcium Response Assay—Intracytoplasmic free calcium was measured with Fura-2/AM (Molecular Probes, Leiden, Netherlands). HEK cells (3×10^6) were washed once and loaded for 45 min at 37 °C, in the dark, with 2 μM Fura-2/AM and 2 μM pluronic acid in 1 ml of HBSS buffer supplemented with 10 mM HEPES, 0.5 mM $MgCl_2$, and 1 mM $CaCl_2$. After centrifugation, the pellet was resuspended in 2 ml of the same buffer and transferred to a quartz cuvette for reading. CX3CL1 was added to the cell volume at various concentrations. Fluorescence was monitored with a SAFAS spectrofluorometer (SAFAS S.A., Monaco) in cuvettes thermostatically controlled at 37 °C and stirred continuously. The cell suspension was excited alternately at 340 and 380 nm and fluorescence measured at 510 nm. 10-nm slit widths were used for both excitation and emission. Graphic representation of intracellular calcium concentrations were computed with Equation 1,

$$[Ca^{++}] = 225 \times R/(R_{max} - R) \times Sf_{380}/Sb_{380} \qquad \text{(Eq. 1)}$$

which was previously determined by Grynkiewicz (30), with R the ratio of the fluorescence measured at the 340 and 380 nm excitations. R_{max} was evaluated by lysing the cells with 0.5% Triton X-100, and R_{min} determined by adding the excess EGTA. Sb_{380} and Sf_{380} were the fluorescence levels at 380-nm excitation, both determined under the same conditions.

Chemotactic Migration Assay—Chemotaxis was assayed in a 96-well chemotaxis chamber with a filter porosity of 10 μm (NeuroProbe, Cabin John, MD) for HEK cells and 5 μm for PBMC. The cells were washed twice with PBS, resuspended in serum-free RPMI 1640 medium (Invitrogen) containing 5 mg/ml BSA, then labeled for 30 min at 37 °C with 5-(and-6)-carboxyfluorescein diacetate, succinimidyl ester (Molecular Probes) in RPMI 1640. Cells were then washed in PBS and resuspended in HBSS buffer supplemented with 10 mM HEPES, 0.5 mM $MgCl_2$, and 1 mM $CaCl_2$ (10^6 cells/ml). 80 μl of this cell suspension was loaded onto the filter. A final volume of 28 μl of medium with various concentrations of CX3CL1 was placed in the lower chamber. The 96-well plate was then incubated for 2–3 h at 37 °C, 100% humidity, and 5% CO_2. The filter top surface was rinsed with PBS, and the plate centrifuged for 2 min at 1500 rpm. Fluorescence was measured with a Packard Fusion microplate analyzer (PerkinElmer Life Sciences).

Parallel Plate Laminar Flow Chamber Adhesion Assay—Adhesion experiments used the parallel plate flow technique and the chamber previously described (31). The coverslips we used were either cultured with adherent HEK cells (HEK-pBlast or HEK-FKN clones) or coated with CX3CL1 (Fig. 1*C*), as follows: the coverslip was coated with 10 μl of anti-His_6 antibody (25 μg/ml in PBS plus 0.5 mM $MgCl_2$ and 1 mM $CaCl_2$) for 30 min at 37 °C, washed in PBS, coated with 10 μl of 100 nM CX3CL1-His_6 (RnD Systems, Lille, France) for 1 h at 37 °C, and then coated with saturating solution (PBS plus 3 mg/ml BSA and 50 mg/ml sucrose) for 1 h at 37 °C. The coverslip was pressed by a screwed steel plate against a drilled plexiglass block that contained a cavity measuring $0.1 \times 8 \times 20$ mm^3 surrounded by a toric gasket (Satim, Evenos, France). The chamber was set on the stage of an inverted microscope (TE300, Nikon, France) equipped with a phase contrast 10× objective (Nikon, n.a. 0.25) and a cooled CCD camera (Sensicam, PCO, Kelheim, Germany). HEK-CX3CR1 clone cells or PBMC were suspended in PBS, incubated for 30 min at 37 °C with 1 μM 5-(and-6)-carboxyfluorescein diacetate, succinimidyl ester (Molecular Probes), for labeling and resuspended in flow buffer (HBSS supplemented with 2.5 mM EDTA, 2.5 mM EGTA, 10 mM HEPES, 2 mg/ml BSA) at 10^6 cells per ml for HEK clones and at 4×10^6 cells per ml for transiently transfected HEK and PBMC. For the tests assessing the impact of divalent cations, the buffer contained 0.5 mM $MgCl_2$ and 1 mM $CaCl_2$ rather than EGTA or EDTA. A syringe pump (PHD 2000; Harvard Apparatus, Les Ulis, France) drove 0.5 ml of cell suspension through the chamber at a wall shear stress of 1.5 dynes·cm^{-2}. The buffer was warmed to 37 °C before the syringes were filled and maintained at 37 °C by plunging the tubing into a thermostatically controlled bath. After a 10-min wash at 1.5 dynes·cm^{-2}, fluorescent images of two separate 0.5 mm^2 fields were recorded to count the adherent cells (excitation 450–500 nm, emission 510–560 nm, dichroic filter Q505lp, Chroma, Brattleboro, VT). The shear stress was then set at 15 dynes·cm^{-2} for 5 min, 75 dynes·cm^{-2} for 2 min, and finally 150 dynes·cm^{-2} for 2 min. The adherent cells were counted at each step. The number of cells was expressed as the mean of the count of the two 0.5 mm^2 fields. The number of adherent PBMC cells was expressed as the percentage of the total number of CX3CR1$^+$ injected cells, evaluated by flow cytometry with a CX3CR1-specific monoclonal antibody (MBL, Nagoya, Japan). Specific adhesion was obtained by subtracting the number of cells adhering to the HEK-pBlast coverslip from the number adhering to the HEK-CX3CR1. The results were expressed as the mean ± S.E. of four or more measurements.

Dual Pipette Aspiration Technique—The dual pipette adhesion assay

was performed on the stage of a Leica inverted microscope, positioned on an anti-vibration platform with a digitally controlled thermostat and equipped with ×10 and ×63 objectives. The incubation chamber consisted of the bottom of a 90-mm Petri dish covered with the inverted bottom of a second dish of the same size. All surfaces in contact with the cells were precoated with BSA, inactivated for 3 min at 80 °C (3 mg/ml). Before the assay, the chamber was loaded with CO_2-independent medium (Invitrogen) supplemented with 2 mM glutamine, penicillin (100 IU/ml), streptomycin (100 μg/ml), 2.5 mM EGTA, and 2.5 mM EDTA. To obtain an inner diameter of between 4.0 and 5.5 μm, we pulled (with a Sutter instrument, model P-2000), cut, and then fire-polished micropipettes with a homemade microforge. Before the adhesion assay, pipettes were filled with sterile isotonic sucrose solution (300–330 mosM) and preincubated in BSA. Cells were manipulated with two micropipettes, each held in its own micromanipulator and connected to a combined hydraulic/pneumatic system that provided the necessary control of the aspiration force applied to the cells.

The protocol we used is very similar to that of Chien and co-workers (32). Two cells, collected by gentle aspiration onto the tip of each pipette (cell number 1 in pipette A, cell 2 in pipette B), were brought into contact through the use of the micromanipulators and allowed to remain in contact for different periods of time (Fig. 3*C*, 2–30 min). To separate the cells, aspiration in pipette B was maintained at a level sufficiently high to hold cell number 2 tightly, while the aspiration in pipette A was increased in steps measured with a pressure sensor (Validyne: model DP103–38; ranging from 0 to 50,000 Pascal units). After each step, the pipettes were moved apart in an effort to detach the adherent cells from one another. A pair pulled intact from pipette A was moved back to the pipette orifice, the aspiration in the pipette was increased, and another attempt was made to detach the cells from each other. The cycle was repeated until the level of aspiration in pipette A was sufficient to pull one cell apart from the other. The aspiration employed in each cycle was monitored continuously. In most cases, cell deformation and contact area variation during the separation process were very limited (less than 20% for the contact area), and the separation took place suddenly, in less than a tenth of a second. The cells appeared to behave more like rigid structures than like two adhering deformable capsules. The usual approach (33, 34) of measuring contact angles at the end of the pipette and at the edge of the contact thus did not seem useful. The separation force (F) for rigid structures can be deduced from the data.[2] The values recorded for each of the last two cycles in the series (P_{n-1} and P_n) were used to calculate F for the pair tested, with Equation 2,

$$F = \pi(d/2)^2(P_{n-1} + P_n)/2 \qquad \text{(Eq. 2)}$$

with d the internal diameter of pipette A. This relation assumes that the pressure inside the cell is the same as that in the chamber; valid in our case since the tension of the cell is essentially zero. The results were expressed as mean ± S.E. for 13 or more measurements.

Western Blot Analysis of p44/42 MAP Kinase Phosphorylation—HEK cells were starved for 18 h in DMEM without SVF and suspended at 10^7 cells/ml in RPMI 1640 medium supplemented with 1 mM HEPES and 1 mg/ml BSA. After addition of 50 nM CX3CL1 for the indicated time, the samples (10^6 cells) were washed in 1 ml of PBS at 4 °C. Pellets were resuspended in 20 μl of Tris, 20 mM, pH 7.5, 1 mM EDTA 1 mM orthovanadate, 25 mM NaF, 5 mM pyrophosphate (Sigma), and 1 mM dithiothreitol supplemented with Complete protease inhibitor from Roche Applied Science for 30 min at 4 °C. Nuclear and cellular debris were removed by centrifugation for 10 min at 10 000 × g. The samples were then assayed for protein content, diluted in sample buffer (50 mM Tris, pH 7, 3% SDS, 10% glycerol, 5% 2-mercaptoethanol, and bromphenol blue) and heated for 3 min at 95 °C. Proteins were separated by standard SDS-PAGE. Gels were electrotransferred to Hybond-P nitrocellulose membrane (Amersham Biosciences), and the blots probed with polyclonal antibodies raised against phospho-p44/42 MAP kinase (Thr^{202}/Tyr^{204}) or p44/42 MAP kinase (Cell Signaling, New England Biolabs, Hitchin, UK) in accordance with the manufacturer's instructions. For detection, we used horseradish peroxidase-conjugated goat anti-mouse IgG (Bio-Rad) and an enhanced chemiluminescence detection system (Amersham Biosciences), in accordance with the manufacturer's instructions, on Curix Blue x-ray film (Agfa, Mortsel, Belgium). LY-294002 and PD-98059 (2′-amino-3′-methoxyflavone) were purchased from New England Biolabs and Biomol, respectively.

[2] Y.-S. Chu, S. Dufour, J. P. Thiery, E. Perez, and F. Pincet, submitted manuscript.

RESULTS

Enhanced Cell Adhesive Functioning for PBMC That Express CX3CR1-IM—We used the parallel plate adhesion method to compare the adhesion of PBMC from donors with different CX3CR1 genotypes to a monolayer of CX3CL1-expressing HEK. At low perfusion rates (1.5 dynes·cm^{-2}), we repeatedly found that cells from donors heterozygous for the 249 and 280 positions (VI-TM) of CX3CR1 (Fig. 1*A*, *solid squares*) were captured in significantly larger numbers than cells from those homozygous for the wild-type genotype (VV-TT) (Fig. 1*A*, *solid triangles*). Cells from individuals with both genotypes began to dissociate at a shear stress higher than 15–20 dynes·cm^{-2} (Fig. 1*A*, *solid symbols*). Nonspecific adhesion, *i.e.* capture on CX3CL1-negative HEK cells, was very low and very similar for cells of both genotypes (Fig. 1*A*, *open symbols*). Pretreatment of PBMC with 100 nM CX3CL1 for 45 min at 37 °C almost totally abolished the adhesion, which indicates that PBMC capture by CX3CL1+ HEK was mostly specific for the CX3CR1/CX3CL1 pair and operated through the interaction between the two molecules. Moreover, our adhesion experiments were performed in the presence of divalent chelators to prevent the activity of other adhesion molecules, such as integrins, that are Ca^{2+}- and Mg^{2+}-dependent. Finally we tested the PBMC adhesion with a more physiological type of CX3CL1+ cell: our results were similar when the CX3CL1+ HEK layer cells were replaced by a smooth muscle aortic cell line that expresses CX3CL1 after pretreatment with TNFα and INFγ (35, 36) (data not shown).

The differences we observed in the adhesion behavior of cells with these CX3CR1 variants were not due merely to differences in receptor expression. Instead, we found that the frequency of $CX3CR1^+$ cells was regularly lower in PBMC with the CX3CR1-VI-TM than in cells expressing the nonmutated receptor CX3CR1-VV-TT (Table I). Similarly, the ^{125}I-CX3CL1 binding assay indicated that, as we noted previously (26), cell suspensions with the CX3CR1-VI-TM genotype had only 67 ± 11% (n = 7) as many binding sites (B_{max}) as suspensions with CX3CR1-VV-TT cells. Yet, although there were fewer $CX3CR1^+$ cells, there were more cells adhering to membrane CX3CL1. The effect of CX3CR1 mutations was therefore underestimated. Accordingly, we expressed the specific adhesion by calculating the ratio of $CX3CR1^+$ cells specifically adhering to membrane CX3CL1 (see "Experimental Procedures"). Fig. 1*B* reports PBMC-specific adhesion for each CX3CR1 allele. No significant differences in adhesion were observed between the PBMC expressing CX3CR1 that differed only at the 280 position (Fig. 1*B*, compare VI-TT with VI-TM and II-TM with II-MM). In contrast, the Ile^{249} substitution appeared crucial. Adhesion was already significantly greater with the PBMC from heterozygous VI-TT individuals than from the VV-TT homozygote (Fig. 1*B*). Moreover, PBMC from carriers homozygous for position 249 (*i.e.* II-TM and II-MM, Fig. 1*B*, *right*) adhered significantly more than PBMC from heterozygous (*i.e.* VI-TT and VI-TM, Fig. 1*B*, *center*) donors. The amplitude of extra adhesion therefore appears to be directly correlated with the number of Ile^{249} alleles, according to a simple gene dosage effect.

To verify the absence of nonspecific cell-cell interaction, we performed experiments with immobilized CX3CL1. We found that PBMC from CX3CR1-VI-TM donors adhered to coverslip coated with recombinant CX3CL1 at a rate more than twice that of cells from CX3CR1-VV-TT individuals, and this was the case regardless of the presence of divalent cations (Fig. 1*C*, *solid bars*). This confirms that the excess adhesion in the presence of the Ile^{249}–Met^{280} CX3CR1 mutations is due solely to its interaction with the CX3CL1 ligand. More specifically, it dem-

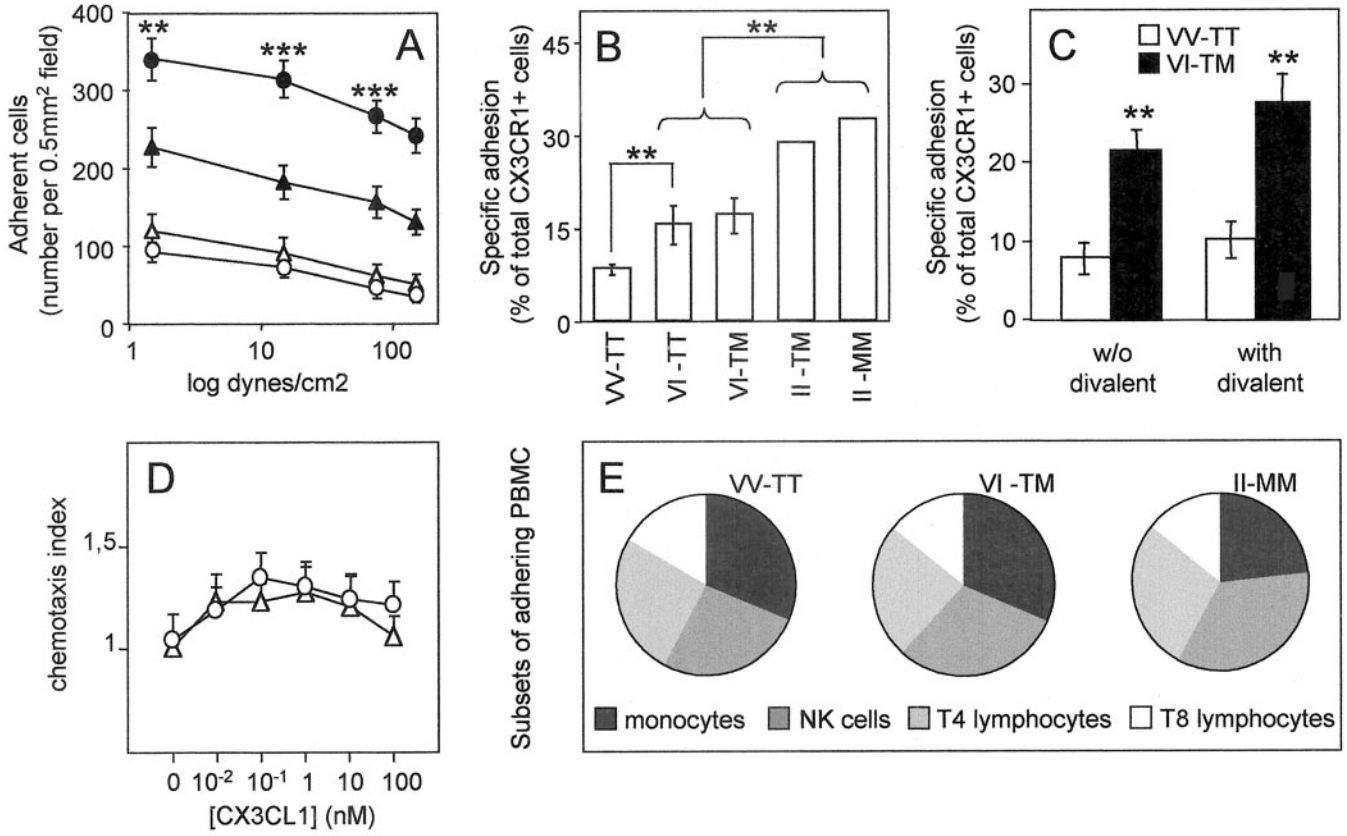

FIG. 1. **Adhesive and migration properties of PBMC with various CX3CR1 genotypes.** *A*, PBMC from individuals with CX3CR1-VV-TT (*triangles*, $n = 10$) and with CX3CR1-VI-TM (*circles*, $n = 7$) genotypes were assayed for adhesion in a parallel plate laminar flow chamber, with coverslips coated with adherent HEK-pBlast (*open symbols*) or HEK-FKN clones (*solid symbols*). Adherent cells were counted after each flow change. The difference between VV-TT and VI-TM was significant (**, $p < 0.05$; ***, $p < 0.005$) for the first three flow steps. *B*, PBMC from individuals with CX3CR1-VV-TT ($n = 10$), VI-TT ($n = 4$), VI-TM ($n = 7$), II-TM ($n = 2$), or II-MM ($n = 2$) was assayed for adhesion as in *A*. We report the number of adherent cells after the first flow step (10 min at 1.5 dynes·cm^{-2}). Specific adhesion was obtained by subtracting the cells adhering to the HEK-pBlast from the total number adhering to the HEK-CX3CL1 coverslip and then dividing this number by the total number of CX3CR1$^+$ cells quantified in the PBMC preparation, as assayed by flow cytometry (Table I). The difference in adherence for different genotypes (VV-TT *versus* VI-TT; VI-T/M *versus* II-MT/M) was significant ($p < 0.005$). *C*, PBMC from individuals with CX3CR1-VV-TT ($n = 5$, *white bars*) or VI-TM ($n = 5$, *black bars*) were assayed for adhesion as in *A*, in the absence (*left*) or in the presence (*right*) of divalent cations (0.5 mM $MgCl_2$, 1 mM $CaCl_2$) with coverslips coated with immobilized FKN-His_6. We report the number of adherent cells after the first flow step (10 min at 1.5 dynes·cm^{-2}). Specific adhesion was obtained by subtracting the number adhering to the control coverslip (coated only with anti-His_6 antibody) from the number adhering to the FKN-His_6 coverslip. The difference in adherence for different genotypes was significant ($p < 0.005$), both in the presence (*right*) or absence (*left*) of divalent cations. *D*, PBMC from individuals with CX3CR1-VV-TT ($n = 5$, *triangles*) or VI-TM ($n = 5$, *circles*) were assayed for chemotactic migration, as indicated under "Experimental Procedures." *E*, the percentage of the different subsets of adhering PBMC from individuals with three different CX3CR1 genotypes were quantified by flow cytometry, as detailed under "Experimental Procedures."

TABLE I
Characteristics of the PBMC samples used in the study

The percent of CX3CR1-positive cells in each PBMC preparations was quantified by flow cytometry (see "Experimental Procedures"). This frequency was found to be significantly lower in PBMC from CX3CR1-VI-TT and from CX3CR1-II-MM individuals than in PBMC from CX3CR1-VV-TT individuals ($p < 0.05$).

	VV-TT	VI-TT	VI-TM	II-TM	II-MM
% CX3CR1$^+$ cells ± S.E.	29.2 ± 2.6	22.5 ± 4.2	21.0 ± 2.4	21.9 ± 3.3	16.6 ± 3.4
n^a	10	4	7	2	2

[a] Number of individuals.

onstrates that the phenomenon is independent of the divalent ions as is the basal adhesion caused by the CX3CR1-VV-TT molecule (5, 11, 12) (see Fig. 1*C*, *open bars*).

Finally, we assayed the chemotactic migration of PBMC from individuals with the CX3CR1-VV-TT and CX3CR1-VI-TM genotypes (Fig. 1*D*). Surprisingly, no difference was detected between these variants in response to soluble CX3CL1, in contrast to the notable differences in their responses to membrane-anchored CX3CL1 (Fig. 1, *A–C*). It thus appears that these CX3CR1 variants can discriminate between the two forms of the ligand.

The enhanced adhesiveness of the mutated CX3CR1 was observed with whole PBMC. We then considered whether this effect was specific for a single leukocyte population. Phenotyping the adherent PBMC revealed that all the CX3CR1$^+$ PBMC subpopulations (*i.e.* monocytes, NK, CD4+, and CD8+ lymphocytes) contributed to this effect in similar proportions (Fig. 1*E*). This indicates that the excess adhesion we observed is caused by the intrinsic potency of the mutated CX3CR1. We checked this finding further with purified monocytes from various individuals. We found that CX3CR1-VI-TM monocytes adhered at a rate three times higher than the CX3CR1-VV-TT monocytes (data not shown). In contrast, both monocyte populations were indistinguishable in their chemotactic response to

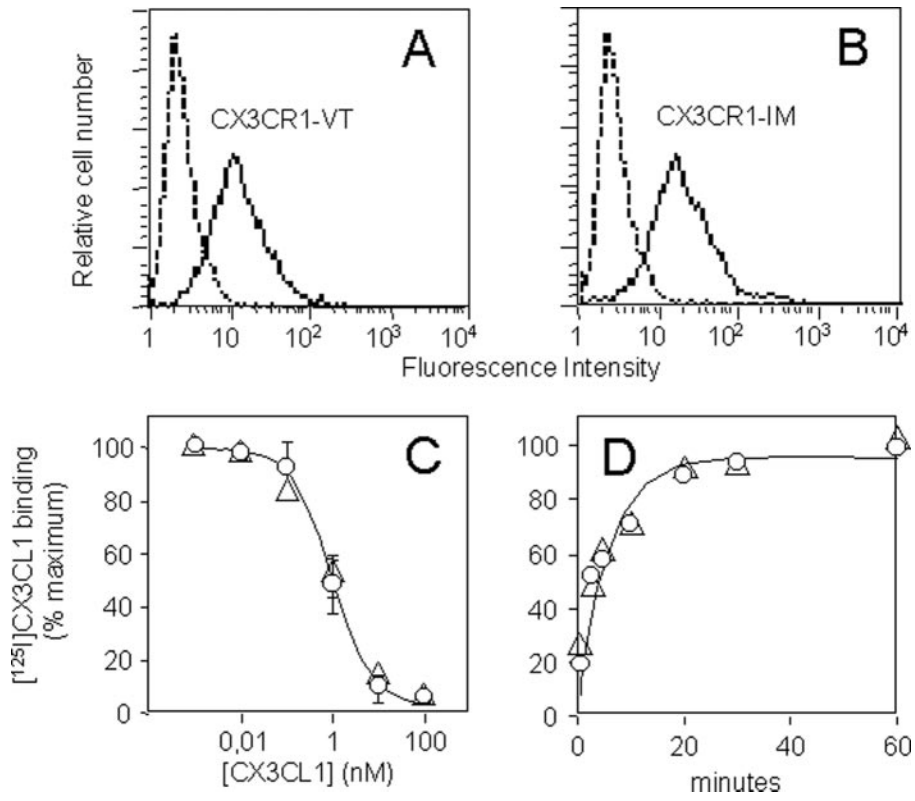

FIG. 2. **CX3CL1 binding characteristics of the HEK-CX3CR1-VT and HEK-CX3CR1-IM clones.** *A* and *B*, the expression of CX3CR1 in both HEK clones was assayed by flow cytometry after staining with and without the FITC-conjugated anti-CX3CR1 monoclonal antibody. *C*, HEK clones expressing CX3CR1-VT (*open triangles*) or CX3CR1-IM (*solid circles*) were assayed for ^{125}I-CX3CL1 binding for 2 h at 37 °C with increasing amounts of unlabeled CX3CL1, as indicated. The data were fitted with a hyperbolic curve and a K_d of 0.6 nM. *D*, the same clones were assayed for ^{125}I-CX3CL1 binding for the time indicated. The data were fitted with a hyperbolic curve and a k_{on} of 0.18 min^{-1}.

CX3CL1. These findings agree with those obtained with whole PBMC (Fig. 1*D*). We therefore concluded that the excess adhesion we observed with PBMC bearing the Ile^{249} CX3CR1 allele (Fig. 1*B*) was not specific to one particular leukocyte subpopulation, but occurs once the mutation is present. Moreover, this change can only be observed when CX3CR1 binds the membrane form of CX3CL1 (Fig. 1, *A–C*) and not in response to its soluble form (Fig. 1*D*).

Enhanced Cell Adhesive Functioning for HEK Clones That Express CX3CR1-IM—To characterize the adhesive properties of the CX3CR1 variants further, we generated HEK clones expressing the wild-type (CX3CR1-VT) and mutated (CX3CR1-IM) forms of the receptor. Using flow cytometry, we confirmed that the clones we chose expressed similar levels of CX3CR1 isoforms (Fig. 2, *A* and *B*). Using ^{125}I-CX3CL1 binding, we found that the mean expression of CX3CR1-IM (B_{max}) was slightly lower than that of CX3CR1-VT (84%± 19%, $n = 8$). Finally, using competition experiments (Fig. 2*C*; $K_i = 0.95 \pm 0.45$ nM for CX3CR1-VT and 0.86 ± 21 nM for CX3CR1-IM, $n = 4$) and association kinetics (Fig. 2*D*; $k_+ = 0.183 \pm 0.028$ min^{-1} for CX3CR1-VT and 0.178 ± 0.024 min^{-1} for CX3CR1-IM, $n = 4$), we found that both CX3CR1 variants displayed similar affinity for soluble CX3CL1. Similar results were obtained with the dissociation kinetic assay (data not shown).

Two different clones of each type were tested independently with flow adhesion. As with PBMC, the clones expressing CX3CR1-IM (Fig. 3*A*, *solid circles*) adhered more than those expressing CX3CR1-VT (Fig. 4*A*, *solid triangles*): the number of CX3CR1$^+$ HEK cells adhering specifically to membrane CX3CL1 at a low perfusion rate (1.5 dynes/cm^2) was almost twice as high for the mutated CX3CR1-IM form than for the standard CX3CR1-VT. Both types of clones began to dissociate at shear stress higher than 15–20 dynes·cm^{-2}, as previously reported (5, 11). Nonspecific adhesion of the clones was assessed with a CX3CL1-negative adherent cell layer (Fig. 3*A*, *open triangles* and *circles*). A control HEK clone expressing the chemokine receptor CCR5 adhered equally poorly to the CX3CL1-expressing cells (Fig. 3*A*, *diamonds*). Moreover, the adhesion of the HEK clones that expressed CX3CR1 was almost wholly suppressed when the cells were preincubated with soluble CX3CL1 for 45 min at 37 °C (data not shown). Again this indicates that this adhesion is specific to the CX3CR1/CX3CL1 pairing.

We verified that no particular property selected by clone generation caused these adhesion features in the stable HEK clones: they were also found with HEK transiently transfected with either CX3CR1-VT or CX3CR1-IM plasmids (Fig. 3*B*, compare VT and IM). In addition, we assayed the HEK transfected with the CX3CR1 plasmid carrying only the V249I mutation, *i.e.* CX3CR1-IT. Surprisingly these cells adhered at a rate similar to that of the double mutant CX3CR1-IM (Fig. 3*B*). Moreover the cells expressing the no naturally occurring variant CX3CR1-VM adhered at a rate similar to that observed with CX3CR1-VT cells (Fig. 3*B*). These findings provide further support for the hypothesis that the excess adhesion is due only to the mutation at position 249.

To confirm and quantify this enhanced adhesion with the CX3CR1-IM variant, we used another cell-cell adhesion assay, the dual pipette aspiration technique, previously used to verify CTL target adhesion (32). Briefly, this method consists in determining the force required to dissociate a pair formed by two cells brought into contact by micropipettes. The dissociation force is measured at a given time after pair formation. We found that paired CX3CR1-VT/CX3CL1 HEK cells adhered after only 2 min of contact with a separation force of about 6 nanoNewtons (Fig. 3*C*, *solid triangles*), at a level similar to the intercellular adhesiveness due to N-cadherins.[3] This CX3CR1-VT/CX3CL1 adhesion was independent of time, as expected from previous data (4, 5, 11), and lasted for 30 min without attenuation (Fig. 3*C*, *solid triangles*). After 2 min of contact, the strength of the CX3CR1-IM/CX3CL1 axis was similar to that of the CX3CR1-VT/CX3CL1 pair. In contrast, after contact of 4 min or more, the cells expressing CX3CR1-IM adhered more

[3] S. Dufour, personal communication.

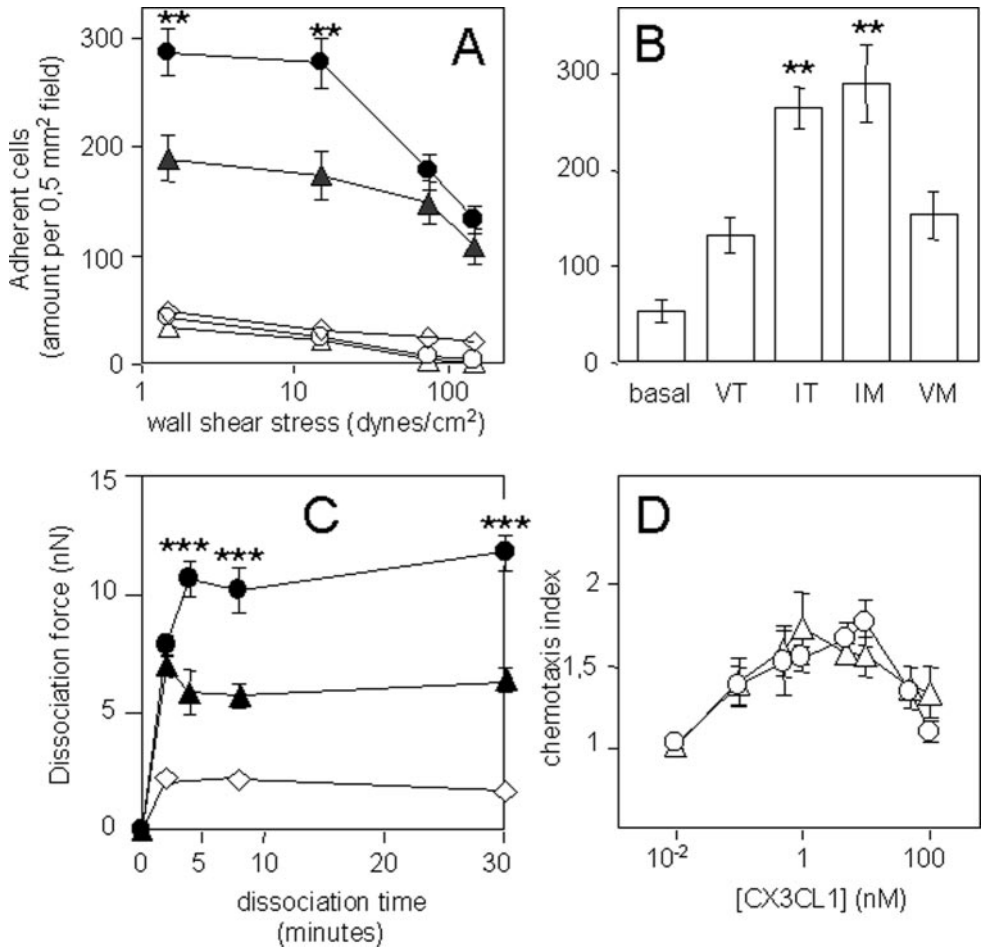

FIG. 3. **Adhesive and migration properties of HEK cells stably or transiently transfected with CX3CR1-VT or CX3CR1-IM.** *A*, HEK clones expressing CX3CR1-VT (*triangles*) or CX3CR1-IM (*circles*) were suspended and assayed for adhesion in a parallel plate laminar flow chamber, with coverslips with adherent HEK-pBlast (*open symbols*) or HEK-CX3CL1 clones (*solid symbols*), as described in the legend to Fig. 1*A*. The difference between adhesion of the CX3CR1-VT/CX3CL1 and CX3CR1-IM/CX3CL1 pairs was significant ($p < 0.005$) after the steps at 1.5 and 15 dynes·cm^{-2} ($n = 12$). The adhesion of the HEK clone expressing CCR5 on adherent HEK-FKN is also reported (*diamonds*). *B*, HEK cells transiently transfected with empty plasmid (*basal*), CX3CR1-VT, CX3CR1-IT, CX3CR1-IM, or CX3CR1-VM constructions were assayed for flow adhesion on HEK-CX3CL1 clones ($n = 5$). We checked that the different HEK populations expressed similar levels of CX3CR1 by ^{125}I-CX3CL1 binding. *C*, HEK clones expressing CX3CR1-VT (*triangles*), CX3CR1-IM (*circles*), and CCR5 (*diamonds*) were suspended and assayed for adhesion by the micropipette aspiration technique with HEK-CX3CL1 clone cells. The dissociation force was evaluated after the indicated time of adhesion. The HEK-CCR5 clone does not bind CX3CL1 according to the ^{125}I-CX3CL1 binding assay. Its adhesion assessed nonspecific adhesion between HEK cells. The difference between adhesion of the CX3CR1-VT/CX3CL1 and CX3CR1-IM/CX3CL1 pairs was significant ($p < 0.0005$) for the durations 4, 8, and 30 min ($n > 13$). *D*, HEK clones expressing CX3CR1-VT (*triangles*) or CX3CR1-IM (*circles*) were assayed for chemotactic migration, as indicated under "Experimental Procedures."

strongly to the CX3CL1+ cell partners, thereby requiring a dissociation force of 10–12 nanoNewtons, *i.e.* about twice as high as for CX3CR1-VT (Fig. 3*C*, *solid circles*). This did not weaken within 30 min of testing. The nonspecific adhesion of both CX3CR1 clones to CX3CL1-negative cells was weak (<2 nanoNewtons) for all the time periods tested (data not shown), as was the adhesion of a HEK clone transfected with a control receptor (CCR5) to cells expressing CX3CL1 (Fig. 3*C*, *diamonds*). Similar low adhesion was obtained with the CX3CR1/CX3CL1 cell pair, when the CX3CR1$^+$ clones were pretreated for 45 min at 37 °C with soluble CX3CL1 (data not shown). As with the parallel plate flow adhesion technique, these experiments were performed in the absence of divalent cations. In their presence, however, we also observed a difference between the dissociation forces measured with two CX3CR1 variants, but only after 30 min of cell to cell contact (data not shown). We tested the chemotactic responses of the transfected HEK cell clones to the CX3CL1 gradient. As with PBMC (Fig. 1*D*), we found no differences between the clones expressing the two CX3CR1 variants (Fig. 3*D*).

The Excess Adhesion Caused by the Mutated CX3CR1 Is PTX-dependent—Although most signals triggered by CX3CR1 ligation with the soluble CX3CL1 are G-protein-dependent, the adhesive properties of the CX3CR1/CX3CL1 pair are independent of the G_i pathway, *i.e.* they are still present after PTX treatment (4, 5, 11). We confirmed this finding here with flow chamber dynamic adhesion assays that used PBMC from CX3CR1-VV-TT donors (Fig. 4*A*, *open bars*) or HEK cells expressing CX3CR1-VT (data not shown). Surprisingly, the adhesion observed with cells expressing the CX3CR1-IM variant was reduced after PTX treatment to the level observed with the CX3CR1-VT (Fig. 4*A*, *solid bars*). The same result was observed with PBMC adhering to immobilized CX3CL1, either in the presence or absence of divalent ions (data not shown) or using the dual pipette assay with HEK cell pairs (Fig. 4*B*). This result suggests that the adhesive feature of the mutated CX3CR1 is composed of two additive events: one basal adhesion common to both variants and one specific to the CX3CR1-IM conformation. In contrast, the excess adhesion obtained with the CX3CR1-IM haplotype was insensitive to other pharmaco-

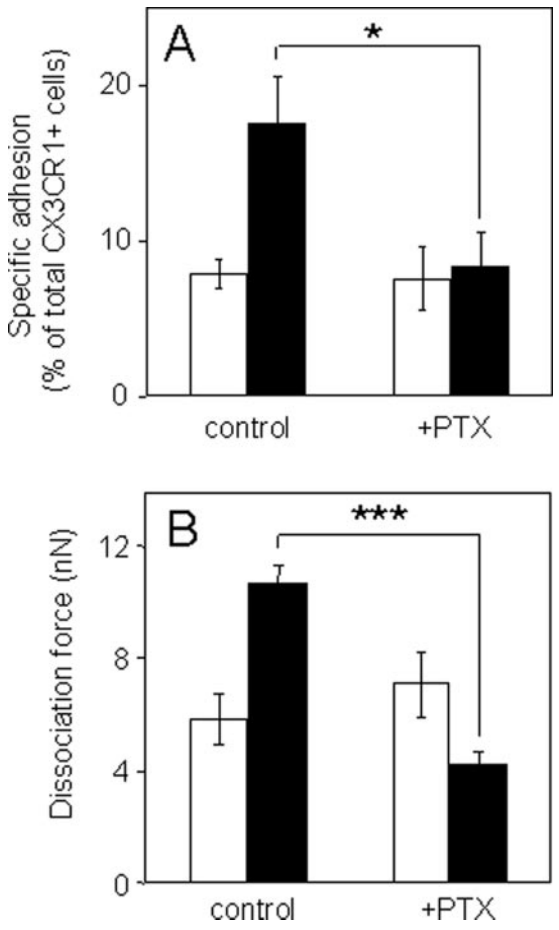

FIG. 4. **Effect of PTX pretreatment upon the adhesion characteristics of CX3CR1-VT- and CX3CR1-IM-expressing cells.** *A*, PBMC of individuals with CX3CR1-VV-TT (*open bars*) or CX3CR1-VI-TM (*solid bars*) genotypes were incubated for 150 min at 37 °C in RPMI 1640 medium supplemented with 1 mM HEPES and 1 mg/ml BSA with ($n = 5$) or without (*control*) 0.2 μg/ml of PTX. They were then suspended and assayed for adhesion with the parallel plate chamber as described in the legend to Fig. 1*B*. *B*, HEK clones expressing CX3CR1-VT (*open bars*) and CX3CR1-IM (*solid bars*) were incubated for 18 h at 37 °C in culture medium with or without (*control*) 0.2 μg/ml of PTX. They were then suspended and assayed for dissociation force by the dual pipette technique with HEK-CX3CL1 clone cells after 4 min of adhesion, as described in the legend to Fig. 3*C*. The specific adhesion was calculated at each experiment by subtracting the dissociation force observed between the HEK-CX3CR1 and the HEK-CX3CL1 clones from the nonspecific adhesion obtained with the HEK-CCR5 and the HEK-CX3CL1 clones.

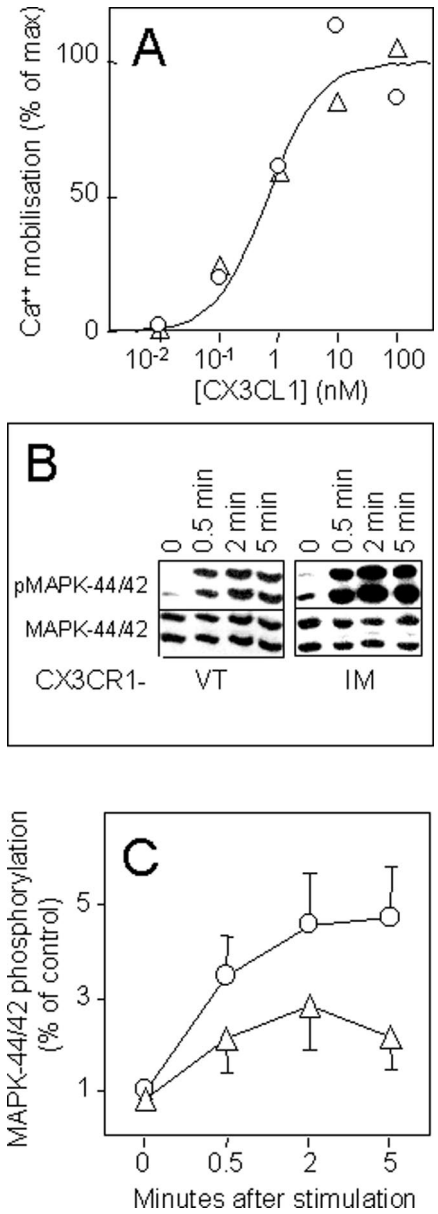

FIG. 5. **Various cellular responses of the HEK-CX3CR1-VT and HEK-CX3CR1-IM clones to soluble CX3CL1.** *A*, HEK clones expressing CX3CR1-VT (*triangles*) or CX3CR1-IM (*circles*) were assayed for intracellular calcium mobilization in response to various concentrations of CX3CL1. The amplitude of the responses was normalized to the maximal amplitude, which is 33 nM for the CX3CR1-VT clone and 40 nM for the CX3CR1-IM clone. *B*, HEK clones were also assayed for p44/42 MAP kinase phosphorylation during the indicated times in response to 50 nM CX3CL1. *C*, quantification of p44/42 MAP kinase phosphorylation in HEK clones, from Western blot scanning.

logical agents, including LY-294002 and PD-98059, which inhibit, respectively, phosphatidylinositol 3-kinase and p44/42 MAP kinase enzymes (data not shown).

Signaling Pathways Mediated by CX3CR1 Variants—Possible differences between the CX3CR1 variants were tested by assaying two other cellular responses. We first examined the calcium response of HEK cell clones that expressed each of the CX3CR1 variants (Fig. 5*A*); the dose-response curves were indistinguishable. We also tested the activation of the cellular MAP kinase pathway, which CX3CL1 triggers in neurons (37), intestinal epithelial cells (38), microglia cell lines (16), and monocyte cell lines (39). In both of our HEK cell line clones, the maximum p44/42 MAP kinase stimulation was reached within 2 min of CX3CL1 application (Fig. 5, *B* and *C*). The extent of MAP kinase phosphorylation was slightly higher in the CX3CR1-IM than in the VT HEK clone (Fig. 5, *B* and *C*), but the difference was not statistically significant.

DISCUSSION

In view of its effect on prognosis in AIDS (18, 19) and in cardiovascular diseases (26–28), understanding the molecular modifications caused by the chemokine receptor CX3CR1-IM mutation is an important challenge. We found here that intercellular adhesion mediated by the CX3CR1/CX3CL1 pair was substantially greater with cells that express the CX3CR1-IM variant than with those expressing the CX3CR1-VT variant (Figs. 1, 3, and 4). Moreover, the data from both PBMC (Fig. 1*B*) and HEK (Fig. 3*B*) indicate that the V249I mutation alone is responsible for the high level of adhesion we observed. Finally, adhesion mediated by CX3CR1-IM was independent of divalent ions and involved only CX3CL1 as counterligand (Fig. 1), as was the adhesion mediated by CX3CR1-VT (5, 11, 12).

This surprisingly enhanced adhesiveness of the CX3CR1 variant was demonstrated with two different techniques that determined distinct indicators. The parallel plate method furnishes the fraction of adhering cells under shear stress, while the dual pipette procedure directly assesses the force required to dissociate cell pairs under axial stress. Both techniques indicate that the CX3CL1-specific adhesion force generated by the CX3CR1-IM variant is significantly greater than that induced by the CX3CR1-VT genotype. Moreover, the dual pipette procedure indicates that this excess adhesion occurs slowly, after a few minutes, thereby suggesting that the adhesive potency of CX3CR1-IM results from the addition of two phenomena: first, immediate adhesion, as observed for CX3CR1-VT, followed by a time-dependent attachment that seems specific to CX3CR1-IM. This slow time course may point to a signaling-dependent mechanism, a hypothesis supported by our experiments with PTX (Fig. 4). Thus the mutated CX3CR1 form may specifically trigger a signal that, added to the basal and instantaneous adhesion because of the CX3CR1/CX3CL1 interaction, yields excess adhesion. Although our data show that MAPK-p44/42 activation is somewhat higher in CX3CR1-IM cells (Fig. 5, *B* and *C*), the testing of specific inhibitors ruled out the involvement of the MAP kinase-dependent and the phosphatidylinositol 3-kinase pathways in generating this extra adhesion.

The enhanced adhesiveness of the CX3CR1-IM variant was observed in both transfected HEK cells and peripheral blood cells. All the $CX3CR1^+$ PBMC subpopulations adhered to membrane CX3CL1 (5) and showed enhanced adhesiveness when they had the CX3CR1-IM haplotype (Fig. 1, *B* and *E*). The association of the CX3CR1-IM genotype with a reduced risk of cardiovascular disease was previously thought to be due to the receptor's reduced capacity to bind its ligand, and frozen PBMC from HIV patients with a mutated genotype showed less ligand affinity (18). A recent report proposes that the Ile^{249} mutation is associated with a promoter mutation that may result in differential CX3CR1 expression (40). This might explain the significantly lower number of receptors per cell on PBMC from VI compared with VV donors (Refs. 18 and 26 and this report). It cannot, however, account for the excess adhesion we observed here. Our experiments indicate that the differences we observed between CX3CR1 variants are due to intrinsic molecular properties.

While our article was under review, a study appeared, reporting that CX3CR1-IM cells have globally impaired responses to CX3CL1, *i.e.* ligand binding and calcium response, as well as impaired adhesive and chemotactic functions (28). We cannot account for these discrepancies in the responses to soluble CX3CL1 observed in transfected HEK cells (ligand binding, calcium mobilization). It is conceivable that, under different manipulation conditions, the CX3CR1-IM cells might respond somewhat less than the CX3CR1-VT cells. These discrepancies do not really affect our main conclusion. On the other hand, the adhesion data from this report also diverge sharply from ours: the adhesion to an endothelial cell line of K562 cell line transfected with CX3CR1-IM was far lower than that of K562 cells transfected with CX3CR1-VT (28). In contrast, our data were obtained with both PBMC and transfected HEK cell lines in an adhesion assay over immobilized CX3CL1 as well as different layer cells (HEK and smooth muscle cells). Moreover, we performed a supplementary parallel plate adhesion test with either PBMC or transiently transfected K562 cell line using precisely the McDermott's method, *i.e.* a loading phase at a shear stress of 0.25 dynes·cm^{-2} instead of 1.5 dynes·cm^{-2}, a progressive washing and a final wash at 10 dynes·cm^{-2} instead of 15 dynes·cm^{-2}. In these conditions, we still observed the excess adhesion of the CX3CR1-IM-expressing cells (data not shown). We should state moreover that this extra adhesion was observed with two different techniques (Fig. 4). It is not impossible that some features of the cell lines used by McDermott *et al.* (binding sites per cell, actual signaling pathways, adhesion molecules on the 926 endothelial cell line) may explain the discrepancies with our data. The identification of the various steps underlying the CX3CR1-IM effect may illuminate the divergences between these reports.

Our study implies that CX3CR1 behaves differently when addressing soluble or membrane ligand. A similar difference was recently observed for IFNγ production by NK cells (41). Our work also shows that the specific mechanism triggered by CX3CR1-IM binding to membrane CX3CL1 is dependent on the PTX-sensitive G-protein family G_i (Fig. 4). This signal-dependent adhesion might be due to more effective oligomerization of CX3CR1-IM at the adhesive interface, possibly related to a differential association with membrane lipid rafts. It has been suggested that the association of membrane protein to lipid rafts involves fatty acylation, specifically palmitoylation. This post-translational modification might be inhibited with 2-bromopalmitate (42), as for the CCR5 receptor (43). Our preliminary work with 2-bromopalmitate did not show a clear difference between the CX3CR1 variants in their palmitoylation potential: both were equally sensitive to the pharmacological compound.[4] Further work is required to assess the aggregation rate and the lateral diffusion factor of both variants. Another possible explanation is differential inactivation of the mutated CX3CR1; it would thus interact with the membrane-anchored ligand for a longer period. This slower inactivation may be due to specific signaling; the inactivation of the G-protein-coupled receptor is signal-dependent, through arrestin, GRK, or tyrosine kinase (44, 45). Our preliminary work, however, did not confirm this hypothesis. Both CX3CR1-VT and CX3CR1-IM receptors seem to be internalized at the same rate, after soluble CX3CL1 binding.[5]

To our knowledge, our study is the first to report a chemokine receptor mutation associated with increased functions. It appears to originate in a single mutation, replacement of a valine residue by an isoleucine at position 249. This increase in functioning seems to be mediated by gene dosage (Fig. 1*B*) rather than by a dominant effect. Further studies are nonetheless needed to ensure that the Met^{280} position is not implicated using PBMC from CX3CR1-II-TT donors and HEK stably transfected with CX3CR1-IT and CX3CR1-VM. For now we can only speculate as to why or how a semi-conservative mutation (Val to Ile) has so dramatic an outcome. Recent structural studies describing the conformation changes in G-protein-coupled receptors (46, 47) often note that the relative movement of helices 6 and 7, where the CX3CR1 natural mutations are located, appears to play an important role. These helices may also be involved in the potential dimerization interface between G-protein-coupled receptor monomers (48).

Recent reports show that inactivating the *CX3CR1* gene leads to a decrease in the risk of atherogenesis (49, 50). It was therefore paradoxical to find that mutations that appear to protect against cardiovascular diseases (26–28) actually enhance the molecule's adhesive properties. The monocytes recruited in the intima layer to form atherosclerotic plaque should first adhere and cross the endothelium barrier (51, 52). The reduction of this transmigration step in the presence of CX3CL1 (53) indicates that the adhesion function of CX3CL1 may counteract the migration driven by inflammatory che-

[4] A. Bourdais and P. Deterre, unpublished data.
[5] S. Faure, P. Deterre, and C. Combadière, unpublished data.

moattractants. It is thus conceivable that excess adhesion might further diminish monocyte extravasation and hence weaken atherogenesis.

The additional adhesion we observed may also be involved in NK or CTL cell target interactions in ganglia, especially in HIV patients. The lymph nodes of such patients overexpress CX3CL1 (54), while disease severity is correlated with CX3CR1 expression (14). Hence, the excess adhesion we describe here may profoundly affect both innate and acquired immunity.

Acknowledgments—We thank Véronique Ollivier for providing us with smooth muscle cell lines, Cédric Lécureuil for help with the flow cytometry, Jean-Pierre Lagarde for help in sequencing plasmid constructions, and Eric Perez for continuing support.

REFERENCES

1. Lawrence, M. B., and Springer, T. A. (1991) *Cell* **65,** 859–873
2. Springer, T. A. (1990) *Nature* **346,** 425–434
3. Pan, Y., Lloyd, C., Zhou, H., Dolich, S., Deeds, J., Gonzalo, J. A., Vath, J., Gosselin, M., Ma, J., Dussault, B., Woolf, E., Alperin, G., Culpepper, J., Gutierrez-Ramos, J. C., and Gearing, D. (1997) *Nature* **387,** 611–617
4. Imai, T., Hieshima, K., Haskell, C., Baba, M., Nagira, M., Nishimura, M., Kakizaki, M., Takagi, S., Nomiyama, H., Schall, T. J., and Yoshie, O. (1997) *Cell* **91,** 521–530
5. Fong, A. M., Robinson, L. A., Steeber, D. A., Tedder, T. F., Yoshie, O., Imai, T., and Patel, D. D. (1998) *J. Exp. Med.* **188,** 1413–1419
6. Matloubian, M., David, A., Engel, S., Ryan, J. E., and Cyster, J. G. (2000) *Nat. Immunol.* **1,** 298–304
7. Nakayama, T., Hieshima, K., Izawa, D., Tatsumi, Y., Kanamaru, A., and Yoshie, O. (2003) *J. Immunol.* **170,** 1136–1140
8. Papadopoulos, E. J., Sassetti, C., Saeki, H., Yamada, N., Kawamura, T., Fitzhugh, D. J., Saraf, M. A., Schall, T., Blauvelt, A., Rosen, S. D., and Hwang, S. T. (1999) *Eur. J. Immunol.* **29,** 2551–2559
9. Tsou, C. L., Haskell, C. A., and Charo, I. F. (2001) *J. Biol. Chem.* **276,** 44622–44626
10. Garton, K. J., Gough, P. J., Blobel, C. P., Murphy, G., Greaves, D. R., Dempsey, P. J., and Raines, E. W. (2001) *J. Biol. Chem.* **276,** 37993–38001
11. Haskell, C. A., Cleary, M. D., and Charo, I. F. (1999) *J. Biol. Chem.* **274,** 10053–10058
12. Haskell, C. A., Cleary, M. D., and Charo, I. F. (2000) *J. Biol. Chem.* **275,** 34183–34189
13. Nishimura, M., Umehara, H., Nakayama, T., Yoneda, O., Hieshima, K., Kakizaki, M., Dohmae, N., Yoshie, O., and Imai, T. (2002) *J. Immunol.* **168,** 6173–6180
14. Combadiere, B., Faure, S., Autran, B., Debre, P., and Combadiere, C. (2003) *AIDS* **17,** 1279–1290
15. Dichmann, S., Herouy, Y., Purlis, D., Rheinen, H., Gebicke-Harter, P., and Norgauer, J. (2001) *Inflamm. Res.* **50,** 529–533
16. Maciejewski-Lenoir, D., Chen, S., Feng, L., Maki, R., and Bacon, K. B. (1999) *J. Immunol.* **163,** 1628–1635
17. Nishiyori, A., Minami, M., Ohtani, Y., Takami, S., Yamamoto, J., Kawaguchi, N., Kume, T., Akaike, A., and Satoh, M. (1998) *FEBS Lett.* **429,** 167–172
18. Faure, S., Meyer, L., Costagliola, D., Vaneensberghe, C., Genin, E., Autran, B., Delfraissy, J. F., McDermott, D. H., Murphy, P. M., Debre, P., Theodorou, I., and Combadiere, C. (2000) *Science* **287,** 2274–2277
19. Faure, S., Meyer, L., Genin, E., Pellet, P., Debre, P., Theodorou, I., and Combadiere, C. (2003) *J. Acquired Immune Defic. Syndr.* **32,** 335–337
20. McDermott, D. H., Colla, J. S., Kleeberger, C. A., Plankey, M., Rosenberg, P. S., Smith, E. D., Zimmerman, P. A., Combadiere, C., Leitman, S. F., Kaslow, R. A., Goedert, J. J., Berger, E. A., O'Brien, T. R., and Murphy, P. M. (2000) *Science* **290,** 2031
21. Hendel, H., Winkler, C., An, P., Roemer-Binns, E., Nelson, G., Haumont, P., O'Brien, S., Khalilli, K., Zagury, D., Rappaport, J., and Zagury, J. F. (2001) *J. Acquired Immune Defic. Syndr.* **26,** 507–511
22. Brumme, Z. L., Dong, W. W., Chan, K. J., Hogg, R. S., Montaner, J. S., O'Shaughnessy, M. V., and Harrigan, P. R. (2003) *AIDS* **17,** 201–208
23. Reeves, J. D., McKnight, A., Potempa, S., Simmons, G., Gray, P. W., Power, C. A., Wells, T., Weiss, R. A., and Talbot, S. J. (1997) *Virology* **231,** 130–134
24. Rucker, J., Edinger, A. L., Sharron, M., Samson, M., Lee, B., Berson, J. F., Yi, Y., Margulies, B., Collman, R. G., Doranz, B. J., Parmentier, M., and Doms, R. W. (1997) *J. Virol.* **71,** 8999–9007
25. Combadiere, C., Salzwedel, K., Smith, E. D., Tiffany, H. L., Berger, E. A., and Murphy, P. M. (1998) *J. Biol. Chem.* **273,** 23799–23804
26. Moatti, D., Faure, S., Fumeron, F., Amara, M., Seknadji, P., McDermott, D. H., Debre, P., Aumont, M. C., Murphy, P. M., de Prost, D., and Combadiere, C. (2001) *Blood* **97,** 1925–1928
27. McDermott, D. H., Halcox, J. P., Schenke, W. H., Waclawiw, M. A., Merrell, M. N., Epstein, N., Quyyumi, A. A., and Murphy, P. M. (2001) *Circ. Res.* **89,** 401–407
28. McDermott, D. H., Fong, A. M., Yang, Q., Sechler, J. M., Cupples, L. A., Merrell, M. N., Wilson, P. W., D'Agostino, R. B., O'Donnell, C. J., Patel, D. D., and Murphy, P. M. (2003) *J. Clin. Investig.* **111,** 1241–1250
29. Gugl, A., Renner, W., Seinost, G., Brodmann, M., Pabst, E., Wascher, T. C., Paulweber, B., Iglseder, B., and Pilger, E. (2003) *Atherosclerosis* **166,** 339–343
30. Grynkiewicz, G., Poenie, M., and Tsien, R. Y. (1985) *J. Biol. Chem.* **260,** 3440–3450
31. Pierres, A., Feracci, H., Delmas, V., Benoliel, A. M., Thiery, J. P., and Bongrand, P. (1998) *Proc. Natl. Acad. Sci. U. S. A.* **95,** 9256–9261
32. Sung, K. L., Sung, L. A., Crimmins, M., Burakoff, S. J., and Chien, S. (1986) *Science* **234,** 1405–1408
33. Tozeren, A., Sung, K. L., and Chien, S. (1989) *Biophys. J.* **55,** 479–487
34. Evans, E., Berk, D., and Leung, A. (1991) *Biophys. J.* **59,** 838–848
35. Ludwig, A., Berkhout, T., Moores, K., Groot, P., and Chapman, G. (2002) *J. Immunol.* **168,** 604–612
36. Ollivier, V., Faure, S., Tarantino, N., Chollet-Martin, S., Deterre, P., Combadiere, C., and de Prost, D. (2003) *Cytokine* **21,** 303–311
37. Meucci, O., Fatatis, A., Simen, A. A., and Miller, R. J. (2000) *Proc. Natl. Acad. Sci. U. S. A.* **97,** 8075–8080
38. Brand, S., Sakaguchi, T., Gu, X., Colgan, S. P., and Reinecker, H. C. (2002) *Gastroenterology* **122,** 166–177
39. Cambien, B., Pomeranz, M., Schmid-Antomarchi, H., Millet, M. A., Breittmayer, V., Rossi, B., and Schmid-Alliana, A. (2001) *Blood* **97,** 2031–2037
40. DeVries, M. E., Cao, H., Wang, J., Xu, L., Kelvin, A. A., Ran, L., Chau, L. A., Madrenas, J., Hegele, R. A., and Kelvin, D. J. (2003) *J. Biol. Chem.* **27,** 27
41. Yoneda, O., Imai, T., Nishimura, M., Miyaji, M., Mimori, T., Okazaki, T., Domae, N., Fujimoto, H., Minami, Y., Kono, T., Bloom, E. T., and Umehara, H. (2003) *Eur. J. Immunol.* **33,** 53–58
42. Webb, Y., Hermida-Matsumoto, L., and Resh, M. D. (2000) *J. Biol. Chem.* **275,** 261–270
43. Percherancier, Y., Planchenault, T., Valenzuela-Fernandez, A., Virelizier, J. L., Arenzana-Seisdedos, F., and Bachelerie, F. (2001) *J. Biol. Chem.* **276,** 31936–31944
44. Miller, W. E., and Lefkowitz, R. J. (2001) *Curr. Opin. Cell Biol.* **13,** 139–145
45. Pierce, K. L., Premont, R. T., and Lefkowitz, R. J. (2002) *Nat. Rev. Mol. Cell. Biol.* **3,** 639–650
46. Meng, E. C., and Bourne, H. R. (2001) *Trends Pharmacol. Sci.* **22,** 587–593
47. Decaillot, F. M., Befort, K., Filliol, D., Yue, S., Walker, P., and Kieffer, B. L. (2003) *Nat. Struct. Biol.* **10,** 629–636
48. Bouvier, M. (2001) *Nat. Rev. Neurosci.* **2,** 274–286
49. Combadiere, C., Potteaux, S., Gao, J. L., Esposito, B., Casanova, S., Lee, E. J., Debre, P., Tedgui, A., Murphy, P. M., and Mallat, Z. (2003) *Circulation* **107,** 1009–1016
50. Lesnik, P., Haskell, C. A., and Charo, I. F. (2003) *J. Clin. Investig.* **111,** 333–340
51. Glass, C. K., and Witztum, J. L. (2001) *Cell* **104,** 503–516
52. Reape, T. J., and Groot, P. H. (1999) *Atherosclerosis* **147,** 213–225
53. Umehara, H., Goda, S., Imai, T., Nagano, Y., Minami, Y., Tanaka, Y., Okazaki, T., Bloom, E. T., and Domae, N. (2001) *Immunol. Cell Biol.* **79,** 298–302
54. Foussat, A., Bouchet-Delbos, L., Berrebi, D., Durand-Gasselin, I., Coulomb-L'Hermine, A., Krzysiek, R., Galanaud, P., Levy, Y., and Emilie, D. (2001) *Blood* **98,** 1678–1686

Specific Recognition of Macroscopic Objects by the Cell Surface: Evidence for a Receptor Density Threshold Revealed by Micrometric Particle Binding Characteristics

Stéphanie Sarda,* David Pointu,† Frédéric Pincet,‡ and Nelly Henry*†

*Laboratoire Chimie Bioinorganique Médicale, Institut Universitaire Technologique Paul Sabatier, Castres, France; †Institut Curie, Laboratoire Physico Chimie Curie, Centre National de la Recherche Scientifique, Unité Mixte de Recherche 168, Paris, France; and ‡Laboratoire de Physique Statistique–Ecole Normale Supérieure, Paris, France

ABSTRACT The establishment of specific molecular bonds between a cell and a facing surface is involved in many physiological and technological situations. Using micrometric magnetic particles, we have explored the formation of specific molecular bonds between the cell and surfaces bearing complementary ligands under passive conditions. Streptavidin-coated particles were targeted to the cell surface of a B-cell line through a specific biotinylated antibody against the CD19 receptor. Flow cytometry, optical microscopy, and micropipette experimental techniques have been used. Main findings have been that cell surface receptor density acted like a switch for particle capture with a threshold value found here equal to 1.6×10^3 receptor/μm^2. This led to exclusion from binding of the cells of lowest receptor density. The density threshold was modulated by the length of the binding link and the physics of the cell/particle collision. We suggest that the shear stress is one of the main determinants of the characteristics of binding. We also show that several thousand receptors were involved in the cell particle contact at the end of the binding process, although only eight bonds are required for the initial capture of a particle. A passive binding inhibition process due to link concentration by the initial contact was proposed to account for the small number of particles per cell.

INTRODUCTION

Many crucial biological events depend on specific molecular recognition at the cell surface. Significant progress has been made, in the past few years, toward understanding details of refined receptor-ligand interactions in terms of bond formation between a unique site and the complementary molecule (e.g., Helm et al., 1991; Verkhivker et al, 2002; Pierres et al., 2002; Jung et al., 2000). Ever-increasing amounts of structural data (Stuart and Jones, 1995) and the emergence of single molecule approaches have particularly contributed to enlightening the field of molecular recognition (Merkel et al., 1999; Evans, 2001). However, in many instances, the recognition at the cell surface appears to involve much higher complexity through multiple factors such as cell surface composition and architecture, membrane mechanics, receptor dynamics and complexation, connection with the cytoskeleton network, etc. This becomes of most importance when the ligands themselves are presented to another surface, as is the case for many specific cell interactions such as those of cells in tissues (Gumbiner, 1996) or in immunological complexes such as those formed by T cells and antigen-presenting cells (van der Merwe, 2002). It now clearly appears that cell interactions engage molecular assemblies rather than unique ligand-receptor interaction (Hutchinson et al., 2003). Moreover, the cell surface is covered by the glycocalix—a hydrophilic, negatively charged, carbohydrate polymer layer whose thickness can reach up to several tens of nanometers depending on cell type (Braun and Fromherz, 1998). It very likely supports a steric repulsive barrier that avoids interactions with interfaces lacking specific complementary ligands or a sufficient number of positive charges (Chenevier et al., 2000; Ravaine et al., 2002). This surrounding layer actually creates a surface force field that superimposes the net receptor-ligand binding potential. Because of the high heterogeneity of the cell surface, this potential cannot be described by using the theoretical Derjaguin-Landau-Verwey-Overbeek approach or measured using surface-force techniques, as has been achieved with model surfaces (e.g., Leckband et al., 1994; Wong et al., 1997).

In this article, we report an experimental approach aimed to evidence a few consequences of the complex biological environment offered at the cell surface, on the formation of a well-known key-lock molecular link, the streptavidin-biotin bond. We depict the association characteristics of model macroscopic objects, constituted by streptavidin-covered micrometric beads, with the surface of a B-cell line. We chose to target the CD19 receptor, a B-cell-specific transmembrane glycoprotein of 80 kDa, which is involved in the MHC class II signaling complex (e.g., Lévéille et al., 2002; Bradbury et al., 1993) and the interaction with T cells. The link with streptavidin-covered particles is established through a biotinylated antibody specific for the CD19 receptor. The cell-to-particle binding was analyzed using a flow cytometry technique that allowed statistic and quantitative measurements of the association parameters, in parallel with optical microscopy and micropipette experiments that allowed evaluation of the characteristics of individual events. We found that the binding at the cell

Submitted June 23, 2003, and accepted for publication January 2, 2004.

Address reprint requests to Nelly Henry, Institut Curie, CNRS, UMR 168, Physico Chimie Curie, 11 rue P. et M. Curie, Paris, France 75005. Tel.: 33-01-42-34-6495; E-mail: nelly.henry@curie.fr.

0006-3495/04/05/3291/13 $2.00

surface obeyed a receptor density threshold that depended both on the accessibility of the receptor within the surface layer and on the mechanics of the collision between the hard sphere and the soft material of the cell surface. We also evidenced that in the final stage of the particle adhesion on the cell surface, several thousand links were engaged in the cell-to-particle contact. The obtained results supported the idea of a collective, dynamic binding mechanism, which will be discussed. Above the better understanding of the mechanism of interaction, the question of the molecular recognition at the cell surface is also crucial in more applied situations involving protein-coated synthetic implants or in cell-sorting processes using specific colloids to select a cell subpopulation identified by a surface marker. This will be also considered in light of our results.

MATERIALS AND METHODS

Reagents and particles

Streptavidin and biotin, conjugated both with and without fluorescein, were supplied by Molecular Probes (Eugene, OR). Antibodies, anti-CD19 purified or FITC- or biotin-conjugated, were from BD Biosciences Pharmingen (San Diego, CA) and anti-cytokeratine-FITC was from Miltenyi Biotec (Bergisch Gladbach, Germany). Magnetic latex particles were 2.8-μm diameter, purchased from Dynal (Compiègne, France), either functionalized with carboxylic acid groups or grafted with streptavidin.

Cell culture and labeling

The B-cell lymphoma cell line, line Bernard (LB), EBV-transformed, was a gift from J. Dechanet-Merville (UMR CNRS 5540, Université Bordeaux II, Bordeaux, France). Cells were cultured suspended in Dulbecco's Modified Eagle Medium supplemented with 10% fetal calf serum, 2 mM L-glutamine, 50 U/ml streptomycin, at 37°C in 5% CO2. For particle-binding experiments, the cells were labeled with biotinylated anti-CD19 as follows. The whole procedure was carried out in ice; cells from an exponentially growing culture were washed with PBS and their concentration adjusted to 5×10^6 cells/ml, then incubated with the antibody above saturating concentration (4 μg/ml) for 1 h and washed twice in PBS to remove biotinylated antibody excess. The cells were then ready to be put in contact with streptavidin particles. Titrations with anti-CD19-FITC or anti-cytokeratin-FITC were performed in the same conditions. When required and as stated below, PBS was added with 0.1% sodium azide.

Cell-particle contact

Cells were put into contact at time $(t) = 0$ by gentle mixing in a tube of 2 ml of cell suspension adjusted at the desired concentration with a few microliters of the particle suspension. To ensure proper mixing of the samples all along the interaction process, the tubes containing the cell-particle suspensions were placed on the radii of a rotating disk spinning at 5 rpm, either at 4°C or ambient temperature. This stirring was interrupted only to carry out regular 10-s flow cytometry acquisitions.

Flow cytometry

Flow cytometry data were acquired using a FACScan (Becton Dickinson, Le Pont de Claix, France) equipped with an air-cooled 488-nm argon-ion laser. Fluorescence measurements were collected using dichroic mirrors and filter sets: a 530/30-nm bandpass on the FL1 channel and a 650-nm longpass on the FL3 channel. Ten-thousand events were the typical number collected, except for the most diluted samples, where only 2000 events were acquired to maintain short time resolution for each sample. Data were analyzed using the multivariate analysis software CellQuest (BD Biosciences, San Diego, CA), except in a few cases where more detailed analysis was performed on list-mode data files stored in flow cytometry standard (FCS) format.

Fluorescence absolute calibration was performed using the following autocalibration method: α, the coefficient giving the proportionality between the mean fluorescence provided by the cytometer photomultiplier and the amount of fluorescent-bound molecules per cell, was obtained directly from the slope of the titration curve giving the fluorescence per cell as a function of increasing fluorescent ligand concentration in the initial linear part. Indeed, for high affinities, the amount of free ligand may be neglected when ligand concentration is low and receptors are in excess. The amount of complex is then very closely equal to the total amount of ligand. In the range-of-affinity constant expected for the binding of an antibody to its receptor, this consisted of a maximum approximation of 1% of the signal and avoided all the drawbacks related to calibration performed with beads having different optical properties than cells.

Binding equilibrium analysis

Equilibrium data were analyzed according to the following Scatchard-like method, wherein the binding affinity of a ligand L, for a receptor R, which is present in a mean number of n copies on a cell C, is considered.

This analysis is performed on the basis of a simple binding equilibrium described by the mass action law,

$$K_a = \frac{[R - L]}{[R] \times [L]},$$

where $[R]$, $[L]$, and $[R{-}L]$ are the molar concentrations of ligand, receptor, and receptor-ligand complex. $[L]$ and $[R]$ are given by the mass conservation laws,

$$[L] = [L]_{tot} - [R\text{-}L],$$

where $[L]_{tot}$ is the total ligand molar concentration, and it is the experimental variable

$$[R] = [R]_{tot} - [R\text{-}L]$$
$$[R]_{tot} = n \times [C],$$

where $[C]$ is the cell molar concentration. $[R{-}L]$ is given by the fluorescence values obtained by flow cytometry (FL) converted according to the autocalibration method with the proportionality factor α,

$$[R - L] = \alpha \times (FL).$$

Then, it becomes

$$[L]_{tot} - \alpha \times (FL) = \frac{\alpha \times (FL)}{K_a(n \times [C] - \alpha \times (FL))},$$

where $[L]_{tot} - \alpha \times (FL)$ is plotted as a function of $\alpha \times (FL)$ with K_a and n as adjustable parameters. This method was applied to characterize the binding

equilibrium of anti-CD19 on its receptor on the B-cell line, and FITC-coupled anti-CD19 was used.

Micropipette experiments

Pipettes with a 0.5–1-μm inner radius, r_p, were used to manipulate the cell and the bead. The experimental approach consisted of micromanipulating them to ensure contact and then holding them together for a few seconds to allow bond formation. The pipettes were then moved apart over a few micrometers. During this process, the cell was enduring an axisymmetric stretch. The analysis of the equilibrium geometry allowed us to evaluate the adhesion energy, inasmuch as the local tension γ around the contact line was known. Neglecting the pressure difference between the inside of the cell and the solution, γ can be deduced (Tozeren et al, 1989) from the angle θ_1 that the cell makes with the radial direction at the tip of the pipette, as

$$\gamma = \Delta P \times \frac{r_p^2}{2r_c} \times \frac{\sin\theta_1}{\sin\phi_1},$$

where ΔP is the aspiration pressure inside the pipette, r_c is the contact radius, and ϕ_1 is the angle formed by the cell and the radial direction at particle contact. Assuming adhesion is uniform, the adhesive energy per unit area, w_a, is given by Young's equation (Berk and Evans, 1991), as

$$w_a = \gamma(1 - \cos\theta_c),$$

where θ_c is the contact angle between the bead and the cell.

RESULTS

CD19 receptors: number, ligand affinity, and distribution

Before entering into the detailed analysis of particle binding, we carried out experiments to precisely quantify the occurrence of the CD19 receptor on the cell surface using FITC-coupled anti-CD19. The equilibrium binding data were collected by incubating a range of anti-CD19–FITC concentrations with the cells and by measuring the fluorescent signal on the flow cytometer. Background due to unspecific binding was evaluated using an anti-cytokeratin-FITC antibody (no receptor on the surface). The data, giving the fluorescence per cell, were converted into bound anti-CD19-FITC according to the autocalibration method explained in Materials and Methods and plotted in Fig. 1 *A*. Data analysis was performed according to the Scatchard-like method described above. Parameters adjustment (Fig. 1 *B*) provided a value of $(8.2 \pm 2) \times 10^8\ M^{-1}$ for the association constant, K_a, of anti-CD19 with CD19. The number of binding sites was found equal to $(4.1 \pm 0.9) \times 10^5$ per cell.

Fig. 2 details the CD19 receptor distribution through the whole cell population. The histogram was acquired in the FL1 channel for a saturating concentration of anti-CD19-FITC. The distribution over the cell population was found to be monomodal, very close to a Gaussian profile with only a slight right skew. The whole distribution (mean fluorescence value = 46) was detached from the background (mean fluorescence value = 2) and the FL1 versus forward-light-scatter dot-plot displayed only one dot cluster, indicating that CD19 protein was present on every cell of the distribution.

We also checked using fluorescent streptavidin that these receptors were able to specifically anchor anti-CD19-biotin at the cell surface in a quantitative way. For that, we first incubated cells with saturating concentrations of anti-CD19-biotin at 4°C, washed off antibody excess, and performed the cell-surface cytofluorometric titration of the biotins present using increasing concentrations of streptavidin-FITC. We obtained a mean number of 5×10^5 streptavidin molecules bound per cell, which is close to the number of CD19 receptors measured above, suggesting that, for steric purposes, only one streptavidin was bound per biotinylated antibody fixed on the cell surface.

Cell-particle binding profile: evidence for a subpopulation selection

On this basis, our purpose has been to characterize the specific binding on the cell surface of micrometric particles under passive conditions, i.e., low temperature and poor physiological buffer. Cells labeled with biotinylated anti-CD19 were put into contact with streptavidin-grafted particles ($t = 0$). Immediately 10-s flow cytometry acquisitions were initiated and regularly recorded all along the binding process, providing sequential snapshots of the situation within the cell-particle suspension. Fig. 3 shows the biparametric dot-plots acquired on mixtures of 1.5×10^5 cells/ml and to 1.5×10^6 particles/ml, i.e., 10 particles per cell, at 1 and 30 min of contact, together with the dot-plots acquired before any particle contact and after 30-min contact between unlabeled cells and streptavidin particles. Forward-light scatter (FSC) versus side-light scatter (SSC) and fluorescence emission at the highest wavelength (FL3) are shown. Dead cells and debris were gated out. The dot cluster of the living cells, initially concentrated in the lower-left region of the scatter plot extended toward the region of higher side scatter, revealed the capture of particles by the cells. This particle-bearing cell population was also clearly identified by its higher fluorescence in the FL3 vs. FSC plots. The number of events associated with this cluster increased with time. Control plots did not undergo significant alteration. It can be seen that particle binding onto the cell did not affect their size-related forward-scatter parameter. Unbound particles, at least a fraction, appeared in cytograms at lowest-forward-scatter values as expected from their 2.8-μm diameter. They displayed rather high values of side scatter and FL3, due to their iron oxide payload, which conferred to the particle both a high optical index and a large fluorescence spectrum as confirmed using fluorescence microscopy. Each cytogram also allowed us to discriminate and quantify free particles (small size, high SSC, and FL3), and free cells (defined size and low SSC) from cells having bound particles (same defined size as free cells and increased FL3 and SSC) in any

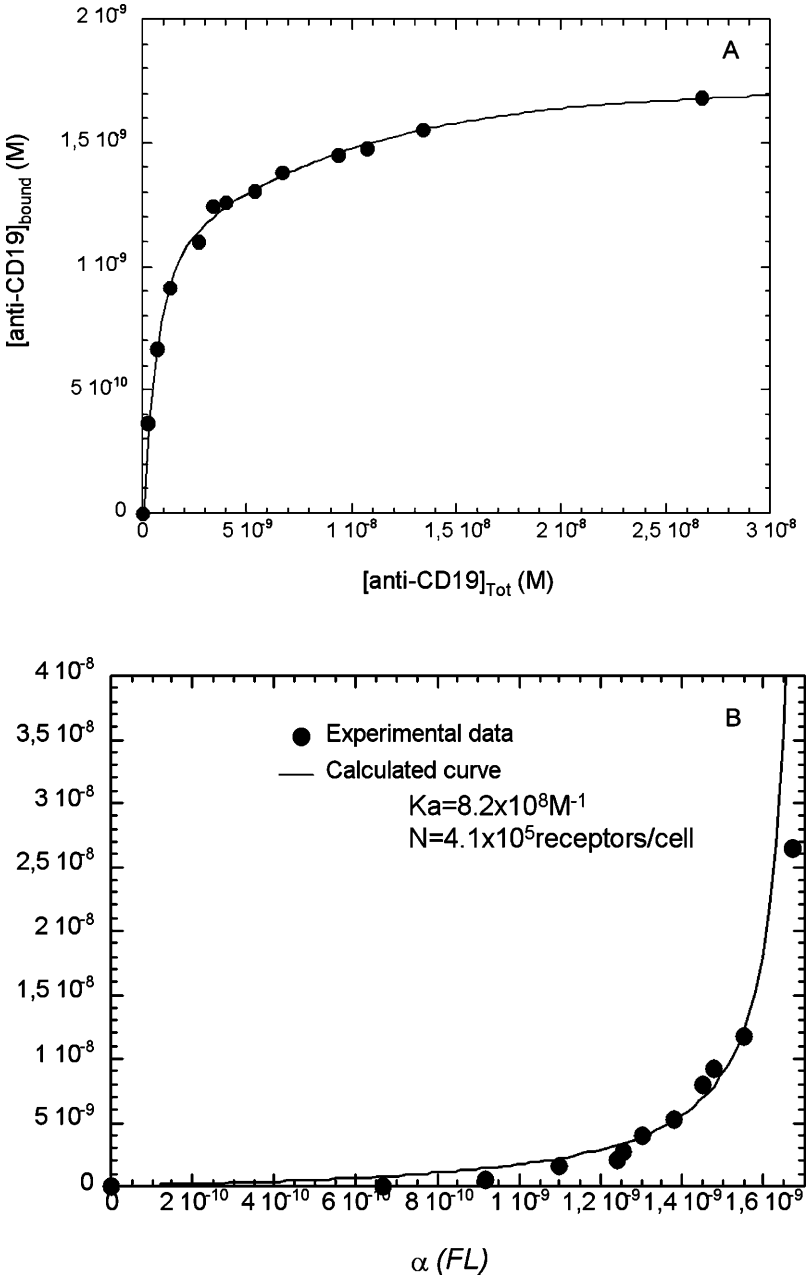

FIGURE 1 CD19 receptors titration: the number of CD19 receptors per cell has been determined using increasing concentrations of FITC-labeled anti-CD19 and measuring fluorescence per cell using flow cytometry. The arbitrary values obtained were converted into bound anti-CD19 applying the autocalibration methods described in Materials and Methods and plotted as a function of antibody concentration (*A*). Experiments were performed at 4°C, in PBS buffer, pH 7.4. Cell concentration for these experiments was equal to 2.5×10^6 cells/ml. Here is a representative experiment of at least three separate titrations. Anti-CD19 binding analysis (*B*) was performed according to the Scatchard-like method (see Materials and Methods). The adjustment of the experimental points (●) to the analytical formula obtained (—) provided an association constant K_a equal to 8.2×10^8 M^{-1} and a mean number of sites equal to 4.1×10^5 receptors per cell.

suspension. A crucial point to underline, in these results, was the splitting of the cell population into two classes—cells with bound particles and cells without. The particles actually operated a selection within the cell population, despite the one-mode distribution, in regard to CD19 receptor occurrence for this cell line. In the following, the parameter f_c, the fraction of cells holding at least one particle, will be used to characterize this selection. On the basis of the fluorescence data, it was determined as the ratio of the events acquired in the upper-left region of the FL3 vs. FSC plot (living cells of higher fluorescence) to the total number of events acquired in both the upper and lower regions (all living cells). The number of events comprised in the upper-left region at $t =$ 0 constituted the background and was subtracted from all numbers. Fig. 4 shows the evolution of the fraction f_c as a function of time of cell/particle contact. Obviously, the fraction of cells having bound particles reached a plateau value equal to 0.4 after 30 min of cell/particle contact. At this plateau, using optical microscope observations, we checked that the samples still exhibited significant amounts of free cells and free particles together with cells having bound particles (Fig. 5).

At this point, two parameters were retained to describe this specific cell/particle binding profile: 1), the value f_c, the fraction of captured cells when the binding is achieved (i.e., binding plateau), and 2), the apparent characteristic time τ

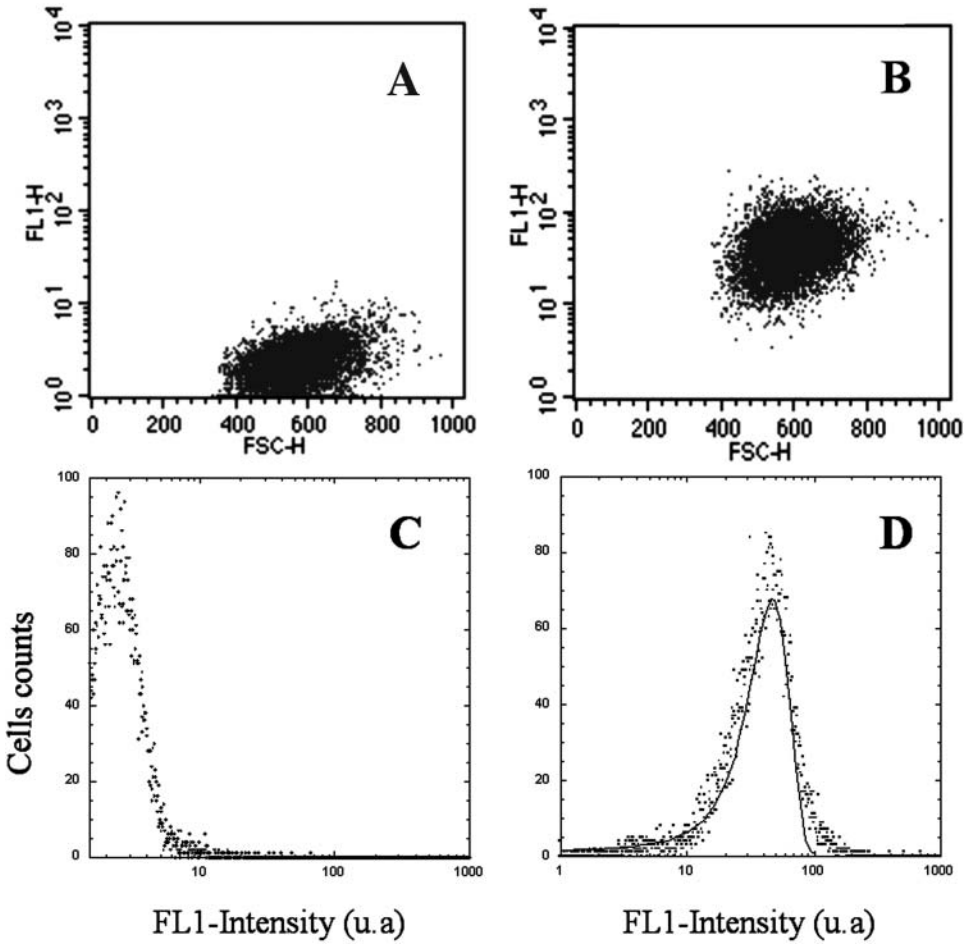

FIGURE 2 Flow cytometry biparametric dot-plots and histograms showing CD19 receptors distribution. LB cells were incubated at 4°C during 1 h with 4 μg/ml FITC-conjugated anti-cytokeratin (*A* and *C*) and with FITC-conjugated anti-CD19 (*B* and *D*). The fluorescence distribution of the labeled cells clearly displayed only one mode; it has been adjusted to a Gaussian distribution (—) of the form $(1/\sigma\sqrt{2\pi})e^{-(x-\bar{x})^2/2\sigma^2}$, which provided a mean value of 47.

(i.e., the time to reach a fraction of captured cells equal to $f_c/2$). In the previous experimental conditions (1.5×10^5 cells/ml; 1.5×10^6 particles/ml; 5 rpm stirring; standard molecular link), we found $f_c = 0.42$ and $\tau = 210$ s.

Density threshold

We then aimed to gain more insight into the understanding of the binding profile and focused our interest on the origin of the selection operated by the particles within the cell population. We took advantage of the paramagnetic properties of the particles used in this study to physically separate cells that were without particles from cells with at least one particle under a magnetic field gradient. The streptavidin-binding sites of the particle-free cells were then probed on the flow cytometer using streptavidin-FITC. Fig. 6 shows the fluorescence distribution obtained on these particle-free cells together with the distribution acquired on the initial whole-cell population before any contact with particles. It appeared that those cells (which did not capture particles) displayed a binding-sites distribution that was shifted to the lower values, indicating a lower binding-site density exposed on the cell surface by these cells (Table 1). The histograms were converted into number of binding sites per cell and normalized to the same number of cells. The particle-free cell distribution was then multiplied by 0.6 to account for the fraction of discriminated cells previously measured by flow cytometry. This fraction was also corroborated by the results of the magnetic separation, which gave 43 $\pm$ 3% of cells in the pellet and 57 $\pm$ 2% of cells remaining in the supernatant. We then subtracted the calculated histogram from the histogram of the entire population. The result is shown in Fig. 7. The ascending part of the curve gives the surface density cutoff for the binding of a particle onto the cell surface. It shows that, below 2.9×10^5 receptors per cell, no particle may adhere steadily onto the cell surface; the probability to stabilize at least one particle on the surface then becomes 1, inasmuch as the mean number of binding sites attains the value of 3.8×10^5 per cell.

Number of particles per cell and binding order

Some experiments were performed using a particle batch displaying a size distribution narrower than the current samples. Because of this small size dispersion, we were able to distinguish, inside the particle-bearing cells cluster, subclusters of cells characterized by n (the number of particles

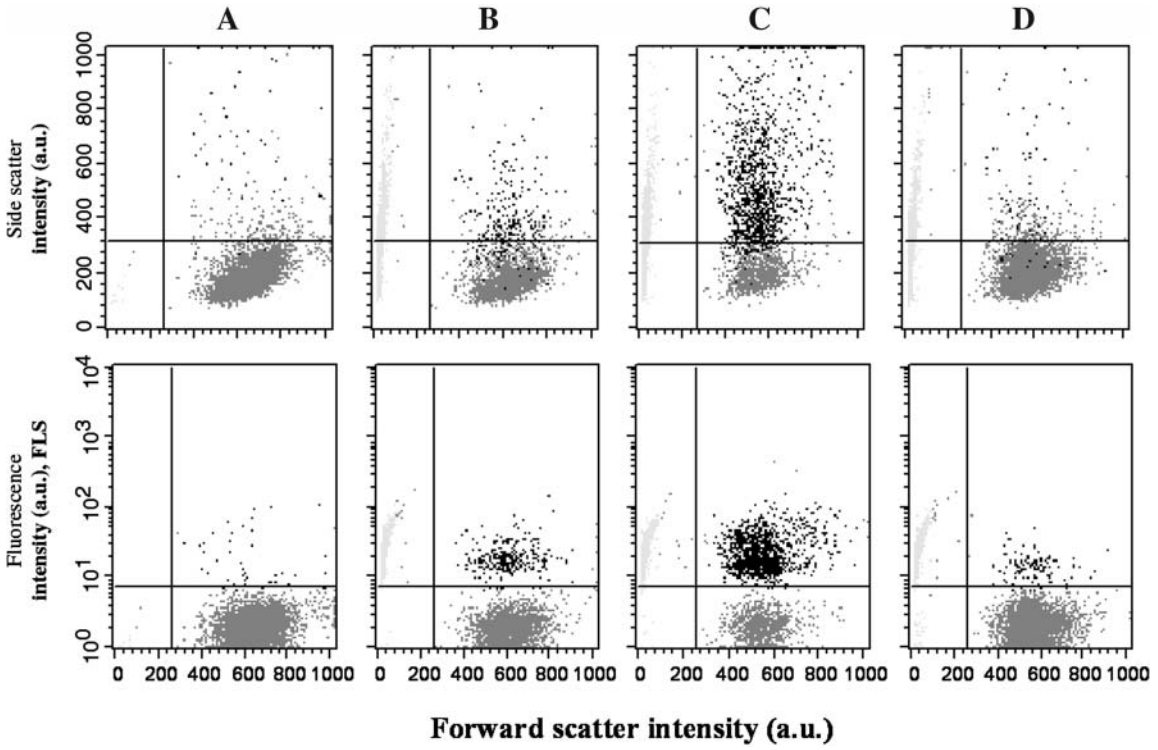

FIGURE 3 Scattering (*upper frames*) and fluorescence (*lower frames*) biparametric dot-plots of interacting particles and cells. 1.5×10^5/ml LB cells were labeled (*A*, *B*, *C*) or not (*D*) with biotinylated anti-CD19 and put into contact with 1.5×10^6/ml streptavidin-coated particles. Flow cytometry data were acquired at various times after particle contact; (*A*) $t = 0$, (*B*) $t = 1$ min, and (*C* and *D*) $t = 30$ min. Incubation was performed at 4°C, measurements at 20°C, all in PBS buffer, pH 7.4.

per cell); see Fig. 8. Then, we plotted ν, the frequency of cells bearing n particles, as a function of n when the binding was achieved (Fig. 8). The curve obtained was adjustable to an exponential decrease like

$$\nu(n) = p \times e^{-\delta \times n}.$$

This behavior suggested that the energy barrier encountered by a particle to bind on the cell surface increased with the number of particles already bound to the cell. The value p is a prefactor depending on experimental conditions such as the number of cells and particles, i.e., the value of the binding threshold. The value δ accounts for the energy barrier increase occurring between the binding of a particle at the order $(n+1)$ and the binding of a particle at the order n.

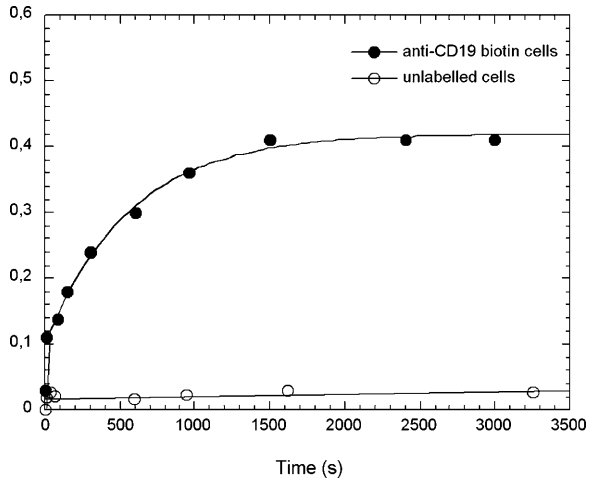

FIGURE 4 Cells and particles interaction kinetic profile. The ratio of the number of cells having acquired enhanced fluorescence, i.e., located in the upper quadrant of the FL3 dot-plot (see Fig. 3), to the total number of living cells has been plotted as a function of time of contact with the particles. Cells had previously been labeled (●) or not (○) with biotinylated anti-CD19. Same experimental conditions as in Fig. 3.

Parameters affecting the binding profile

The effect of four experimental parameters on the particle-binding characteristics f_c and τ were tried.

The role of particle/cell ratio

The results shown in Fig. 9 demonstrated that the decrease of the particle/cell number ratio did not affect f_c, the fraction of particle-bearing cells, but induced the increase of the kinetic parameter τ. These results evidenced an irreversible binding, the kinetics of which was determined by the number of collisions per time unit.

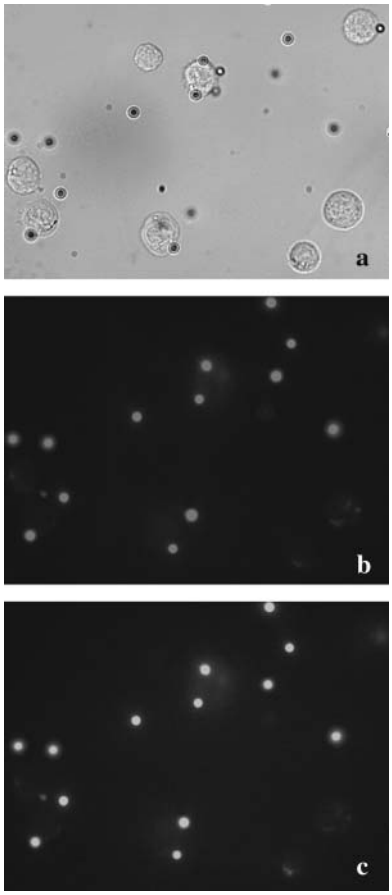

FIGURE 5 Optical (*a*) and fluorescence microscopy (*b* and *c*) pictures of labeled cells and particles sample. Fluorescence images of particles were recorded under epifluorescence lightening using a FITC (*b*) or a rhodamine (*c*) filter setup, showing the large spectra of the particles' fluorescence.

The length of the molecular link

We increased the length of the molecular link using an additional binding level made of biotinylated polyclonal anti-mouse (Fab)′2 fragments directed against the mouse anti-CD19 already bound to the cell. Fig. 10 illustrates the increase of the parameter f_c in the lengthened configuration. It also appears that the characteristic binding time was increased with this longer link.

The rotation speed

We found that the rotation speed of the sample during the stirring also influenced f_c and τ. The value f_c increased with the stirring speed, whereas τ decreased as shown in Fig. 11. Actually, this stirring mode induced the sample to flow from bottom to top of the tube twice per rotation. Each liquid inversion occurred on a rather small angle ($'10°$ for a 2-ml sample at 5 rpm), submitting the sample to shear flows, the intensity of which depended upon the disk rotation speed. The speeding-up of the stirring induces an increase of: the collision probability per unit of time; the shear; and the kinetic energy of the particles.

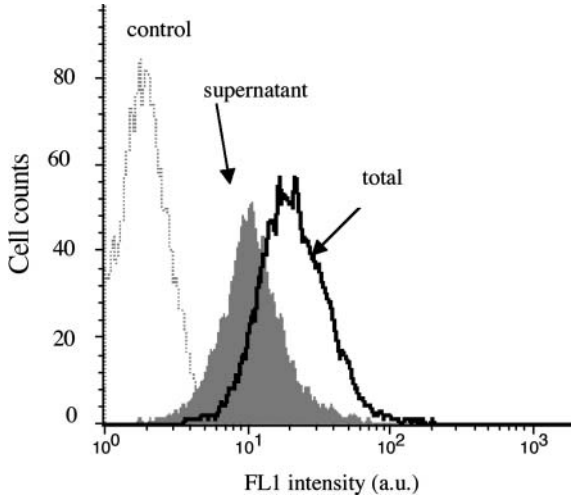

FIGURE 6 Binding sites distribution of particle-free and particle-bound cells. 5×10^5/ml LB cells labeled with biotinylated anti-CD19 were incubated with 5×10^6/ml particles for 60 min. Once the binding process was achieved, cells with particles and cells without particles were physically sorted under magnetic field gradient. The cells in the supernatant, without particles, were then labeled with a saturating (1 μg/ml) FITC-coupled streptavidin and their fluorescence histogram (*dark shaded*) recorded in the FL1 flow cytometer channel. The same labeling was performed in parallel on biotinylated cells before the incubation with the particles (*open black*). These are shown together with an unlabeled control cells histogram (*dotted line*); mean values in Table 1.

The cell energetic poisoning

To estimate the contribution of the cell active processes to the binding profile, we performed all experiments in the presence of 0.1% sodium azide, which abolished the ATP resources of the cell. Upon this treatment, the captured cell's fraction increased 15%. This effect was accompanied by a small change in the number of particles per cell distribution, which causes the exponential decay to display an s-shaped dependence on the number of already bound particles (Fig. 12).

Contact area and binding potential

Contact area between particle and cell was estimated from geometric considerations (Fig. 13) and image analysis of 50

TABLE 1 Mean fluorescence (FL1) and binding site values of cell treated with biotinylated anti-CD19 and labeled with saturating concentrations of streptavidin FITC

Cell population	Mean fluorescence	Mean number of sites per cell	Mean number of sites/μm^2
Control	2	—	—
Particle-free	10.5	2.2×10^5	1.1×10^3
All cells	19.8	4.1×10^5	2.1×10^3

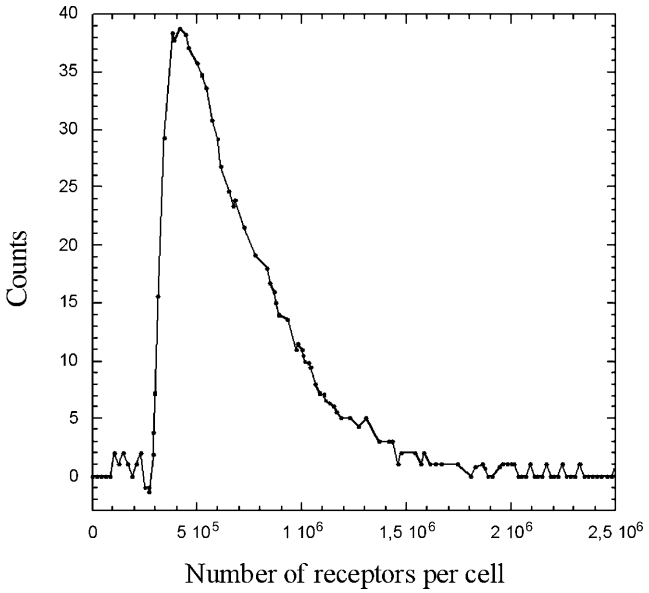

FIGURE 7 Receptor density cutoff for the binding of a particle, obtained after subtraction of the particle-free cells distribution to the total cells distribution, normalization of each histogram to the same number of cells, and multiplication of each by their respective mean frequency, i.e., 0.4 and 0.6.

microscopy images. The key length of the problem was h^*, the height of the particle cap that entered into contact with the cell surface. The corresponding contact area is then

$$S_c = 2\pi \times h^* \times r_b,$$

with a radius r_c equal to

$$r_c = r_b \times \sin\theta,$$

or

$$r_c = r_b \times \sin\left[\cos^{-1}\left(\frac{r_b - h^*}{r_b}\right)\right].$$

The value h^* was measured on samples at the kinetic plateau. We obtained h^* values comprised between 1.4 and 3.5 μm^2 with a mean value and standard deviation equal to 2.5 μm^2 and 0.7 μm^2, respectively. Considering the mean surface receptor density, a 2.5-μm^2 cell surface should gather a mean binding potential of 2×10^3 receptors as compared to the global mean distribution and 4×10^3 receptors as compared to cutoff density. On the other side, the particle presented a number of potential links equal to 5×10^5 on a 2.5-μm^2 surface. These numbers reflect the mean distributions and do not take into account possible local receptor concentrations. Under these static conditions, a mean contact should be able to connect a maximum number of 4×10^3 molecular streptavidin-biotin links.

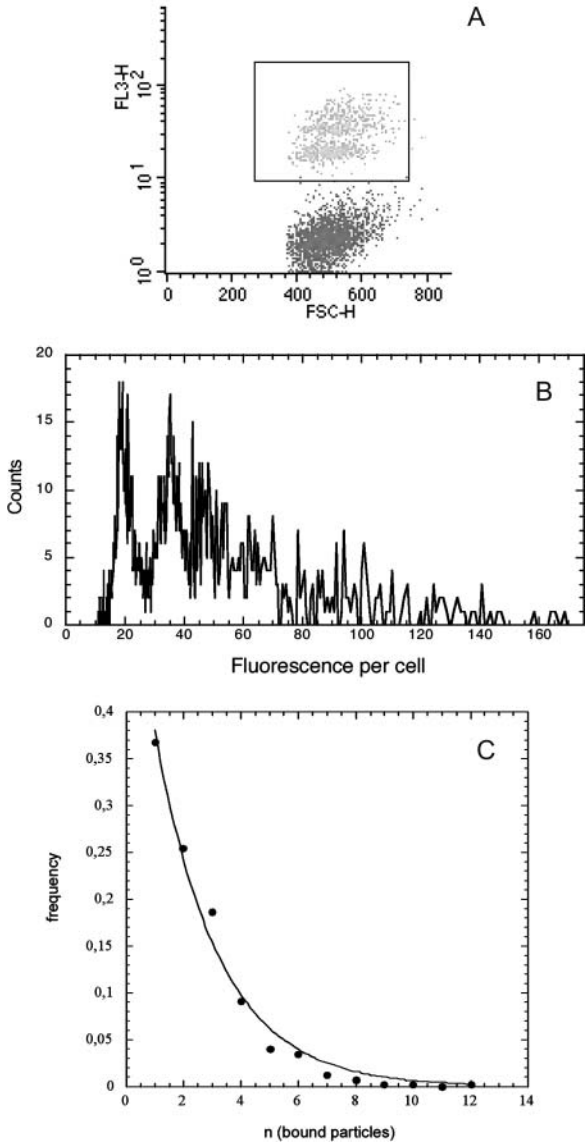

FIGURE 8 Number of bound particles per cell: the cluster of the cells having bound particles (*black frame*) was selected on the biparametric dot-plot (*A*), at the kinetic plateau of the binding (same experimental conditions as in Fig. 2). Its fluorescence distribution was plotted according to a linear scale (*B*), which allowed resolving discrete populations of cells according to their bound-particles' number. The fluorescent increment per bound particle was found equal to 17 arbitrary units. The number of cells per subpopulation (with 1, 2, 3, . . . , n particles) was counted and plotted as a function of n, the number of bound particles per cell (*C*). The experimental points (●) were adjusted to an exponential decay (—) of the form $\nu(n) = p \times e^{-\delta \times n}$.

Estimation of density of molecular links in a contact

To estimate the number of links actually participating in a contact, we carried out micropipette experiments on a single cell. The binding energy stored in a contact was evaluated from the mechanic equilibrium obtained after pulling apart cell and particle in the axis of the contact (Fig. 14). We measured the contact angles using an automatic-edges re-

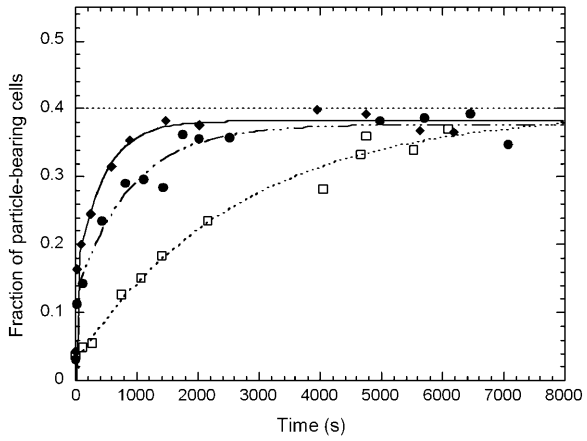

FIGURE 9 Effect of particles/cells ratio. Cells and particles were put into contact as described in Fig. 3 except the particles/cells ratio was decreased. Ratios are equal to 2 (□), 7 (●), and 15 (♦).

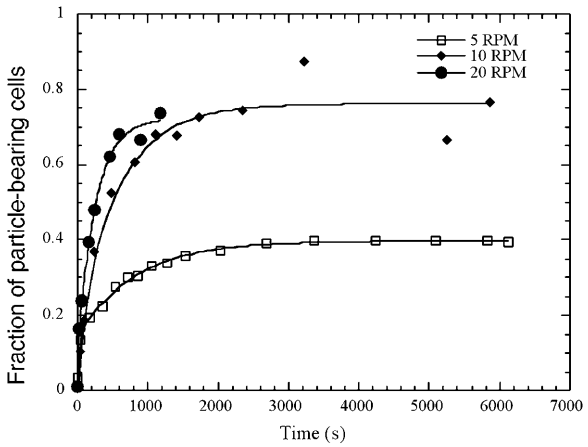

FIGURE 11 Effect of stirrer rotation speed. The kinetics of the cell/particle binding process was followed as described in Fig. 3 for three different rotation speeds of the stirring setup: 5 RPM (□), 10 RPM (♦), and 20 RPM (●).

search program. However, we should mention that the contact-angle measurements at the cell surface were rather inaccurate due to halo effects, inducing high standard error on the value of W_a. Following the analysis of Tozeren et al. (1989), explained in Materials and Methods, we obtained a density of energy of the order of $(1 \pm 0.5) \times 10^5$ kT/μm^2, i.e., according to the mean area of a contact $(2.5 \pm 1.25) \times 10^5$ kT per contact. At this point, it is difficult to straightforwardly extract a defined number of links, N, from this energy of adhesion. The first reason is that we do not exactly know the energy of such a link within the contact at the cell surface. Indeed, it has been shown, for instance in Pérez-Luna et al. (1999), that the kinetic constants for the dissociation of the streptavidin-biotin link at an interface were affected by the structure of the surface itself. The second reason is that we have no precise description of the thermodynamics of the contact. However, it can be reasonably accepted (Brochard-Wyart and de Gennes, 2003) that this energy of adhesion is comprised between $N \times (kT)$ and $N \times \varepsilon_b \times (kT)$, where ε_b is the energy of a link. Then using the energy of streptavidin-biotin link formed in solution, we found that the number of links within a 2.5-μm^2 contact should be comprised between $(7 \pm 0.35) \times 10^3$ and $(2.5 \pm 1) \times 10^5$.

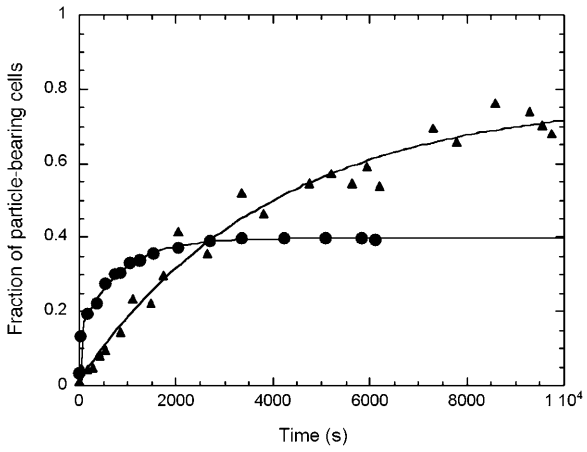

FIGURE 10 Effect of the length of the molecular link. Cell/particle binding process was followed as in Fig. 3 except the molecular link presented by the cell was extended using a biotinylated (Fab)$'_2$ fragment directed against the mouse anti-CD19 already bound on the B-cell (▲). Data obtained with the shortest link, i.e., biotinylated anti-CD19 (●).

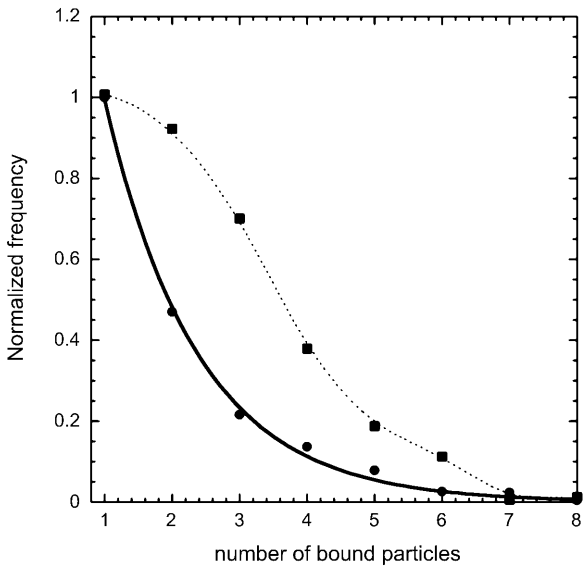

FIGURE 12 Distribution of the number of particles per cell. The number of cells, n_i, in each subpopulation of cells bearing i particles was plotted as a function of i, for experiments performed with (■) or without (●) 0.1% sodium azide. The normalized frequency for a subpopulation of cells bearing i particles is equal to $\frac{n_i}{\sum_{i=1}^{n} n_i} \times \frac{1}{\nu_{max}}$, where ν_{max} is equal to the highest frequency of the sample.

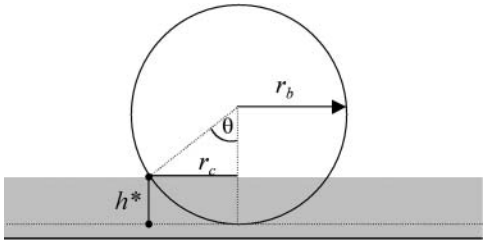

FIGURE 13 Geometry of the contact. This figure gives the parameters allowing the description of particle/cell contact, where r_c is the radius of the contact area, r_b is the radius of the particle, and h^* is the penetration depth of the particle in the cell surface layer.

DISCUSSION

We have depicted here a few passive biophysical aspects of the binding of colloidal particles, mediated by a collection of molecular links, on the surface of a B-cell line. This question of the establishment of molecular bonds in the bushy material of the cell surface deserves to be addressed to better understand the strategies developed by the cell to interact with the macroscopic objects of its environment. This also happens in physiological situations where cells have to cooperate through specific association, such as, for example, in the formation of the immunological synapse (Grakoui et al., 1999), rather than in more technological situations such as specific cell sorting using magnetic colloids (Chalmers et al., 1998).

As a tool, we have employed well-defined micrometric particles bearing streptavidin, and a biotinylated antibody targeted to the B-cell specific receptor CD19, and then followed the phenomenology of the particles binding to the labeled cells. The most striking feature of this binding process was that only a fraction of the cell population appeared to be competent for particle binding, even though the cell line was probed for its CD19 surface expression and proved to display a monomodal CD19 distribution with a mean value of 4×10^5 receptors per cell. We have shown here that this cell selection originated in the existence of a receptor surface density threshold governing the binding. The association of a particle to a cell occurred only if the receptor surface density reached a minimal limiting value that was found equal to 1.6×10^3 receptors/μm^2. Depending on the receptor distribution, this threshold value determined the fraction f_c of cells that were able to bind one or more particles. Similar behavior was also observed with another B-cell line (JY) and with a T-cell line (Jurkat) labeled using a biotinylated anti-CD3 antibody (data not shown). Still, we have shown that the binding threshold shifted toward the lower density values when the molecular link was lengthened, suggesting that steric hindrance created by the glycocalix restrained the binding site's accessibility.

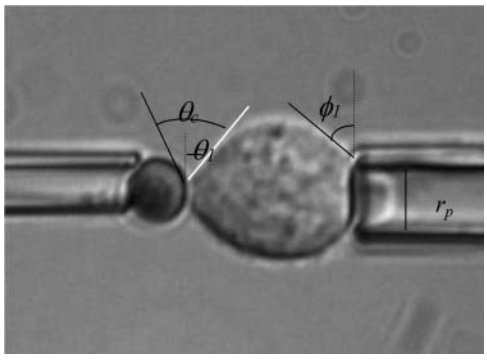

FIGURE 14 Evaluation of cell-particle energy of adhesion. Cell and particle are pulled apart with micropipette. The various angles used for the calculation of the energy of adhesion are shown. Experiments were performed at room temperature.

Considering that the mean surface densities of receptors and ligands on cell and particle, together with the estimation of the contact area, were found to be ~2.5 μm^2, it can be calculated that a contact may potentially assemble 4×10^3 links. This is the mean number of receptors presented by the cell over a 2.5-μm^2 area. On the particle side, the same area presents 5×10^5 binding sites. The micropipette experiments have provided limit-values telling us that the number of links within a contact should be comprised between 7×10^3 and 2.5×10^5. Despite the large values-interval provided, these experiments indicated that a high number of sites were, in fine, actually connected between cell and particle; these numbers are much higher than we would have expected for the retaining of such a particle in a hydrodynamic flow. For a given system in which the nature of the molecular link and the surface densities of receptor and ligand are fixed, the two parameters governing the number of links, N, necessary to retain a particle on a surface are γ, the shear stress and r_c, the radius of the contact area. Indeed, the theoretical framework introduced by Bell (1978) and detailed in Cozens-Roberts et al. (1990) allowed us to calculate N from the expression

$$N = (160\lambda/k_BT)[\gamma/Ln(K_a\rho_L)](r_b^3/r_c), \quad (1)$$

where λ is the range of the interaction; k_B is the Boltzmann constant; T is the temperature; γ is the shear stress; K_a is the two-dimensional association constant of the binding link; ρ_L is the ligand surface density; and r_b is the radius of the particle. Here, to evaluate N from Eq. 1, we took λ to be equal to 5×10^{-8} cm, just as for the antigen-antibody bond (Cozens-Roberts et al., 1990). Considering that the rupture will take place at the site of the weakest junction (Saterbak and Lauffenburger, 1996), we took for K_a the affinity constant of the association of anti-CD19 with its CD19 target determined above (8.2×10^8 M^{-1}). At this point, it should be noted that the constant entering in Eq. 1 is a two-dimensional constant whereas the constant we have determined is a three-dimensional constant. We made the volume-to-surface conversion following the considerations of Dustin et al. (1997), i.e., introducing a characteristic

length of the order of the molecule size (10 nm). The ligand surface density, ρ_L, was equal to $2 \times 10^{13}/cm^2$, the streptavidin surface density of the particles, and r_b was equal to 1.4×10^{-4} cm. The shear stress applied in our experimental setup was of course strongly heterogeneous but we have been able to estimate from the fluid volume in the tube and from the speed of liquid inversion that γ reasonably ranged between 1 and 10 dyn/cm^2. We then calculated N for a range of r_c-values providing contact areas comprised between 10^3 and 10^4 nm^2. Afterwards we calculated the number of links offered by the cell surface for the same range of contact area considering the surface density at the binding threshold. We then obtained that, at the threshold density, the cell was able to bind a particle (i.e., to gather enough receptor for the particle not to be detached by the fluid) only if the contact area was at least equal to 5000 nm^2, the number of necessary links being equal to 8. At lower receptor densities, the number of links presented by the cell for this contact area decreases below this limiting stabilizing number—explaining why the cells could no longer bind any particles, with those being immediately detached by the shear flow.

On the other hand, we observed that increasing the rotation speed of the stirring machine decreased the binding threshold value and we attributed this effect to the increase of the shear stress. Now, Eq. 1 predicts that the threshold should increase, inasmuch as N is proportional to the shear stress but only if γ and r_c are independent variables—which is the case for solid surfaces as described in Cozens-Roberts et al. (1990), Saterbak et al., (1993), and Pierres et al. (1998, 2001). Here, the cell surface is a soft material offering a viscoelastic layer, having a plastic response in the collision with the particle, the extent of which should depend strongly on the torque and force imposed by the fluid on the particle, and then from the shear stress. Our working hypothesis is now that the shear stress has two counteracting effects in the binding. On the one hand, it increases the detaching force; on the other hand, it increases the contact area between cell and particle—decreasing the number of required links to stabilize the particle at the surface, thereby decreasing the threshold value. This idea is now under investigation in our group using homogeneous shearing in a cone-plate setup. At this point, we guess that the characteristics of the binding profile originate in the existence and the properties of the glycocalyx and that describing the response to the shear will help us to better understand the role of this structure in the regulation of the cell-surface interactions. Sabri et al. (2000) has already shown in activated human monocytes that such a regulating role could take place through compression or displacement of the bulky structures of this layer.

The binding scheme proposed above entails that the contact area delineated by the collision may grow from approximately eight links, distributed over 500 nm^2, to reach a few thousand occupying a few μm^2—as was measured at the plateau of the interaction. This contact area may simply grow as the particle locally rolls over the cell with an amplitude depending on the cell membrane and the initial link's elasticity (Schmid-Schonbein et al., 1981; Dong et al., 1988). Then, the ligands and receptors align, allowing much additional molecular binding. In a static vision of ligands and receptors distribution, the particle connects only the locally facing receptors. However, in this hypothesis, the cell should accommodate particles almost up to close packing, whereas only cells having bound a few particles (10 at the very most) were evidenced. Moreover, we have shown in this report that the probability for a cell-particle contact to occur decreased exponentially with the particle order, suggesting that the binding of the particle n^{th} affected the binding of the particle $(n+1)^{th}$. This might have something to do with some spatial orientation effect induced by the already bound particles. Indeed, once a cell has bound one particle, it is no longer a spherical object and in a shear field, it might well adopt a preferential orientation that would affect the subsequent binding events. However, this is rather difficult to evaluate and our preferred hypothesis is that of a dynamic process where the binding initiation would induce migration of receptors toward the contact. This receptor migration would then also drive the arrest of the binding of particles of higher order by decreasing the mean receptors surface density below the binding threshold. This implies that migration of receptors occurs with a characteristic time significantly lower than the characteristic time of particle binding. The ratio of these two times is contained in the constant δ, which gives the exponential decrease of the binding probability with the binding order of the particle. This migration of receptors toward the contact area seems to be a mainly passive process driven by the thermodynamic equilibrium of the unbound receptors at the cell surface. Indeed, the energetic poisoning of the cell only slightly affected the interaction characteristics. A small density threshold decrease and a binding inhibition retardation were observed using sodium azide treatment. This suggests that cell active processes, which were likely of very low level in the conditions we used, only tended to facilitate or accelerate the migration of the receptors but not to trigger it. CD19 is actually a co-receptor of the B-cell receptor engagement and is known for being able to translocate in lipid rafts upon stimulation (Cherukuri et al., 2001). It forms transitory noncovalent complexes with CD21 and CD81, obviously holding the intrinsic aptitude to diffuse freely in the membrane.

To summarize the main findings of this work, we propose a model for the specific cell-surface interaction where:

1. The binding involves a large collection of links.
2. The cell surface receptor density operates like a switch for binding.
3. The strength of the collision between cell and the surface (here, colloidal surface) is a key parameter of the binding, because it determines the receptor surface density threshold value that allows the binding. This collision strength is determined by the physical conditions of

cell-surface contact, in particular the shear stress applied. This is of most importance for technological applications such as those consisting of sorting cells on specific criteria using ligand-bearing particles (immunodiagnostic applications). Adapting the incubation setup to apply a control shear stress will lead to a net higher and accelerated capture of the cells of interest.

4. The length of the molecular link appeared to increase the number of efficient binding events, strengthening the idea of the role of the steric repulsion and the important role of the glycocalyx. This is also for consideration in conceiving cell-sorting tools: if some latitude is permitted on the receptor serving for the capture, it has to be chosen to be as long as possible; if not, the ligand architecture has to be a long one, eventually involving bonds in series.
5. The initial limiting contact, which allows the cell-surface binding and which is established at the moment of the collision, spreads up to a few μm^2, providing a strong adhesion involving thousands of links.
6. It seems that the establishment of the contact concentrates the binding molecules within the contact zone. This phenomenon appears to operate like a switch-off to further binding.

The receptor clustering in adhesive phenomena has often been observed, both experimentally and theoretically, as the result of spontaneous thermodynamic equilibrium upon binding mostly in biophysical model systems (e.g., Torney et al., 1986; Albersdörfer et al., 1997; Bruinsma et al., 2000; Brochard-Wyart and de Gennes, 2002). Depending upon the physical and chemical conditions offered, this clustering might provide to the cell some sort of basic means for regulating its interaction with the environment.

We are grateful to Pierre Nassoy for valuable discussions and to Christophe Hubert for skillful technical assistance.

The Fonds Européen de Développement Régional Objectif 2 and Bioengineering Program from the French Ministry of Research and Technology have contributed financial support for this work.

REFERENCES

Albersdorfer, A., T. Feder, and E. Sackmann. 1997. Adhesion-induced domain formation by interplay of long-range repulsion and short-range attraction force: a model membrane study. *Biophys. J.* 73:245–257.

Bradbury, L. E., V. S. Goldmacher, and T. F. Tedder. 1993. The CD19 signal transduction complex of B lymphocytes. Deletion of the CD19 cytoplasmic domain alters signal transduction but not complex formation with TAPA-1 and Leu^{13}. *J. Immunol.* 1993. 151:2915–2927.

Braun, D., and P. Fromherz. 1998. Fluorescence interferometry of neuronal cell adhesion on microstructured silicon. *Phys. Rev. Lett.* 81: 5241–5244.

Brochard-Wyart, F., and P. G. de Gennes. 2002. Adhesion induced by mobile binders: dynamics. *Proc. Natl. Acad. Sci. USA.* 99:7854–7859.

Bruinsma, R., A. Behrisch, and E. Sackmann. 2000. Adhesive switching of membranes: experiment and theory. *Phys. Rev. E.* 61:4253–4267.

Bell, G. I. 1978. Models for the specific adhesion of cells to cells. *Science.* 200:618–627.

Berk, D., and E. Evans. 1991. Detachment of agglutinin-bonded red blood cells. III. Mechanical analysis for large contact areas. *Biophys. J.* 59:861–872.

Chalmers, J. J., M. Zborowski, L. Sun, and L. Moore. 1998. Flow through, immunomagnetic cell separation. *Biotechnol. Prog.* 14:141–148.

Chenevier, P., B. Veyret, D. Roux, and N. Henry-Toulme. 2000. Interaction of cationic colloids at the surface of J774 cells: a kinetic analysis. *Biophys. J.* 79:1298–1309.

Cherukuri, A., P. C. Cheng, H. W. Sohn, and S. K. Pierce. 2001. The CD19/CD21 complex functions to prolong B-cell antigen receptor signaling from lipid rafts. *Immunity.* 14:169–179.

Cozens-Roberts, C., J. A. Quinn, and D. A. Lauffenberger. 1990. Receptor-mediated adhesion phenomena. Model studies with the radical-flow detachment assay. *Biophys. J.* 58:107–125.

de Gennes, P. G., P. H. Puech, and F. Brochard-Wyart. 2003. Adhesion induced by mobile stickers: a list of scenarios. *Langmuir.* 19:7112–7119.

Dong, C., R. Skalak, K. L. Sung, G. W. Schmid-Schonbein, and S. Chien. 1988. Passive deformation analysis of human leukocytes. *J. Biomech. Eng.* 110:27–36.

Dustin, M. L., D. E. Golan, D. M. Zhu, J. M. Miller, W. Meier, E. A. Davies, and P. A. van der Merwe. 1997. Low affinity interaction of human or rat T-cell adhesion molecule CD2 with its ligand aligns adhering membranes to achieve high physiological affinity. *J. Biol. Chem.* 272:30889–30898.

Evans, E. 2001. Probing the relation between force-lifetime and chemistry in single molecular bonds. *Annu. Rev. Biophys. Biomol. Struct.* 30:105–128.

Grakoui, A., S. K. Bromley, C. Sumen, M. M. Davis, A. S. Shaw, P. M. Allen, and M. L. Dustin. 1999. The immunological synapse: a molecular machine controlling T-cell activation. *Science.* 285:221–227.

Gumbiner, B. M. 1996. Cell adhesion: the molecular basis of tissue architecture and morphogenesis. *Cell.* 84:345–357.

Helm, C. A., W. Knoll, and J. N. Israelachvili. 1991. Measurement of ligand-receptor interactions. *Proc. Natl. Acad. Sci. USA.* 88:8169–8173.

Hutchinson, S. L., L. Wooldridge, S. Tafuro, B. Laugel, M. Glick, J. M. Boulter, B. K. Jakobsen, D. A. Price, and A. K. Sewell. 2003. The CD8 T-cell coreceptor exhibits disproportionate biological activity at extremely low binding affinities. *J. Biol. Chem.* Apr 15, 2003 [*epub ahead of print*]. 278:24285–24293.

Jung, L. S., K. E. Nelson, P. S. Stayton, and C. T. Campbell. 2000. Binding and dissociation kinetics of wild-type streptavidins on missed biotin-containing alkylthiolate monolayers. *Langmuir.* 16:9421–9432.

Leckband, D. E., F. J. Schmitt, J. N. Israelachvili, and W. Knoll. 1994. Direct force measurements of specific and nonspecific protein interactions. *Biochemistry.* 33:4611–4624.

Lévéille, C., J. G. Castaigne, D. Charron, and R. Al-Daccak. 2002. MHC class II isotype-specific signaling complex on human B-cells. *Eur. J. Immunol.* 32:2282–2291.

Merkel, R., P. Nassoy, A. Leung, K. Ritchie, and E. Evans. 1999. Energy landscapes of receptor-ligand bonds explored with dynamic force spectroscopy. *Nature.* 397:50–53.

Pérez-Luna, V., M. J. O'Brien, K. A. Opperman, P. D. Hampton, G. P. López, L. A. Klumb, and P. S. Stayton. 1999. Molecular recognition between genetically engineered streptavidin and surface-bound biotin. *J. Am. Chem. Soc.* 121:6469–6478.

Pierres, A., A. M. Benoliel, and P. Bongrand. 1998. Use of a laminar flow chamber to study the rate of bond formation and dissociation between surfce-bound adhesion molecules: effect of applied force and distance between surfaces. *Faraday Discuss.* 111:321–330.

Pierres, A., A. M. Benoliel, C. Zhu, and P. Bongrand. 2001. Diffusion of microspheres in shear flow near a wall: use to measure binding rates between attached molecules. *Biophys J.* 81:25–42.

Pierres, A., D. Touchard, A. M. Benoliel, and P. Bongrand. 2002. Dissecting streptavidin-biotin interaction with a laminar flow chamber. *Biophys. J.* 2002 82:3214–3223.

Ravaine, V., J. Bibette, and N. Henry. 2002. Wetting of liquid droplets on living cells. *J. Colloid Interface Sci.* 255:270–273.

Sabri, S., M. Soler, C. Foa, A. Pierres, A. Benoliel, and P. Bongrand. 2000. Glycocalyx modulation is a physiological means of regulating cell adhesion. *J. Cell Sci.* 113:1589–1600.

Saterbak, A., and D. A. Lauffenburger. 1996. Adhesion mediated by bonds in series. *Biotechnol. Prog.* 12:682–699.

Saterbak, A., S. C. Kuo, and D. A. Lauffenburger. 1993. Heterogeneity and probabilistic binding contributions to receptor-mediated cell detachment kinetics. *Biophys. J.* 65:243–252.

Schmid-Schonbein, G. W., K. L. Sung, H. Tozeren, R. Skalak, and S. Chien. 1981. Passive mechanical properties of human leukocytes. *Biophys. J.* 36:243–256.

Stuart, D. I., and E. Y. Jones. 1995. Recognition at the cell surface: recent structural insights. *Curr. Opin. Struct. Biol.* 5:735–743.

Torney, D. C., M. Dembo, and G. I. Bell. 1986. Thermodynamics of cell adhesion. II. Freely mobile repellers. *Biophys J.* 49:501–507.

Tozeren, A., K. L. Sung, and S. Chien. 1989. Theoretical and experimental studies on cross-bridge migration during cell disaggregation. *Biophys J.* 55:479–487.

Van der Merwe, P. A. 2002. Formation and function of the immunological synapse. *Curr. Opin. Immunol.* 14:293–298.

Wong, J. Y., T. L. Kuhl, J. N. Israelachvili, N. Mullah, and S. Zalipsky. 1997. Direct measurement of a tethered ligand-receptor interaction potential. *Science.* 275:820–822.

Verkhivker, G. M., D. Bouzida, D. K. Gehlhaar, P. A. Rejto, S. T. Freer, and P. W. Rose. 2002. Complexity and simplicity of ligand-macromolecule interactions: the energy landscape perspective. *Curr. Opin. Struct. Biol.* 12:197–203.

Eur. Phys. J. E **14**, 269–276 (2004)
DOI 10.1140/epje/i2003-10151-2

THE EUROPEAN PHYSICAL JOURNAL E

Hemifusion and fusion of giant vesicles induced by reduction of inter-membrane distance

J. Heuvingh[1,a], F. Pincet[2], and S. Cribier[1]

[1] Laboratoire de Physico-Chimie Moléculaire des Membranes Biologiques, URD-CNRS UMR 7099, IBPC, 13 rue Pierre et Marie Curie, 75005 Paris, France
[2] Laboratoire de Physique Statistique, ENS, 24 rue Lhomond 75231 Paris cedex 05, France

Received 22 July 2003 and Received in final form 26 May 2004 /
Published online: 3 August 2004 –

Abstract. Proteins involved in membrane fusion, such as SNARE or influenza virus hemagglutinin, share the common function of pulling together opposing membranes in closer contact. The reduction of inter-membrane distance can be sufficient to induce a lipid transition phase and thus fusion. We have used functionalized lipids bearing DNA bases as head groups incorporated into giant unilamellar vesicles in order to reproduce the reduction of distance between membranes and to trigger fusion in a model system. In our experiments, two vesicles were isolated and brought into adhesion by the mean of micromanipulation; their evolution was monitored by fluorescence microscopy. Actual fusion only occurred in about 5% of the experiments. In most cases, a state of "hemifusion" is observed and quantified. In this state, the outer leaflets of both vesicles' bilayers merged whereas the inner leaflets and the aqueous inner contents remained independent. The kinetics of the lipid probes redistribution is in good agreement with a diffusion model in which lipids freely diffuse at the circumference of the contact zone between the two vesicles. The minimal density of bridging structures, such as stalks, necessary to explain this redistribution kinetics can be estimated.

PACS. 87.16.Dg Subcellular structure and processes: Membranes, bilayers, and vesicles – 87.15.Vv Biomolecules: structure and physical properties: Diffusion – 64.70.Nd Structural transitions in nanoscale materials

1 Introduction

Membrane fusion is a topic of essential interest in diverse areas of biological science, such as transport inside the cell, viral infection, delivery of hormones and neurotransmitters, or fertilization. In the recent years, progresses have been achieved in the description and understanding of the molecular machinery of membrane fusion. For intracellular transport, SNARE proteins are believed to be responsible for fusion. Reconstituted in artificial vesicles in the absence of any other protein, their presence was sufficient to promote fusion [1].

SNARE proteins in opposing membranes can interact, forming a SNAREpin, and pulling together the membranes in which they are embedded. The reduction of inter-membrane distance could directly induce a transition state of the phospholipids [2] triggering fusion. A mechanical effect of the SNAREs could also be involved in the merging of the distal monolayers [3]. Another hypothetical pathway to fusion [4] reduces the role of lipids and involves primarily proteins as constituents of the initial fusion pore leading to fusion.

Viral fusion proteins are believed to trigger fusion between the virus and the host cell membrane by a similar mechanism of pulling membranes together [5,6].

The aim of this work is to mimic these systems in an entirely artificial protein-free system, by bringing the membranes of two vesicles into closer contact and show that lipid layers alone can fuse or partly fuse. More precisely, we will point out that if the lipid layers are brought close enough to each other, fusion or an intermediate state called hemifusion can occur. The idea of studying hemifusion or fusion in model systems by the reduction of inter-membrane distance induced by dehydration is not new. For example, dehydration has been either directly induced [7] or mediated by poly(ethylene glycol) [8]. However, some quantitative features are difficult to control and measure in these systems (*e.g.*, tension, dynamics of the lipid redistribution, volume and membrane surface variations, initial time of contact between the membranes, ...). The use of giant unilamellar vesicles allows to circumvent most of these difficulties.

[a] e-mail: julien.heuvingh@univ-paris5.fr

The forces applying in the interaction between two lipidic membranes are: the van der Waals attraction, the double layer electrostatic repulsion between the zwiterionic lipids, the repulsion by Helfrich's thermal undulation [9], and several short-range repulsion forces (hydration, protrusion, steric hindrance) [10,11]. For membranes of dioleoyl-phosphocholine, a separation distance of 3 nm was measured by X-ray diffraction by Rand and Parsegian [12]. By adding in our system functionalized lipids bearing the DNA bases thymidine or adenosine as headgroups, we introduce a supplementary force (the H-bond between nucleosides), enhancing attraction between the membranes. Numerical estimation of the interaction energy as a function of the intermembrane distance shows a decrease of the equilibrium distance from 3 nm without the supplementary force to 1 nm with the supplementary force (calculated by Pincet *et al.* [13]). The interaction between the nucleosides lipid derivative and their behavior have been previously described [14]. The decrease of the intermembrane distance is only effective where the specific force is applying, *i.e.* where two functionalized lipids, or stacks of functionalized lipids [15] from the membranes come into vicinity. The membranes might therefore be 3 nm distant, with patches of membrane protruding toward each other. Such a protrusion is similar to the deformation observed in exocytosis [16] that may be induced by fusogenic proteins [17]. It has also been theoretically shown that these protrusions facilitate the formation of stalk intermediates between two bilayers [18]. When stalks are formed, the topological structure of the membranes is similar to the commonly called hemifusion state where the contacting leaflets of both bilayers have merged whereas the inner leaflets remain independent. Such stalk structures have recently been observed by X-ray diffraction [7].

2 Materials and methods

2.1 Materials

The functionalized lipids with thymidine or adenosine as headgroups (later referred to as adenosine or thymidine lipids) were obtained by coupling the unprotected nucleosides to 2-(1,3-dioleyloxy) propylhemisuccinic acid using a modified DCC/DMAP method [19]. Dioleoyl-*sn*-phosphatidylcholin (DOPC), fluorescein isothiocyanate dextran (MW: 9300kDa) and bovine albumin were purchased from SIGMA. 1,2-dioleoyl-*sn*-glycero-3-phosphoethanolamine-N-(lissamine rhodamine B sulfonyl) (RhPE) was purchased from Avanti Polar Lipids. Vitrex sigilium paste was purchased from Modulohm A/S (Herlev, Denmark). Coated ITO glass was purchased from Thales Electron Device (Vélizy, France).

2.2 Preparation of GUV

Giant unilamellar vesicles were produced by the electroformation method [20]. Briefly, the preparation chamber is made of two glass plates coated with an indium tin oxide (ITO) film, which renders them conductive. Phospholipids were dissolved in chloroform/methanol (5/3). For each sample, 10 μg were carefully deposited as homogenous pitch on the conductive side of each glass plate. They were then put under vacuum for 1 hour in order to eliminate the remaining solvent. The two plates with the conductive faces opposing each other, together with a 1 mm thick Teflon spacer form a 2ml chamber, which is sealed with sigillum paste. The chamber is filled with a 300 mM sucrose solution. An AC field (8 Hz) was then applied between the two plates of the chamber, quickly after the filling, in order to prevent the spontaneous formation of vesicles. The lipid film swelled as the electric voltage was progressively increased to 1 volt over one hour, remaining at this value overnight. The giant vesicles are finally detached from the glass plate by the application of an electric AC tension of higher voltage and shorter period (4 Hz). The vesicles used for the experiments were directly taken from the preparation chamber with a capillary pipette inserted through a hole in the Teflon spacer. Giant vesicles prepared in this manner are mostly unilamellar [21].

The osmolarity of each solution used in these experiments was carefully checked with a micro-osmometer (Roebling, Germany). The glucose and sodium chloride solutions in which the vesicles were observed were adjusted at a slightly higher osmolarity than the swelling sucrose solution, in order to deflate the vesicles. This is required for pipette holding and to obtain a suitable contact area during aggregation of the vesicles.

2.3 Observation of liposomes and micromanipulation

Liposomes were observed by epi-fluorescence and phase contrast optical microscopy, using an inverted microscope (Zeiss IM35). The objective lens was X32 (N.A. 0.40, Zeiss, Germany). The fluorescence was excited by an argon laser (Coherent Innova 90-4) tuned at 514 nm (green) for rhodamine-labeled lipids and at 488 nm (blue) for fluorescein-labeled dextran. The images were acquired on a Micromax 5 MHz digital camera (Roperscientific, USA) with a PI 782 $\times$ 582 Interline CCD Array.

Transfer micromanipulation was used in order to maneuver independent vesicles and to transfer vesicles from a stock chamber to an observation chamber where the conditions were well defined. The micromanipulation device was made up of two micromanipulators (Leitz, Germany) and three pipette holders (Narishige, Japan). Two types of micropipettes were used: small suction pipettes (internal diameter 5–10 μm) and larger transfer pipettes (internal diameter 100–300 μm). The aspiration was controlled by hydrostatic pressure up to 500 Pa. The transfer pipette was made and used as indicated by Kwok and Evans [22].

The micromanipulation chamber was made up of two metal plates and four thin glass slides. The glass slides formed two independent parallel chambers of approximately 300 μl, into which the solutions stand by capillarity on two sides, allowing pipettes to enter the solution or to pass through it. The two chambers along with the pipettes

were incubated in a solution of 10% BSA in pure water during one hour to prevent adhesion of vesicles with the pipettes or glass slide, and were then emptied and rinsed out twice from the solution. One of the chambers (the stock chamber) was then filled with a 310 mOsm glucose solution, the other one (the observation chamber) with a 320 mOsm NaCl solution. The vesicles were put in the stock chamber with a capillary pipette. The vesicles sunk to the bottom of the chamber in a few minutes, due to the density difference between the sucrose solution inside the vesicle and the glucose solution outside. We selected a suitable vesicle and held it by a suction pipette. It was then transferred and put down on the bottom of the observation chamber. This operation was repeated with another vesicle of the appropriate type and of similar size. The second vesicle was placed near the first one. A flow was then set by a pipette aspiration in order to displace the two vesicles, and to bring them into contact.

2.4 Fluorescence quantification

For quantification purpose, we usually determined the mean density of fluorescence probes on a vesicle. A rectangular selection was chosen around the center of the vesicle's projected image. The intensity of the fluorescence signal in the selection was averaged, and we took as error bars the standard deviation of the fluorescence intensity in the selection. This choice of selection allowed us to avoid errors due to a higher projection of the membrane closer to the border, and to the drift caused by the polarization of the laser light source and by the mean orientation of the dipolar momentum of probes in the membrane. This quantification was done with the *Image J* software, provided by the National Institute of Health (USA).

3 Results and discussion

3.1 Observation

In a first set of experiments we used two types of vesicles, both predominantly made of DOPC. The first type contained a fixed amount of adenosine lipids (ranging from 1% to 10% of the total lipids), and 2% RhPE as fluorescent label. The second type bore thymidine lipids (same amount as adenosine on the former type), and had no fluorescence apart from the intrinsic fluorescence of DOPC. This intrinsic fluorescence is at least 5 orders of magnitude smaller than the RhPE fluorescence. Two vesicles of different types were selected from the stock chamber and transferred to the observation chamber. The two vesicles were then brought into close proximity. Aggregation of the vesicles (deformation with formation of an adhesion area between the vesicles) happened spontaneously within minutes or was triggered by displacing the vesicles with a flow of the pipette.

Immediately after aggregation (within 5 seconds, the time resolution of the experimental setup), a fluorescent signal was observed on the non-labeled vesicle. During a few minutes the fluorescence intensity on the thymidine-bearing vesicle increased, while the fluorescence intensity decreased on the adenosine-bearing vesicle. In most of the experiments an equilibrium, stable for several hours, was reached.

In five percent of the experiments (7 occurrences), the vesicles collapsed, forming a bigger one. In the other cases, the fluorescence transfer reached equilibrium. These observations and their kinetics were the same for vesicles containing 1, 2, 5 and 10% of functionalized lipid (adenosine and thymidine).

Control experiments were conducted with vesicles containing neither adenosine nor thymidine lipids. The aggregation was still observed, but no fluorescence transfer was detected over more than an hour, in agreement with results of Pincet *et al.* [13]. No collapse of two vesicles into a bigger one was observed during control experiments.

3.2 Equilibrium

When an equilibrium was reached, the fluorescence intensity of the formerly non-fluorescent vesicle was still inferior to the intensity of the formerly fluorescent vesicle (see Fig. 1).

3.2.1 Hemifusion

The relative difference in the fluorescence of the two vesicles at equilibrium suggests that the system may have reached a state known as hemifusion state where the contacting leaflets of both bilayers have merged whereas the inner leaflets (as well as the interior of the vesicles) remain independent. This can be shown in three complementary ways: i) by directly quantifying the fluorescence ratio of the vesicles at equilibrium; ii) by labeling the aqueous content of one vesicle; and iii) by trying to separate the vesicles. The results of these three approaches are described in this section.

Fluorescence microscopy images were recorded and analyzed to compare the fluorescence intensity on the membrane of both vesicles, after transfer has reached equilibrium. The ratio of fluorescence between the two vesicles (*i.e.* the fluorescence density on the formerly non-fluorescent vesicle divided by the fluorescence density on the formerly fluorescent vesicle) was collected for about fifty couples of vesicles. This ratio was found to be close to one third for vesicles of the same size. In the case of hemifusion, this result is expected, as the fluorescent markers on the outer leaflet of the originally labeled vesicle redistributed between the two vesicles, whereas the markers of the inner leaflet stay in the membrane of the originally labeled vesicle. The expected fluorescence ratio for vesicles of different size enduring hemifusion is calculated in Appendix A. The experimental equilibrium transfer ratio is found to be very close to the calculated theoretical ratio, denoting a lipid mixing of the outer leaflets of both vesicles, without the mixing of inner leaflets (see Fig. 2).

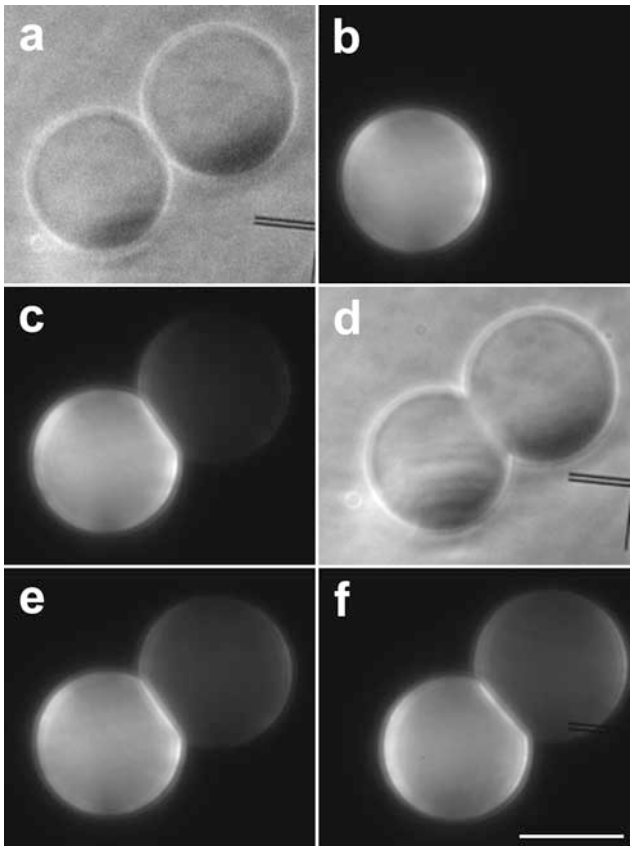

Fig. 1. Two tangent vesicles seen by phase contrast microscopy (a) and epi-fluorescence (b). One of the vesicles is functionalized by adenosine lipids and labeled by RhPE, the other one is functionalized by thymidine lipids. Just after aggregation of the two vesicles, as attested by membrane deformation in the contact area (d), a fluorescent signal appeared on the non-labeled vesicle (c), denoting a lipid mixing. Fluorescent lipids carry on their redistribution after 3 minutes (e) until they reached equilibrium after 6 minutes (f). The fluorescence density on the thymidine-bearing vesicle was still inferior to the fluorescence density of the adenosine-bearing vesicle. The bar is 20 μm.

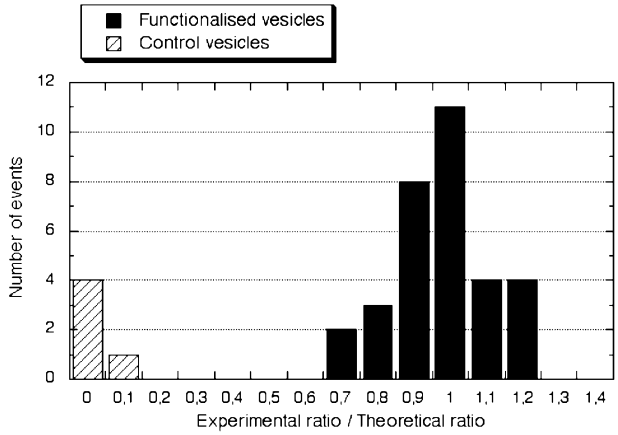

Fig. 2. Comparison between experimental and theoretical ratio of fluorescence density between the two vesicles, after redistribution has reached an equilibrium. The experimental ratio is the fluorescence density measured on the formerly non-fluorescent vesicle divided by the fluorescence density measured on the formerly fluorescent vesicle. The theoretical ratio of two vesicles enduring a mixing of their outer monolayer, but no mixing of their inner monolayer, was calculated according to Appendix A. For vesicles' couple containing adenosine and thymidine lipids, the experimental ratio is close to the theoretical one. For control vesicles bearing no functionalized lipids the experimental ratio is close to zero (no lipid redistribution).

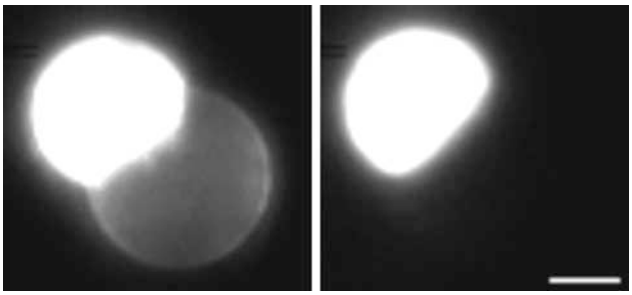

Fig. 3. Two aggregated vesicles. One of the vesicles is functionalized by adenosine lipids and labeled by RhPE on surface and by FITC-dextran in volume; the other one is functionalized by thymidine lipids. Fluorescence imaging with a laser tuned on the excitation wavelength of rhodamine (514 nm) shows lipid mixing (left). Fluorescence imaging with a laser tuned on the excitation wavelength of fluoresceine (488 nm) shows no aqueous content mixing (right). The bar is 10 μm.

In a separate set of experiments, we grew the adenosine fluorescent vesicles in a fluorescent solution. The solution contained 1 mM dextran (9300 Da) labeled with fluorescein. Sucrose was added in order to maintain a 300 mOsm osmolarity. The vesicles are therefore fluorescently labeled on their surface by rhodamine and in volume by fluoresceine. These vesicles, along with thymidine vesicles, were as previously put in the stock chamber, and transferred to the observation chamber. The dextran concentration was set to give a fluorescence emission one order of magnitude stronger than the membrane emission. As the vesicles aggregated, fluorescence emissions were checked on the thymidine vesicle with the laser set alternatively on the fluorescein absorption wavelength (488 nm) and on the rhodamine absorption wavelength (514 nm). Minutes after aggregation, a good fluorescent rhodamine signal was seen on the thymidine vesicle, denoting lipid mixing, but no fluorescence signal was detected for the fluorescein absorption wavelength more than one hour after lipid mixing (see Fig. 3). Therefore, if any leakage had occurred during this time, it was below the resolution of our system (less than one percent of the fluorescent dextran leaked to the other vesicle). This denotes a lack of significant content mixing, at least for molecules with a radius of more than 3 nm [23].

Finally, when we tried to separate the vesicle doublet after equilibrium was reached, we were not able to revert it to two completely independent vesicles. This was checked by holding tightly both vesicles by pipettes with a high suction pressure. Provided that the vesicles were not destroyed by the mechanical stress, the pipettes were pulled

apart. The vesicles seemed then completely separated in phase contrast microscopy. This result gives a strong indication that both vesicles still have distinct interior media.

In reality, this separation was not complete since a lipid filament (tether) of unknown structure could still be seen linking the vesicles by fluorescence. When one of the vesicles was released, it hurled back toward the other vesicle, indicating strong tension in the tether. However, this tether is not characteristic of hemifusion as has already been observed before in adhering systems [24]. This was confirmed in control experiments where two adhering vesicles containing neither adenosine nor thymidine lipids were separated.

These three different approaches show unambiguously that hemifusion is indeed reached in our system: the outer leaflets are shared while the inner leaflets, as well as the interior of the vesicles, are completely distinct.

3.2.2 The decrease in separation distance triggers hemifusion

The physical factor that triggers hemifusion has also to be discussed. Since the functionalized lipids are able to decrease the equilibrium distance between adhering bilayers from 3 nm down to 1nm, the hydration of the lipids in the contact area tends to be smaller than its most favorable one [25]. This process is similar to what happens when pushing on membranes very strongly. It has already been observed that supported membranes that were pushed against each other with high forces were indeed able to hemifuse [26]. These experiments showed that fusion needs less force to be achieved when the contact area is more depleted in lipids [26,27]. A recent paper by Safran [28] showed how the decrease of lipid density in the contact area can induce hemifusion. With our functionalized molecules, the lipids in the contact area are frustrated by the dehydration. Therefore, their chemical potential becomes higher than the one in the non-frustrated state before adhesion and, since they have to equilibrate with the lipids in the outer region, there must be a slight depletion to equalize the chemical potentials. This depletion would expose the hydrophobic parts of the lipids and could produce hemifusion.

3.2.3 Structure of the contact zone

Even though the hemifusion state is clearly established, the organization of the lipids in the contact area remains unknown. In other terms, the intermediary state toward fusion in which the system is blocked still has to be elucidated. The structure of the contact zone remains unclear.

When two vesicles endure hemifusion, the membranes in the contact area must rearrange from a bilayer to another structure. The model currently favored for the fusion of purely lipidic membranes is the stalk hypothesis [29, 30]. In this model, the first intermediary state toward fusion is the formation of a thin lipid bridge (stalk) linking the two outer monolayers. A slight evolution of the stalk structure would then allow a contact between the two inner monolayers. Two scenarios are proposed to go from the stalk intermediate to the formation of a pore in the membrane, leading to fusion. The first one is the direct formation of a pore. The second one is the enlargement of the stalk, creating a diaphragm, *i.e.* a bilayer formed by the inner monolayers of both vesicles. Destabilization of the diaphragm would then trigger pore formation.

According to this stalk hypothesis, the structure of the contact area of the hemifused doublets in our experiments could be either a stalk structure or a diaphragm. However, the picture of a diaphragm spanning the whole contact area seems unrealistic at such scales (the typical contact area of the two giant vesicles is hundreds of square microns). In particular, the very high elastic modulus (about 0.1 N/m for a vesicle membrane [31]) prevents such a high compression of the membrane, which means there is no space for the lipids of the outer membranes to be driven away from the interface. We tried to get direct evidence of the presence of two bilayers at the interface, instead of the single diaphragm bilayer. Unfortunately, quantification of the straight vertically oriented contact area proves difficult to obtain in a convincing way. However, no fluorescence loss of the interface was observed between images taken immediately before and after the start of the hemifusion (data not shown).

We can therefore, with reasonable confidence, hypothesize that the structure of the contact area is a stalk structure with a sufficient number of stalks or of equivalent "bridging structures" which could be, for instance, diaphragms of limited extent.

Since the lipids have to pass through these bridging structures, it can be suspected that their diffusion would be slowed down during their transfer from one vesicle to the other. This could be checked by directly quantifying the kinetics of fluorescence redistribution. Fluorescence ratios were compiled for different times before equilibrium was reached. In this way, we obtained the kinetics of the lipid redistribution between the two hemifused vesicles. This kinetics was compared to a model for lipid redistribution based on Rubin *et al.* [32] where the outer membrane's lipids freely diffuse on the surface of two truncated spheres picturing the hemifused doublet (see Fig. 4). This model will thereafter be referred as the "peanut model", because of its geometrical aspect. We numerically solve the diffusion equation in this geometry (see App. B) with a diffusion coefficient of 3 $\mu m^2/s$ [33]. The redistribution of lipids can then be predicted, given only the radius of the vesicles and the contact angle between them. The experimental kinetics of redistribution compare very well with the model kinetics for all vesicles' couples (see Fig. 5) showing that the lipid diffusion is not significantly slowed down during their transfer from one vesicle to the other. This indicates that there must be a sufficient number of bridging structures for the lipids reaching the contact area to rapidly get into a stalk as they diffuse on the interface, and cross it to the other vesicle. A lower bound of the stalks density can be roughly estimated by analogy with the so-called "trap model" [34] which gives the relation between this density

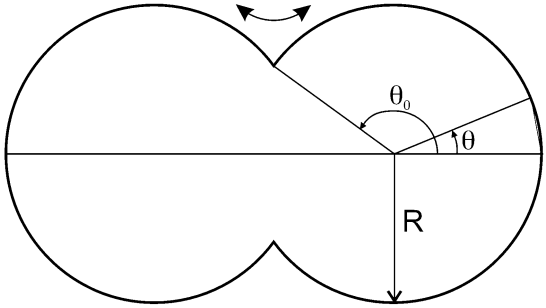

Fig. 4. Schematic drawing of the cross-section of the outer monolayer of a vesicle couple enduring unrestricted hemifusion. This model geometry is used to calculate the kinetics of lipid probe redistribution. At time 0, all lipid probes are located on the left vesicle. The partial derivative diffusion equation is numerically solved in this geometry (see App. B).

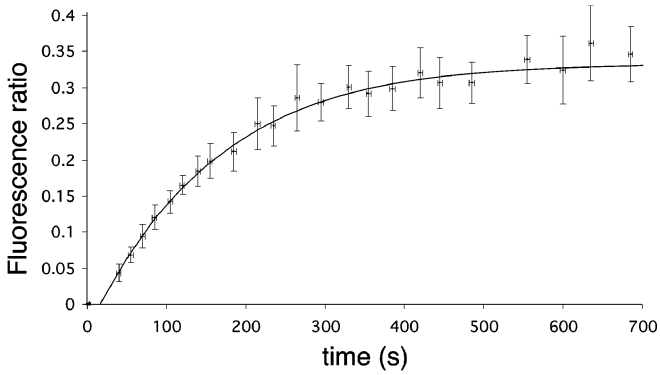

Fig. 5. Typical kinetics of lipid redistribution in a functionalized vesicles' couple. Fluorescence ratios between the two vesicles were measured during lipid redistribution. The curve is derived from the numerical calculation of a model of diffusion on the surface of two truncated spheres, using the dimensions of both vesicles ($R = 14.1$ μm, $\theta_0 = 2.3$ rad). The curve encompasses all experimental points within their error bars. Note that this curve is not a fit but the expected one from the experimentally measured diffusion coefficient D (3 $\mu m^2 s^{-1}$ [33]). Time 0 is defined as the time of the last measure before the start of a detectable fluorescence transfer (start of hemifusion) and the theoretical curve is slightly translated in time (within the 20 seconds for the start of the fluorescence transfer) to match the experimental data.

and the delay in the diffusion caused by the presence of the stalks. As we know this delay is smaller than the experimental error, this model shows that very few stalks per 100 μm^2 would be sufficient to explain the experimental results. This result may seem surprising; however, it has to be remembered that the lipids have a very high diffusion coefficient (3 $\mu m^2 s^{-1}$) meaning that they cover 10 μm^2 in about 3 s. As stalks could be structures with a short lifetime [30], this estimate has to be considered as the minimal amount required at a given time.

Since all proportions of functionalized lipids down to one percent lead to an agreement between the "peanut model" and the experiment, it is likely that the number of stalks present at the interface between two vesicles bearing ten percent of functionalized lipids is larger. Some authors have proposed an alternative to the stalks in which there would be transverse diffusion of lipids where the hydrophobic tails cross the water gap between the membranes to explain lipid exchange [35]. Such a transfer cannot be present in our system as the characteristic time of lipid residence in a bilayer is at least three orders of magnitude greater [10] than what we observed.

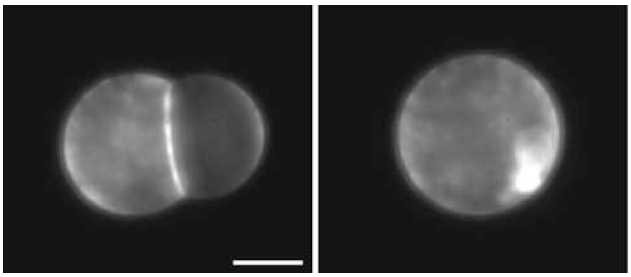

Fig. 6. Fluorescence images of a hemifused doublet enduring full fusion. The two original vesicles (left) and the resultant vesicle (right) are seen by fluorescence microscopy. The internal volume is conserved during the transformation. The total area of the membrane is not conserved; a highly fluorescent region, probably due to an aggregate of supernumerary lipids, can be seen inside the resultant vesicle. The bar is 10 μm.

3.3 Fusion

The collapse of two adhering vesicles in one spherical vesicle (see Fig. 6) is a fusion process. In the fusion events that were observed, fusion frequency did not seem to depend on the functionalized lipid concentration. In all cases, the resulting vesicle was also spherical, indicating that either some outer medium had entered the final vesicle (increase in the total volume) or part of the membrane was not any more present on the spherical surface (decrease of the total area). The contrast between inner and outer medium was still present, showing that no major leakage took place in the process. This is confirmed by direct measurement of the vesicles radii before and after fusion. The volume of the resultant vesicle was always very similar (less than ten percent increase) to the sum of the volume of the two original vesicles. The total area was never conserved during fusion. The excess of membrane is observable inside the resultant vesicle (see Fig. 6). It can be located in invaginations or in lipidic aggregates.

Tension of the vesicle membranes is often claimed to play a role in fusion processes [36]. In our system, the adhesion of the vesicles induces a tension of at least 10^{-5} N/m (this latter corresponds to the tension between two pure DOPC vesicles). To test the role of tension, in several occasions, we induced a tension of about $5 \cdot 10^{-4}$ N/m to both vesicles enduring hemifusion, with suction micropipettes. This did not trigger any fusion, even though it lies within the regime where the membranes are highly stretched [22].

The process of the full fusion of two giant vesicles was an unintuitive result, as conservation of both volumes and

areas would have led to an unstable non-spherical resultant vesicle. Actually, this irreversible process seems to favor volume conservation, characteristic for a fusion without leakage.

4 Conclusion

Transfer micromanipulation offers many improvements from usual experiments. First, it allowed us to study an independent vesicles' couple without any aggregation of supernumerary giant vesicles. We also avoided the aggregation of sub-micronic vesicles (LUV or SUV produced concomitantly with GUV by the electroformation method) which could increase the fluorescence signal on both giant vesicles.

For aqueous content labeling of the vesicles, we grew the GUV in a highly concentrated fluorescent dextran solution. When a vesicle sample was put in the deposit chamber, a high fluorescent background was present, due to the diluted fluorescent dextran solution. Transfer to the observation chamber allowed us to avoid this background, which would have hampered our measurements.

The approach presented here allowed to observe fusion and a fusion intermediate, hemifusion, triggered by the addition of short-range specific forces in a couple of purely lipidic giant vesicles. Even though the fusion events did not occur very often, their frequency is sufficiently high (5%) for this system to be used as a fusion model in aqueous media. This result widens the field of applications of model systems to full fusion studies.

For hemifusion, accordance between the observed and calculated ratios of fluorescence of the two vesicles, after lipid redistribution reached equilibrium, along with the absence of redistribution of an aqueous dye, allowed us to identify this fusion intermediate as hemifusion. The redistribution kinetics of lipid probes (in accordance with our diffusion model) is compatible with a stalk structure of the contact zone, provided there is a sufficient number of stalks. This intermediate is stable over hours in most cases, although destabilization leaded to full fusion in a limited number of experiments. The absence of coupling between the proximal and distal leaflets could be responsible for the scarceness of full fusion events in our system [3,37].

The authors wish to thanks Jean-Philippe Bouchaud for useful discussions about convective effects in diffusion and Eric Brunet for his help in the numerical solving of diffusion equations. J.H. was recipient of a fellowship from the Ministère de l'Education, de la Recherche et de la Technologie.

Appendix A. Theoretical fluorescence ratio for vesicles of different sizes

Let N be the total number of fluorescent labels on the vesicle, A_1 and A_2 the areas of the initially fluorescent and initially non-fluorescent vesicles. In the case of hemifusion, after equilibrium is reached, half of the fluorescent labels are still present in the inner monolayer of the initially fluorescent vesicle, whereas the other half is divided between the outer monolayers of both vesicles. The surface densities of fluorescent probes on the vesicles are therefore proportional to

$$F_1 \propto \frac{1}{2}\frac{N}{A_1} + \frac{1}{2}\frac{N}{(A_1+A_2)}\,,$$
$$F_2 \propto \frac{1}{2}\frac{N}{(A_1+A_2)}\,.$$

Hence the fluorescence ratio between the vesicles is

$$R = \frac{F_2}{F_1} = \frac{A_1}{2A_1+A_2}\,.$$

By measuring the radius of both vesicles, we can therefore predict their theoretical fluorescence ratio, when the vesicles endure hemifusion, and after the complete redistribution of the lipids.

Appendix B. Model for the kinetics of lipid's redistribution

In this model, the outer membrane's lipids freely diffuse on the surface of two truncated spheres picturing the hemifused doublet (see Fig. 6). On each vesicle, the surface density of fluorescent probes $C(\theta,t)$ obeys the spherical diffusion equation:

$$\frac{\partial C}{\partial t} = \frac{D}{R^2}\frac{1}{\sin\theta}\frac{\partial}{\partial\theta}\left(\sin\theta\frac{\partial C}{\partial\theta}\right)\,, \quad 0\leqslant\theta\leqslant\theta_0\,, \qquad \text{(B.1)}$$

where D is the lateral diffusion coefficient for PE probes in DOPC at 20 °C, R the radius of the vesicle and θ_0 the contact angle between the two vesicles. The surface density and the diffusive flux must be continuous at the junction of the two vesicles. The surface density at $t=0$ is equal to the initial concentration C_0 per monolayer on the initially fluorescent vesicle and to zero on the other vesicle.

For vesicles of the same size, the problem is symmetrical with respect to the plane where the vesicles join. As the two diffusion equations are linear, the difference $M(\theta,t)$ between the surface density at two symmetrical points on the sphere obeys the diffusion equation (B.1). The sum of the surface density at these points, which also obeys equation (B.1), is always equal to the initial concentration C_0. Continuity of the surface density at the junction imposes $M(\theta_0,t)$ to be null at all times.

Given the partial differential equation (B.1), the initial and boundary conditions, Mathematica® resolved numerically the function $M(\theta,t)$, for all angles and times.

From $M(\theta,t)$, the ratio of fluorescence between the two vesicles is easily derived:

$$R(\theta,t) = \frac{C_0 - M(\theta,t)}{3\times C_0 + M(\theta,t)}\,.$$

For comparison between the model and the experimental ratios of fluorescence, $R(\theta,t)$ were calculated at θ corresponding to the center of the rectangular selection chosen for quantification (see Sect. 2.4).

The variation along the θ coordinate of fluorescence density at fixed time, although predictable in our model, proved difficult to fit with experiment because of quantification problems.

The necessities of simplification for numerically solving the diffusion model restricted us to the case of vesicles' couple of equal radius.

References

1. T. Weber *et al.*, Cell **92**, 759 (1998).
2. S.M. Small, *The Physical Chemistry of Lipids. From Alkanes to Phospholipids* (Plenum Publishing Corporation, New York, 1986).
3. J.A. McNew *et al.*, J. Cell Biol. **150**, 105 (2000).
4. W. Almers, F.W. Tse, Neuron **4**, 813 (1990).
5. P. Durrer *et al.*, J. Biol. Chem. **271**, 13417 (1996).
6. R. Jahn, T.C. Südhof, Annu. Rev. Biochem. **68**, 863 (1999).
7. L. Yang, H.W. Huang, Science **297**, 1877 (2002).
8. B.R. Lentz, J.K. Lee, Mol. Membr. Biol. **16**, 279 (1999).
9. W. Helfrich, R.-M. Servuss, Nuovo Cimento D **3**, 137 (1984).
10. J. Israelachvili, *Intermolecular and Surface Forces* (Academic Press, San Diego, 1985).
11. L. Lis *et al.*, Biophys. J. **37**, 667 (1982).
12. R.P. Rand, V.A. Parsegian, Biochim. Biophys. Acta **988**, 351 (1989).
13. F. Pincet, L. Lebeau, S. Cribier, Eur. Biophys. J. **30**, 91 (2000).
14. F. Pincet *et al.*, Phys. Rev. Lett. **73**, 2780 (1994).
15. E. Perez *et al.*, Eur. Phys. J. B **6**, 1 (1998).
16. R.L. Ornberg, T.S. Reese, J. Cell Biol. **90**, 40 (1981).
17. M.M. Kozlov, L.V. Chernomordik, Biophys. J. **75**, 1384 (1998).
18. P.I. Kuzmin, J. *et al.*, Proc. Natl. Acad. Sci. USA **98**, 7325 (2001).
19. L. Lebeau *et al.*, Chem. Phys. Lipids **62**, 93 (1992).
20. M.I. Angelova *et al.*, Progr. Colloid Polym. Sci. **89**, 127 (1992).
21. L. Mathivet, S. Cribier, P.F. Devaux, Biophys. J. **70**, 1112 (1996).
22. R. Kwok, E. Evans, Biophys. J. **35**, 637 (1981).
23. M. Arrio-Dupont *et al.*, Biophys. J. **70**, 2327 (1996).
24. E. Evans *et al.*, Science **273**, 933 (1996).
25. T.J. McIntosh, D. Magid, in *Phospholipids Handbook*, edited by G. Cevc (Dekker, New York, 1993).
26. C. Helm, J.N. Israelachvili, P. Mc Guiggan, Biochemistry **31**, 1794 (1992).
27. T. Kuhl *et al.*, Langmuir **12**, 3003 (1996).
28. S.A. Safran, T.L. Kuhl, J.N. Israelachvili, Biophys. J. **81**, 659 (2001).
29. L. Chernomordik *et al.*, Biophys. J. **69**, 922 (1995).
30. D. Siegel, Biophys. J. **65**, 2124 (1993).
31. E. Evans, D. Needham, J. Phys. Chem. **91**, 4219 (1987)
32. R.J. Rubin, Y. Chen, Biophys. J. **58**, 1157 (1990).
33. L.K. Tamm, H.M. McConnell, Biophys. J. **47**, 105 (1985).
34. H.C. Berg, E.M. Purcell, Biophys. J. **20**, 193 (1977).
35. V. Marchi-Artzner *et al.*, J. Phys. Chem. **100**, 13844 (1996).
36. F.S. Cohen *et al.*, J. Cell Biol. **98**, 1054 (1984).
37. G.B. Melikyan, J.M. White, F.S. Cohen, J. Cell Biol. **131**, 679 (1995).

Ultraweak Sugar-Sugar Interactions for Transient Cell Adhesion

Frédéric Pincet,* Tugdual Le Bouar,* Yongmin Zhang,† Jacques Esnault,† Jean-Maurice Mallet,† Eric Perez,* and Pierre Sinaÿ†

*Laboratoire de Physique Statistique de l'Ecole Normale Supérieure, UMR 8550 associée au CNRS et aux Universités Paris 6 et Paris 7, and †Département de Chimie de l'Ecole Normale Supérieure, UMR 8642, 75231 Paris cedex 05, France

ABSTRACT Carbohydrate-carbohydrate interactions are rarely considered in biologically relevant situations such as cell recognition and adhesion. One Ca^{2+}-mediated homotypic interaction between two Lewis^x determinants (Le^x) has been proposed to drive cell adhesion in murine embryogenesis. Here, we confirm the existence of this specific interaction by reporting the first direct quantitative measurements in an environment akin to that provided by membranes. The adhesion between giant vesicles functionalized with Le^x was obtained by micropipette aspiration and contact angle measurements. This interaction is below the thermal energy, and cell-cell adhesion will require a large number of molecules, as illustrated by the Le^x concentration peak observed at the cell membranes during the *morula* stage of the embryo. This adhesion is ultralow and therefore difficult to measure. Such small interactions explain why the concept of specific interactions between carbohydrates is often neglected.

INTRODUCTION

Molecular features governing the selectivity in cell-cell recognition and adhesion are key elements to understanding morphogenesis and organogenesis. All living organisms are characterized by the presence of glycoproteins and glycosphingolipids on the cytoplasmic membrane. Carbohydrate chains, as exposed structures at the cell surface, should play a key role in early events of cell-cell recognition. Indeed, they have firmly been recognized as interaction sites in cell adhesion processes such as leukocyte recruitment or host-pathogen interaction. Such events are commonly attributed to lectin or lectin-like proteins and the corresponding specific carbohydrate ligands. It has been suggested that specific carbohydrate-carbohydrate interactions may also play this important role (Hakomori, 1991). Several direct measurements of adhesion between surfaces decorated with glycolipids have been reported in the past (Marra, 1985, 1988; Evans, 1987; Rand and Parsegian, 1989; Luckham et al., 1993; Yu et al., 1998; Ricoul et al., 1998). These strong adhesions, obtained through various techniques (surface force apparatus, osmotic stress method, and vesicle micropipette aspiration), were due to van der Waals or other nonspecific forces. However, some carbohydrate-carbohydrate interactions found in biological processes have been proposed to be specific (Hakomori, 1991; Sharon and Lis, 1993; Bovin, 1996). One of them, the Lewis^x determinant (Le^x), has been identified as presumably playing a biological role by means of intermembrane interactions. According to a current hypothesis, it has a calcium-mediated specific interaction with itself.

Le^x has been shown to be involved in murine and human embryogenesis. This carbohydrate is present on the cell membrane in the polar headgroup of glycolipids. It is not expressed at the cell surface until the eight-cell stage, shows maximal expression at the *morula* stage of mouse embryogenesis, and declines after compaction (Solter and Knowles, 1998; Fenderson et al., 1986). This compaction stage could be inhibited either by anti-Le^x antibodies or Le^x itself, or by inactivating the calcium with EDTA. As Le^x is not charged, the role of the calcium is not electrostatic in nature. These results (Eggens et al., 1989; Kojima et al., 1994) led the authors to propose a calcium mediated Le^x-Le^x-specific homotypic interaction as a basis of cell adhesion in preimplantation embryos, and in various tumor cells. Other observations also strongly suggest that Le^x-Le^x interactions exist in the presence of Ca^{2+} (Boubelik et al., 1998; Siuzdak et al., 1993; Henry et al., 1999; Geyer et al., 2000).

Here we report the first direct quantitative measurements of this putative interaction in a physicochemically well defined system and in conditions similar to the natural environment of the glycolipid, i.e., lipid bilayers. This was done through the adhesion between two giant vesicles functionalized with synthetic glycolipids. Sufficient to promote cell-cell adhesion, this ultraweak interaction explains why this concept is often underestimated.

EXPERIMENTAL SECTION

We have measured directly the adhesion between electrically neutral giant vesicles that included synthetic lipids bearing Le^x groups at the vesicle surface. These vesicles were made of stearoyl-oleoylphosphatidylcholine (SOPC; purchased from Avanti Polar Lipids, Alabaster, AL) as the main component.

Received for publication 12 May 2000 and in final form 15 December 2000.

Address reprint requests to Eric Perez, Laboratoire de Physique Statistique de l'Ecole Normale Supérieure, UMR 8550 associée au CNRS et aux Universités Paris 6 et Paris 7, 24 rue Lhomond, 75231 Paris Cedex 05, France. E-mail: perez@physique.ens.fr or to Pierre Sinaÿ, Département de Chimie de l'Ecole Normale Supérieure, UMR 8642, 24 rue Lhomond, 75231 Paris Cedex 05, France. E-mail: pierre.sinay@ens.fr.

0006-3495/01/03/1354/05 $2.00

Measurements of vesicle adhesion

To measure their adhesion, two vesicles of cellular dimensions (10–50 μm) were aspirated in micropipettes and micromanipulated into contact. The (negative) pressure, ΔP, in each pipette controlled the (positive) hydrostatic pressure in the vesicle and thus the mechanical tension, τ_m, in its membrane:

$$\tau_m = \frac{\Delta P}{2\left(\frac{1}{r_p} - \frac{1}{r_v}\right)} \quad (1)$$

where r_p and r_v are, respectively, the radius of the micropipette and that of the vesicle. The two osmotically controlled vesicles are observed in interference contrast microscopy. One of them is pressurized into a tight, rigid sphere with large bilayer tension, whereas the adherent vesicle is held with low pressure and remains deformable. The adhesion energy W_{adh} is obtained by determining the contact angle θ_c of the two vesicles (cf. Fig. 1) and the tension τ_m of the flaccid vesicle membrane (Evans, 1990):

$$W_{adh} = \tau_m(1 - \cos\,\theta_c) \quad (2)$$

By combining Eqs. 1 and 2, it is easy to relate ΔP to W_{adh}:

$$\Delta P = C \cdot W_{adh} \quad (3)$$

where C depends only on the geometry of the system:

$$C = \frac{2\left(\frac{1}{r_p} - \frac{1}{r_v}\right)}{1 - \cos\,\theta_c} \quad (4)$$

The measurement of θ_c was deduced numerically from geometrical parameters as indicated in Evans (1990).

Glycolipids

The Le^x determinant is a trisaccharide (Galβ1 $\rightarrow$ 4 [Fucα 1 $\rightarrow$ 3] GlcNAc). It is neutral in physiological conditions. In classical natural sphingolipids, the Le^x trisaccharide is attached to the ceramide through a lactose group. Although they are available in large quantities by chemical synthesis, they have not been used in this study. With their large hydrophilic pentasaccharide headgroups and their relatively small hydrophobic chains, they are rather soluble in water and their distribution in vesicles cannot be controlled. We therefore synthesized a less water-soluble lipid (Esnault et al, 2001) with a Le^x headgroup attached via a so-called spacer group to ensure its mobility (Fig. 2 *a*) that we will refer to as Le^x lipid.

In this synthetic glycolipid, a rather low solubility in water combined with a good bilayer cohesion were obtained by using three hydrophobic chains, instead of two as in ceramide. To ensure good accessibility of the Le^x groups for interaction, they were provided with translational mobility by branching the chains. This hinders the bidimensional crystallization of the chains and keeps the layers in a fluid state. An orientational mobility was provided by means of a flexible spacer between the chains and the Le^x. This allowed the Le^x groups to take the exact orientation and position for which the specific interaction can occur.

For the controls, a glycolipid with the same features but without Le^x was synthesized (Fig. 2 *b*); we will refer to it as Lac lipid.

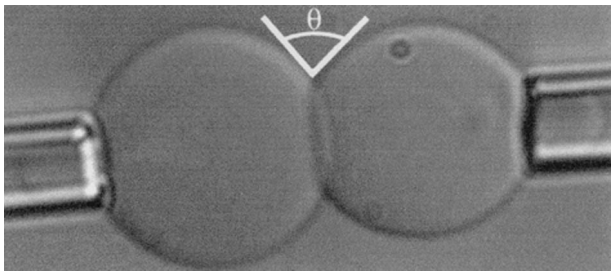

FIGURE 1 The two osmotically controlled vesicles held in micropipettes by aspiration are observed in interference contrast microscopy. The suction pressure applied to the micropipettes allows control of the tension of the vesicle bilayers. One of them (*left*) is pressurized into a tight-rigid sphere with large bilayer tension, whereas the adherent vesicle (*right*) is held with low pressure and remains deformable. The adhesion energy W_{adh} is obtained by determining the contact angle θ_c of the two vesicles and the tension τ_m of their membrane (θ): $W_{adh} = \tau_m(1 - \cos\theta_c)$.

Experimental procedure

Giant vesicles were formed by lipid hydration after evaporation from chloroform solution in 320 mOsm sucrose solution (Needham, 1993; Needham and Evans, 1988). The Le^x-functionalized vesicles, hereinafter referred to as Le^x vesicles, were made from a mixture of SOPC and the synthetic Le^x lipid (90:10 by mol). Two types of control vesicles were prepared: one made of pure SOPC and the other made of SOPC and Lac lipid (90:10 by mol) that we call Lac vesicles.

The vesicle suspension was added to an aqueous glucose solution chamber of a slightly higher osmolarity (360 mOsm) than that of the vesicles, in order to deflate them and make them micromanipulable. Two vesicles were then transferred into another chamber filled with salt solution, either NaCl or $CaCl_2$, at 360mOsm. Both vesicles were micromanipulated into tangential contact. The contact angle was measured for several tension values of the flaccid vesicle membrane by decreasing the aspiration and then increasing it in order to check the reversibility of the adhesion (Evans, 1990).

The experiments consisted of comparing the adhesion of two Le^x vesicles in NaCl and in $CaCl_2$ (Le^x/Le^x experiments). As calcium is known to produce sometimes peculiar effects on bilayer interactions (Marcelja, 1992), many controls were required. First, it was necessary to compare Le^x/Le^x experiments with experiments in which the Le^x groups from one of the vesicles were absent (Le^x/Lac experiments). Second, it was useful to replace the Le^x groups with another sugar in both vesicles (Lac/Lac

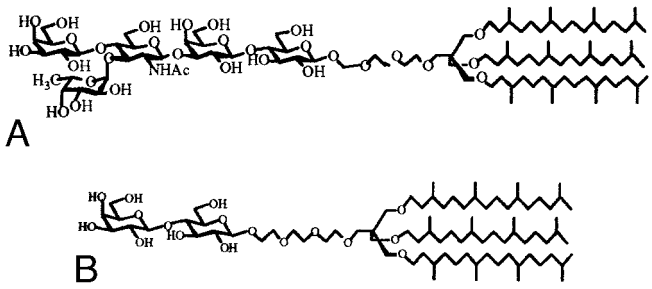

FIGURE 2 (*a*) The Le^x determinant is a trisaccharide (Galβ1 $\rightarrow$ 4 [Fucα 1 $\rightarrow$ 3] GlcNAc). It is neutral in physiological conditions. In a classical natural sphingolipid, the Le^x trisaccharide is attached to the ceramide through a lactose group. In the synthetic glycolipid, a rather low solubility in water together with a good bilayer cohesion were obtained by using three hydrophobic chains instead of two, as in ceramide. To ensure good accessibility of the Le^x groups for interaction, they were provided with translational and orientational mobilities by branching the chains, thus keeping the layers in a fluid state by hindering their crystallization, and by means of a flexible spacer between the chains and the Le^x. (*b*) The same lipid without the Le^x group.

experiments). Third, as SOPC was the main component of our vesicles, it was interesting to compare the adhesions obtained with that of pure SOPC vesicles.

RESULTS AND DISCUSSION

Fig. 3 shows the aspiration pressure as a function of C (cf. Eq. 4) for the controls and Le^x/Le^x experiments. The slopes are equal to the vesicles' adhesion free energies. These slopes are independent of the vesicle size. Adhesion energy values for the controls and for the Le^x/Le^x experiments are given in the table. The effect of adding calcium on the Le^x vesicles is clearly seen in Table 1 and Fig. 3. The adhesion energy in $CaCl_2$ is 2.5 times higher than in NaCl, whereas the Le^x/Lac and Lac/Lac experiments showed a small decrease of the adhesion energy in calcium (3.10^{-6} J/m^{-2}). For comparison, calcium has no influence on the adhesion of pure SOPC vesicles. These results show unambiguously that Le^x groups are necessary on both vesicles for the calcium-induced adhesion enhancement to occur. This is in agreement with the specific interaction scheme advocated by Hakomori (1991).

Because a fraction of the vesicles produced in this way are multilamellar (about 40%; Kwok and Evans, 1981), it is necessary to check that what was seen was really adhesion and not fusion, which would look the same under a microscope. Adhesion experiments were performed in which one of the adhering Le^x vesicles contained fluorescent phospholipids added to its membrane, while the other did not. The vesicles were left in contact 30 min and then observed. It was checked that the fluorescence of the first vesicle did not diffuse into the membrane of the second vesicle.

TABLE 1 Adhesion energy of vesicles in aqueous media

	Adhesion energy (10^{-6} J/m^2)	
Left vesicle/right vesicle	in NaCl 0.2 M	in $CaCl_2$ 0.11 M
Le^x/Le^x	4.5 ± 2	11 ± 2
Le^x/Lac	5.4 ± 1	2.5 ± 2
Lac/Lac	9.5 ± 0.5	6 ± 1
pure SOPC vesicles	14 ± 2	15 ± 4

Adhesion energy of vesicles (10^{-6} J/m^2) in aqueous media between Le^x- or Lac-functionalized vesicles (Le^x means that the vesicle composition is SOPC:Le^x 90:10; same for Lac), and between pure SOPC vesicles, in NaCl and in $CaCl_2$.

The adhesion, in the case of NaCl and for all types of vesicles, is the result of a balance between van der Waals attractions and short-range repulsions that include entropic and structural contributions (Rand and Parsegian, 1989; Israelachvili and Wennerström, 1990). Because 90 percent of the surface of the Le^x and Lac vesicles is made of SOPC, van der Waals forces may be expected to be the same for all

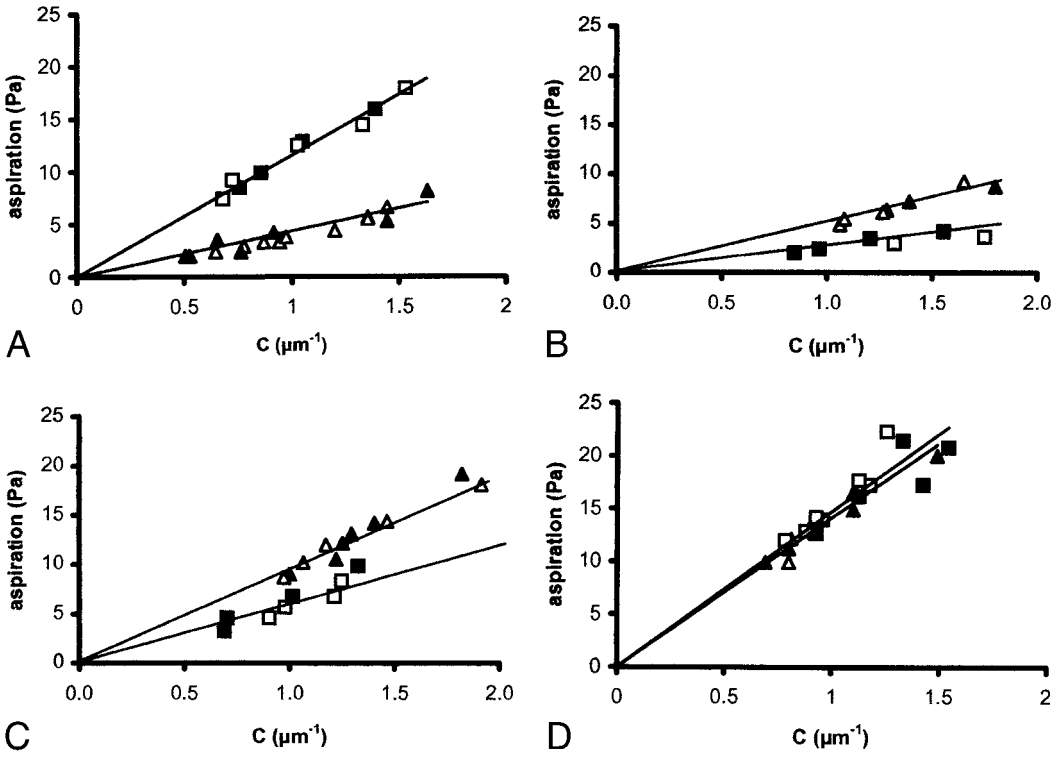

FIGURE 3 Aspiration pressure as a function of parameter C given in Eqs. 3 and 4. (*a*) Le^x/Le^x experiment (two vesicles with SOPC:Le^x of 90:10); (*b*) Lex/Lac experiment (one vesicle is SOPC:Le^x 90:10; the other is SOPC:Lac 90:10); (*c*) Lac/Lac experiment (two vesicles with SOPC:Lac 90:10); (*d*) pure SOPC vesicles. The closed symbols represent decreasing aspiration, and open ones represent increasing aspiration. *Triangles* are for NaCl solution and *squares* for $CaCl_2$. The *straight lines* are least-squares fits.

types of vesicles. Therefore, the higher adhesion in NaCl with pure SOPC, as compared to SOPC/Le^x, may seem surprising. However, one may note that the sugar groups are bound to the lipid chains by a flexible spacer (Fig. 2). The thermal fluctuations of this spacer can give rise to steric repulsions, as polymer brushes do (Taunton et al., 1990). We have performed measurements that show that our Le^x lipid spacers fluctuate like an ideal polymer chain, generating steric repulsions (in preparation). This explains why the adhesion of SOPC vesicles is reduced by the presence of sugars. In agreement with these considerations, Table 1 shows that the adhesion energies vary according to the size of the sugar headgroup present on the vesicle: the larger the headgroup (Le^x), the larger the steric repulsion, and therefore the smaller the adhesion energy ($Le^x/Le^x < Le^x/Lac <$ Lac/Lac $<$ SOPC/SOPC). This difference between Le^x and control vesicles is not relevant for our purpose, since van der Waals forces do not play much role in cell membrane interactions. Usually the adhesions are governed by cell adhesion molecules such as proteins or lipids, given that there are many steric repulsions produced by the glycocalix. For this reason, two biomembranes will not adhere in the absence of specific adhesion sites.

The specific contribution W_{spe} of the Le^x groups to the adhesion energy of our vesicles is equal to the difference between the effects of calcium on adhesion energy in the Le^x/Le^x and in the Le^x/Lac experiments (i.e., the control that is the most similar to the experiment). The table shows that $W_{spe} = 10 \pm 5\ \mu J/m^{-2}$. Even though it is usually delicate to deduce molecular information about a single bond from global adhesion energy measurements (Evans, 1985a,b), the case of Le^x is favorable because of the weakness of the interactions. A single slope for the contact formation and separation of the vesicles features a continuous and reversible adhesion. This implies that the lifetime of the involved bonds is so short that the association/dissociation process can be considered instantaneous compared to the time scale of the distribution of the lipids in the vesicle membrane. The Le^x vesicles thus constitute a highly dynamic system, in contrast to vesicles that bear much stronger binding sites (Noppl-Simson and Needham, 1996). The adhesion molecules are expected to diffuse toward the contact zone, which therefore should contain a higher density of them, leaving the non-contacting part of the vesicle depleted, especially for large contact areas. According to the theoretical approaches proposed in the mid-eighties (Bell et al., 1984; Evans, 1985b), it is possible to deduce directly this enrichment $\Delta\rho$ of the contact zone from W_{spe}:

$$\Delta\rho = W_{spe}/k_BT$$

which gives, in our case, an enrichment $<2\%$. Therefore, the density can be considered constant. This has the consequence that the bonds between the vesicles come from Le^x groups that randomly face each other. The density of such sites is equal to p^2/A, where A is the average area per lipid (here 0.7 nm^2, obtained from Rand and Parsegian (1989) and from monolayer compression isotherms; strictly speaking, A is the area over which the field of attraction of one site is felt by a site on the other vesicle) and p the proportion of Le^x lipids in the vesicle (here 0.1). W_{spe} is equal to the actual number of bonds per unit area in the contact zone times the bond energy e. The weakness of $\Delta\rho$ indicates that e is small. Assuming that it is smaller than k_BT, only half of the facing sites are actually bound. This leads to

$$W_{spe} = (p^2/2A)e \quad (5)$$

This gives an upper estimate of e (because this would underestimate the real number of bonds).

In Eq. 6, assumption is made that the glycolipids are not clusterized in the vesicle membrane. From this equation, e ranges between 0.17 and 0.5 k_BT (i.e., 0.1 and 0.3 kcal/mol). Previous glycolipid studies showed strong van der Waals interactions (Rand and Parsegian, 1989; Yu et al., 1998; Evans, 1987; Marra, 1985, 1988; Ricoul et al., 1998; Luckham et al., 1993). In the present work, the calcium-induced interaction is specific and comes in addition to van der Waals forces. It is worthwhile to note that these molecules are neutral and, therefore, this interaction is not intrinsically electrostatic.

This ultraweak interaction energy validates the assumption that the e is substantially below k_BT. A rough estimate of the bond lifetime can be obtained by comparison with the streptavidin/biotin system (30 k_BT bond energy and lifetime of several days) and assuming an Arrhenius law. It is well below 1 μs. It is most unusual to measure molecular interaction energies well below the thermal energy. This only shows that cell-cell adhesion will require a large number of these molecules, as is, indeed, observed during the *morula* stage of mouse embryogenesis. The molecular mechanism of the Le^x interaction remains mysterious. The mediation by Ca^{2+} could result from the setting up of an appropriate coordination shell around the cation (Bugg, 1973).

These measurements with synthetically tailored Le^x containing neoglycolipids directly confirm the involvement of neutral cell surface oligosaccharides in cell-cell adhesion and illustrate why, when the Le^x sites are blocked, the compaction stage of the embryo does not occur (Eggens et al., 1989). Le^x can, in the presence of Ca^{2+}, substantially enhance the deformation and adhesion of lipid vesicles, i.e., objects with mechanical features akin to those of the cell membranes. The interaction scaled down to one molecule is well below thermal energy. It produces transient and dynamic adhesion that is indeed what cell differentiation requires.

In contrast to these neoglycolipids, the natural glycolipids bearing Le^x are generally glycosphingolipids based on ceramide. This may noticeably influence the adhesion energy, either because of their arrangements in the membrane or

because of their functionalities. For example, in our case, a bidimensional clustering of Le^x lipids in the vesicles' contact region would generate a higher adhesion energy, because a higher number of sites would be involved in the adhesion. It is likely, therefore, that in their biological environment, the Le^x groups would be distributed unevenly in the membranes and generate a higher adhesion than the one measured here on our model vesicles. Here, we have quantified the Le^x-Le^x interaction regardless of the rest of the lipid, which may modulate the resulting adhesion.

This first direct measurement of biologically relevant ultraweak carbohydrate-carbohydrate interaction shows that it is now possible to quantify them even if they are smaller than the thermal energy and opens up a new, promising field of inquiry in biology.

F. P. and E. P. thank E. Evans and J. Wolfe for helpful discussions

REFERENCES

Bell, G. I., M. Dembo, and P. Bongrand. 1984. Cell adhesion: competition between non-specific repulsion and specific binding. *Biophys. J.* 45: 1051–1064.

Boubelik, M., D. Floryk, J. Bohata, L. Draberova, J. Macak, F. Smid, and P. Draber. 1998. Le^x glycosphingolipids-mediated cell aggregation. *Glycobiology.* 8:139–146.

Bovin, N. V. 1996. Carbohydrate-carbohydrate interactions: a review. *Biochemistry (Moscow).* 61:694–704.

Bugg, C. E. 1973. Calcium binding to carbohydrates: crystal structure of a hydrated calcium bromide complex of lactose. *J. Am. Chem. Soc.* 95: 908–913.

Eggens, I., B. Fenderson, T. Toyokuni, B. Dean, M. Stroud, and S. Hakomori. 1989. Specific interaction between Le^x and Le^x determinants, a possible basis for cell recognition in preimplantation embryos and in embryonal carcinoma cells. *J. Biol. Chem.* 264:9476–9484.

Esnault, J., J.-M. Mallet, Y. Zhang, P. Sinaÿ, T. Le Bouar, F. Pincet, and E. Pérez. 2001. New highly hydrophobic Lewis X glycolipids: synthesis and monolayer behavior. *Eur. J. Org. Chem.* 2001:253–260.

Evans, E. 1985a. Detailed mechanics of membrane-membrane adhesion and separation, II. Continuum of molecular cross-bridges. *Biophys. J.* 48:175–183.

Evans, E. 1985b. Detailed mechanics of membrane-membrane adhesion and separation, I. Discrete kinetically trapped molecular bridges. *Biophys. J.* 48:185–192.

Evans, E. 1987. Physical properties of surfactant bilayer membranes: thermal transitions, elasticity, rigidity, cohesion and colloidal interactions. *J. Phys. Chem.* 91:4219–4228.

Evans, E. 1990. Adhesion of surfactant-membrane covered droplets: special features and curvature elasticity effects. *Colloids Surfaces.* 43: 327–347.

Fenderson, B. A., E. H. Holmes, Y. Fukushi, and S. Hakomori. 1986. Coordinate expression of X and Y haptens during murine embryogenesis. *Dev. Biol.* 114:12–21.

Geyer, A., C. Gege, and R. R. Schmidt. 2000. Calcium dependent carbohydrate-carbohydrate recognition between $Lewis^x$ blood group antigens. *Angew. Chem. Int. Ed.* 39:3246–3249.

Hakomori, S. 1991. Carbohydrate-carbohydrate interaction as an initial step in cell recognition. *Pure Appl .Chem.* 63:473–482.

Henry, B., H. Desvaux, M. Pristchepa, P. Berthault, Y. Zhang, J-M. Mallet, J. Esnault, and P. Sinaÿ. 1999. NMR study of a $Lewis^x$ pentasaccharide derivative: solution structure and interaction with cations. *Carbohydr. Res.* 315:48–62.

Israelachvili, J. N., and H. Wennerström. 1990. Hydration or steric forces between amphiphilic surfaces. *Langmuir.* 6:873–876.

Kojima, N., B. A. Fenderson, M. R. Stroud, R. I. Goldberg, R. Habermann, T. Toyokuni, and S. Hakomori. 1994. Further studies on cell adhesion based on Le^x-Le^x interaction, with new approaches: embryoglycan aggregation of F9 teratocarcinoma cells, and adhesion of various tumour cells based on Le^x expression. *Glycoconjugate J.* 11:238–248.

Kwok, R., and E. Evans. 1981. Thermoelasticity of large lecithin bilayer vesicles. *Biophys. J.* 35:637–652.

Luckham, P., J. Wood, and R. Swart. 1993. The surface properties of gangliosides. *J. Colloid Interface Sci.* 156:173–183.

Marcelja, S. 1992. Electrostatics of membrane adhesion. *Biophys. J.* 61: 1117–1121.

Marra, J. 1985. Controlled deposition of lipid monolayers onto mica and direct force measurements between galactolipid bilayers in aqueous electrolyte solutions. *J. Colloid Interface Sci.* 107:446–455.

Marra, J. 1988. Direct measurements of attractive van der Waals and adhesion forces between uncharged lipid bilayers in aqueous solutions. *J. Colloid Interface Sci.* 109:11–20.

Needham, D., and E. Evans. 1988. Structure and mechanical properties of giant lipid (DPMC) vesicle bilayers from 20°C below to 10°C above the liquid cristal-cristalline phase transition at 24°C. *Biochemistry.* 27: 8261–8269.

Needham, D. 1993. Measurement of interbilayer adhesion energies. *Methods Enzymol.* 220:111–129.

Noppl-Simson, D. A., and D. Needham. 1996. Avidin-biotin interactions at vesicle surfaces: adsorption and binding, cross-bridge formation, and lateral interactions. *Biophys. J.* 70:1391–1401.

Rand, R. P., and V. A. Parsegian. 1989. Hydration forces between phospholipid saccharide bilayers *BBA.* 988:351–376.

Ricoul, F., M. Dubois, L. Belloni, T. Zemb, C. André-Barrès, and I. Rico-Lattes. 1998. Phase equilibria and equation state of a mixed cationic surfactant-glycolipid lamellar system. *Langmuir.* 14:2645–2655.

Sharon, N., and H. Lis. 1993. Carbohydrates in cell recognition. *Scientific Am.* 74–81.

Siuzdak, G., Y. Ichikawa, T. J. Caulfield, B. Munoz, C.-H. Wong, and K. C. Nicolaou. 1993. Evidence of Ca^{2+}-dependent carbohydrate association through ion spray mass spectrometry. *J. Am. Chem. Soc.* 115: 2877–2881.

Solter, D., and B. B. Knowles. 1978. Monoclonal antibody defining a stage-specific mouse embryonic antigen (SSEA-1). *Proc. Natl. Acad. Sci. USA.* 75:5565–5569.

Taunton, H. J., C. Toprakciaglu, L. J. Fetters, and J. Klein. 1990. Interaction between surfaces bearing end-adsorbed chains in a good solvant. *Macromolecules.* 23:571–580.

Yu, Z. W., T. L. Calvert, and D. Leckband. 1998. Molecular forces between membranes displaying neutral glycosphingolipids: evidence for carbohydrate attraction. *Biochemistry.* 37:1540–1550.

From Macroscopic Adhesion Energy to Molecular Bonds: A Test of the Theory

Frédéric Pincet,[1,*] Eric Perez,[1] Jean-Christophe Loudet,[1] and Luc Lebeau[2]

[1]*Laboratoire de Physique Statistique de l'Ecole Normale Supérieure, associé au CNRS et aux universités Paris VI et Paris VII, 24, rue Lhomond, 75231 Paris Cedex 05, France*

[2]*Laboratoire de Synthèse Bio-organique, CNRS, Unité de Recherche Associée 1386, Faculté de Pharmacie, 74 Route du Rhin, 67401 Illkirch, France*

(Received 5 July 2000; published 9 October 2001)

We present a statistical mechanical treatment relating the macroscopic adhesion energy of two surfaces, which can be obtained by micropipette aspiration studies, to the microscopic adhesion energy between individual bonds. The treatment deals with the case of weak reversible bonds, so that the equilibrium partition function has significance. This description is coherent with previous theories. Experiment and theory are compared to probe the nature of weak bonds in membranes, where local equilibria can be obtained. The case of a bead and a vesicle decorated by nucleosides was considered.

DOI: 10.1103/PhysRevLett.87.178101 PACS numbers: 87.15.Kg, 68.35.Md, 87.15.By

Biological media provide a great variety of physicochemical phenomena through molecular recognition. Everything biological is accomplished with weak interactions and bonds. Strong interactions would stop the dynamical processes which are indispensable to life. The adhesion of surfaces exhibiting binding sites has been widely investigated theoretically [1–4]. Because of the diffusion process, the adhesion sites are attracted to the contact zone. A previous pioneering work [5] has indeed analyzed and confirmed the kinetics of the enrichment in the contact zone of two vesicles. In contrast, the experimental test of the theory was hindered by the lack of available weak binding sites with reversible adhesion. Recently designed lipid molecules and end-functionalized polymers now allow such experiments. The aim of this paper is to extend the equilibrium models and test them with these new molecular tools: the static adhesion energy was measured between a lipid vesicle and a polymer bead both functionalized with nucleosides that provide weak binding sites. The lipid vesicle can act as a reservoir of adhesion molecules which equilibrate with the contact zone while the adhesion groups on the bead are relatively immobile. Experiment and theory are compared to probe the nature of weak bonds in membranes, where local equilibria can be obtained. These are limiting physical behaviors, of general interest in biological and nonbiological applications.

The adhesion measurements are carried out by the micropipette aspiration technique developed by Evans [6]. Observations are made by differential interferometric contrast microscopy in order to see the vesicle (Fig. 1). To measure their adhesion, the osmotically controlled vesicle and the bead are aspirated in micropipettes and micromanipulated into contact. The (negative) pressure ΔP in the pipette controls the (positive) hydrostatic pressure in the vesicle and thus the mechanical tension τ_m in its membrane [5],

$$\tau_m = \frac{\Delta P}{2(\frac{1}{r_p} - \frac{1}{r_v})}, \tag{1}$$

where r_p and r_v are, respectively, the radius of the micropipette and of the vesicle. The adherent vesicle is held with low pressure and remains deformable. The adhesion free energy W_{adh} is obtained by determining the contact angle θ_c (Fig. 1) and the tension τ_m of the flaccid vesicle membrane,

$$W_{\mathrm{adh}} = \tau_m(1 - \cos\theta_c). \tag{2}$$

By combining (1) and (2), it is easy to relate ΔP to W_{adh},

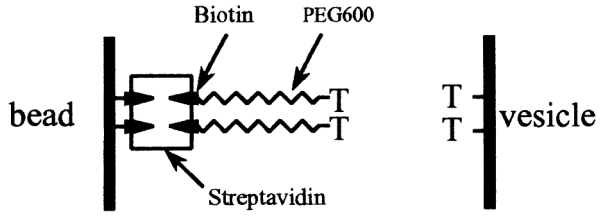

(a)

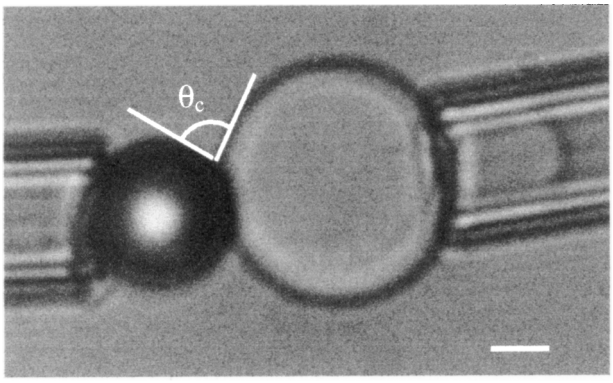

(b)

FIG. 1. (a) Functionalized bead with an end-grafted polyethylene glycol (PEG) bearing biotin at one end and one nucleoside at the other. (b) Micromanipulated vesicle in contact with a bead held by a micropipette. The bar represents 5 μm.

$$\Delta P = C \cdot W_{\mathrm{adh}}\,, \tag{3}$$

where C depends only on the geometry of the system,

$$C = \frac{2(\frac{1}{r_p} - \frac{1}{r_v})}{1 - \cos\theta_c}\,. \tag{4}$$

The measurement of θ_c was numerically deduced from geometrical parameters as indicated by Evans [7]. Following Eq. (3), the slope of ΔP as a function of C is W_{adh}.

Lipids carrying one nucleoside (adenosine, A, or thymidine, T) as a polar headgroup were synthesized [8]. Giant vesicles were formed by hydrating a lipid mixture stearoyl-oleoyl phosphocholine (SOPC)/nucleoside lipid (9/1) in 320 mOsm sucrose solution [9,10]. The vesicle suspension was added to an aqueous glucose solution chamber of a slightly higher osmolarity (360 mOsm) than that of the vesicle in order to deflate it and make it micromanipulable.

Superavidin coated polystyrene beads were purchased from Bangs Labs. The average area per attachment site for biotin was between 50 and 180 nm^2 [11]. In order to coat them with nucleosides, a polyethyleneglycol (PEG) spacer arm (containing 14 ethyleneoxide units) was dissymmetrically functionalized at one end with biotin, and at the other end with A or T (Fig. 1) [8]. The beads were incubated in water (50 μg/ml) with one of these heterobifunctionalized PEG arms (1 mg/ml) for one day. The contact angle was measured for several tension values of the flaccid vesicle membrane by decreasing the aspiration and then increasing it in order to check for the reversibility of the adhesion. This decreasing/increasing aspiration process was repeated several times on the same vesicle/bead couple, and it was indeed observed that this adhesion was reversible within the experimental error [12].

Four adhesion situations were investigated: bead A–vesicle A, bead T–vesicle T, bead T–vesicle A, and bead A–vesicle T. A control experiment was performed in which the vesicle was made of only SOPC and adhered to a T-coated bead. It gives the nonspecific contribution W_{nspe} to the adhesion.

Figure 2 shows the aspiration pressure as a function of C [cf. Eq. (4)] for these cases. According to Eq. (3), the slopes in Fig. 2 are equal to W_{adh}. The values of W_{adh} are independent of the vesicle size. The specific adhesion energies W_{spe} are given by $W_{\mathrm{spe}} = W_{\mathrm{adh}} - W_{\mathrm{nspe}}$ (cf. Table I).

Given the experimental error, the bead A-vesicle T and bead T-vesicle A systems have the same adhesion energy as expected. The specific adhesion energies follow the increasing order: $W_{\mathrm{spe}}(T/T) < W_{\mathrm{spe}}(A/A) < W_{\mathrm{spe}}(A/T)$. This is consistent with the data reported in the literature [13,14]. The short lifetime of the bonds is illustrated by the small fraction of occupied bead sites (5%) that can be estimated from the specific adhesion energy, the known bond energy, and the bead site density.

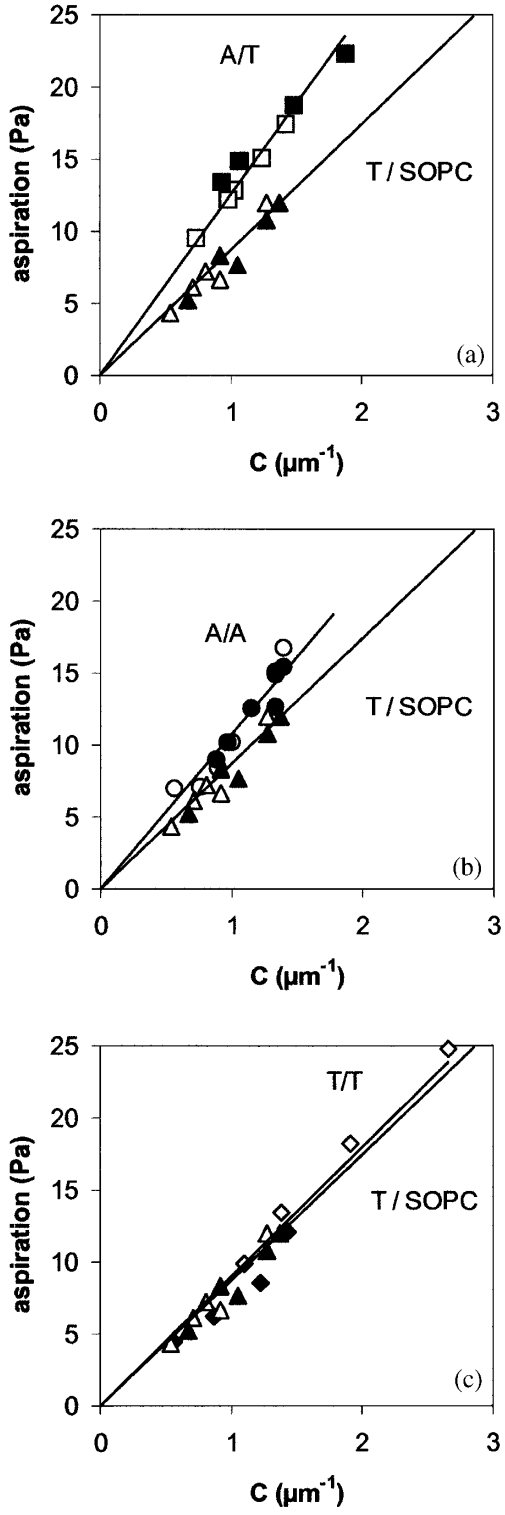

FIG. 2. Aspiration pressure as a function of C [cf. Eq. (4)] for a specific interaction and comparison with the nonspecific case T/SOPC (control). According to Eq. (3), the slopes are equal to W_{adh}. The solid lines are fits forced through zero and they roughly represent the adhesion energy. However, the values reported in Table I are averages from fits not forced through zero and in which the increasing pressure is treated separately from the decreasing one. Closed (open) symbols correspond to the increase (decrease) of the aspiration pressure. (a) bead A/vesicle T, (b) bead A/vesicle A, (c) bead T/vesicle T.

TABLE I. Adhesion energy values (W_{adh}) averaged as indicated in Fig. 2, from at least two separate experiments and six cycles. The error is $\pm 1 \times 10^{-6}$ J · m^{-2}. W_{spe} is equal to $W_{adh} - W_{nspe}$ where W_{nspe} is the T/PC adhesion energy.

	A/T	T/A	A/A	T/T	T/PC
W_{adh} (10^{-6} J/m^2)	12.0	12.9	9.9	9.3	8.6
W_{spe} (10^{-6} J/m^2)	3.4	4.3	1.3	0.7	

The expression of W_{spe} for stronger bonds has already been derived in the mid 1980s [1,2] but was never experimentally checked. It relates W_{spe} to the enrichment of the contact zone in adhesion sites,

$$W_{spe} = (\rho_c - \rho_{nc}) k_B T , \quad (5)$$

where ρ is the surface density of sites at the vesicle surface; c refers to the contact zone and nc to the rest of the vesicle.

Here we extend this approach through a microcanonical description that allows one to directly relate W_{spe} to the bond energy. We consider a bead with immobile adhesion sites with a density $1/A_0$. This bead interacts with a vesicle of area A_V displaying N mobile sites. We assume that each adhesion site has a field of attraction with an area α. A vesicle site can be bound to a given bead site if it is located within an area α around the bead site. Such a vesicle site can have two states, bound or unbound. α is assumed to be the same for thymidine and adenosine. Finally, we call A_f the part of the bead surface located in the contact zone A_c in which a site of the vesicle can be bound: $A_f = A_c \alpha / A_0$. In our case, A_f is very small as compared to A_V. In this system, the partition function Z is obtained by summing over all the configurations in which n sites are in A_f, and among them, m are bound [15],

$$Z = K \sum_{n=0}^{N} \sum_{m=0}^{n} \frac{N!}{n!\,(N-n)!} \frac{n!}{m!\,(n-m)!} \times (A_v - A_f)^{N-n} \left(\frac{1}{2}\right)^n A_f^n e^{m e_b}, \quad (6)$$

where e_b is the binding energy and can represent in the more general sense an exchange energy; K is independent of A_c. Because the sites in A_f can be bound or not bound while the sites out of A_f have only one state, the factor $1/2^n$ is necessary to avoid counting twice the ones in A_f. By summing over m and then over n, one obtains

$$Z = K \left[A_v + A_f \left(\frac{e^{e_b} - 1}{2} \right) \right]^N . \quad (7)$$

Our experiments provide a measurement of W_{spe} which is formally equal to [1]

$$W_{spe} = -\frac{\partial F}{\partial A_c}\bigg|_{V,T} = k_B T \frac{\partial \ln Z}{\partial A_c}\bigg|_{V,T} \quad (8)$$

where F is the free energy and A_c the contact area, and therefore

$$W_{spe} = \frac{\frac{\alpha N}{A_0}\left(\frac{e^{e_b}-1}{2}\right) k_B T}{A_v + \frac{\alpha A_c}{A_0}\left(\frac{e^{e_b}-1}{2}\right)} \approx \frac{\alpha \rho_v}{A_0}\left(\frac{e^{e_b} - 1}{2}\right) k_B T , \quad (9)$$

where $\rho_v = N/A_v$. It is worth noting from Eqs. (7) and (9) it is possible to reobtain exactly Eq. (5) [15]. By using Eq. (9) one directly obtains e_b from the measured specific adhesion energy values provided that A_0/α is known. As the same grafting technique was used for the A and T beads, A_0/α should also be the same in all the cases and is expected to be of the order of 10^3. $A_0/\alpha = 2100$ gives values that are in closest agreement with the known binding energy values [13,14] (Table II).

Since it generally takes about 15 min for lipids to diffuse around a giant vesicle, it is surprising that for each change of aspiration pressure, the equilibrium seems to be reached in less than a minute. Given W_{spe} and Eq. (5), the enrichment is around 1% at the true equilibrium obtained within 15 min. The resulting change in W_{spe} is within the experimental error and can be neglected. We have checked it experimentally by measuring for several aspiration pressures the contact angle for 20 min. In this approximation, equilibrium can be obtained locally because of the excess of sites on the vesicle and lateral diffusion does not bring significant change. The local equilibrium time is typically the one needed for a lipid to explore an area A_0, which is less than a second. This explains the fast equilibrium and also why the observed hysteresis is not stronger than for nonfunctionalized vesicles [16].

In contrast, if there were more sites on the bead or less sites on the vesicle, the diffusion of the vesicle sites towards the contact region would change noticeably the equilibrium time. It may be noted that decreasing the site density on the vesicle would decrease the adhesion energy which is already borderline; beads with a higher site density were not available. One may also note that even though global equilibrium is not achieved, the measured adhesion energy value is not affected beyond the experimental error, and therefore it is possible to obtain, through Eq. (5), the excess of sites at global equilibrium.

A_0/α is the parameter deduced from the experimental data. The values of A_0 and α cannot be determined, and we will only briefly discuss them. As a first approximation, we may assume that the bead is saturated with nucleosides which are all accessible. As discussed above, A_0 is then expected to be comprised between 50 and 180 nm^2, giving

TABLE II. Binding energy values e_b as deduced from Eq. (9) for different values of A_0/α.

A_0/α	1600	2100	2600	Literature values
Bead/vesicle				
A/T	2.9	3.2	3.4	3.6
T/A	3.1	3.4	3.6	3.6
A/A	2.0	2.3	2.5	1.9
T/T	1.5	1.7	1.9	1.5

for α a value comprised between 0.025 and 0.086 nm^2. This seems compatible with the fact that the nucleosides A and T bind through one donor and one acceptor H-bond separated by about 2 Å [17]. Since the PEG spacer arm is flexible, in a more realistic model, the sites should be accessible only for a fraction of its conformations. In this respect, A_0 may have been underestimated as well as α since only the ratio A_0/α is known.

This microcanonical description relating adhesion energy measurements to binding energies is coherent with the experiments and can be applied to other systems. The requirement of knowing A_0/α is limiting because it is not easy to obtain, but numerical simulations may provide good estimates in some cases. The precision of the technique is given by the dispersion of the adhesion energy data and is illustrated in Table II. In the case of A/T, the error is about $0.5k_BT$.

The present approach was made possible by the use of weak bonds. Functionalization by nucleosides produces a reversible adhesion and therefore enables one to measure a relevant adhesion energy which is not the case from stronger bonds [18].

The authors thank E. Evans who initiated this work, B. Derrida, C. Gourier, and J. Vannimenus for useful discussion, and L. Montagne, R. Marchand, and A. Le Sauze for their help in the micropipette setup.

*To whom correspondence should be addressed.
Email address: pincet@lps.ens.fr

[1] E. Evans, Biophys. J. **48**, 175–183 (1985).
[2] G. I. Bell, M. Dembo, and P. Bongrand, Biophys. J. **45**, 1051–1064 (1984).
[3] R. Lipowski, Phys. Rev. Lett. **77**, 1652–1655 (1996).
[4] D. Zuckerman and R. Bruinsma, Phys. Rev. Lett. **74**, 3900–3903 (1995).
[5] D. A. Noppl-Simson and D. Needham, Biophys. J. **70**, 1391–1404 (1996).
[6] E. Evans, Colloids Surf. **43**, 327–347 (1990).
[7] E. Evans, Biophys. J. **31**, 425–432 (1980).
[8] L. Lebeau, F. Pincet, and E. Perez (to be published).
[9] D. Needham, Methods Enzymol. **220**, 111–129 (1993).
[10] D. Needham and E. Evans, Biochemistry **27**, 8261–8269 (1988).
[11] As specified by Bangs Labs, the superavidin coated beads could adsorb 397.3 ng of biotin alkaline phosphatase (BAP) per mg of beads. Given the molecular weight of BAP (160 000 g), and the size of the beads (11 μm), the area per adsorbed BAP was 360 nm^2 which is of the order of the size of BAP. As this protein is larger than superavidin, the area per superavidin is at most 360 nm^2, and therefore, A_0 is at most 180 nm^2. As the diameter of superavidin is 5.5 nm, A_0 is at least 50 nm^2.
[12] A possible extraction of the lipids from the vesicle during this process cannot be ruled out in spite of a good reversibility: even if all the connected lipids were extracted, the adhesion measured in the subsequent cycle would not be modified within the experimental error, as it can easily be seen *a posteriori* from Table I by estimating the number of actual bonds in the contact zone, which is at least 10^3 times smaller than the initial quantity of lipids.
[13] F. Pincet, W. Rawicz, E. Perez, L. Lebeau, C. Mioskowski, and E. Evans, Phys. Rev. Lett. **79**, 1949–1952 (1997).
[14] F. Pincet, E. Perez, L. Lebeau, and C. Mioskowski, Mod. Phys. Lett. B **10**, 81–99 (1996).
[15] A detailed calculation of the adhesion energy with mobile or immobile sites will be found in F. Pincet, J. Vannimenus, C. Gourier, and E. Perez (to be published).
[16] See, for instance, Fig. 2 of E. Evans and D. Needham, Macromolecules **21**, 1822–1831 (1988).
[17] W. Saenger, *Principles of Nucleic Acid Structure* (Springer-Verlag, New York, 1984).
[18] E. Evans, Biophys. J. **48**, 185–192 (1985).

Electrostatic Nanotitration of Weak Biochemical Bonds

F. Pincet,[2] W. Rawicz,[1] E. Perez,[2] L. Lebeau,[3] C. Mioskowski,[3] and E. Evans[1]
[1]*Departments of Physics and Pathology, University of British Columbia, Vancouver, British Columbia, Canada, V6T 1W5*
[2]*Laboratoire de Physique Statistique de l'Ecole Normale Supérieure, associé aux universités Paris VI et Pairs VII, 24, rue Lhomond, 75231 Pairs Cedex 05, France*
[3]*Laboratoire de Synthèse Bio-organique, CNRS, Unité de Recherche Associée 1386, Faculté de Pharmacie, 74 Route du Rhin, 67401 Illkirch, France*
(Received 30 December 1996)

We introduce a new method to measure the energetics and range of weak biochemical bonds using functionalized vesicles. Large bilayer regions are held in molecular proximity by osmotic depletion forces to enable rapid specific bonding. By fixing an electrical charge to the tethering site of the functional group on one surface, persistent adhesion of the vesicles after removal of the depletion stress is titrated against the clamped electrostatic potential of the opposite surface. We demonstrate the method with DNA bases and obtain new information on the range of their specific interactions. [S0031-9007(97)04018-0]

PACS numbers: 87.15.Kg, 68.18.+p, 68.35.Md, 87.15.By

Nature has chosen weak biochemical bonds to play important roles in biology—e.g., the interaction energy between a complementary pair of nucleic bases of DNA is perhaps only $\approx 5\ k_BT$. Yet, bonds of a few k_BT in energy are extremely difficult to probe by any of the existing force techniques (atomic force microscopy [1], surface forces apparatus [2], optical tweezers [3], bead force probe [4], etc.) because these bonds have very short lifetimes with little strength on the time scale of experiments. Thus, we have developed a new method to titrate the specific chemical interaction of a weak bond against a controlled electrostatic bias. The concept is based on forced confinement of the reactant groups to a molecularly thin layer. When the surfaces are sufficiently close, the specific bonds equilibrate rapidly; but if separated beyond the range of the specific interaction, no bonding occurs [5]. Simultaneously, specific bonds that form are armed with a controlled repulsive potential which is triggered simply by release of the confining stress. If this potential exceeds the binding energy, the surfaces unbind; if not, they remain adherent. The experimental approach is to chemically graft a functional group [6] to the headgroup of a membrane lipid bearing a single electrical charge, which is then mixed with neutral lipids into the surface of a lipid bilayer vesicle #1. The counter structure (receptor group) is grafted to a neutral lipid, which is mixed with neutral and electrically charged bare lipids in the surface of a second bilayer vesicle #2. The charged lipids clamp the surface potential of vesicle #2. Then, using a novel preassembly technique, vesicle #1 is brought into molecular proximity with vesicle #2 and released to test for adhesive bonding. By titrating the electrolyte concentration in the aqueous environment and the surface charge density in vesicle #2 against adhesion, both the range and magnitude of the specific chemical interaction can be established. Here, we demonstrate the nanotitration method for weak hydrogen bonding between *A* and *T* nucleosides.

Three new diacyl lipids were synthesized [6] by grafting nucleosides to lipid chains, a negatively charged adenosine lipid (DOSPA), a neutral adenosine lipid (DOSA), and a neutral thymidine lipid (DOST) (see Fig. 1). Negatively charged bare lipids stearoyl-oleoyl-phosphatidylserine (SOPS) and neutral stearoyl-oleoyl-phospatidylcholine lipids (SOPC), were also used. Large vesicles were formed by hydration of mixtures (the compositions are listed in Table I) of these nucleoside lipids with the bare lipids (dried from chloroform-methanol solution) in 0.3 M sucrose [7]. The composition of the lipid mixtures was chosen according to the required charge. These lipids chains were unsaturated. This provided membrane vesicles in a fluid state, which ensured good mixing of the lipids. Vesicles labeled #1 contained DOSPA and vesicles labeled #2 contained either DOSPA or DOST plus SOPS to set the surface charge density. All experiments were performed at a fixed *p*H of 5.5.

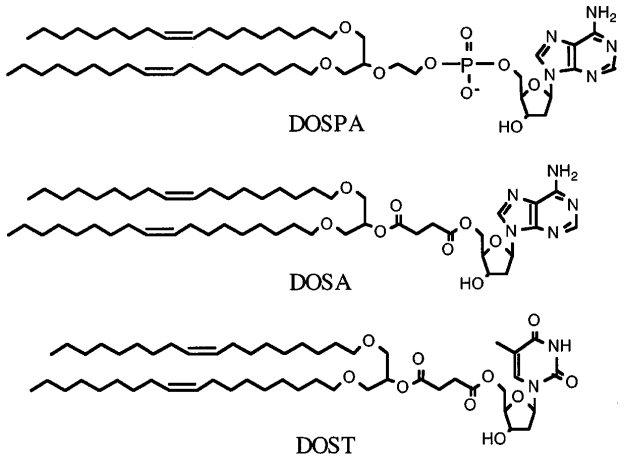

FIG. 1. Structures of the functionalized lipids. DOSPA is negatively charged while DOSA and DOST are neutral.

TABLE I. First two columns: composition of the vesicles; third column: range of ionic strengths that brackets the crossover C^* from bound to unbound vesicles; the limits on binding energy E_b that correspond to the bracket of ionic strengths as calculated with Eq. (1) (using an area per lipid [11] of 0.65 nm^2 and a single negative charge for DOSPA and SOPS with DOST, DOSA, and SOPC uncharged).

Vesicle #1	Vesicle #2	C^* (mM)	Binding energy (k_BT)
DOSPA/SOPC (5:95)	DOST/SOPS/SOPC (5:5:90)	$1 < C^* < 10$	$1.83 < E_b < 3.83$
DOSPA/SOPC (5:95)	DOST/SOPS/SOPC (5:10:85)	$1 < C^* < 10$	$2.97 < E_b < 5.18$
DOSPA/SOPC (5:95)	DOSA/SOPS/SOPC (5:5:90)	$5 < C^* < 50$	$0.90 < E_b < 2.37$

Using micropipets, single vesicles were selected from a dilute suspension in a chamber on the microscope stage and transferred to an adjacent chamber that contained NaCl (plus glucose needed for osmotic balance) and PEG 20000 polymer. To identify vesicles in the initial suspension, the two types of vesicles were prepared with different optical densities, which could be easily discriminated in the Hoffman modulation contrast microscopy. After transfer to the polymer solution, the vesicles were maneuvered to just touch in the second chamber where a macroscopic-size contact ($\approx 10\ \mu m^2$) was formed immediately, driven by the attractive depletion force (Fig. 2) [8]. Next, the adherent vesicle pair was released from the depletion stress by transfer into a third chamber that contained only NaCl (plus glucose). At this point, the only interaction left to sustain persistent adhesion of the vesicles in opposition to the electrostatic repulsion was the specific nucleoside attraction. If the internucleoside binding energy was smaller than the electrostatic double-layer energy, the vesicles separated; otherwise, they remained in contact. In accordance with Gouy-Chapman theory [9], the double-layer energy, scaled to one DOSPA molecule, E_{dl} depends on the charge density ρ_e (number of charges per nm^2) and ionic strength c_i (mol/l) : $\sinh(E_{\mathrm{dl}}/2k_BT) \approx 1.36\,\frac{\rho_e}{\sqrt{c_i}}$ (1). The double-layer energy E_{dl} was adjusted, by varying the salt concentration c_i (from 1 to 200 mM) and the SOPS density ρ_e in the #2 vesicles.

First, we titrated the nucleoside binding interaction against the ionic strength for fixed concentration of charged SOPS lipid. The ionic strength was reduced until the electrostatic repulsion was sufficient to unbind the adherent vesicles after transfer from the polymer solution. To stabilize initial contact in the polymer solution, the long-range electrostatic repulsion was overcome by a strong depletion stress in a 5% to 10% w/w concentration of PEG. As seen in Table I, the crossover between persistent adhesion and separation established bounds for the binding energy based on the discrete value of ionic strength used in the experiments. The binding energies deduced from the results in Table I for A/T and A/A interactions are in good agreement with values measured by other methods as seen in Table II.

Second, to test the range of the specific interaction, the concentration of PEG polymer was lowered until the persistent adhesion vanished, even though a stable depletion-driven contact existed before transfer from the initial PEG solution. For example, specific bonding of vesicles with 10 mol % charged SOPS lipid and 5 mol % reactant lipids (cf. second line of Table I) disappeared when the PEG concentration was reduced from 10%

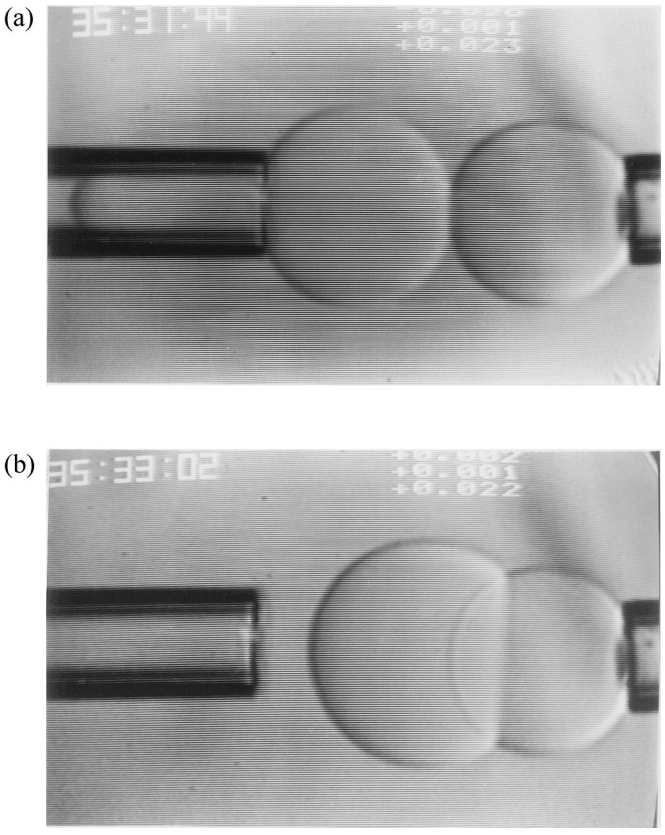

FIG. 2. Video micrographs of vesicle adhesion driven by polymer depletion in a 10% solution of PEG 20000. (a) The vesicles are maneuvered into point contact by micropipets. (b) The left hand vesicle is released from its holding pipet to enable adhesion to the right hand vesicle. The adherent vesicle pair was then transferred to a polymer-free solution to test persistent bonding after removal of depletion force.

TABLE II. Comparison of experimental values with published binding energies [10,11].

Binding energy (k_BT)	Experimental values	Literature values
A/T	$2.97 < E_b < 3.83$	3.5
A/A	$0.90 < E_b < 2.37$	1.7

to 5% (w/w) even in 20 mM salt. Analyzing the balance of osmotic depletion stress and electrostatic repulsion for these polymer concentrations shows that the initial separation between the surfaces increased from near molecular contact (stabilized by repulsive hydration and steric forces) in the 10% PEG solution to ≈2 nm in 5% PEG, which was the approach used to obtain a bound for the range of the specific interactions. The range of 2 nm for the A/T interaction is much smaller than the long-range attraction (≈38 nm) seen in SFA experiments with the functionalized lipids supported on mica substrates [10,11].

This new titration technique provides a simple approach to evaluate binding energies (from $2-25\ k_BT$) [12] and ranges of biochemical bonds under conditions most relevant for biology. In particular, the reactants are restricted to soft-flexible interfaces whose stiffness can be controlled, which provides an environment similar to bonding between semiflexible polymer chains. As such, the electrostatic and steric microenvironment around the binding sites can be preset by introducing membrane lipids with special charge and polymer moieties grafted to the headgroups. With this approach, it is possible to examine the nontrivial consequences of membrane conformational degrees of freedom and mobile-focal adhesion sites, which remain as unresolved issues between recent theoretical models [13].

This work was supported by the Medical Research Council of Canada through Grant No. MT7477, the Canadian Institute for Advanced Research Program in "Science of Soft Surfaces and Interfaces."

[1] G. Binnig, C. F. Quate, and C. H. Gerber, Phys. Rev. Lett. **56**, 930 (1986).

[2] J. N. Israelachvili and G. E. Adams, J. Chem. Soc. Faraday Trans. **174**, 975 (1978).

[3] A. Ashkin, Biophys. J. **61**, 569 (1992).

[4] E. Evans, K. Ritchie, and R. Merkel, Biophys. J. **68**, 2580 (1995).

[5] At equilibrium, the adhesion energy between surfaces with mobile reactants (ligands and receptors tethered to lipids) is simply the surface pressure produced by the crossbridged groups confined to the contact region (i.e., energy/area $\approx \rho_b k_B T$ where ρ_b = bound sites/area). The concentration of bound sites in the contact zone is set by the 2D equilibrium between bound and free sites [i.e., $\ln(\rho_b/\rho_f) \approx$ binding energy]. See Appendix of E. Evans, Biophys. J. **48**, 175 (1985); M. Dembo, Proc. R. Soc. London B **234**, 55 (1988). Rapid diffusion of the ligand/receptor groups is essential to the success of this measurement. The key question is what is the equilibration time ($t_D \sim 4\pi R^2/D$)? For 10 μm size vesicles and fluid lipids with diffusivity of order $D \sim 10\ \mu m^2/sec$, the equilibration time is of order 1 min, which is well within the waiting period at each step in the experiment.

[6] Functionalized lipids were synthesized by coupling the unprotected nucleosides with 2-(1,3-dioleyloxy) propyl hemisuccinate using a modified DCC/DMAP method. L. Lebeau, S. Olland, P. Oudet, and C. Mioskowski, Chem. Phys. Lipid **62**, 93 (1992).

[7] D. Needham and E. Evans, Biochem. **27**, 8261 (1988).

[8] Depletion-driven attraction arises as a subsequence of steric repulsion of the polymer chains from nonadsorbing surfaces. When separation between the surfaces reaches the scale of the correlation length of the polymer in solution, chains are excluded from the gap and the osmotic imbalance in the solvent pulls the surfaces together [J. F. Joanny, L. Leibler, and P. G. Gennes, J. Polym. Sci. **17**, 1073 (1979)]. See E. Evans and D. Needham, Macromol. **21**, 1822 (1988); E. Evans, Macromol. **22**, 2277 (1989); E. Evans, D. Klingenberg, and F. Szoka, Langmuir **12**, 3031 (1996) for details of depletion-driven attraction between lipid bilayer vesicles and methods used in testing bilayer vesicle adhesion in concentrated solutions of nonadsorbing PEG and Dextran polymers.

[9] R. M. Peitzsch and S. Mc Laughlin, Biochemistry **32**, 10 436 (1993).

[10] F. Pincet, E. Perez, G. Bryant, L. Lebeau, and C. Mioskowski, Phys. Rev. Lett. **73**, 2780 (1994).

[11] F. Pincet, E. Perez, G. Bryant, L. Lebeau, and C. Mioskowski, Mod. Phys. Lett. B **10**, 81 (1996).

[12] To determine a sensitivity limit for the novel technique presented in our manuscript, many subtle aspects must be taken into account. The most important to consider is steric repulsion and unbinding driven by confinement of collective bending excitations as originally worked out by Helfrich [W. Helfrich, Z. Naturforsch. **33A**, 305 (1978); W. Helfrich and R.-M. Servuss, Nuovo Cimento Soc. Ital. Fis. **D3**, 137 (1984); R. Lipowsky and S. Leibler, Phys. Rev. Lett. **56**, 2541 (1986); E. Evans and V. A. Parsegian, Proc. Natl. Acad. Sci. U.S.A. **83**, 7132 (1986)]. The most restrictive estimate is based on the critical level of short-range adhesion energy ($c_0 E_b^*$) below which the unbinding transition is expected in the absence of lateral tension [R. Lipowsky, Europhys. Lett. **7**, 255 (1988); E. Evans, Langmuir **7**, 1900 (1991)]. As shown by Lipowsky and coworkers [R. Lipowsky *et al.*, Phys. Rev. Lett. **77**, 1652 (1996), and references therein], this threshold is determined by the magnitude of the steric interaction in the range of the attraction l_a, i.e., $c_o E_b^* \sim 0.2\ (k_BT)^2/(k_c l_a^2)$. Given the 1 nm range of attraction found here and the membrane bending stiffness for these bilayers of $\sim 25\ k_BT$, the critical level of bare adhesion energy would be on the order of 10^{-2} mJ/m^2, which for ligand-receptor fractions in the membrane above one mole percent ($c_o > 0.014\ nm^{-2}$) predicts unbinding at an energy/bond of a small fraction of

$E_b^* < 0.2\ k_BT$. For weak bonds of order k_BT, the fraction of adhesive molecules is raised to 5 mol % or more so that fluctuations are not expected to significantly affect the sensitivity.

[13] D. Zuckerman and R. Bruinsma, Phys. Rev. Lett. **74**, 3900 (1995); R. Lipowsky, Phys. Rev. Lett. **77**, 1652 (1996).

Quantitative Analysis of Holes in Supported Bilayers Providing the Adsorption Energy of Surfactants on Solid Substrate

Patricia Bassereau*,† and Frédéric Pincet‡

Laboratoire de PhysicoChimie Curie, UMR 168 CNRS-Curie, Institut Curie, 11 rue P. et M. Curie, 75231 Paris Cedex 05 France, and Laboratoire de Physique Statistique de l'Ecole Normale Supérieure, associé aux universités Paris VI et Paris VII, 24 rue Lhomond, 75231 Paris Cedex 05 France

Received May 19, 1997. In Final Form: October 9, 1997⊗

We investigated the topography of mixed bilayers consisting of a first monolayer of DMPE (dimyristoylphosphatidylethanolamine) and of a second monolayer of DOPC (dioleoylphosphatidylcholine) that were Langmuir−Blodgett deposited on mica. Using transfer ratio measurements and tapping mode atomic force microscopy experiments, we show that the subnanometric holes in the bilayers result from the desorption of lipids of the first monolayer during the transfer of the second monolayer. We present a new simple technique based on the quantitative analysis of these holes that allows determination of the adsorption energy of amphiphilic molecules on solid surfaces. This technique is valid for relatively low adsorption energies in the range 1 to 10 k_BT.

Introduction

Supported lipid bilayers were commonly considered as model membranes.[1] In this respect, Langmuir-Blodgett bilayers have been used for a long time in many force measurements and were described as perfectly smooth films.[1−4] These last years, atomic force microscopy (AFM) experiments allowed imaging of these bilayers, but most of the results concentrated on the molecular scale description of the bilayers.[5−7] On a larger scale, the existence of holes in these films has been observed for several years.[7,8] Different surfactants (lipids, fatty acids) and different types of substrates (hydrophilic or hydrophobic) were used. The depth of these holes that most of the authors measured usually corresponds to the thickness of the bilayer, which suggests that the first monolayer peels off during the deposition of the second layer. Up to now, only qualitative observations were reported and, to our knowledge, no quantitative analysis has been published to explain the origin of the holes. This lack of quantitative analysis may hinder a correct interpretation of some force measurements for which a precise understanding of the surface arrangement of the molecules is required.

In this paper, we have combined transfer ratio and AFM measurements on mixed bilayers consisting of a first monolayer of DMPE (dimyristoylphosphatidylethanolamine) and of a second monolayer of DOPC (dioleoilphosphatidylcholine). We were able to demonstrate that, as suspected before, the holes in these supported bilayers originate in the desorption of molecules of the first monolayer during the second transfer. This effect is shown to be related to the balance between the adsorption energy of the molecules on the solid substrate and their energy at the air−water interface. As the surface pressure of the monolayer at the liquid interface is controlled, the knowledge of the number of molecules peeling off provides directly the adsorption energies of amphiphilic molecules on solid substrates.

Experimental Section

Langmuir-Blodgett Deposition. We prepared asymmetric bilayers consisting of a first monolayer of DMPE and of a second monolayer of DOPC. This system is commonly used in surface force apparatus (SFA) experiments.[9] DMPE and DOPC were purchased from Avanti Polar Lipids Inc., dissolved in chloroform, and stored under argon at −20 °C. The layers were Langmuir-Blodgett deposited on freshly cleaved mica translated vertically in the home-made trough[10] (15 × 25 cm²). The size of the mica was ∼1 × 1 cm² for the AFM experiments and 1.5 × 8 cm² for the transfer ratio measurements. A schematic representation of the samples is given in Figure 1. For the DMPE layer, the substrate was raised from the trough. In all the experiments described in this paper, the surface pressure and deposition velocity of the substrate were, respectively, 42 mN/m corresponding to the solid phase[11]) and 200 μm/s. The DOPC layer was then transferred during the vertical dipping of the substrate into the trough, resulting in an hydrophilic bilayer. This transfer was performed at different deposition velocities (3 and 200 μm/s) and surface pressures (Π_{DOPC}) between 2 and 40 mN/m. The DOPC is in a liquid phase for this pressure range (data not shown). To prevent any dewetting problem, the samples always remained immersed in highly pure water.

* Author to whom correspondence should be addressed.
† Laboratoire de PhysicoChimie Curie.
‡ Laboratoire de Physique Statistique de l'Ecole Normale Supérieure.
⊗ Abstract published in *Advance ACS Abstracts,* December 1, 1997.

(1) Israelachvili, J. N. *Intermolecular and Surface Forces*; Academic: London, 1992.
(2) Helm, C. A.; Knoll, W.; Israelachvili, J. N. *Proc. Natl. Acad. Sci. U. S. A* **1991**, *88*, 8169.
(3) Pincet, F.; Perez, E.; Bryant, G.; Lebeau, L.; Mioskowski, C. *Phys. Rev. Lett.* **1994**, *73*, 2780.
(4) Solletti, J. M.; Botreau, M.; Sommer, F.; Brunat, W. L.; Kasas, S.; Duc, T. M.; Celio, M. R. *Langmuir* **1996**, *12*, 5379.
(5) Weisenhorn, A. L.; Egger, M.; Ohnesorge, F.; Gould, S. A.; Heyn, S. P.; Hansma, H. G.; Sinheimer, R. L.; Gaub, H. E.; Hansma, P. K. *Langmuir* **1991**, *7*, 8.
(6) Zasadsinski, J. A.; Helm, C. A.; Longo, M. L.; Weisenhorn, A. L.; Gould, S. A.; Hansma, P. K. *Biophys. J.* **1991**, *59*, 171.
(7) Bourdieu, L.; Silberzan, P.; Chatenay, D. *Phys. Rev. Lett.* **1991**, *67*, 2029.
(8) Hui, S. W.; Viswanathan, R.; Zasadsinski, J. A.; Israelachvili, J. N. *Biophys. J.* **1995**, *68*, 171.
(9) See for example Helm, C. A.; Israelachvili, J. N.; McGuiggan, P. M. *Biochemistry* **1992**, *31*, 1794; and Pincet, F.; Perez, E. Wolfe, J. *Cryobiology* **1994**, *31*, 531.
(10) Perez, E.; Wolfe, J. *Langmuir* **1994**, *10*, 974.
(11) Dörfler, H.-D.; Rettig, W. *Colloid Polym. Sci.* **1980**, *258*, 415.

S0743-7463(97)00515-5 CCC: $14.00

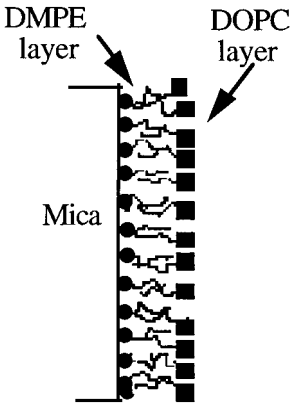

Figure 1. Schema of the deposited bilayer on the mica.

All our experiments were performed at room temperature.

Transfer Ratio. The difference between the total area of the DOPC monolayer before and after transfer (ΔA) at the air/water interface was recorded. The ratio between ΔA and the area of the mica (A) will be referred as the "transfer ratio" and denoted R ($R = \Delta A/A$). A value for R of 1 reflects that the monolayer is properly transferred on the substrate and that no desorption of molecules occurs during the transfer.

Atomic Force Microscopy. The topography of the surface of the bilayers was observed with a Nanoscope III (Digital Instruments) AFM setup. The images were obtained in tapping mode in water to prevent any damage of the bilayer structure. The sample had to remain immersed under water after lipid deposition, so the mica substrate was transferred under water and taped on the center of a Teflon disc with a small groove on its periphery. This simple system allowed a large water drop to be maintained over the mica when the sample was installed on the scan head. The commercial tapping liquid cell was then placed over the sample. We used a medium scan head (15×15 μm^2) and commercially available silicon nitride tips on a cantilever with a spring constant (k) of 0.56 N/m, oscillating at a frequency of 90 kHz. The images were obtained with a scan rate of 2 Hz. Prior to every experiment, we exposed the tips for 30 min to an ozone flux to oxidize any contaminant. The first image was usually obtained between 30 min and 1 h after the deposition. For the AFM experiments, the DOPC layer was deposited at a velocity of 200 μm/s (similar to classical SFA experiments and to some previous AFM experiments[3,6,12]). We insured that the force plot was correct and not modified before and after every experiment to check that the tip had not been contaminated during the scans.

Results and Discussion

Desorption of the DMPE Layer. The DMPE monolayer in the air is smooth and defect free, as observed with AFM (see Figure 2a). This result is confirmed by the transfer ratio ($R = 1.04 \pm 0.03$), which indicates that the monolayer was slightly denser on the mica than at the air/water interface. If moved through the monolayer-free air/water interface at 3 μm/s, the DMPE monolayer is then covered with holes. The proportion of the surface covered by holes (x) is very high $x = 38 \pm 4\%$ (see Figure 2b)], confirming that the DMPE molecules desorb at least in the extreme case where there are no DOPC molecules ($\Pi_{DOPC} = 0$ mN/m) at the air/water interface.

For DOPC, the deposition ratio decreased with both the surface pressure of the monolayer and the transfer velocity (see Table 1). The transfer ratio (R) is commonly considered as direct evidence of the good quality of a transfer. In fact, this ratio reflects the balance between molecules desorbing from the substrate and molecules of the monolayer transferred onto the substrate. The fact that R is always <1 (see Table 1) is not proof for a low quality transfer but could be equally well interpreted as desorption from the substrate of some DMPE molecules. Moreover, the decrease of R with Π_{DOPC} indicates that the number of DMPE molecules desorbed from the mica increases when Π_{DOPC} decreases. Eventually, $R = -0.04$ (see Table 1), which is evidence of a very large desorption from the substrate at low surface pressure.

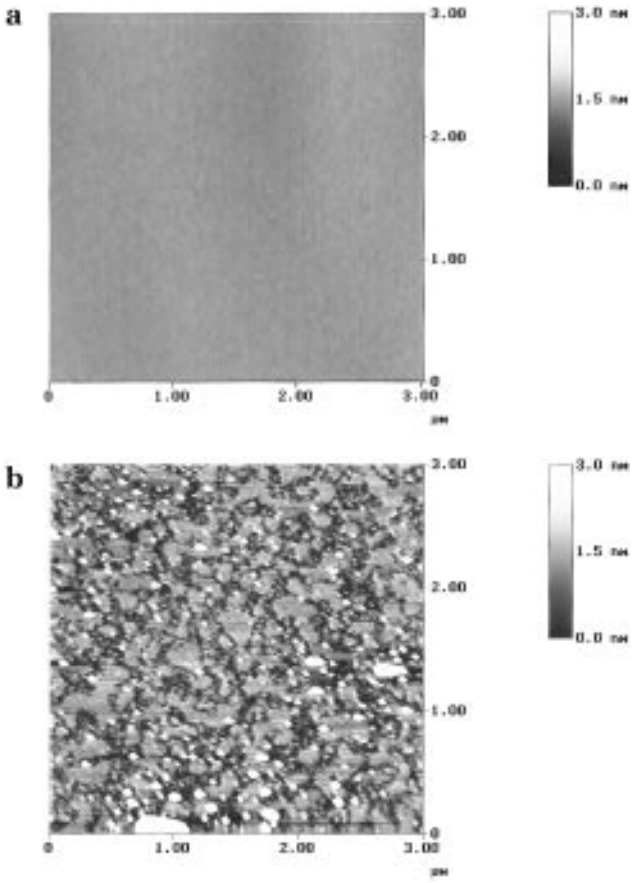

Figure 2. (a) AFM image (tapping mode in air) of a DMPE monolayer deposited on mica at 42 mN/m. (b) AFM image (tapping mode in water) of the same DMPE monolayer after it was passed through the air/water interface. The coexistence of holes, monolayers, and multilayers (white spots) is similar to the results described in ref 4.

Table 1. Evolution of the Transfer Ratios of DOPC Monolayer from the Air/Water Interface onto DMPE-Coated (42 mN/m) Mica at Deposition Speeds of 200 μm/s (R_{fast}) and 3 μm/s (R_{slow})

Π_{DOPC} (mN/m)	R_{fast}	R_{slow}
40	0.94 ± 0.05	0.92 ± 0.05
25	–	0.71 ± 0.05
15	0.74 ± 0.05	0.42 ± 0.05
2	0.41 ± 0.05	-0.04 ± 0.05

Bilayer-Deep Holes. The AFM images clearly exhibit holes in the bilayers (see Figure 3) at every transfer pressure. The proportion and size of the holes depend on the deposition pressure (see Table 2 and Figure 3). These defects are very stable; that is, their shape and position do not change over at least 30 min. Besides, we never observed any growth of these holes over a few hours. For the high-pressure transfer, the depth of the holes cannot be obtained with a good accuracy because their lateral size is of the order of the size of the tip radius (≈30 nm). For the low pressures (15 and 2 mN/m), the holes are larger (up to 500 nm); their typical sizes are, respectively, 100 and 250 nm. A depth of 3.2 ± 0.6 nm could be

(12) Helm, C. A.; Israelachvili, J. N.; McGuiggan, P. M. *Biochemistry* **1985**, *24*, 4608.
(13) Wolfe, J.; Perez, E.; Bonanno, M.; Chapel, J.-P. *Eur. Biophys. J.* **1991**, *19*, 275.

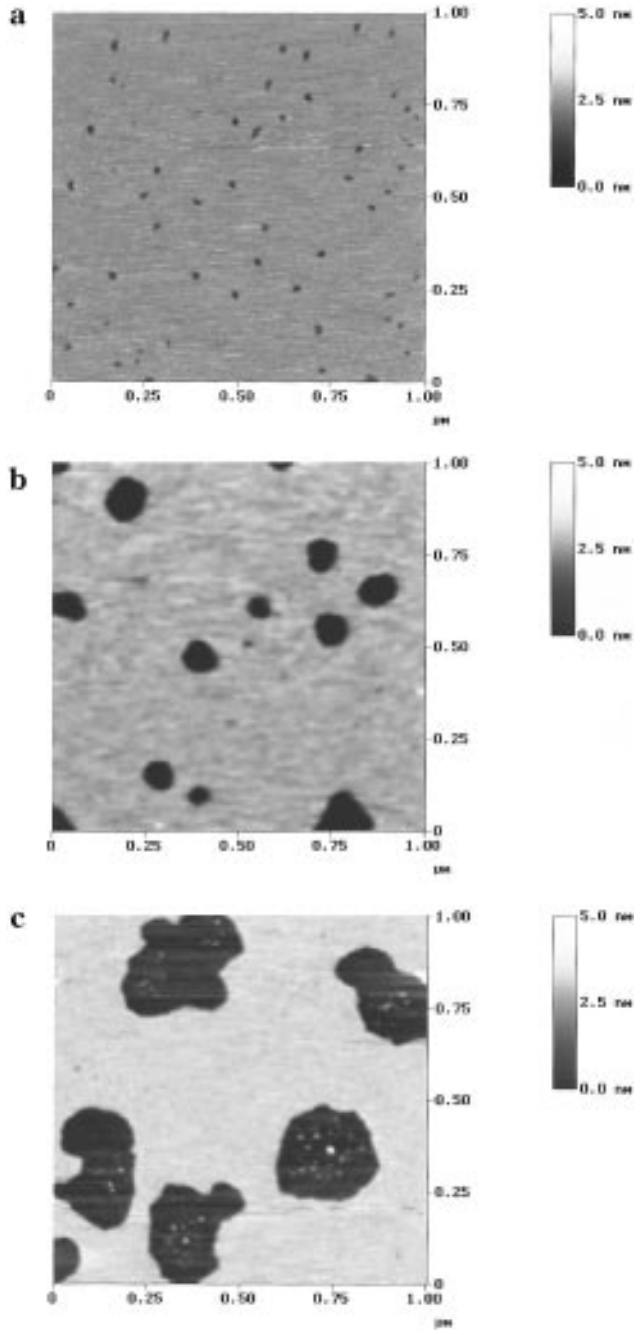

Figure 3. AFM images in tapping mode of lipid bilayers deposited on mica surface. The first monolayer is made of DMPE (42 mN/m), and the second monolayer is made of DOPC deposited at (a) 40, (b) 15, and (c) 2 mN/m.

Table 2. Fraction of the Surface Covered by Holes in the DMPE/DOPC Bilayer Surface at Various DOPC Deposition Pressures (Π_{DOPC}) Obtained with AFM Experiments (x_{AFM}) and By Transfer Ratio Measurements from Equation 1 (x_R)

Π_{DOPC} (mN/m)	x_{AFM} (%)	x_R (%)
40	4 ± 3	3 ± 3
15	10 ± 3	12 ± 3
2	19 ± 3	21 ± 3
0	38 ± 4	—

measured. The thickness of the DMPE monolayer on a silicon substrate is 2.4 nm as measured by ellipsometry. The thickness of a DOPC monolayer is ~2.0 nm in the dense phase at $\Pi_{DOPC} = 40$ mN/m.[13] Consequently, as the thickness of this monolayer at lower surface pressure is <2.0 nm, the defects are extending over a bilayer. At high pressures, the holes have probably the same physical origin and, consequently, should also be one bilayer thick.

Moreover, monolayer-deep holes would not be stable for two reasons. Firstly, hydrophobic chains of the DMPE would be in contact with water. Secondly, we performed fluorescence recovery after photobleaching (FRAP)[14] experiments to estimate the in-plane diffusion coefficient (D) of the lipids in the transferred layers. The DMPE or the DOPC lipids were mixed with 5% of their fluorescent NBD analogs (synthesized at the Laboratoire de Physico-Chemie Moléculaire des Membranes Biologiques—Paris[15]). The lipids of the outer monolayer diffuse rapidly, and D is between 0.1 and 1 $\mu m^2/s$, slightly smaller than the diffusion coefficient of phosphatidylcholine (PC) in oriented multilayers.[16] This result indicates that monolayer-deep holes would spontaneously close up in 1 s at the most, and could not be observed on several consecutive AFM images. At the contrary, bilayer-deep holes are stable because no noticeable diffusion of the lipids of the first monolayer on the mica was observed with FRAP experiments over measurable time scales (30 min). This result explains the immobility and shape invariance of the holes.

Holes Origin. The two previous results, desorption of the DMPE and bilayer-deep holes, suggest the following scenario for the arrangement of the bilayers on the mica. When the first DMPE monolayer is dipped in through the DOPC monolayer, some DMPE lipids desorb from the mica to the air/water interface. The DOPC molecules cover only the hydrophobic surface of the remaining DMPE chains, leading to the coexistence of bare mica and lipid bilayers in contact with the water. In addition, if we assume that the molecular area of the DOPC is unchanged after deposition and that holes are due exclusively to DMPE desorption, the proportion of bare mica (i.e., the proportion of holes; x) should be related to the transfer ratio R by eq 1:

$$x = \frac{1 - R}{1 + \frac{a_w}{a_m}} \tag{1}$$

where a_m is the molecular area of DMPE on the mica (0.41 nm^2/molecule) and a_w is the molecular area of DMPE at the DOPC transfer pressure of Π_{DOPC}. The term a_w can easily be obtained from the pressure isotherm of the DMPE monolayer. The error bars on R, a_w, and a_m are, respectively, 0.05, 0.02 nm^2, and 0.02 nm^2, as deduced from statistical analysis. Therefore, the precision on x is greater than 0.03.

The term x can also be measured from the AFM images by applying a threshold before processing them. The error bars (see Table 2) were deduced from the precision on the threshold and from the statistical analysis over several images and samples.

For the same deposition velocity (200 μm/s), the x values calculated from the transfer ratio measurements agree perfectly with the ones deduced from AFM (see Table 2). The same comparison has also been performed with pure bilayers (DOPC/DOPC and DMPE/DMPE, not shown). The agreement is again excellent between the two techniques.

This agreement shows unambiguously that the holes are created in the bilayers by the peeling off of the DMPE molecules during the transfer of the second monolayer.

(14) Cribier, S.; Morrot, G.; Neuman, J. M.; Devaux, P. F. *Eur. Biophys. J.* **1990**, *18*, 33.
(15) Colleau, M.; Herve, P.; Fellmann, P.; Devaux, P. F. *Chem. Phys. Lipids* **1991**, *57*, 29.
(16) Devaux, P. F.; McConnell, H. J. M. *Eur. Biophys. J.* **1972**, *94*, 4475.

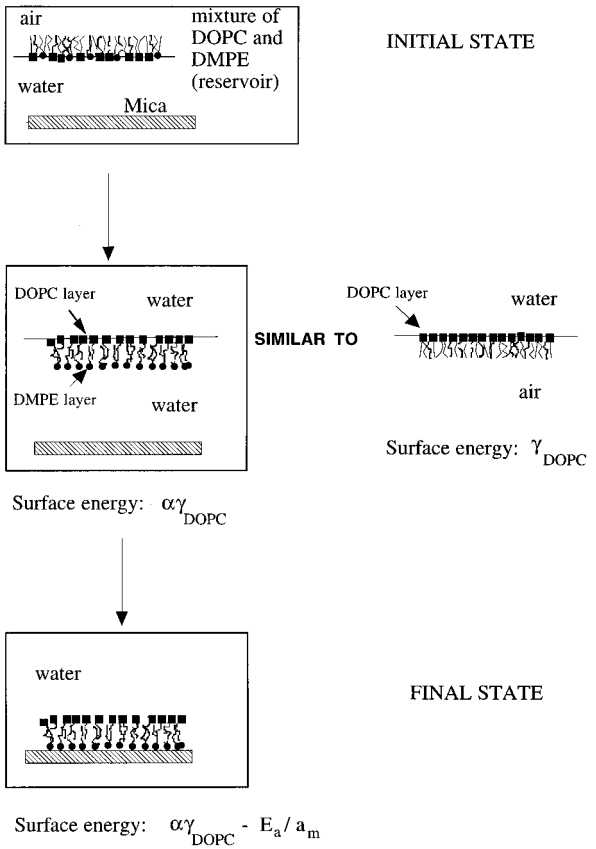

Figure 4. Description of the ΔE term, which is the the free-energy difference between the bilayer phase adsorbed on the mica and the bare mica with the lipids in the reservoir at the air/water interface, for a reference area a_m (a_m is the DMPE molecular area). Only surface terms are used. ΔE is obtained through an intermediate state (a DOPC/DMPE bilayer in water). The relative surface energy of this intermediate state can be estimated to be $\alpha\gamma_{DOPC}$ by analogy with the air/water interface.

Adsorption Energy of DMPE on Mica. The hole density is related to the transfer velocity. The diffusion of DMPE lipids in the monolayer at the contact line air/water/mica might limit the desorption of lipids and explain the transfer velocity dependence. The diffusion coefficient of lipids at the air/water interface is of the order of a few $\mu m^2/s$, so the lipids diffuse over a few microns per second. Therefore, at slow velocity (3 μm/s), it can be assumed that equilibrium is achieved. For the calculation of the proportion of holes x, the simplest approach is to describe the system as two phases in equilibrium : (1) the bilayer phase adsorbed on the mica, and (2) the bare mica with the lipids in the reservoir at the air/water interface. The ratio ρ between the total surface covered by holes and the total bilayer surface ($\rho = x/1 - x$) is given by eq 2:

$$\rho = \exp(-\Delta E/k_B T) \qquad (2)$$

where ΔE is the free-energy difference between both phases for a reference area a_m. The term ΔE represents the energy cost to detach the DMPE polar head from the mica (i.e. the adsorption energy per DMPE molecule E_a) minus the interfacial tension of DOPC on DMPE (see Figure 4). This last term is the surface energy required to create a mixed DOPC/DMPE bilayer from the corresponding lipids in the reservoir (see Figure 4). In the absence of exact model or of experimental data, we can make the analogy between the DMPE/water interface and the air/water interface and assume that the DOPC/DMPE interfacial tension is proportional to the surface tension

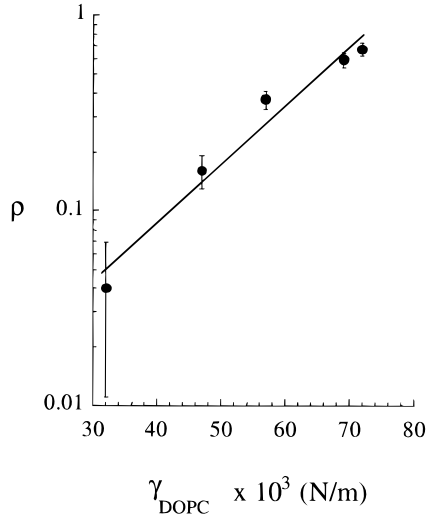

Figure 5. Ratio (ρ) between the surface covered by holes and the surface covered by the bilayer (●) as a function of the surface tension of the DOPC monolayer at the air/water interface (γ_{DOPC} = 72 mN/m − Π_{DOPC}). The straight line represents the best fit deduced from eq 2. The correlation coefficient is 0.979.

of DOPC at the air/water interface γ_{DOPC} (γ_{DOPC} = 72 mN/m − Π_{DOPC}) during the transfer of this molecule. Therefore, for the area a_m, ΔE is given by eq 3:

$$\Delta E = E_a - a_m \alpha \gamma_{DOPC} \qquad (3)$$

The two unknowns are the proportionality factor α and E_a. The terms a_m and γ_{DOPC} are directly deduced from the compression isotherm, and α will depend on the DMPE deposition pressure, which is constant in our experiments.

This simple model fits well the transfer ratio data at 3 μm/s (see Figure 5). The deduced DMPE/mica adsorption energy is $5.2 \pm 0.5\ k_B T$, and $\alpha = 0.7$. These values validate *a posteriori* our assumptions because the observed desorption reflects a moderate energy E_a. Moreover, the interfacial tension between the DMPE chains and water is >25 mN/m[17] and is weaker than the pure water surface tension of 72 mN/m.[18] Therefore, α was expected to be in the range 0.35 − 1.

The sensitivity of the transfer ratio technique to x does not exceed 3%. We have estimated the strongest adsorption energy accessible with this simple technique to be 10 $k_B T$.

Conclusion

As a conclusion, we have shown that the large scale defects observed in the DOPC/DMPE bilayers on mica are bilayer-deep holes. The holes originate from the balance between the relatively low lipid/substrate adsorption energy (few $k_B T$) and the pressure in the second monolayer at the air/water interface. The size of the holes decreases as the deposition pressure increases and the proportion of the holes may easily be deduced from the transfer ratio. This phenomenon is probably common in any supported bilayer system and has been observed previously by different groups but never been explained. Consequently, in the case of asymmetric bilayer, the second bilayer is never perfectly pure; that is, some lipids from the inner monolayer are present in the outer one (this is very relevant for SFA experiments). The propor-

(17) Pincet, F.; Perez, E.; Bryant, G.; Lebeau, L.; Mioskowski, C. *Mod. Phys. Rev. Lett. B* **1996**, *10*, 81.

(18) van Oss, C. J. *Interfacial Forces in Aqueous Media*; Dekker: New York, 1994.

tion of contaminant is hard to determine. Some bare mica is exposed to the water, possibly generating double-layer repulsion in force measurements. This phenomenon has been previously observed but not understood.[13] We have used the simplest model for analyzing our experimental results. Because our free energy contains only surface terms, we are unable to predict the size and the shapes of the holes.

Additionally, we propose a novel simple technique for measuring the adsorption energy of amphiphilic molecules on solid substrate. This technique could be widely used with numerous systems, possibly even with copolymers, as long as they can form bilayers. For typical lipids, this technique is appropriate in the range $1-10\ k_BT$.

Acknowledgment. We are grateful to S. Cribier for the FRAP experiments at the LPCMMB, and to G. Debregeas, E. Perez, and T. Lebouar for useful discussions.

LA970515C